



The
University
Of
Sheffield.

Modelling the Axial Polarity in the Developing Zebrafish Ear

By: R D Hartwell

A thesis submitted in partial fulfilment of the requirements for the degree of
Doctor of Philosophy

The University of Sheffield Department of Biomedical Science

September 2016

Abstract

The developing zebrafish ear, along with the inner ear of all jawed vertebrates, must undergo a symmetry-breaking event as it progresses from an ectodermal placode to an elaborate structure with morphological and functional asymmetry around the body axes. This asymmetry is apparent soon after the specification of the otic placode, established through localised domains of expression across the otic anterior-posterior (AP) axis (reviewed in Whitfield and Hammond 2007). In the zebrafish it has previously been established that Fibroblast growth factor (Fgf) and Sonic hedgehog (Shh) signalling are primarily responsible for AP patterning of the otic placode sensory epithelia and strikingly, alterations of these pathways can produce duplications of the anterior or posterior otic character. However, the propensity of the equipotent otic placode to adopt either an anterior or posterior fate is progressively restricted over this early developmental period (Hammond et al., 2003; Hammond and Whitfield, 2011).

The currently known posterior otic markers are expressed from 24 hours post fertilisation (hpf), after the zebrafish otic placode is thought to have become restricted in its ability to adopt either anterior or posterior character. However, there are no markers within the early posterior otic domain that might indicate any transcriptional difference prior to 24hpf. The early transcriptional differences that define anterior otic character are better defined but it is not clear how otic extrinsic Fgf and Shh signalling are integrated to establish this differential expression.

I have identified two novel markers of the posterior otic domain that are expressed prior to 24hpf, which appear to reflect different events occurring across the AP otic axis. Alongside this I have also demonstrated that the early anterior otic markers *hmx3a* (previously *nkx5.1*) and *hmx2* (previously *nkx5.2*) represent good candidates for integrating Fgf and Shh signalling to establish the extent of the anterior otic character. By combining these data I have built upon the previous model of Hammond et al. proposing a model that better accounts for the dynamic expression observed across the AP axis of the zebrafish otic placode (Hammond and Whitfield, 2011).

Contents

1	Introduction	5
1.1	The zebrafish as a vertebrate model	5
1.2	The function and structure of the inner ear	6
1.2.1	The vestibular system	6
1.2.2	The auditory system	7
1.3	Early development of the inner ear; the otic placode	7
1.3.1	The otic-epibranchial placodal domain	7
1.4	Patterning of the zebrafish otic placode across the anterior-posterior axis	11
1.4.1	Signals acting across the zebrafish otic anterior-posterior axis	11
1.4.2	Transcriptional differences across the anterior-posterior otic axis	15
1.4.3	Competence of the otic placode to adopt anterior-posterior identity	18
1.5	Patterning of the chick and mouse otocyst along the anterior-posterior axis	23
1.6	Congenital hearing loss	26
1.7	Aims and objectives	27
1.7.1	Aims	27
1.7.2	Objectives	27
2	Materials and Methods	28
2.1	Materials	28
2.2	Methods	28
2.2.1	Zebrafish husbandry	28
2.2.2	Zebrafish lines	29
2.2.3	Microscopy	29
2.2.4	PCR	30
2.2.5	Injection	30
2.2.6	Morpholino (MO) knockdown	30
2.2.7	<i>cdrl:eGFP</i> construct injection	31
2.2.8	CRISPR Mutagenesis	32
2.2.9	Recombineering	33
2.2.10	Screening	36
2.2.11	Genotyping by sequencing or restriction digest	37
2.2.12	Fluorescence-Activated Cell Sorting (FACS) and flow-cytometry	38
2.2.13	In Situ Hybridisation (ISH)	39
2.2.14	Phalloidin staining of actin-rich stereocilia	44
2.2.15	Joint acetylated-tubulin antibody and phalloidin staining	45
2.2.16	Heat-shock inducible misexpression	45
2.2.17	Embryo chemical treatment	45
2.2.18	Vestibular analysis	46

2.2.19	Statistics	46
3	Identification of novel early markers of the posterior otic domain	47
3.1	Introduction	47
3.2	Results	48
3.2.1	Search of expression data for genes with early restriction to the anterior and posterior otic domains	48
3.2.2	<i>Cdr2l</i> expression persists in the anterior otic domain after loss of Fgf signalling but only transiently	54
3.2.3	Otic <i>cdr2l</i> expression appears down regulated in response to over-expression of <i>fgf3</i>	56
3.2.4	Otic <i>cdr2l</i> expression does not appear duplicated or strongly up-regulated when Hh signalling as constitutively active	58
3.3	Discussion	60
3.4	Conclusions	61
4	The role of <i>cdr2l</i> in otic placode development	62
4.1	Introduction	62
4.2	Results	63
4.2.1	<i>cdr2l</i> morphant morphology	63
4.2.2	<i>Cd2rl</i> morphants show largely unaffected patterning of the anterior-posterior otic axis but a possible reduction in overall length	65
4.2.3	Markers of the delaminating otic neuroblasts and their subsequent differentiation display a modest reduction in expression in the <i>cdr2l</i> morphants	67
4.2.4	<i>Cdr2l</i> morphants have no apparent vestibular defects but a possible swim-bladder inflation phenotype by 5dpf	68
4.2.5	The <i>cdr2l</i> ATG morpholino inhibits translation of the <i>cdr2l</i> CDS <i>in vivo</i>	70
4.2.6	Generation of <i>cdr2l</i> CRISPR mutants	71
4.2.7	<i>Cdr2l</i> mutants do not show any otolith, vestibular or swim bladder defects but do have a reduced anterior-posterior otic vesicle length	73
4.2.8	<i>Cdr2l</i> 4bp deletion mutants show a loss of <i>cdr2l</i> full-length wild-type transcript by 14-16ss but no up-regulation of the potential paralogue <i>cdr2a</i>	76
4.2.9	Otic expression of the positive cell cycle regulator <i>mycb</i> was not clearly altered in <i>cdr2l</i> mutants	77
4.2.10	Expression of <i>neurog1</i> , <i>neurod1</i> and <i>fsta</i> in the <i>cdr2l</i> mutants	79
4.3	Discussion	79
4.4	Conclusions	81
5	Development of a transcriptomics approach to identifying differential gene expression associated with posterior otic identity	82
5.1	Introduction	82
5.2	Results	83
5.3	Discussion	89
6	Integration of Fgf and Hh signalling across the early otic placode	90
6.1	Introduction	90
6.2	Results	91
6.2.1	Posterior otic morphology is lost in embryos treated with 100 μ M cyclopamine (CyA) between 14-15 and 22.5hpf	91

6.2.2	Inhibition of Hh signalling between 14-15 and 22.5hpf leads to delayed ectopic posterior otic expression of the anterior otic factors <i>fgf3</i> , <i>fgf8a</i> and <i>pax5</i> . . .	93
6.2.3	Inhibition of Hh signalling between 14-15 and 22.5hpf directly results in a medial expansion of the early anterior otic factors <i>hmx2</i> and <i>hmx3a</i> by 22.5hpf	96
6.2.4	The ventromedial expansion of <i>hmx2</i> and <i>hmx3a</i> expression after inhibition of Hh signalling between 14-15 and 22.5hpf persists at 36hpf	101
6.2.5	Aberrant activation of Hh signalling does not lead to strong down-regulation of <i>hmx3a</i> by 14-16ss	103
6.2.6	Over-expression of <i>fgf3</i> leads to an initially broad expansion in expression of anterior transcription factors which gradually resolves to the anterior and posterior otic poles	105
6.2.7	Localisation and maintenance of <i>fgf</i> expression within anterior and posterior otic domains	109
6.2.8	Both <i>fgf3</i> or <i>fgf8a</i> have the ability, when over-expressed at 14hpf, to result in morphological duplications of anterior otic identity which is reduced by >18hpf	112
6.2.9	Inhibition of retinoic acid signalling weakly potentiates the early loss of Hedgehog signalling transcriptional phenotype in the ear	117
6.3	Discussion	121
6.4	Conclusions	124
7	Overall Discussion	125
7.1	Overview of Results	125
7.2	Early markers of the posterior otic domain; a role for Cdr2l in otic development? .	126
7.2.1	Dynamic expression of <i>cdr2l</i> across the early otic AP axis, reflective of maturation?	126
7.2.2	A role for otic Cdr2l in proliferation?	127
7.2.3	Does expression of <i>cdr2l</i> in other neural cell types provide an indication of a possible function?	128
7.3	Early integration of extra-otic signalling in defining the anterior and posterior otic domains during otic development	129
7.3.1	Are <i>hmx3a</i> and <i>hmx2</i> sufficient to assign posterior identity?	130
7.3.2	Is posterior otic identity duplicated after knock-down of <i>hmx3a</i> and <i>hmx2</i> ?	131
7.3.3	Insight into assignment of posterior otic identity in zebrafish	132
7.3.4	A new model for patterning of the otic AP axis in zebrafish	132
7.4	Future work	134

Chapter 1

Introduction

1.1 The zebrafish as a vertebrate model

The use of zebrafish as a vertebrate model has become increasingly popular over the last three decades. This is because the early development, along with a number of cell, tissue and organ characteristics, is strikingly conserved between zebrafish and other vertebrates and therefore can provide insight into the underlying mechanisms. The zebrafish model also has a number of other advantages over amniote models. The maintenance of large zebrafish stocks have low overheads compared to other vertebrate models and a high fecundity allows generation of high experimental numbers. Zebrafish are also oviparous with external fertilisation; this allows easy observation of development from the single cell stage. The rate at which zebrafish develop is also quicker than other model vertebrates, with embryos being responsive to contact by 24hpf and able to independently feed by 5 days post fertilisation (dpf) (Kimmel et al., 1995).

As well as being diploid, zebrafish are also highly amenable to genetic manipulation. This initially was exploited through forward mutagenesis screening techniques such as N-Ethyl-N-nitrosourea (ENU) mutagenesis and retroviral insertion. However, more recently due to increasingly comprehensive sequencing of the zebrafish genome, targeted reverse genetic techniques ranging from transient morpholino knock-down and TILLING mutagenesis to highly-precise CRISPR/Cas9-based genome editing have been exploited (reviewed in Huang et al. 2012 and Lawson 2016). This genetic tractability of zebrafish also allows fluorescent transgenics to be generated, which coupled with the early transparency of zebrafish embryos makes this a powerful tool for imaging (reviewed in Weber and Köster 2013).

A number of disease models have been established in zebrafish, including a number for deafness (reviewed in Lieschke and Currie 2007 and Whitfield 2002) (Section 1.6). Along with providing a better understanding of disease pathogenesis; these models, in conjunction with the advantages of the zebrafish model outlined above, provide an ideal system for the screening of chemical compounds for treatment (Murphey and Zon, 2006).

1.2 The function and structure of the inner ear

1.2.1 The vestibular system

The role of the inner ear in detecting different stimuli is reflected in its morphological and functional asymmetry around all three body axes. This is clearly seen in the highly conserved core structure for detection of vestibular stimuli. The vestibular system is, in part, comprised of three fluid-filled semicircular canals (SCCs) positioned orthogonally to each other, which gives the otic vesicle a labyrinthine structure. Each canal has an associated domain of sensory hair cells, the cristae, at their base within a widened region referred to as the ampulla. This allows the SCCs to detect angular acceleration along their respective axes through the movement of the canal and their respective crista, relative to the fluid within. Ventral to the SCCs are endolymph filled chambers containing the sensory epithelia of the utricular and saccular maculae. The position of these is largely conserved between vertebrates, with the utricle situated anterodorsal to the saccule (Figure 1.1). Unlike the cristae, both the utricular and saccular maculae are mounted by calcium-carbonate deposits known as otoliths or otoconia (Stooke-Vaughan et al., 2012). The attachment of the otoliths, initially to the tether cells and subsequently the kinocilia of the hair cell bundles, allows the utricle and saccule to detect linear acceleration and gravity through the movement of the kinocilia relative to the suspended otolith (Riley and Moorman, 2000). In fish and avians another otolithic sensory macula, the lagena, forms later during development (15dpf in zebrafish) branching off from the saccule. In some vertebrates, such as zebrafish, another non-otolithic macula, the neglecta, also forms later from the utricle (reviewed in Whitfield et al. 2002 and Wu et al. 1998).

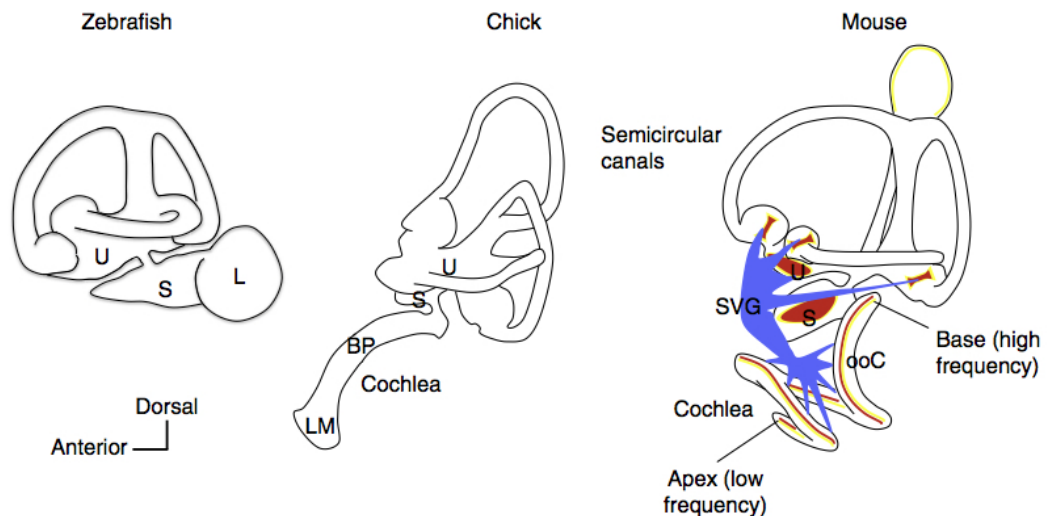


Figure 1.1: Schematic of the zebrafish, chick and mouse inner ear structure

Comparison of the inner ear structure of zebrafish, chick and mouse shows a highly conserved dorsal vestibular apparatus with a clear difference in the ventral domains associated with auditory perception. BP: Basilar Papilla, L: Lagena, LM: Lagenar macula, ooC: organ of Corti, SVG: Spiral and Vestibular Ganglion, U: Utricle. Sensory (red), neuronal (blue). Reproduced with kind permission from T. Whitfield *Current Opinion in Genetics & Development* 2015, 32:112–118.

The dorsally positioned endolymphatic sac and duct, which extends from the dorsomedial region of the ear, is another conserved structure within the vertebrate inner ear. This endolymphatic system regulates the endolymph, a unique ionic extra-cellular fluid, within the ear. The presence of endolymph is necessary during development of the otic vesicle for otolith formation, with a later role also in hair cell depolarisation and maintaining pressure within the labyrinth of the inner ear (Li et al., 2013; Abbas and Whitfield, 2009) and reviewed in Nin et al. 2016.

1.2.2 The auditory system

Whilst the vestibular system, which requires morphological asymmetry to function, retains a highly conserved function and morphology between vertebrates as discussed above, the auditory system shows a greater degree of variation between vertebrates (Figure 1.1). In teleosts such as zebrafish, the utricle is thought to primarily detect vestibular stimuli, whereas the saccule is thought to predominantly play a role in the detection of auditory stimuli (Lu and DeSmidt, 2013; Riley and Moorman, 2000; Popper and Fay, 1973). However, in chick and mouse auditory stimuli are detected by a specialised ventrally-located organ called the cochlear duct. The cochlear duct differs structurally and functionally between mammals and avians, with the auditory sensory epithelium in mammals being referred to as the organ of Corti compared to the basilar papilla in avians and reptiles. Despite their differences both are tonotopic, being organised along their length according to frequency sensitivity (reviewed in Alsina et al. 2009 and Whitfield 2015).

The variation in the auditory system is also reflected in the manner in which sound is conducted from the external environment to the auditory sensory epithelium. In mammals and avians, this is achieved through the ossicles, of which mammals have three but avians only one. These ossicles conduct the movements of the tympanic membrane of the outer ear in response to pressure waves to the respective auditory epithelium (Thompson et al., 2012; Zou et al., 2012). In adult zebrafish, due to the constraints of an aquatic environment, the initial detection of sound is thought to be primarily achieved through deflections of the inflated swim-bladder wall. These deflections are subsequently conducted to the sensory utricle and lagena of the inner ear via the Weberian ossicles; a structure unique to the otophysi series of teleosts (Popper and Fay, 1973; Bang et al., 2001). However, direct stimulation of the maculae by particle motion has also been observed in zebrafish and due to the swim-bladder only inflating around 4-5dpf, it is also likely to be the primary method of auditory detection in embryonic and larval zebrafish (Lu and DeSmidt, 2013).

1.3 Early development of the inner ear; the otic placode

1.3.1 The otic-epibranchial placodal domain

In all vertebrates the intricately structured inner ear is firstly specified as a cranial sensory placode. This simple thickening of non-neural ectoderm arises from the posterior domain of a horseshoe-shaped region of preplacodal ectoderm extending around the anterior edge of the neural plate (Figure 1.2A) (reviewed in Ladher 2016). The initial competence to form the preplacodal ectoderm in zebrafish is dependent on the expression of a self-regulating network of transcription factors, *tfap2a* and *tfap2c*, *foxi1* and *gata3*, which are induced within this ectodermal region early during gastrulation (~6hpf) primarily by members of the Bone Morphogenetic Protein (BMP) family, which are ventrally expressed within the ectoderm (Figure 1.2A-1) (Kwon et al., 2010; Bhat et al., 2013; Tucker et al., 2008; Dick et al., 2000). Whilst the requirement for TFAP2 in establishing the preplacodal ectoderm in mouse and chick is unreported, *Foxi3* and *Gata3* show similar expression in these vertebrates to *foxi1* and *gata3* in the zebrafish preplacodal ectoderm

and have been shown to be required in a comparable manner (Khatri and Groves, 2013; Ohyama and Groves, 2004; Khatri et al., 2014; Birol et al., 2016).

The expression of *tfap2a/c*, *foxi1* and *gata3* within the preplacodal ectoderm permits the expression of other transcription factors belonging to the *dlx*, *six*, *eya* to follow shortly, being expressed by the mid-gastrula stages (~ 8 hpf). This expression of the various *dlx*, *six*, *eya* transcription factors within this ectodermal domain are thought to further establish the preplacodal domain both in zebrafish and other vertebrates (reviewed in Ladher 2016). The Pax, Eya and Six transcription factors are thought to act in a network with another cofactor, Dach in the development of a number of placode-derived sensory structures in vertebrates (reviewed in Streit 2007). However, it is not clear if this network is acting during establishment of the preplacodal ectoderm (Hammond et al., 2002). The expression of the *six* and *eya* family members within the preplacodal ectoderm during its establishment has also been reported to be dependent on the attenuation of ventrolateral sources of BMP via the dorsal expression of BMP antagonists (Kwon et al., 2010; Wang et al., 2011; Yao et al., 2014). In zebrafish, the expression of such an antagonist, *cv2*, within the preplacodal ectoderm appears to be dependent on *dlx3b/4b* (Figure 1.2A-2) (Esterberg and Fritz, 2009). The preplacodal expression of the *six* and *eya* family members has also been shown to be weakly dependent on Fibroblast growth factor (Fgf) and Platelet-derived growth factor A (Pdgf) signalling in zebrafish, with Foxi1, Gata3 and Dlx3b/4b all appearing to regulate Fgf signalling within this region (Esterberg and Fritz, 2009; Yao et al., 2014; Kwon et al., 2010). A similar requirement for Fgf signalling in inducing expression within the preplacodal is also seen in chick and mouse (reviewed in Ladher 2016).

Adjacent to the preplacodal ectoderm, bordering the medially-positioned neural plate ectoderm, a domain of premigratory neural crest (NC) cells is also established mid-way through gastrulation (7-8hpf) (Figure 1.2A-2.) (Wang et al., 2011). These NC cells eventually migrate from this dorsal position and contribute to the cartilage within the head along with pigment, neuronal and glial cell lineages (reviewed in Knecht and Bronner-Fraser 2002). In zebrafish this border domain is established through the expression of a number of genes such as *foxd3*, *snai1b* and members of the *pax3/7*, *irx* and *zic* families are induced during gastrulation (reviewed in Simões-Costa and Bronner 2015). A number of genes expressed within the preplacodal ectoderm such as *tfap2a/c* and the members of the SoxE transcription family, *sox9a*, *sox9b* and *sox10*, also show overlapping expression within the neural crest domain (Figure 1.2A) (Dutton et al., 2009; Li and Cornell, 2007). The expression of these genes within this domain is thought to occur in a step-wise manner, responding to Wnt signalling emanating from the vegetal (posterior) marginal zone and an adjacent dorsoventral domain of ectoderm, as well as dorsal sources of Fgf signalling, low-levels of BMP signalling from the ventrolateral ectoderm and localised-Notch signalling (reviewed in Stuhlmeier and García-Castro 2012). Similar to the preplacodal ectoderm establishing this border domain is also likely dependent on regulation of BMP and Wnt signalling through the expression of their antagonists within this region (Stevenson et al., 2009; Wang et al., 2011). Establishment of this neural crest domain on the neural plate border via BMP, Wnt and Fgf is thought to be similar in chick and mouse (reviewed in Groves and LaBonne 2014).

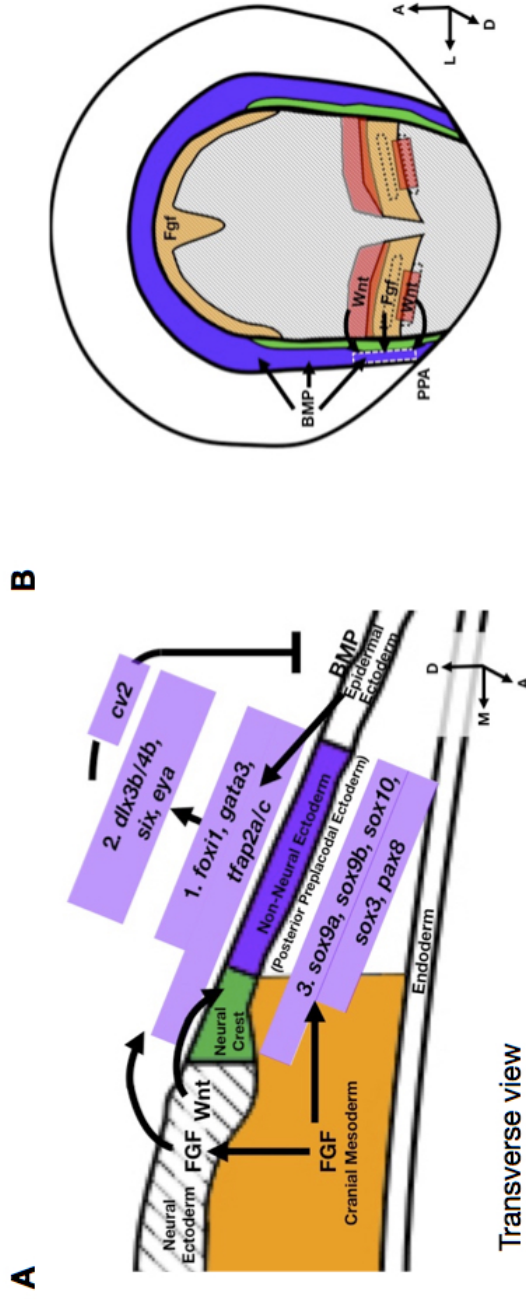
By mid-late gastrulation (~ 9 hpf), localised FGF signalling from the adjacent neural ectoderm of the presumptive mid-hindbrain boundary and rhombomere 4, along with Wnt8 signalling, which by late gastrula is expressed in a similar domain (Figure 1.2A-2.), induce expression of the paired-box transcription factor *pax8* within the preplacodal ectoderm (Lekven et al., 2001)(Phillips et al., 2004). This dorsolateral source of Fgf signalling is also required for expression of the SoxB1 family transcription factor *sox3* within a similar domain to *pax8* (Sun et al., 2007; Padanad and Riley,

2011). This expression of *pax8* and *sox3* within the posterior domain of preplacodal *foxi1* expression establishes an otic-epibranchial placodal domain (OEPD), which will give rise to both the otic and epibranchial tissues (Hans et al., 2004; Solomon et al., 2004, 2003; Lekven et al., 2001; Phillips et al., 2004). This localisation of FGF and Wnt within the neural ectoderm also subsequently leads to the progressive restriction of *foxi1* expression to this posterior domain at approximately 1ss (~10.5hpf) (Hans et al., 2013; Yao et al., 2014; Padanad et al., 2012). Expression of another preplacodal marker, *gata3*, also shows a later restriction to this region by 10ss (14hpf) (Bhat et al., 2013). The localisation of Fgf signalling adjacent to the OEPD also appears to be required for the persistent expression of *dlx3b* and *sox9a/b* within this domain in zebrafish (Liu et al., 2003).

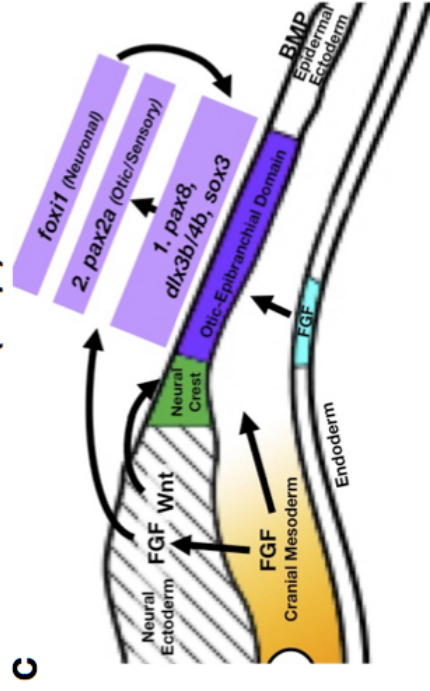
Shortly after the induction of *pax8* within the posterior preplacodal ectoderm, *Dlx3b* and *Dlx4b*, *Pax8* and Fgf signalling induce the expression of *pax2a* within this domain by 3ss (11hpf), with the broader expression of *foxi1* thought to specify a neuronal ground state for OEPD neuronal derivatives within this domain in zebrafish (Figure 1.2C) (Hans et al., 2013, 2004; Solomon et al., 2004). In chick, mouse and zebrafish, the dorsal source of Wnt signalling is then thought to maintain high expression of *pax2* within the dorso-medial region by 6ss (12hpf) to specify the otic placode with low Wnt signalling within the ventrolateral region leading to low *pax2* expression, specifying the epibranchial placode (Figure 1.2B) (Freter et al., 2008; McCarroll et al., 2012; Ohyama et al., 2006). In zebrafish, this medial domain of high *pax2a* expression, in combination with *pax8* further drives otic differentiation via a down-regulation of *Foxi1* (Padanad and Riley, 2011). A paralogue of *pax2a*, *pax2b* is also expressed within the domain of *pax8*, albeit slightly later than *pax2a* and has been suggested to act redundantly with *pax2a* (Mackereth et al., 2005). Later *pax2a* expression is restricted to the sensory structures of the maculae and cristae, likely dependent on *Dlx3b/4b*, with *pax8* expression being progressively lost from the otic tissue (Hans et al., 2013) (reviewed in Whitfield et al. 2002).

After the induction of *pax2a* expression within the OEPD (~11hpf), expression of *sox3* is progressively lost (~12hpf) from the future otic domain expressing *pax8* and high *pax2a*, resulting in a lateral domain of expression within the domain fated to become the developing epibranchial placodes (Figure 1.2). This maintenance of *sox3* within the lateral epibranchial domain of the zebrafish OEPD has been suggested to result from a balance of otic Fgf24 signalling and later lateral BMP signalling within this domain rather than reflecting otic specification through *Pax2a* (Sun et al., 2007; Padanad and Riley, 2011). From 10ss (14hpf) in zebrafish another member of the SoxB1 family, *sox2*, is also broadly expressed within a broad medial domain of the otic placode, later refining to the two sensory domains marking the sensory epithelia of the utricle and saccule and is required for maintenance and regeneration of the hair cells within these domains (Millimaki et al., 2010). A similar role for *Sox2* has also been reported in chick and mice (Neves et al., 2011; Kiernan et al., 2005).

Establishment of the Posterior Preplacodal Domain bud (10hpf)



Induction of the Otic-Epibranchial Domain 3ss (11hpf)



Segregation of the Otic-Epibranchial Domain 3-6ss (11-12hpf)

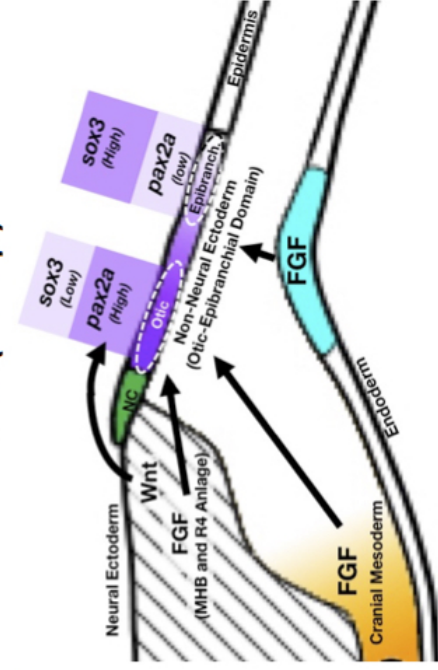


Figure 1.2: Establishment of the otic domain from the posterior preplacodal ectoderm
 (A) Definition of the non-neural ectoderm and the posterior preplacodal region by 10hpf (bud stage). (B) Dorsal view at 10hpf highlighting the signalling pathways acting to define the posterior preplacodal domain during late epiboly. (C) Induction of the otic-epibranchial domain with Pax2a establishing sensory fates and Foxr1 a neuronal ground state. (D) Segregation of the otic-epibranchial domain into a dorsal otic domain and a ventral epibranchial domain driven by high and low levels of *pax2a* expression respectively. Figures A, C and D are transverse view and Figure B is a dorsal view.

1.4 Patterning of the zebrafish otic placode across the anterior-posterior axis

Once established, the otic placode in fish progressively undergoes cavitation to form the otic vesicle, with the otic placode in aminotes invaginating to form an otocyst following an intermediate otic cup stage. However, before these morphological changes occur otic asymmetry across all three body-axes has been established. In zebrafish, asymmetry across the mediolateral (ML) axis of the otic placode is the first apparent with a ML gradient of *pax2a* expression in response to a hindbrain source of Wnt signalling, present at around 3ss (11hpf), as discussed above (McCarroll et al., 2012). This specification of the ML axis is quickly followed by the AP otic axis, which is reported to show anterior-localised expression of *hmx3a* from 4ss (11.5hpf) onwards (Feng and Xu, 2010). The dorsoventral (DV) axis appears to be specified later in zebrafish with *dlx3b* expression appearing dorsally localised from 14ss (16hpf) and *eya1* expression ventrally localised from 22ss (20hpf) onwards, both restricting from initially broad domains of expression (Sahly et al., 1999; Ekker et al., 1992) (reviewed in Whitfield and Hammond 2007).

A feature of the otic anterior-posterior axis is that it appears prone to adopt either the anterior or posterior character following perturbation early during its development with this being shown from as early as the 1930s in salamanders following rotation of the otic tissue and a similar result also being reported in chick more recently (Harrison, 1936; Wu et al., 1998). In zebrafish and xenopus, it has also been shown that duplications of the anterior-posterior axis can show mirror symmetry of both the anterior and posterior sensory structures and expression of normally localised genes (Waldman et al., 2007; Hammond et al., 2003; Hammond and Whitfield, 2011). These results support the importance of exogenous signalling pathways action on the early otic tissue in establishing anterior and posterior character across an initially equipotent tissue and also highlight the value of this system as a model for generally understanding the mechanisms involved in establishing asymmetry across tissues during development. Therefore both this project and the remainder of the introduction are focussed on the signalling events and character assignment occurring across the otic anterior-posterior axis.

1.4.1 Signals acting across the zebrafish otic anterior-posterior axis

Fibroblast growth factor (Fgf)

From late gastrulation until around prim-5 (24hpf) *fgf3* is strongly-expressed within rhombomere 4 (R4), which by the end of gastrulation is positioned anteriorly to the otic placode (Maves et al., 2002). This is also augmented by sources of Fgf3 present within the ventral mesoendoderm underlying the otic placode (McCarroll and Nechiporuk, 2013) (Figure 1.3). *Fgf8a* is also expressed strongly within the anlage of the mid-hindbrain boundary (MHB) and R4 during the induction of the otic placode, persisting within this domain until around 8ss (13hpf) after which it is primarily expressed within the anterior mid-hindbrain boundary (Maves et al., 2002).

Later, *fgf3* is also expressed within the zebrafish otic ectoderm in an anterior domain from 20-26ss (19-22hpf) (Millimaki et al., 2007) (Figure 1.3). From the 18ss (18hpf) *fgf8a* is also expressed within an anterior otic domain and later (prim-5, 24hpf) also shows weak and transient expression within a posterior otic domain (Figure 1.3) (Léger and Brand, 2002). A similar otic expression profile is seen with *fgf10a* being expressed in an anterior otic domain from 10-14ss (14-16hpf) onwards and later in a posterior domain (Figure 1.3) (McCarroll and Nechiporuk, 2013).

However, this posterior expression of *fgf10a* is not lost as with *fgf8a*, persisting to eventually be present within the posterior crista (Thisse and Thisse, 2004; Ma and Zhang, 2015).

Along with being required for establishing the otic placode (see Section 1.3), Fgf3 and 8a signalling both external to and within the otic tissue is also crucial for patterning the anterior domain of the otic placode in zebrafish. Perturbation of the hindbrain and the R4 domains of *fgf3* and *8a* expression resulting in corresponding changes in the expression of anterior and posterior markers within the otic tissue (Kwak et al., 2002b). Mutations or knock-down of either *fgf3* or *fgf8a*, despite having differences in their phenotypes, have both also been shown to lead to a reduction in expression of genes known to be required for normal development of the anterior sensory domains with loss of *fgf3* also having been shown to result in a partial loss of anterior sensory morphology (Léger and Brand, 2002; Hammond and Whitfield, 2011). This supports *fgf3* and *8a* having some redundancy in their ability to assign anterior otic character in zebrafish. This redundancy is further supported by inhibition of Fgf signalling using the pan-Fgf inhibitor, SU5402, which shows a stronger reduction in anterior otic character than loss of either *fgf3* or *fgf8a* individually (Léger and Brand, 2002; Hammond and Whitfield, 2011). Misexpression of either *fgf3* or *fgf8a* also emphasises the ability of both these Fgfs to duplicate anterior markers (Sweet et al., 2011; Hammond and Whitfield, 2011). Whilst *fgf10a* has also been suggested to play a role in patterning the anterior otic domain in zebrafish, its effect on this appears to be very weak (McCarroll and Nechiporuk, 2013).

Two other Fgfs, *fgf17* and *fgf24*, have also been reported to be expressed later within anterior and broadly posterior domains of the zebrafish otic placode respectively. However, neither has been reported to be associated with determining either anterior or posterior otic character (Reifers et al., 2000; Padanad and Riley, 2011; Draper et al., 2003).

Sonic hedgehog (Shh)

Induction of the posterior otic domain in zebrafish has been shown to be dependent on Sonic hedgehog a and b (Shh), signalling redundantly from the ventrally-position, midline structures of the floorplate and notochord (Figure 1.3) (Hammond et al., 2003). This ventral source of Shh signalling also appears to be important in influencing the dorsoventral (DV) axis of the zebrafish otic placode (Hammond et al., 2010). Expression of canonical read-out genes for Hedgehog signalling, *ptch1* and *ptch2* from >20ss reflect the ventral sources of Hh signalling, being expressed in a ventromedial otic domain. *Ptch2* is reported to be initially expressed across the AP axis at 15ss (16.5hpf), progressively strengthening in a domain midway along the AP length of the otic tissue and extending weakly into the posterior domain (Hammond et al., 2003). The lack of *ptch* expression within the anterior otic domain has been suggested to possibly reflect the combination of the anterior otic domain being further away from the midline structures and also roughly adjacent to the anterior limit of the notochord (Figure 1.3) (Hammond et al., 2003). However, *brachyury* mutants, which lack a differentiated notochord, do not show any defects in posterior otic morphology suggesting this is not the main factor (Hammond et al., 2003).

The data discussed above have led to a model for specification of the zebrafish otic anterior-posterior axis, whereby a gradient of Fgf signalling from the anterior hindbrain and anteroventral mesoendoderm is responsible for assigning anterior otic identity with Shh signalling across the length of the otic placode, originating from the ventral midline structures, assigning posterior identity (Hammond and Whitfield, 2011).

In patterning the otic AP axis, Fgf and Shh have been shown not to directly inhibit the signalling of the other, based on the expression of canonical Fgf and Shh signalling targets (Hammond and Whitfield, 2011). This infers that the difference in anterior and posterior identity is due to differential regulation of intrinsic otic gene expression by both of these pathways.

Retinoic acid (RA)

RA cannot be visualised directly due to it being a metabolite of vitamin A, therefore the expression of RA synthesising aldehyde dehydrogenase enzymes have been used in lieu as an indicator of sources of free RA within embryos. This use of aldehyde dehydrogenase expression as an indicator of RA within the embryo is supported by transgenic RA sensors, which appear to correlate with the expression domains of the aldehyde dehydrogenases (Mandal et al., 2014; Waxman and Yelon, 2011). In contrast, the expression of RA metabolising cytochrome p450 enzymes within various regions of the developing embryo are thought to represent sinks for free RA within the embryo and together with the aldehyde dehydrogenases create source-sink gradients of free-RA (White et al., 2007). Such a RA source-sink gradient has been proposed to be present across the otic domain, with a domain of *aldehyde dehydrogenase 1 family, member A2 (aldh1a2)* expression in a ventrolateral domain, posterior to the otic placode in zebrafish from 16hpf (14ss) onwards and an anterior medial domains of the cytochrome p450 enzyme, *cyp26c1* expression present later at around 22hpf (Figure 1.3) (Maier and Whitfield, 2014). Later, from 22ss (20hpf), as the posterior expression of *aldh1a2* becomes weaker another aldehyde dehydrogenase, *aldh1a3* is expressed within the anterior otic tissue (Figure 1.3) (Maier and Whitfield, 2014).

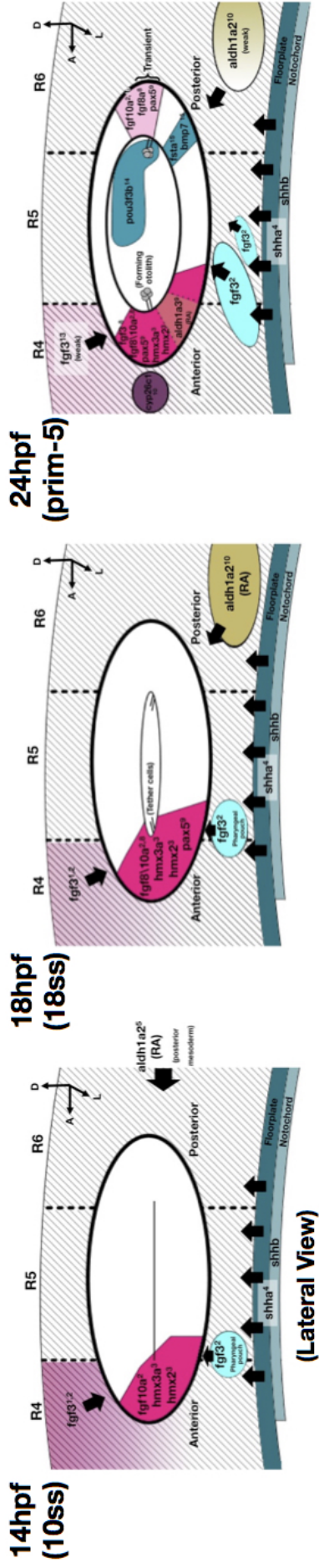
In zebrafish, RA signalling is involved in patterning the hindbrain during gastrulation (Hans and Westerfield, 2007). However, it has not been reported to directly affect the development of the anterior-posterior character of the otic tissue, instead having a clear role in regulating the balance between the anterior sensory and neurogenic domains relative to the posterior non-neurogenic domain along the ventral otic edge (Figure 1.3) (Radosevic et al., 2011; Maier and Whitfield, 2014).

Wnt and Bone morphogenetic proteins (BMP)

At the time during which the developing otic placode is thought to be patterned in zebrafish (>11hpf), a number of Wnt family members are expressed in the dorsal hindbrain adjacent to the otic placode. *Wnt1, 3a, 7a, 7b* and 10b, all appear in the hindbrain posterior to the otic placode by 16ss (14hpf) with *wnt8b*, which at late gastrula stages is present along with *wnt8a* in a domain of neuroepithelium adjacent to the OEPD (Section 1.3), showing restricted expression within R3 and R5 by 14ss (16hpf) (Beretta et al., 2011; Lecaudey et al., 2007; Buckles et al., 2004; Lekven et al., 2003, 2001; Kelly et al., 1995).

Misexpression of *wnt8a* in zebrafish, as well as altering the size of the OEPD due to its role in establishing this domain as discussed in Section 1.3, can lead to changes in the expression of *fgf3* and *fgf8a* within the hindbrain (Phillips et al., 2004). Such changes in hindbrain patterning can indirectly alter the anterior-posterior patterning of the otic vesicle (Lecaudey et al., 2007). However, the otic vesicle in such embryos has been reported to develop normally (Kelly et al., 1995).

Anterior-Posterior Identity



Sensory, Neurogenic and Non-neurogenic Domains

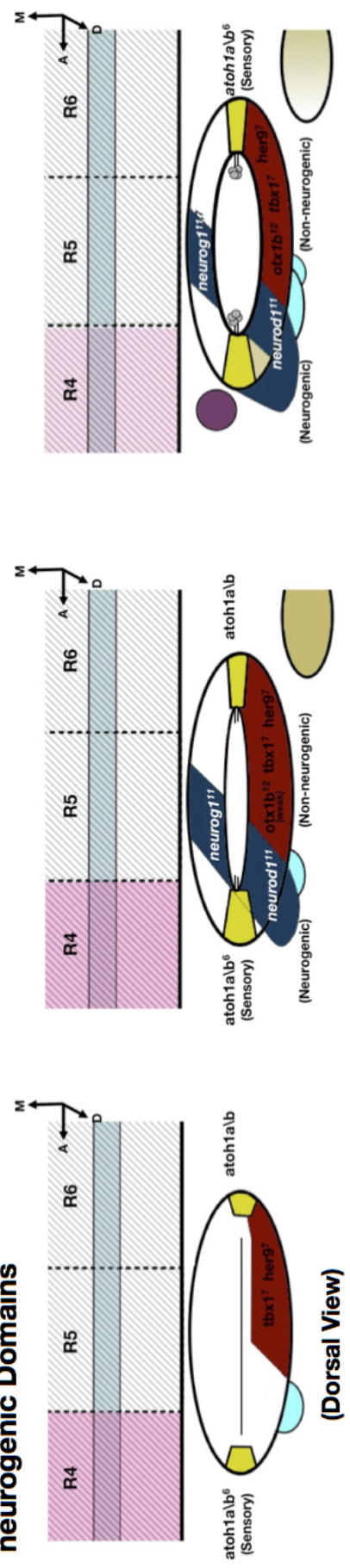


Figure 1.3: Development across the anterior-posterior axis of the zebrafish otic placode from 14-24hpf

Anatomy, signalling pathways and genes patterning the anterior-posterior axis of the otic tissue between 10ss (14hpf) and prim-5 (24hpf). The top row of lateral figures shows the assignment of anterior and posterior character whereas the bottom row of dorsal figures shows the defining of the neurogenic and non-neurogenic domains. Sources of exogenous signalling pathway components acting on the otic placode are consistent between figure rows. All figures are with anterior to the left.

1= Nechiporuk et al. 2007, 2= McCarroll and Nechiporuk 2013, 3= Feng and Xu 2010, 4= Hammond et al. 2003, 5= Grandel et al. 2002, 6= Millimaki et al. 2007, 7= Radosevic et al. 2011, 8= Léger and Brand 2002, 9= Kwak et al. 2006, 10= Maier and Whitfield 2014, 11= Andermann et al. 2002, 12= Mercier et al. 1995, 13= Walshe and Mason 2003, 14= Maulding et al. 2014, 15= Mowbray et al. 2001 and 16= Thisse and Thisse 2004

Other Wnt family members are also unlike to directly influence otic anterior-posterior patterning, with knock-down of *wnt8b* alone, as well as knock-down of *wnt3a* in a *wnt10a* mutant background, not being reported to result in changes in otic AP patterning or morphology in zebrafish (Buckles et al., 2004; Hans and Westerfield, 2007). This is supported by inhibition of canonical Wnt signalling through misexpression of the Wnt antagonist, *dkk1* (Phillips et al., 2004; Kawano and Kypta, 2003). This misexpression of *dkk1* results in otic vesicles with a smaller but seemingly normal morphology, as highlighted by the otolith position. Whilst these various alterations in Wnt signalling may have subtle or unobserved effects on the transcription of markers of otic anterior-posterior character, overall it appears that despite the presence of these numerous Wnt sources close to the otic placode, Wnt signalling does not appear to be directly patterning the otic anterior-posterior axis.

BMP signalling, despite being important in establishing the otic domain (see Section 1.3) has not been implicated in patterning the anterior-posterior axis of the developing zebrafish ear. Bmp ligands do show localised expression within the zebrafish otic tissue with *bmp2b* expressed in a dorsal domain that extends posteriorly and *bmp7* expressed within a ventral posterior domain (Figure 1.3). Other mediators of the BMP pathway also show localised expression within both the anterior and posterior lateral domains. However, all these components are expressed >22 ss (20hpf), after the period over which anterior and posterior otic character are thought to be assigned (Mowbray et al., 2001). Bmp2b and Bmp7 also are reported to be involved in patterning events other than AP patterning, with Bmp2a being required for development of all three canals and Bmp7 implicated in mediating neurogenic differentiation in response to Tfap2a (Kantarci et al., 2015; Hammond et al., 2009).

1.4.2 Transcriptional differences across the anterior-posterior otic axis

The medial otic domain

Early transcriptional differences across the AP axis in response to extrinsic sources of Fgf and Shh localised across the early otic AP axis are crucial in defining anterior and posterior otic identity, which manifest as morphological differences within the anterior and posterior domains as development progresses (Figure 1.4). Expression of such markers associated with developing anterior and posterior otic character is primarily within a more medial domain of the otic tissue in zebrafish from which the sensory maculae form and marked by an initially ($<$ prim-5, 24hpf) broad domain of *pax2a* (Riley et al., 1999).

The earliest localised expression across the anterior-posterior axis of this medial domain is that of the homeobox H6 family transcription factor *hmx3a* (previously *nkx5.1*) from 4ss (11.5hpf) onwards. *Hmx3a* is expressed within a ventromedial anterior domain and is shortly followed by expression of another Hmx family member, *hmx2* (previously *nkx5.2*) at 10-12ss (14-15hpf) within the same region, which has been reported to act redundantly with Hmx3a in specifying anterior otic character (Figures 1.3 and 1.4) (Feng and Xu, 2010). The anterior and posterior semi-circular canals also later form on the edge of this medial domain of *hmx2* and *hmx3a* expression in zebrafish, although interestingly knock-down of both does not lead to a loss of these structures possibly due to redundancy with other Hmx family members (Feng and Xu, 2010). Hmx3a and Hmx2, along with extrinsic Fgf signalling also maintain the later onset of *pax5* expression (16ss, 17hpf) within the same otic domain (Figures 1.3 and 1.4) (Feng and Xu, 2010). In zebrafish, Pax5 is required for maintaining anterior sensory hair cells later in development (prim-5 onwards, 24hpf). However, this does not appear to be through regulation of the other anterior otic markers and a similar requirement for *pax5* in maintaining hair cells has not been reported in other vertebrate models

(Kwak et al., 2006). *Hmx3a* and *Hmx2* have also been shown to be required for expression of *fgf3*, *fgf8a* and *fgf10a* within this anterior otic domain (Feng and Xu, 2010). These Fgfs are progressively expressed within this otic domain, with *fgf10a* first seen at 10ss (14hpf) and *fgf8a*, followed by *fgf3*, expressed later (Section 1.4.1, Figures 1.3 and 1.4) (Léger and Brand, 2002; McCarroll and Nechiporuk, 2013).

The presence of *fgf3*, *8a* and possibly *fgf10a* within the anterior otic domain also likely reflects a feedback loop acting within this domain to reinforce and maintain anterior otic character. This is supported by data showing that in zebrafish loss of *fgf3* or *fgf8a* leads to the reduction/loss of the anterior otic markers, *hmx2*, *hmx3a* and *pax5*, of which *hmx2*, *hmx3a* are required for maintaining expression of these Fgfs within the anterior domain (Kwak et al., 2006; Feng and Xu, 2010; Léger and Brand, 2002). Conversely misexpression of either *fgf3* or *fgf8a* also leads to a posterior expansion of these anterior otic markers (Sweet et al., 2011; Hammond and Whitfield, 2011). Interestingly, it has also been reported that two of the anterior otic markers, *pax5* and *fgf8a*, show transient expression within the posterior otic domain around 24hpf (Figure 1.3) (Léger and Brand, 2002; Kwak et al., 2006). However, no suggestion as to what this might be reflecting has been made.

Duplications of the anterior markers, *pax5* and *fgf8a*, have also been reported in the *sox10* (previously *colourless*, *cls*) mutants, although interestingly without any corresponding anteriorisation of the posterior macula morphology (Dutton et al., 2009). The reason for this is unclear, especially given *sox10* appears uniformly expressed across the otic anterior-posterior axis past prim-5 (24hpf) (Dutton et al., 2001).

Within the posteromedial otic domain in zebrafish, the earliest published markers are *pou3f3b* (previously *zp23*); a POU class homeobox transcription factor, *bmp7* and *follistatin A* (*fsta*); a glycoprotein, which is a canonical antagonist of BMP (Hauptmann and Gerster, 2000). All three are reported to be expressed within this otic domain from prim-5 (24hpf) (Figures 1.3 and 1.4) (Dutton et al., 2009; Kwak et al., 2006; Mowbray et al., 2001). Whilst the functions of *Pou3f3b*, *BMP7* and *Fsta* in regulating posterior otic character are unknown, both *pou3f3b* and *fsta* appear to reflect changes in posterior otic character. This is based on the observation that their posterior expression is lost in response to misexpression of *fgf3* with *fsta* also being expressed within the anterior domain after inhibition of Fgf signalling (Kwak et al., 2002a; Hammond and Whitfield, 2011). However, given the progressive restriction in the otic placode to duplicate anterior identity within the posterior domain between 14-20hpf, prior to the reported onset of these posterior markers, it is highly likely that a response from other earlier targets of Hh within this domain are needed to establish posterior otic character.

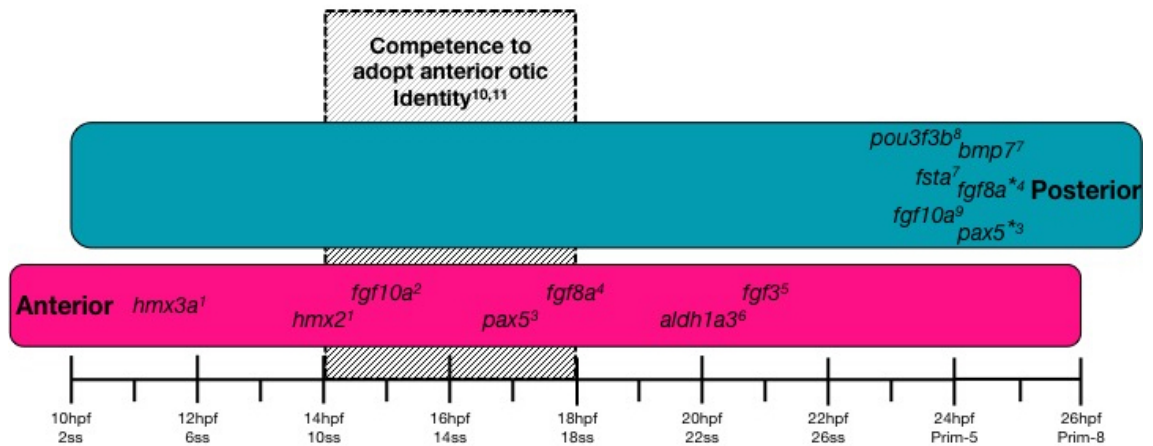


Figure 1.4: Timing vs asymmetric gene expression within the otic medial domain
Onset of expression either within the medial anterior (pink) or posterior (blue) domains for genes associated with developing otic character.

1= Feng and Xu 2010, 2= McCarroll and Nechiporuk 2013, 3= Kwak et al. 2006, 4= Léger and Brand 2002, 5= Millimaki et al. 2007, 6= Maier and Whitfield 2014, 7= Mowbray et al. 2001, 8= Maulding et al. 2014, 9= Thisse and Thisse 2004, 10= Hammond et al. 2003, 11= Hammond and Whitfield 2011. Asterisks highlight transcripts that are only transiently present within the posterior.

The lateral otic domain

Similar to the medial otic domain, the ventrolateral otic domain also shows early asymmetric gene expression across the anterior-posterior axis (Figure 1.3, bottom row). However, this asymmetry rather than reflecting differences in anterior and posterior otic character represents the early segregation of an anterior neurogenic domain from which neuroblasts will delaminate to form the statoacoustic ganglion and a posterior non-neurogenic domain from which the ventral pillar of the lateral canal will later form.

An early marker within this ventrolateral domain is the transcription factor *tbx1*, which is expressed posteriorly within this domain from 10ss (14hpf) (Figure 1.3). In zebrafish, *tbx1* has been shown to define this region as non-neurogenic through its induction of the bHLH proneural antagonist *her9*. The induction of *her9* within this posterior region is then thought to limit the expression of the proneural *neurod1* to a defined anterior neurogenic domain, later also marked by *neurog1*, that establishes a population of delaminating neuroblasts that migrate anteriorly to establish the statoacoustic ganglion (Radosevic et al., 2011). Within the mid-region of the ventrolateral domain marked by *tbx1*, the transcription factor *otx1b* is also expressed from 18hpf (Figure 1.3). Expression of *otx1b* within this region is dependent on Tbx1 and whilst Otx1b has been suggested to also act in limiting the extent of the adjacent neurogenic domain, it is also required for formation of the ventral pillar from this epithelium around which the lateral semicircular canal forms (Whitfield et al., 1996a; Maier and Whitfield, 2014; Hammond and Whitfield, 2006).

Other later (>28hpf) markers of this lateral domain in zebrafish are *hmx1* and *hmx4* (previously *SOHo*). Both of these are reported to also show expression within the anterior statoacoustic ganglion and later the anterior and posterior cristae but their functions in zebrafish otic development are currently unknown (Feng and Xu, 2010).

The initial expression of *tbx1* within this posterolateral domain is dependent on early posterior RA signalling, likely resulting from *aldh1a2* expression within the somitic mesoderm posterior to the otic placode and later within a ventrolateral domain closer to the otic placode (Figure 1.3) (Grandel et al., 2002; Mandal et al., 2014). Unlike the markers of the posterior medial domain, *tbx1* expression within the posterior lateral otic placode appears inhibited by Shh signalling prior to 18ss (18hpf) from the ventral midline structures, which has been suggested to limit expression of *tbx1* to the lateral otic domain (Radosevic et al., 2011). Similarly, expression of *tbx1* and *otx1b* are reported to be upregulated by Fgf signalling rather than inhibited, as seen with markers of the posterior medial domain (Maier and Whitfield, 2014). Interestingly, Fgf also positively regulates the anterior sensory and neurogenic domains with *neurod1* showing a duplicated domain of expression adjacent to the posterior otic vesicle after misexpression of *fgf3* (Hammond and Whitfield, 2011). However, the establishment of the lateral neurogenic domain doesn't appear to be directly linked to anterior otic character as a similar duplication of *neurod1* is not seen after inhibition of Hh signalling during the period over which the otic anterior-posterior axis is thought to be specified (Radosevic et al., 2011).

Anterior Fgf signalling has also been reported to induce expression of RA-producing *aldh1a3* within an anterior domain between the sensory and neurogenic domain from 22ss (20hpf) onwards (Figure 1.3). This anterior source of otic RA has been proposed to further balance the maturation of the delaminating neuroblasts from the neurogenic domain and the anterior limit of the posteriorly situated non-neurogenic domain (Maier and Whitfield, 2014).

1.4.3 Competence of the otic placode to adopt anterior-posterior identity

A key feature of the developing zebrafish ear and why it represents a good model for understanding patterning across the otic anterior-posterior axis in vertebrates is its ability to duplicate either anterior or posterior otic character. This has been clearly shown by Hammond et al. in response to manipulation of either Fgf or Shh signalling (Hammond et al., 2003; Hammond and Whitfield, 2009, 2011). However, the duplication response seen after changes in either Fgf or Shh signalling appears to be dependent on the temporal and spatial competence of the otic tissue to respond, as discussed below. Different alterations of Fgf or Hh signalling also result in varying degrees of change in either anterior or posterior otic character highlighting that both the competence of the otic tissue to respond and the signalling environment are important for determining the ultimate duplication phenotype observed (Maier and Whitfield, 2014; Hammond et al., 2010; Hammond and Whitfield, 2011; Léger and Brand, 2002).

Temporal

The equipotent nature of the zebrafish otic placode to duplicate anterior otic character in response to misexpression of *fgf3* is reported to be restricted to a period of early otic development. Duplication of the anterior otic morphology and expression of anterior markers is observed after heat-shocks from the 10ss (14hpf), with the ability of the otic tissue to produce such duplicated morphology appearing to be progressively lost by the 16ss (17hpf) (Hammond and Whitfield, 2011). Misexpression of *fgf8a* from the 10ss (14hpf) in zebrafish has also been shown to produce an anterior duplication but this has only been reported in the expression of anterior markers rather than the otic morphology (Sweet et al., 2011). A similar progressive loss of competence to duplicate anterior otic character is seen in ears treated with the Hh signalling inhibitor, cyclopamine. Here treatment prior to 15ss (16.5hpf) is reported to show a strong duplication of anterior morphology but similar treatments at later time points results in progressively less extreme duplication phenotypes

(Hammond et al., 2010).

Intriguingly, the morphological duplication of posterior otic character seen in the ears of *ptch1;2* mutants, where Hh signalling is constitutively activated, can be rescued by treatment with the Hh signalling inhibitor cyclopamine from the 17ss (17.5hpf) (Hammond et al., 2010). This suggests that the anterior otic domain is still competent to respond to changes in to the signalling environment at this later time point.

Spatial

Another interesting characteristic of these axial duplications is seen when these are generated through misexpression of *fgf3*, pan-Fgf inhibition by SU5402, constitutive activation of Hh signalling by inhibition of PKA inhibition or injection of Shh RNA. Rather than resulting in the expression of markers associated with either anterior or posterior otic character across the entire AP axis of the otic tissue, as might be expected given the loss of AP-localised positional information, under these conditions certain AP markers are reported to display discrete domains of expression duplicated at either end of the AP axis by prim-15 (30hpf) (Figure 1.5A) (Hammond et al., 2010; Hammond and Whitfield, 2011; Hammond et al., 2003). This suggests that only certain regions of the otic tissue are competent to maintain a transcriptional response following the previously mentioned changes in signalling. A similar response is also observed in the sensory maculae under similar duplicating conditions. In these duplicated maculae the morphology and hair cell polarity, which has distinct regional directionality associated with the anterior and posterior maculae, appears mirrored around the AP axis rather than showing two patches with identical/expanded directional polarity or with no polarity altogether (Figure 1.5B) (Hammond et al., 2003; Hammond and Whitfield, 2011).

The mirrored response observed could reflect the duplication of either an otic extrinsic or intrinsic organiser in response to changes in Fgf or Hh that establishes the localisation of the duplicated domains of expression and maculae morphology at either end of the otic AP axis and also influences the polarity of the hair cells. Whilst hindbrain sources of Fgf signalling have been shown to be important for establishing the anterior domain of markers, patterning of the hindbrain is reported to appear normal in SU5402-treated and double *ptch1;2* mutants with only a slight expansion of rhombomere 5 observed after misexpression of *fgf3* (Lecaudey et al., 2007; Hammond and Whitfield, 2011; Kwak et al., 2002a). This suggests that a duplication of a hindbrain signalling source is unlikely under these duplicating conditions. However, changes in ventral signalling sources such as the epibranchial endoderm could be occurring but there is currently no evidence reported to support any such changes.

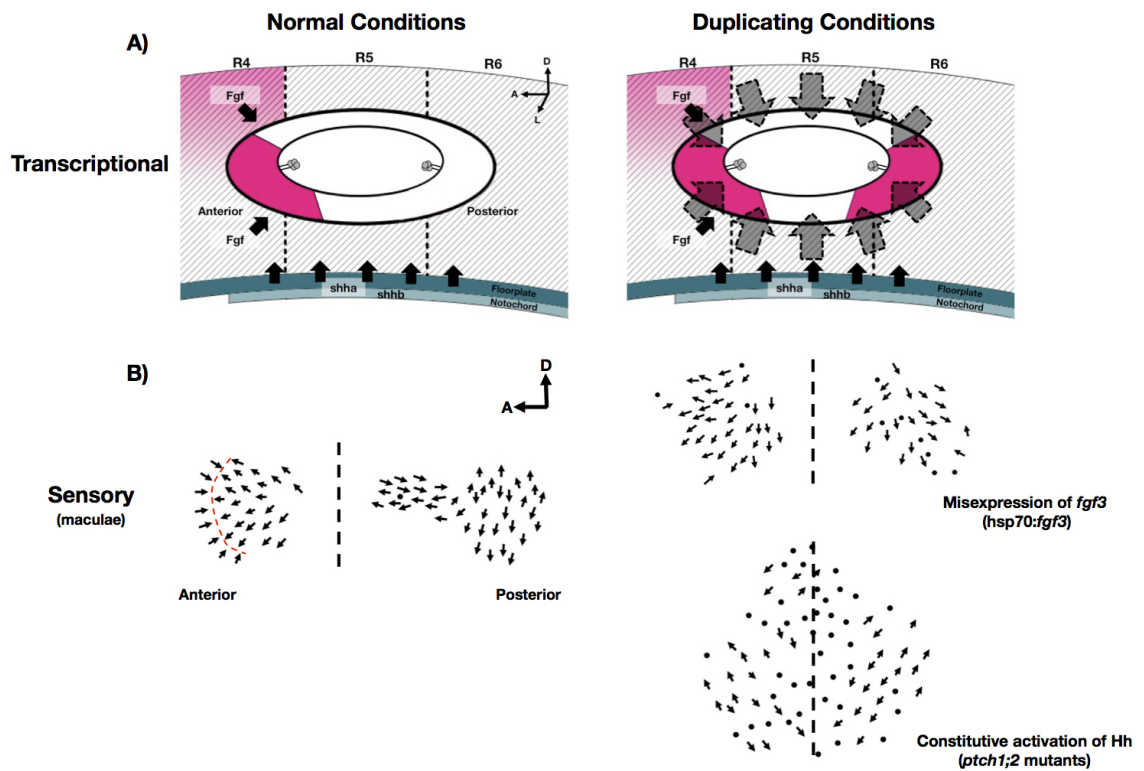


Figure 1.5: Transcriptional and sensory maculae phenotypes seen under conditions that duplicate the otic AP axis.

Phenotypes seen in the A) transcriptional response or B) the sensory maculae after manipulation of either the Fgf or Hh signalling pathways, where positional information is lost either transiently or persistently. In B) the top duplicated hair cell polarity diagram reflects an anterior duplication after misexpression of *fgf3*, whereas the bottom diagram reflects a posterior duplication due to constitutive activation of Hh signalling in *ptch1;2* mutants. Dotted lines are to highlight symmetry around the AP axis and black dots are where the directional polarity could not be determined.

The red line in the normal polarity map in B) represents the stereotypical anterior line of polarity reversal along the AP axis. Polarity diagrams in B are based on those from Hammond and Whitfield 2011; Hammond et al. 2010. All diagrams are from a lateral perspective with the anterior to the left.

Another model has been proposed by Hammond et al., where by extrinsic Fgf and Shh signals induce anterior and posterior character onto an established pre-pattern already present across the otic placode, which establishes organising centres at either pole within the otic tissue (Hammond and Whitfield, 2011). Two potential candidates for establishing such a pre-pattern are the proneural genes, *atoh1b* and *atoh1a*. In the zebrafish otic placode, *atoh1b* is thought to initially specify the tether cells around which the utricle and saccule sensory epithelia form through subsequent rounds of hair cell specification, dependent on *atoh1a*. Both *atoh1b* and *atoh1a* show AP pole-localised expression by 10ss (14hpf), the time from which the otic anterior-posterior axis appears susceptible to changes in patterning, resolving from an initially broad domain of expression (Millimaki et al., 2007). The early segregation of *atoh1b* and *atoh1a* into these two domains appears unaffected by inhibition of either Fgf or Hh signalling, despite these conditions later resulting in fused maculae (Millimaki et al., 2007; Sapède and Pujades, 2010; Hammond and Whitfield, 2011; Hammond et al., 2010).

However, expansion of these *atoh1b/atoh1a* expressing sensory domains after the >18ss (18hpf) does appear positively regulated by Fgf signalling in zebrafish with Notch signalling possibly acting as a negative regulator of such expansion (Millimaki et al., 2007; Sweet et al., 2011).

The misexpression of *atoh1a* can also lead to a posterior expansion of *fgf3* and *fgf8a*, as well as the anterior markers *hmx3a* and *pax5* along the medial otic domain (Sweet et al., 2011). This is despite knock-down of *atoh1a/b* not leading to an obvious decrease in anterior otic expression of anterior markers such as *fgf3* and *fgf8a* by prim-5 (24hpf), possibly reflecting the influence of external Fgf signalling on maintaining this anterior expression (Millimaki et al., 2007; Léger and Brand, 2002; Hammond and Whitfield, 2011; Lecaudey et al., 2007). Therefore, such a feedback loop between the pre-patterned *Atoh1a/b* and the anterior otic markers could reflect why expression of anterior markers after misexpression of *fgf3* are maintained in these discrete domains rather than across the otic tissue (Figure 1.6A).

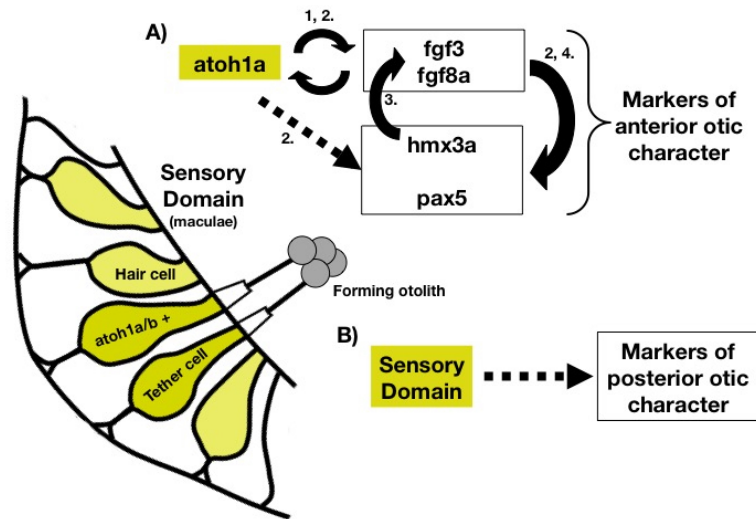


Figure 1.6: Possible mechanism by which an *Atoh1a*/sensory domain pre-pattern might result in localised transcription within the AP poles of the zebrafish otic vesicle

A) A proposed localised feedback loop between *Atoh1a* present within the sensory domains localised at either end of the OV, even under duplicating conditions, and factors known to be involved with establishing anterior otic identity. The dotted line indicates that *Atoh1a* may not be directly regulating *pax5* and *hmx3a* as these are known to be downstream of Fgf signalling within the otic tissue. B) Whilst no evidence has yet been reported for a regulatory link between *Atoh1a* and markers of posterior otic character, the localised sensory domain may still act to regulate these markers.

1= Millimaki et al. 2007, 2= Sweet et al. 2011, 3= Feng and Xu 2010 and 4= Hammond and Whitfield 2011.

For posterior duplications, the posterior marker *fstb* is the only marker reported to show discrete duplicate domains of expression within the otic tissue and only under certain conditions (Hammond et al., 2010, 2003). It is also not clear whether *Atoh1a* or *b* plays any regulatory role with any of the markers of posterior character and localised Hh signalling has not been reported within the otic tissue either during normal development or under duplicating conditions.

This does not mean that there is not a regulatory relationship between the posterior markers and the sensory epithelium expressing *atoh1a* or *b*, which would support the pre-pattern model mentioned above but further work is required to confirm this (Figure 1.6B).

The mechanism by which the polarity of the hair cells in relation to one another within the sensory maculae of the ear are defined in vertebrates is still poorly understood but it is clearly possible to alter this polarity in zebrafish using the duplicating changes in Fgf and Hh signalling mentioned above (reviewed in Sienknecht 2015). However, there must be another level of organisation to ensure that given the loss of positional information from extrinsic sources of signalling, the hair cells of the duplicated patches rather than becoming disorganised show a mirrored symmetry (Figure 1.5B).

In the zebrafish lateral line, which also has directionally polarised hair cells, the polarity of these hair cells has been reported to be influenced by both the Notch and planar cell polarity (PCP) intercellular pathways (Mirkovic et al., 2012). The PCP pathway has also been linked to determining hair cell polarity in the chick and mouse cochlea (Davies et al., 2005; Tarchini et al., 2016; Piast et al., 2005). As a loss of Notch signalling is not reported to clearly perturb the directional polarity of the hair cells within the sensory maculae of the zebrafish ear, the PCP pathway may play a role in determining this (Haddon et al., 2000). The direction of polarity produced through the cell-cell interactions in PCP, whilst having a level of self-patterning can also be biased by external cues such as non-canonical Wnt and possibly Hh signalling (Goodrich and Strutt, 2011; Aw and Devenport, 2016). Therefore, this could represent a mechanism by which changes in signalling cues could also influence the polarity of the hair cells within the otic sensory epithelia. It has also been suggested that the directional polarity of hair cells within regions of the maculae are dependent on asymmetric expression of certain genes such as *emx2* in vertebrates, including zebrafish, which might influence downstream effectors of the PCP pathway (Jiang et al., 2017). Such modifiers of the PCP pathway could also represent another point at which external signals could influence determination of hair cell polarity. However, a clear role for the PCP pathway in specifying hair cell directional polarity in the maculae of the zebrafish ear has not yet been reported and the signalling environment that could be influencing the directional polarity of the hair cells within the maculae of the otic tissue through a different mechanism. It is also unclear as to which signalling sources could produce such symmetry around the AP axis.

1.5 Patterning of the chick and mouse otocyst along the anterior-posterior axis

Early otic patterning in both chick and mouse shows a high degree of similarity in the signalling pathways and transcriptional responses observed across the otic axes to those in zebrafish (reviewed in Whitfield and Hammond 2007 and Groves and Fekete 2012). However, the manner in which these signals and transcriptional responses regulate patterning across the three axes in the chick and mouse ear show some differences when compared to zebrafish, as discussed below.

During otic development in zebrafish, Fgf signalling has been shown to have a clear role in establishing anterior otic character with transcriptional and morphological duplications observed in the medial region of the ear following changes in the Fgf signalling environment (see Section 1.4). Yet a similar role for Fgf signalling in anterior-posterior patterning during the otic development of mouse and chick is less clear, despite the similar localisation of *Fgf* expression within the hindbrain and underlying mesoderm adjacent to the developing otic placode in all three model vertebrates (Alvarez et al., 2003; Alsina et al., 2004; Schimmang, 2007). In mice, it is thought that rather than acting to specify the anterior-posterior axis as in zebrafish, Fgf signalling primarily patterns the dorsal domain of the dorsoventral otic axis with loss of dorsal markers common to both mice and zebrafish such as *Dlx5* and *Gbx2* observed in the mouse *Fgf3* mutants (Hatch et al., 2007; Whitfield and Hammond, 2007; Solomon et al., 2003). Fgf signalling during chick otic development is similarly thought to primarily pattern the dorsoventral otic axis. However, there is less direct evidence for this role and it is in part based on the observation that the dorsal semi-circular canals (SCCs) are truncated following alterations to the hindbrain, where *Fgf3* and *Fgf19* are expressed, and a concomitant removal of the ventral midline structures (Liang et al., 2010).

In all three vertebrate models, localised expression of Fgf10 within the three sensory cristae has also been reported (Sánchez-Guardado et al., 2013; Pauley et al., 2003; Thisse and Thisse, 2004). This may represent a possibly conserved role for Fgfs in DV otic patterning, as whilst it has not been observed in zebrafish, in both chick and mouse the localised expression of *Fgf10* has been shown to be required for regulating development of the associated, dorsally-derived, SCCs (Pauley et al., 2003; Chang et al., 2004). Interestingly, localised expression of Fgfs are also seen within another otic sensory epithelium, the maculae. In all three vertebrate models mentioned, persistent expression of certain Fgf family members within the presumptive maculae have been reported. *Fgf* expression within the maculae does not appear to be restricted to just the anterior utricle or posterior saccule, with *Fgf* expression reported in both, which may suggest a possible conserved requirement for Fgf signalling in developing both maculae (Olaya-Sánchez et al., 2016; Pauley et al., 2003; Thisse and Thisse, 2004).

Shh signalling in zebrafish has been well documented as being crucial for establishing posterior otic character across the the anterior-posterior otic axis in zebrafish (see Section 1.4). Hh signalling in mouse and chick has been not been reported to play a similar role in defining the posterior otic character but instead has been implicated in opposing the dorsalisating activity of Fgf, defining the ventral auditory structures (Hatch et al., 2007; Bok et al., 2005; Riccomagno et al., 2002). The dorsoventral gradient of Hh signalling from the midline structures in chick and mice has been suggested to be reflected by a proposed gradient of the Hh transcriptional effector Gli3 Activator (Gli3A), which with an opposing gradient of Gli3 Repressor (Gli3R) has been suggested to specify differing otic fates across the DV axis in chick and mice (Bok et al., 2007b; Ohta et al., 2016).

In both mouse and chick, reduction of Hh signalling results supports such a model with loss of the ventral cochlear duct with a concomitant ventral expansion of common dorsal markers such as *Dlx5* and *Hmx3* observed. Selective loss of Hh within the mouse otocyst also shows the maculae and cristae to be unaltered suggesting that, unlike in zebrafish, Hh signalling is not required for patterning these sensory epithelia (Brown and Epstein, 2011). Despite this seemingly different role for Hh in the otic patterning of zebrafish and the other vertebrate models, the role of Hh signalling in dorsoventral patterning may reflect a common function between zebrafish, chick and mouse. Hammond et al. reported that in zebrafish, aberrant Hh signalling as well as producing a duplication of posterior otic character resulted in severely ventralised ears, which showed a loss of the dorsal endolymphatic duct and SSC structures (Hammond et al., 2010). This suggests a consistent ventralising role for Hh signalling in zebrafish, mouse and chick. It is also interesting to note that Hh signalling in all three vertebrates models appears to be associated with specification of the sensory domains that primarily detect auditory stimuli, with Hh signalling also thought to regulate the tonotopic gradient of the cochlea and basilar papilla in mouse and chick, respectively (Son et al., 2015; Popper and Fay, 1973).

Another seemingly striking difference between the specification of the anterior-posterior axis in the vertebrate models discussed is the suggestion that an anterior to posterior gradient of RA across the mouse and chick otocyst, similar to that proposed to be present across the zebrafish placode, is primarily responsible for patterning the AP axis (see Section 1.4) (Bok et al., 2011; Niederreither et al., 1997; Fujii et al., 1997). This is based on the ability of transient application of exogenous RA to produce a morphological duplication of the posterior SSC and the associate crista in chick, although these embryos also lose all other otic sensory epithelia. However, a similar transient application of exogenous RA also resulted in a transcriptional duplication of the posterior ventrolateral marker *Tbx1*, as well as a loss of the anterior neurogenic domain markers, *Lunatic Fringe (Lfng)* and *Neurod1* in both mouse and chick (Bok et al., 2011). This is consistent with the role of RA in zebrafish in regulating the extent of the posterolateral non-neurogenic and anterolateral neurogenic domains in the developing zebrafish ear, which are also marked by *tbx1* and *neurod1*, respectively (see Section 1.4.2). The anterior neurogenic domain in chick and mouse, unlike zebrafish, also have expression of *Fgf10* and *Fgf3*, respectively, which have both been shown to expand in *Tbx1* mutants but appearing reduced after treatment with high levels of RA (Raft et al., 2004; Cadot et al., 2012). This therefore supports RA in zebrafish, chick and mouse acting in a well conserved network for regulating the neurogenic versus non-neurogenic domains along the AP axis of the ventrolateral domain rather than patterning the sensory AP axis. Whilst the loss of the maculae in chick embryos following RA exposure makes it hard to observed any changes to the patterning of the sensory epithelium, mouse mutants for the RA-synthesising enzyme, *Raldh3* are not reported to show any morphological changes in the maculae (Romand et al., 2013).

It is not clear why the chick ear appears more sensitive to RA, given no morphological duplications of the posterior semicircular canal have been reported in zebrafish or mice in response to elevated RA, it could reflect different sensitivities of the downstream effectors such as *tbx1* to RA as zebrafish *tbx1* show a complete loss SSC formation and fused maculae, highlighting its importance in patterning otic morphology (Maier and Whitfield, 2014; Cadot et al., 2012; Whitfield et al., 1996b)

In zebrafish, expression of *hmx3a* and *hmx2* represent the earliest markers induced in the anterior otic placode in response to Fgf signalling. However, by 48hpf both also show two patches of dorsal expression at either end of the ear with *hmx3a* also showing a patch of expression within a dorsomedial domain (Feng and Xu, 2010; Hammond and Whitfield, 2011). *Hmx3* in chick along with *Hmx2* and *Hmx3* in mouse, initially show a similar early anteromedial localisation within the otocyst (from HH10 and E9.5, respectively) before later appearing to be primarily localised to the dorsal otic domain (Wang et al., 1998, 2001; Herbrand et al., 1998).

Loss of *Hmx2* and *Hmx3* in mice leads to vestibular defects with a loss of the SCCs consistent with their putative role as markers of the dorsal otic epithelium. However, loss of either *Hmx3* alone or both *Hmx2* and *Hmx3* in mice also leads to a reduction or loss of the sensory utricle and saccule with a merging of the two chambers, suggesting *Hmx2* and *Hmx3* may have an effect on sensory AP patterning (Wang et al., 1998, 2001, 2004). Whilst knock-down of *hmx2* and *hmx3a* in zebrafish is not reported to result in a similar loss of the SCCs, the maculae appear merged with a loss of anterior hair cell polarity, similar to the phenotype observed in the mouse knock-outs (Feng and Xu, 2010). Whilst loss of *Hmx2* and *Hmx3* have not been studied in chick, the similarity between the mouse knock-out and zebrafish knock-down phenotypes could indicate a conserved function for *Hmx2* and *Hmx3* in otic patterning in vertebrates.

Despite the similarity in the expression of *Hmx2* and *Hmx3* observed between model vertebrates and a similar negative regulation by Hh signalling, albeit observed across different axes, in both chick and mice Fgf signalling appears to negatively regulate expression of *Hmx3* in contrast to zebrafish where Fgf signalling has been shown to positively regulate otic *hmx3a* expression (Naidoo et al., 2014; Hatch et al., 2007; Hammond and Whitfield, 2011; Freter et al., 2008). Slight differences in regulation of otic transcription factors such as these could reflect why changes in Fgf and Hh signalling do not result in a similar changes to the sensory otic tissue in these vertebrates, as discussed above.

Another well-used, reliable marker of anterior character in zebrafish is *pax5*, which is required with maintaining hair cells within the utricular macula (Kwak et al., 2006). In chick, *Pax5* has been also been identified as being expressed within the sensory domains of the ear in a transcriptional profiling but its function has not been directly assessed (Kwak et al., 2006). In contrast to zebrafish and chick, *Pax5* is reportedly not expressed or necessary for otic development in mice, indicating *Pax5* likely does not have a strongly conserved role in otic development (Bouchard et al., 2010).

The two markers of zebrafish posterior otic character often used, *follistatin* (*fsta*) and *pou3f3b* do not have any documented expression or function within the developing chick or mouse otocyst making it hard to identify any conserved role in establishing the early posterior otic domain across vertebrates.

1.6 Congenital hearing loss

The importance of patterning during the development of the inner ear is highlighted by a number of congenital human syndromes with associated hearing and balance dysfunction. Many of these have been identified as having underlying mutations in genes associated with a conserved function in specifying domains of the ear during early development in vertebrates such as zebrafish, chick and mouse, such as those discussed above (Table 1.1) (Whitfield, 2002). This has meant that zebrafish models for many of these diseases have been established either through reverse or forward genetics approaches.

Due to the genetic tractability of zebrafish, this model system is ideal for generating such models and testing the genetics underlying these diseases. The use of zebrafish as disease models also has many other benefits such as their upkeep being low, having a short developmental time period, their reproduction being oviparous with high fecundity. These advantages also make it possible to screen therapeutic approaches in a high-throughput manner. However, the use of zebrafish as disease models also has its drawbacks with zebrafish being more highly diverged from humans than other vertebrate models. They also have many differences in their physiology and anatomy as well as having duplication of many genes due to genome duplication (reviewed in Ali et al. 2011).

Human Syndrome	Gene(s) effected	Prevalence	Zebrafish model
DeGeorge Syndrome (22q11 Deletion Syndrome)	<i>TBX1</i>	1:4000 (NHS)	Piotrowski et al., 2003
10q25/6 Syndrome	<i>Possibly; HMX3, HMX2 and FGFR2</i>	unknown/low (NORD)	None currently
Branchial Oto Renal Syndrome	<i>EYA1</i>	1:40,000 (NORD)	Kozlowski et al., 2005
Waardenburg-Shah syndrome	<i>SOX10</i>	1:42,000. 2–5% of all congenitally deaf persons* (Song et al., 2016)	Dutton et al., 2009
Waardenburg syndrome type IIA; Tietz Albinism – Deafness syndrome	<i>MITF</i>		<i>Possibly;</i> Lister et al., 1999
* For Waardenburg syndrome as a whole			

Table 1.1: Congenital human syndromes associated with hearing and balance loss

The table list congenital human hearing and balance syndromes that have a causative mutation in genes known to be involved in early patterning of the vertebrate inner ear.

1.7 Aims and objectives

The aim of this project was to develop a better model to account for how relatively simple directional cues from extrinsic signalling sources acting across the early otic AP axis are integrated into the highly dynamic expression seen within the early otic placode, with a focus on the establishment of the posterior otic domain.

1.7.1 Aims

- Identify novel markers of the posterior otic domain.
- Place any novel posterior markers identified within the current model for patterning of the otic AP axis based on their expression and function.
- Build upon the current model for AP patterning across the zebrafish otic placode proposed by Hammond et al. by identifying how Fgf and Hh signalling pathways are integrated to pattern the already known markers of the anterior and posterior domains.

1.7.2 Objectives

- Initially identify markers which show restricted expression to the posterior domain over the period in which the AP axis are thought to be specified (14-20hpf). This will be approached in two ways;
 - A search of expression pattern data using the ZFIN database
 - Analysis of the transcriptome for differential gene expression in early (<18hpf) otic tissue with posterior character.
- Characterise the expression of any candidate early posterior markers and interrogate these under AP duplicating conditions.
- Disrupt the function of any candidate early posterior markers through knock-down or gene editing techniques to identify any role in defining AP otic identity.
- Integrate this expression and any function with the current model for defining the AP otic axis in zebrafish.
- Study the early response of known otic markers to changes in Fgf and Hh signalling.
- Identify mechanisms by which their expression of otic markers may be localised to either pole.
- Fit the early integration of Fgf and Hh signalling with the previous model and any new early posterior otic markers identified.

Chapter 2

Materials and Methods

2.1 Materials

Water

All water used was ultrapure water, which had been purified using a Synergy Water Purification System with a DNase/RNase filter from Merck Millipore.

Chemicals

All chemicals used were analytical grade or equivalent and purchased from Sigma Aldrich, VWR International or Fluka, unless stated otherwise.

2.2 Methods

2.2.1 Zebrafish husbandry

Zebrafish care

Adult fish were kept in circulating water, maintained at 28.5°C with a 14 hour light/10 hour dark cycle. All experiments were carried out according to Home Office regulations on use of animals in scientific research under the project licence; 40/3655 and personal licence; ID1586BAB.

Embryo collection

Fish were setup either as pairs in single containers which have a mesh bottom over a collection tank and removable partition to allow mating to be timed or marbled as a whole tank, with a container containing marbles and a mesh bottom placed over a collection tank within the main tank to allow spawning from the onset of the light cycle. Embryos were collected in system water and incubated at 28.5°C before being sorted into E3 medium (5mM NaCl, 0.17mM KCl, 0.33mM CaCl₂, 0.33mM MgSO₄) with methylene blue, again at 28.5°C.

Embryo staging

Embryos were staged according to Kimmel et al., 1995 (Kimmel et al., 1995). If needed, embryo development was slowed by placing embryos at 22.5°C after the 70% epiboly stage.

2.2.2 Zebrafish lines

All wild-type fish used were from the AB line as maintained in the University of Sheffield Aquaria.

Transgenic and mutant lines used during the project;

Transgenic/Mutant	Reference	Homozygote Identifier
<i>fgf8a</i> ^{ti282a} (previously <i>ace</i>)	Reifers et al., 1998	Clear loss of cerebellum (Reifers et al., 1998)
<i>fgf3</i> ^{t21142} (previously <i>lia</i>)	Herzog et al., 2004	Small otic vesicle and PCR (see table, Hammond and Whitfield., 2011)
<i>fgf10a</i> ^{tbvbo} (previously <i>dae</i>)	Norton et al., 2005	PCR (see table, Norton et al., 2005)
Tg(<i>hs:fgf3</i>)	Lecaudey et al., 2008	Oedema after heat shock and GFP Mres heart marker
Tg(<i>hs:fgf8a</i>) ^{x17}	Millimaki et al., 2010	Oedema after heat shock
<i>smo</i> ^{hi1640}	Chen et al., 2001	U-shaped somites that lack a horizontal myoseptum and a ventrally curved body, also PCR (see table, Chen et al., 2001)
<i>ptch1</i> ^{tj222} ; <i>ptch2</i> ^{hu1602}	Koudjis et al., 2008	Flattened somites and PCR (see table, Koudjis et al., 2008)
<i>mib1</i> ^{ta52b}	Itoh et al., 2003	Indistinct posterior somites at 22-somite stage and PCR (Zhang et al., 2007)
TgBAC(<i>sp7:kaede</i>)	Generated during the project	eCFP CryA lens marker
<i>cdr2l</i> ^{4bp Del}	Generated during the project	PCR (see table)
<i>cdr2l</i> ^{5bp InDel}	Generated during the project	PCR (see table)

Table 2.1

2.2.3 Microscopy

All lateral images are orientated with the anterior to the left and dorsal images with the anterior at the top.

Brightfield, DIC and Epifluorescence microscopy

Live and fixed embryos were generally imaged using an Olympus BX-51 compound microscope, which has brightfield, DIC and epifluorescence optics, with CellB image acquisition software. For fluorescent imaging requiring large fields of view, a Zeiss Zoom V16 fluorescence stereo microscope with Zen acquisition software was used. FIJI (Fiji Is Just ImageJ) (Schindelin et al., 2012) was used for all image processing.

Confocal microscopy

Fluorescently stained embryos were imaged on a Nikon TIRF A1 using NIS Elements for image acquisition. Again FIJI was used for image processing.

2.2.4 PCR

Primers

All primers for PCR amplification were purchased from IDT (Integrated DNA Technologies). Primers were re-suspended in MQH₂O to give a 100 μ M stock concentration and diluted to a working concentration of 10 μ M. Both were stored at -20°C.

PCR Reactions

PCR reactions were assembled in PCR tubes or 96 well plates whilst on ice. Two polymerases were utilised; for genotyping, 2x Taq Reddymix (ThermoFisher) and for cloning or PCR template synthesis, the high-fidelity polymerase, Q5 (NEB). The reactions were set up as recommended by the manufacturer. The annealing temperatures used for 2x Taq Reddymix reactions were generally 5°C below the melting temperature (T_m) of the primers and for Q5 reactions the NEB T_m calculator (<http://tmcalculator.neb.com>) was used (although usually approximately 3°C above the T_m).

2.2.5 Injection

Glass injection needles were prepared by placing glass capillaries into to a needle puller (Sutter Instrument Company) which produced needles with a tip of specified length/thickness. Needle tips were broken using forceps under a dissection scope and filament capillary needles (Harvard Apparatus) filled through capillary action (for morpholinos) with non-filament capillary needles (Harvard Apparatus) filled using microloader tips (Eppendorf) (for RNA and construct injection). The injection needle was then attached to a PV800 Pneumatic microinjector (Precision Instruments) with the settings adjusted until the droplet size of the desired volume was achieved, injecting into mineral oil over a graticule.

For injection a fresh glass slide was placed in a petri dish lid and washed with distilled H₂O to support the embryos. Once embryos were collected, those identified as being healthy and fertilised at the one-cell stage were transferred to the edge of the glass slide and the solution injected into the yolk as close to the cell as possible.

2.2.6 Morpholino (MO) knockdown

Morpholino oligos are comprised of nucleic acid base with a modified morpholine ring and phosphorodiamidate backbone which sterically block binding of endogenous RNA (Summerton, 1999). MO were purchased from and designed by Gene Tools LLC with the *cdr2l* MO designed against the mRNA NM205564.1 transcriptional start site (see Table 2.2). The *cdr2l* MO was re-suspended in MQH₂O to give a stock concentration of 1mM and was initially stored at room temperature in a parafilm-wrapped glass vial, as recommended by Gene Tools LLC. However in the later stages of the project due to concerns over evaporation the MO was aliquoted out and stored at -20C. The non-specific control (CD63 mismatch) MO was kindly provided by Dr S.Greaves and kept at -20C throughout.

Prior to injection, aliquots of the MO were thawed and heated to 65°C for 5-10 minutes to ensure the MO was in solution before being cooled at room temperature.

MO name	Activity	Sequence (5'-3')
Cdr2l ATG MO	Translation blocker	cggtgcggttttcggttttaacggc
Control MO (Non-specific CD63 Mismatch)	None	tttcctgctgcttatacagcgatg

Table 2.2: Morpholino oligos

2.2.7 *cdr2l*:eGFP construct injection

A DNA construct encoding enhanced Green Fluorescent Protein (eGFP) fused 3', via a Glu-Phe linker, to the coding sequence (CDS) of *cdr2l* along with its upstream Kozak sequence and the *cdr2l* ATG MO binding site was synthesised (Figure 2.1). To achieve this, the eGFP CDS and *cdr2l* CDS were amplified via a Q5 PCR with the same restriction sites attached 3' and 5' to the primers and restriction site complementary to the multiple cloning site in the vector backbone at the alternate ends to allow ligation of the two sequences together and then into the plasmid backbone. These PCR products were purified and then used in a double restriction digest before being ligated together with ExpressLink T4 ligase (ThermoFisher) over-night. Once confirmed that the PCR products had ligated together, the DNA construct was ligated with linearised pCS2+, a plasmid designed for *in vivo* expression with a cytomegalovirus (CMV) promoter regulatory region 5' to the multiple cloning site to drive constitutive expression and a 3' polyA sequence. This construct was then transformed into DH5a (NEB) competent cells and successful transformants were selected and grown up in a Carbenicillin (50µg/mL) LB preparation over-night before being spun down and the plasmid isolated (Qiagen). The construct was injected at a concentration of 150ng/µL.

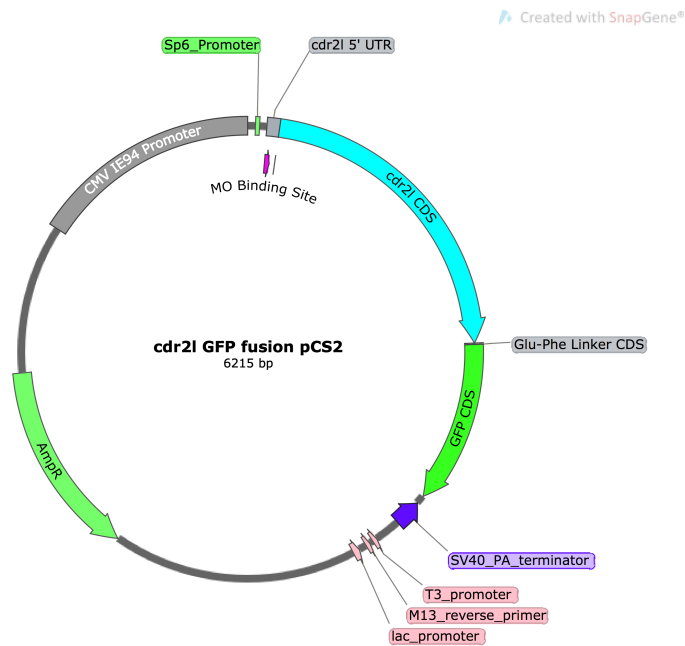


Figure 2.1: *cdr2l*:eGFP construct map

2.2.8 CRISPR Mutagenesis

Oligo design

The CRISPR system is derived from the prokaryotic Clustered, Regularly Interspaced, Short Palindromic Repeats (CRISPR)/Cas9 system. For genomic editing in zebrafish a method based on Hruscha et al, 2013 was used (Hruscha et al., 2013). Here a guide RNA (gRNA) is designed with a 20bp targeting sequence that binds adjacently to a genomic trinucleotide, 5'-NGG-3', proto-spacer adjacent motif (PAM). This targeting sequence is fused to a 5' scaffold sequence and *In vivo* this gRNA forms a tertiary RNA structure that binds to a Cas9 nuclease and can induce double stranded-breaks approximately 3bp 5' of the PAM sequence with subsequent non-homologous end joining (NHEJ) resulting in small insertions or deletions.

For this project a 20bp targeting sequence adjacent to a PAM within the genomic sequence of *cdr2l* (NC 007114.6) was designed utilising the Zhang lab CRISPR design tool (<http://crispr.mit.edu>). This targeting sequence was chosen due to its early position within the second exon of *cdr2l* and because it covers an AluI restriction site located 3bp 5' of the PAM site to allow for genotyping. The targeting sequence should also ideally be designed to have a 5' GG dinucleotide adjacent to the T7 binding site for optimal transcription (Gagnon et al., 2014). However for this project a 5'GC dinucleotide was used due to a limited availability of ideal early sites within the *cdr2l* sequence.

An antisense oligo ultramer with a gRNA scaffold sequence 5' of the target primer sequence and a T7 binding sequence 3' (see Table 2.3) for *in vitro* transcription was subsequently ordered from IDT (<https://eu.idtdna.com>).

	<i>cdr2l</i> exon 2 target sequence	5'-gctccttattgcgctccagc-3'
ss	antisense gRNA scaffold/Target (X)/T7 oligo	5'-aaagcaccgactcggcgccacttttcaagttgataacggactagcctattttaacttgctatttctagctctaaaacxxxxxxxxxxxxxxxxxxxxxxxxctatagtgagtcgtattacgc-3'

Table 2.3: CRISPR oligo design

gRNA Synthesis

The oligo ultramer was suspended to 100 μ M and 5 μ moles of this was annealed to 5 μ moles of a T7 primer in the reaction; 1.5 μ L 100 μ M oligo, 1.5 μ L 100 μ M T7 in 27 μ L linker buffer (linker buffer: 50 mM Tris-HCl pH 8, 100 mM NaCl, 1 mM EDTA). This mixture was incubated for 5 minutes at 95°C before being cooled slowly (to allow annealing) at room temperature for 5 hours. Transcription was carried out using a MEGAshortscript T7 kit (Life Technologies) with the 20 μ L reaction containing;

Component	Volume (μ L) [0.5ex]
Buffer	2 μ L
ATP	2 μ L
CTP	2 μ L
GTP	2 μ L
UTP	2 μ L
Enzyme mix	2 μ L
Annealed oligo	1 μ L
Nuclease-free H ₂ O	7 μ L

Table 2.4: MEGAshortscript T7 gRNA transcription reaction

The reaction was incubated for 2 h at 37°C with 1 μ L of TURBO DNase then added and the reaction incubated for a further 15 min at 37°C. 115 μ L of nuclease-free water and 15 μ L of ammonium acetate stop solution were then added and the reaction transferred to an RNase-free Eppendorf tube where 2 volumes (300 μ L) of ethanol were added and the reaction incubated for >15 min at -20°C to precipitate the RNA. After the -20°C incubation the reaction was centrifuged at 4°C for 15 min at max speed. The supernatant was then removed carefully and the pellet resuspended in 20 μ L MQH₂O, being stored at -80°C.

gRNA/Cas9 protein injection

An injection solution of 400ng/ μ L gRNA, 1 μ g/ μ L of Cas9 protein (kindly provided by Dr H Isaacs) and 0.5 μ L of phenol red was made up to 4.5 μ L in RNase-free H₂O with 1nL injected per embryo. For the *cdr2l* exon 2 CRISPR, embryos from an AB incross were injected. Prior to loading, the solution was kept on dry ice and the loaded injection solution and needle were replaced hourly to ensure protein activity.

2.2.9 Recombineering

Recombineering is based on homologous recombination allowing targeting constructs with homologous "arms" (HA) of sequence to be integrated into bacterial artificial chromosomes (BACs)

utilising bacteriophage-encoded homologous recombination functions. In this project this technique was used to place the photo-convertible protein Kaede within the sequence of *sp7*, a gene expressed within the otic vesicle at an early developmental stage (DeLaurier et al., 2010) contained in BAC CH73-243G6, along with iTol2 transposase long-terminal repeats for subsequent embryo transgenesis.

BAC preparation

BAC CH73-243G6 was ordered from the CHORI BACPAC resource (<http://bacpac.chori.org/>), with the DH10B cells grown out on LB agar chloramphenicol (Cm, 12.5 μ g/mL) plates. Four colonies were then selected and used to setup four 50mL LB chloramphenicol over-night preps. These were subsequently checked for the presence of the *sp7* CDS via PCR and the remaining culture spun down, with the pellet being frozen at -20°C. The pellet for one of the colony preps was then used with a Nucleobond Xtra midi kit (Macherey-Nagel) to isolate the BAC which was resuspended in 15 μ L 1/10th TE with MQH₂O and left over-night at 4°C.

Targeting DNA

Two ultramer oligos were used; one was designed using primer-BLAST (www.ncbi.nlm.nih.gov/tools/primer-blast/) with 20bp of homology to the 5' the Kaede CDS and 60bp of homology to exon 2 of the *sp7* coding sequence. The second ultramer, was previously designed by Delaurier et al, with homology to a more 3' region of the CDS and 3' domain of the pCRII backbone. The pCRII backbone to which these two primers have homology contains the Kaede CDS along with a selectable KanR cassette flanked by Flippase (Flp) *frt* recognition sites (See Table 2.5).

Oligo ultramer	Sequence
L(5') HA <i>sp7</i> exon 2 Kaede	5'-aacactgcaattactctttaaattcttctcaggaggaaacac gttatggatccagtcctcatgagctctgattaaccagaaatga-3'
R(3') HA <i>sp7</i> exon 2 pCRII	5'-ttttaatagggatggtgcttcccggttaccagggtgtggcagaa tctcggactggactggcccgagtgatggata-3'

Table 2.5: *Sp7* exon 2/kaede *frt*:kanR:*frt* targeting oligos

Using the above oligos at a working concentration of 10 μ M, a Q5 (NEB) 100 μ L reaction, split into 5x20 μ L aliquots, was setup (see Table 2.6).

Component	Volume (μ L)
Kaede <i>frt</i> :KanR: <i>frt</i> pCRII plasmid	Variable (200ng)
Q5 Buffer	20 μ L
dNTPS	4 μ L
L(5') HA primer	5 μ L
R(3') HA primer	5 μ L
Q5 polymerase	1 μ L
Annealed oligo	1 μ L
MQH ₂ O	up to 100 μ L

Table 2.6: Targeting DNA PCR

The reactions were pooled and 2 μ L of DpnI (Promega) added at 37°C for 1 hour to remove the plasmid DNA. The whole reaction was then run on a 1.5% SYBRsafe (ThermoFisher) electrophore-

sis gel before the bands were isolated on a safe imager light box (ThermoFisher) and purified with a gel extraction kit (Qiagen) being eluted into 30 μ L of MQH₂O.

EL250 BAC transformation

For recombineering, electro-competent cells that contain temperature-sensitive recombination proteins and an arabinose-inducible flpe gene are required. Therefore the EL250 strain of E coli were used (Lee et al., 2001) and transformed with the CH73-243G6 BAC prior to recombineering, as outlined below.

A culture of EL250 cells was grown from a glycerol stock in no-salt LB to an OD600 of 0.4 to 0.7 and subsequently washed and pelleted. A pellet was then resuspended in 44 μ L of ice cold sterile water and 300ng in 6 μ L of resuspended BAC added. This was transferred to an ice-cold gene pulse cuvette (Biorad) and electroporated at 25 μ F, 1.3kV and 200 Ohms (MicroPulser, Biorad). Immediately after electroporation, 1ml of SOC (NEB) was added and the suspension transferred to a capped round-bottom falcon tube (Fisher Scientific) before being incubated at 32°C for 90 minutes at 250 rpm. After incubation, 0.2 mL were plated onto five Cm (12.5 μ g/mL) plates and grown at 32°C over-night. The following day five colonies were picked and were individually resuspended for use in a 3mL over-night no-salt chloramphenicol LB prep grown at 32°C and a diagnostic PCR alongside a non-electroporated EL250 control.

Once confirmed to contain the BAC, a 3ml prep was subsequently used to setup a 20mL no-salt chloramphenicol LB prep for electroporation with the targeting construct. This was incubated at 32°C until the culture reached an OD600 of approximately 0.6 (<4 hours) with 10mL of this then transferred to a pre-warmed glass flask in a shaking (200rpm), 42°C water bath for 15 mins to induce the recombination enzymes.

kaede frt:kanR:frt / BAC recombineering

In the cold room, 10mL of the EL250/BAC prep was then aliquoted into 5 x 2mL pre-chilled eppendorf tubes and spun briefly with the media then removed and 1mL of ice-cold MQH₂O added to first two tubes. The 1mL re-suspensions were then added to the next two tubes and resuspended before being washed, as previously, and added to the final tube. This final tube was resuspended in 2mL before being washed, twice and placed in a new pre-chilled eppendorf tube, which was then spun down and resuspended with 300ng of the *sp7* exon 2/kaede frt:kanR:frt targeting construct amplicon targeting construct in a 50 μ L total volume of ice cold water. This suspension was transferred to an ice cold cuvette and electroporated at 1.8kV with 1ml of SOC added immediately afterwards and the suspension transferred to a capped round-bottom falcon tube before being incubated at 32°C for 90 minutes at 250 rpm.

After incubation, 0.2 mL were plated onto five Cm (12.5 μ g/mL) plates and grown at 32°C over-night. Five colonies were picked and on Kan (10ug/ml) plates were re-streaked and dotted along with being dotted on ampicillin (Amp, 50 μ g/mL) and Cm (12.5 μ g/mL) plates, before being grown at 32°C. The desired colonies will be Cm and Kan resistant but Amp sensitive with any Amp resistance due to contaminating template plasmid not destroyed by Dpn1. From a plate streaked with a CmR, KanR and AmpS identified colony, a 3mL Kan (50 μ g/mL) culture was setup and grown over-night at 32°C. To remove the KanR cassette from the kaede frt:kanR:frt sequence inserted into the *sp7*-containing BAC, 0.4ml of the Kan over-night prep were added to total 20 mL of Cm (12.5 μ g/mL) containing LB and and grown to OD600 of 0.6 at 32°C. Once at the required density, 0.2mL of 10% L-arabinose was added to the 20mL prep, which was then incubated at

32°C to induce the FLP recombinase and remove the Kan selection cassette. A 1:10 dilution of the 20mL prep in LB with Cm (12.5µg/mL) was then setup and grown for 1h at 32°C. 5 plates were either spread or streaked with 200µL of this dilution and grown overnight at 32°C. The following day three post-FLP colonies were suspended in MQH₂O and spread/dotted on Cm and Kan plates, respectively being grown overnight at 32°C. From these plates, one CmR / KanS colony was selected and grown up at 32°C in a 100ml LB Cm culture, subsequently being spun down as 50ml aliquots and frozen.

iTol2 / BAC recombineering

To help create a stable genomic insertion iTol2, medaka transposase recognition sites were placed into the post-FLP kaede-containing BAC. Primers with HA for the BAC backbone (pTARBAC2.1) were used to amplify a targeting DNA with iTol2 sites flanking both a KanR cassette (pCR8GW backbone) (see Table 2.7) and a *crya* promoter driving eCFP. Both the HA primers and the construct containing the iTol2 and *crya*:eCFP sequence were a gift from M.Tomekca (Roehl lab). The targeting DNA PCR was then setup as before in Table 2.6, digested with DpnI and the product purified through gel extraction (Qiagen).

Oligo ultramer	Sequence
L(5') HA pTARBAC2.1 pCR8GW	5'-gcgtaagcggggcacatttcattacctctttctccgcaccgcacat agatattaccctgttatccctagaaacagctatgaccatgtaa-3'
R(3')HA pTARBAC2.1 iTol	5'-cgcggggcatgactattggcgcgccggatcgatc cttaattaagtctactaattatgatcctctagatcagatct-3'

Table 2.7: iTol2 / *crya*:eCFP targeting oligos

The post-FLP kaede CH73-243G6 BAC was grown up and pre-heated at 42°C, subsequently being electroporated with the iTol2 / *crya*:eCFP PCR product, as outlined in the previous sections. This was plated on to Amp (50µg/mL) LB agar plates and grown at 32°C. The following day colonies were selected, suspended and re-plated on Amp and Spectinomycin (50µg/mL) plates, to test for any residual pCR8GW plasmid, with the suspension also being used for a PCR to confirm the presence of the *sp7* exon 2 CDS and the pTARBAC2.1 backbone with the iTol2 insert. Once a colony was confirmed to have successfully intergrated the post-FLP *sp7*:kaede and iTol2/*crya*:eCFP sequences, it was grown up as a 100ml Amp LB prep and isolated using a Nucleobond Xtra midi kit. This was eluted into six 20µL aliquots which were subsequently pooled.

Recombineered BAC injection

An injection solution of 50ng/µL of *sp7*:kaede iTol2/*crya*:eCFP BAC, 25ng/µL of *transposase* RNA (a gift from E Markham, van Eeden lab) and 10% phenol red was made up in MQH₂O. 1-2nL of this solution were injected into AB embryos which were subsequently raised after screening.

2.2.10 Screening

After injection and subsequent transgenesis or mutagenesis the mosaic G0 embryos were raised for approximately 8-12 weeks.

F1 generation: In the case of transgenic G0s, embryos displaying the expected phenotype were selected prior to raising at 5dpf and after being pair-mated to wildtype ABs, F1 heterozygous

embryos positive for the expected phenotype were selected and raised. For mutagenised G0s these fish were pair-mated to wild-type ABs and subsequently the gDNA extracted from multiple pooled offspring in a 96 well plate (three embryos per well) using the HotSHOT method (outlined below). Using this gDNA, a PCR and restriction digest were used to identify the occurrence of mutations which would suggest successful germline integration of the induced mutation. These identified founders were then outcrossed again to AB embryos and the F1 progeny raised.

F2 generation: Transgenic F1 fish were crossed out to wild-type AB fish; if a single transgenic genomic insertion is present an expected 50% of these F2 offspring would be heterozygous positive for the transgenic insertion. If a single insertion is indicated then the positive F2 embryos, which would all be heterozygous for the same transgenic insertion, were raised as a stable line. Mutagenised F1s were fin-clipped and from this tissue gDNA was extracted for genotyping using PCR followed by sequencing (see below). Once an ideal mutation was identified in an F1, this fish was outcrossed to AB embryos and the F2 progeny raised. At 8-12 weeks the population F2s were screened to identify heterozygous fish positive for the mutation, which were then pooled as a stable mutation.

2.2.11 Genotyping by sequencing or restriction digest

gDNA extraction

For genotyping genomic DNA (gDNA) was extracted from live adult fin clips or live/fixed embryonic tissue using the HotSHOT method described by Meeker et al. 2007 (Meeker et al., 2007). Briefly, the tissue is heated in 50mM sodium hydroxide at 95°C to lyse cells and denature the gDNA. The solution is then cooled, neutralised with TRIS pH 7.5 or 8.2 and centrifuged to pellet cell debris. The supernatant, which contains the gDNA, can then be used in PCR to amplify the relevant section of gDNA. The PCR products were then used either for a diagnostic restriction digest or cleaned using ExoSAP (below) and sequenced.

Gene/Mutant	Genotyping forward (5'-3')	Genotyping reverse	Method of genotyping
<i>fgf8a</i> ^{ti282a} (previously <i>ace</i>)	ttttccaaaagtcacaacgtct	ggtgggattcttctcatgcattc	Sequencing
<i>fgf3</i> ^{t21t42} (previously <i>lia</i>)	tgtccagtcataaatgtcaaag	ccatctcatggccttgttg	NsiI RD - Hammond et al., 2011
<i>fgf10a</i> ^{tbvbo} (previously <i>dae</i>)	gctcttcccagttttccgagctc caggacaatgtgcaaatcg	tccgttcttatcgatcctgag	TaqI RD (65°C) - Norton et al, 2005
<i>smo</i> ^{hi1640}	(1st wildtype tggaagcttttgatgcttt) (2nd viral ins atatcgacggtttccatatggg)	(1st wildtype acatggccaatttctcgaag) (2nd viral ins gtactctataggcttcagctgg)	Presence of viral PCR product - Chung et al, 2008
<i>mib1</i> ^{ta52b}	tatttaccgtctgtctaccacag	attagacgagtttctgtctcctcg	NlaIII RD
<i>cdr2l</i> ^{4bp Del}	ccatatgctgaaacaattatgatgc	ctgctctgtacctcgatttctg	Sequencing
<i>cdr2l</i> ^{5bp Indel}	ccatatgctgaaacaattatgatgc	ctgctctgtacctcgatttctg	AluI RD or Sequencing

Table 2.8: List of genotyping primers

ExoSAP

To remove unused primers and NTPs from the PCR reaction prior to sequencing, 2 μ L of SAP (Shrimp-Alkaline Phosphatase)(NEB) and 0.25 μ L of Exonuclease1 (NEB) (collectively referred to as ExoSAP) were added to 8 μ L of the PCR products, on ice, before immediately being incubated at 37°C for 45 minutes. After this incubation the reaction was heated to 80°C for 15 minutes to deactivate the enzymes. This reaction was then sent for sequencing with the relevant sequencing primer (IDT) (Table 2.8).

2.2.12 Fluorescence-Activated Cell Sorting (FACS) and flow-cytometry

Tissue dissociation

Either dissected tissue or whole embryos (as discussed in the results) were added to a sterile solution of 0.25% porcine trypsin, 1mM Ethylenediaminetetraacetic acid (EDTA) and 10mg/mL proteinase K in PBS with gentle agitation using a p200 (Gilson) for approximately 20 minutes before being stopped with a solution of 1mM CaCl² and 5% fetal calf serum.

1mL of sterile, chilled PBS was then added to the dissociation solution and the suspension spun down at 400g for 3 minutes. The PBS supernatant was then removed and the pellet resuspended in PBS.

For the later experiments utilising FACS, a protocol was developed (outlined below) based on published protocols from the Lawson Lab (<http://lawsonlab.umassmed.edu>), The Zebrafish Book (Westerfield, 2000) and (Baxendale et al., 2009) as well as personal discussion with Dr S Baxendale.

At the time points specified, embryos were dechorionated in pronase (1ml pronase into 3ml of E3 in a 7ml bijou for 10 minutes).

Embryos were then placed into sterile ca²⁺-free Ringer's solution for 10 minutes and passed through a p200 to try and remove as much yolk as possible. The embryos were then separated from any detached yolk and transfer into a sterile 35mm glass dish containing 2mL of collagenase/dispase (1.75mg/mL - Roche) at 28°C. Embryos were then gently pipetted up and down every 10 minutes with a p200 and after \leq 40minutes the majority of the embryonic tissue was dissociated. The suspension was then passed through a 40 μ M filter (Greiner Bio-One) into a sterile 50ml falcon tube to remove any of the larger remaining pieces of tissue. The dish was then rinsed with 2mL of sterile room temperature PBS, which was then poured through the filter. This step was then repeated with the filter alone then rinsed with 2mL of sterile PBS, to give a cell suspension with a total volume of 8mL.

The cell suspension was then spun down at 400g for 3 minutes at 4°C with the PBS supernatant then removed and the pellet resuspended in 5mL of PBS. This was then spun down, again at 400g for 3 mins and the pellet resuspended in 1ml of sterile Hank's Balanced Salt Solution in a 15ml falcon for sorting. The cell suspension was kept in the dark when moved to the FACS facility to prevent UV conversion of Kaede.

Flow-cytometry (cell counting)

Cells were counted on a CyAn analyser (Beckman Coulter) using a 488nm λ excitation laser and either a FITC 530/40 filter or PE 575/25 detection filter. The 488nm laser will excite GFP as well as unconverted and converted Kaede. However only the unconverted Kaede will be detected in the FITC 530/40 (green) channel whereas converted Kaede will be detected in the PE 575/25 (red) channel (Ando et al., 2002).

FACS (cell sorting)

Cells were sorted on a FACSAria IIu sorter (BD Biosciences) at The University of Sheffield Medical School Flow Cytometry Core Facility, using a 488nm λ excitation laser and 530/30 detector.

2.2.13 In Situ Hybridisation (ISH)

ISH Probe Synthesis

The DNA templates used for synthesising RNA ISH probes were produced using either two rounds of PCR with a nested reverse T7 primer or by linearising a modified plasmid containing the cloned sequence of interest. Both protocols, described in further detail below, used cDNA synthesised using SuperScript III Reverse Transcriptase (ThermoFisher) with mRNA initially extracted using TRIzol reagent (Ambion/Invitrogen). Both were carried out as per the manufacturers protocol.

Two-round Nested PCR Template Synthesis

A single forward primer and two reverse primers, one of these being nested at least 50bp 5' of the other, were designed against the mRNA sequence (NCBI) for the gene of interest using primer-BLAST (www.ncbi.nlm.nih.gov/tools/primer-blast/) (Listed in Table 2.9). Primers were designed to be between 23-25bp in length and to the inner, nested reverse primer, a minimal T7 promoter sequence (Table 2.10) was attached at the 5' end. Primers were then ordered from IDT. First Round PCR; A 25 μ L Q5 polymerase PCR was then setup using the forward and outer reverse primer at a working concentration of 10 μ M and 1 μ L of cDNA (synthesised using SuperScript III Reverse Transcriptase following extracted for 35 cycles. This was then checked on a gel to ensure a clean template band of the expected size was present. Second Round PCR; A 50 μ L Q5 polymerase PCR was then setup using the same forward and the inner/T7 reverse primer at a working concentration of 10 μ M and 0.5 μ L of the first round PCR for 30 cycles. This was then checked on a gel to confirm the presence of a clean template band before the reaction was cleaned using a GenElute kit (Sigma) and eluted into 30 μ L MQH₂O and stored at -20°C until required. A table of the primers used is listed below;

Gene	Forward (5'-3')	Outer Reverse	Inner Reverse
aldh1a2 (NM131850.1)	ggagtcgtcaa tattttgccagg	ggtttgagaat gacacgtctctg	ccccgagtgctt tagtatgggta
cdr2a (XM1921397.5)	ccagtcacag agggatttcacag	ttaaaacagcc acaccttactgg	aaacagccaca ccttactgggcc
fgf8a (NM131281.2)	cttcacctctt tgcgttttgcta	cacggtaggaa acctgggataat	atgagctgggta tcttatcgctg
fgfR2 (NM1243006.1)	tggacctttc cagagaagatgg	aagtgagaggc tcctctgatacg	agattgatgatg ttcttgtgccg
fgfR4 (NM131430.1)	gttttcattgc catctgtttca (p308 Roehl lab)	tacgcctcttc ttgagaacctc (p308 Roehl lab)	tctccaccacac aactgtaattc
hmx2 (NM1115098.2)	atgaataatc ggaggacagcg	tgtattttgtacgt cttagtgtgtg	agtgtgtgtaataa tgtgtcatcct
hoxb4a (NM131118.1)	atggccatgag ttctatttgat	ctctgattgct gcacaatgtcg	agttactgcttatt ttggtgttcg
mycb (NM200172.1)	ttctataacca tcagcacggaca	actcatggcataa ccatacaagga	taagccaggcag cttaagaaca

Table 2.9: List of Primers Used for Nested-PCR ISH Probe Template Synthesis

5'-AATACGACTCACTATAGG-3'

Table 2.10: Minimal T7 Promoter Sequence

Synthesis of a plasmid containing a cloned sequence

>23bp primers were designed against the coding sequence for the gene of interest using primer-BLAST (www.ncbi.nlm.nih.gov/tools/primer-blast/) (Table 3.0). These were then used to amplify the sequence from cDNA in a standard high-fidelity Q5 (NEB) PCR, which was subsequently cleaned using a PCR clean-up kit (Qiagen or Sigma) and eluted into 30 μ L of MQH₂O. 3 μ L of the cleaned and original reactions were then run on an ethidium bromide gel to ascertain whether the PCR had produced an amplicon of the expected length. To ligate the cloned sequenced amplified by PCR into a pCR II dual-promoter vector a TA Cloning kit (Invitrogen) was used. This requires 3' A-overhangs to be added to the PCR cloned sequence which is achieved by incubating the PCR with an equal amount of 2xTaq Reddymix (ThermoFisher) at 72°C for 20 minutes.

The ligation reaction was then setup with 1 μ L of the 3' A overhang PCR amplicon added to 2 μ L of pCR II vector, 1 μ L of the ExpressLink T4 DNA Ligase and 2 μ L of Ligation buffer in a 10 μ L reaction on ice before being incubated at 22-25°C (RT) for >15 minutes. The ligation mixture was then added to an aliquot of DH5a competent E.coli (NEB) thawed on ice before being left on ice for 30 minutes. After this period the mixture was heat-shocked at 42°C for 30-45 seconds before being immediately returned to ice for 2 minutes. Following this 250 μ L of RT SOC media (NEB) were added and the suspension outgrown at 37°C, shaking for 1 hour. From this two dilutions, 10¹ and 10² were plated onto carbenicillin (50 μ g/mL) containing (selective) LB agar plates and incubated overnight (<16 hours) at 37°C.

The next morning six colonies were selected from across the plates and suspended in 7 μ L of MQH₂O. The sterile pipette tip used and 3 μ L of the suspension were placed in 3ml of LB broth

Gene	Forward (5'-3')	Reverse	Amplicon Size
ak8(V2) (NM1020644)	agctgaaagg cccctcagaatc	gccgactctcc agtgactcaaac	1400bp
cdr2l(V1) (NM205564)	tgtactgcacg aacgccttgtaa	cagatgtctatgt gggggagtg	1556bp
hmx3a (NM131634.1)	atgccccgaaaca acacaggata	tcccattttctct ctttccctct	976bp
llgl2(V1) (NM212582)	gtgagagagg gcagtttgagtc	tcggaagcaagt ctagaatgaag	3168bp
nav3(/1) (NM1045143.2)	agtaacagcagtaa aggtcctcaaac	gaagctgtactgctc cattaccaccta	1033bp
nav3a (NM1045143.2) (Klein et al., 2011)	ccacgatag gaggacaaa	gtagcgggacag gatgaagaacag	391bp
sp7 (NM212863.1)	ttatggatccagt cccttgctat	catttgctgg cgctttattaga	1444bp

Table 2.11: List of Primers Used for Cloning Probe Template Sequences

with carbenicillin added and incubated at 37°C. The remaining colony suspension was used in a standard 2x Taq Reddymix (ThermoFisher) PCR, albeit with 8 minutes initially at 94°C to ensure bacterial lysis, and the original primers to identify if the clonal PCR insert was present. Colonies identified as having the insert had 100µl of the respective LB culture added to 100mL of fresh LB with carbenicillin and were incubated overnight at 37°C. The following day the cultures were divided into 50mL aliquots and spun down at full speed, 4°C for 15 minutes. The supernatant was removed and the pellets stored at -20°C or used in plasmid midiprep column extraction (Qiagen) where, briefly, the pellet is lysed and cleared before being applied to a tip that selectively binds the plasmid DNA under low-salt and pH. The plasmid DNA is then eluted in a high-salt buffer and desalted through a IPA precipitation before being finally eluted into 1mL of 1/10th TE in MQH₂O and stored at -20°C until required.

Linearisation of plasmid DNA for ISH template

The isolated plasmid containing the cloned sequence was then sent for sequencing and also used for a diagnostic restriction digest to ascertain the cDNA orientation relative to the polymerase promoter sites within the plasmid backbone. A unique restriction site within the plasmid backbone was then identified so that the plasmid could be linearised and used as template in an anti-sense run-off transcription reaction. 3-5µg of the plasmid were digested in a 100µL reaction before being cleaned using a GenElute kit (Sigma), eluted into 1/10th TE in MQH₂O and checked by gel electrophoresis to ensure successful linearisation. This template was then stored at -20°C until required. This protocol was also used to linearise published constructs previously used as a template for ISH probes (listed in Table 3.1).

Gene	Reference	Digest and polymerase for AS transcription
atoh1a	Millimaki et al., 2007	HindIII, T7
fsta	Hammond et al., 2011	SpeI, T7
etv4	Munchberg et al., 1999	NotI, T7
fgf10a	McCarroll et al., 2013	EcoRI, SP6
otx1b	Li Y et al., 1994	EcoR1, T7
ptch2	Hammond et al., 2003	BamHI, T3
pax5	Hammond et al., 2003	EcoR1, T7

Table 2.12: List of previously synthesised/published ISH template constructs

Transcription of Antisense Labelled-RNA Probes for ISH

The transcription reaction was set up on ice as shown in Table 4 using the anti-sense DNA template synthesised previously to transcribe digoxigenin (DIG) or fluorescein UTP-labelled antisense RNA probes. The reaction was incubated for 2-3 hours at 37C before DNase was added and incubated for a further 20 minutes at 37C to remove the DNA template.

Component	Volume (μL)
Template (1 μg)	variable
Nuclease-free water	to 20 μL
10x Transcription Buffer	2 μL
RNase Inhibitor	0.5 μL
100mM Dithiothreitol (DTT)	0.5 μL
DIG or Fluorescein labelled dNTP mix	1 μL
Appropriate polymerase	2 μL

Table 2.13: List of primers used for cloning probe template sequences

The reaction was then placed on ice and purified either using an RNeasy spin filter kit and eluted into 20 μL of RNase-free water (Qiagen, 2012-2014) or by precipitation with ammonium acetate (NH_4Ac). Briefly, the transcription reaction was added to 10 μL of 7.5M NH_4Ac and 75 μL of cold ethanol before being spun at full speed, 4°C for 20 minutes. The supernatant was then removed and the pellet washed with 100 μL of 70% ethanol being spun down at full speed, 4°C for 5 minutes. The ethanol wash was then removed and the pellet suspended in 20 μL of RNase-free water. 1 μL of the resulting RNA was checked by gel electrophoresis and an equal volume of formamide was added to the remaining RNA before being stored at -80°C.

ISH protocol

The following protocol is a modified version of Thisse and Thisse., 2008 Nature Protocols.

Embryo Fixation: Embryos were dechorionated and place in 4%PFA over-night at 4°C. These were then dehydrated through a series of methanol (MeOH) washes at 33%, 66% before finally being stored in 100% MeOH for at least 2 hours at -20°C.

Day 1: Fixed embryos were rehydrated, being washed in 66% MeOH/PBSTw, then 33% MeOH/PBSTw for 5 minutes each. Embryos were then washed four times for 5 mins in PBSTw. A Proteinase K (10 μ g/mL in PBSTw - 1/1000 dil. of 10mg aliquot) solution was made and placed on ice before being added to embryos in a 20°C waterbath for:
<16hpf; 1 min, 16 to 18hpf; 1 1/2 mins, 18 to 22hpf; 2 mins, 22 to 24hpf; 2 1/2 mins, 24 to 26hpf; 4 1/2 mins, 26 to 32hpf; 8 mins, 30 to 36hpf; 16 mins, 36 to 48hpf; 20 mins
After Proteinase K treatment, embryos were transferred from the water bath and placed on ice. The Proteinase K was removed and embryos rinse with PBSTw, being replaced with 4% PFA for 20 minutes on ice. Embryos were then washed four times for 5 mins in PBSTw. (The following steps are all carried out at 65-70°C) Embryos were pre-hybridized in 700 μ L of Hyb+ for 3 hours with 200 μ L of the RNA probe, diluted 1:450 in Hyb+, subsequently added and incubated at 65-70°C overnight.

Day 2: Still at 65-70°C, the RNA probe was removed and returned to -20°C for future use. Embryos were washed in 66% and 33% Hyb- / 2x saline-sodium citrate (SSC) for 10 minutes each, followed by a 100% 2xSSC washed for 10 minutes. Embryos were then wash twice in 0.2xSSC to ensure only high-stringency probe hybridisation for 30 mins each. (The following steps are carried out at room temperature) Following the high-stringency washes, embryos were then progressively washed with 66% and 33% 0.2xSSC / PBSTw for 10 minutes each. They were then washed twice in PBSTw for 10 mins and incubated in blocking buffer for 3 hours. This was replaced with 200 μ L of either anti-DIG or Fluorescein AP-conjugated antibody solution (antibody diluted 1:2000 with blocking buffer) and incubated overnight at 4°C with gentle rocking.

Day 3: The antibody solution was discarded and embryos washed briefly in PBSTw. Embryos were then washed six times in PBSTw for 30 mins each. Subsequently embryos were washed three times for 5 minutes each in staining buffer. After the last wash embryos were transfer to a 24 well plate and the staining buffer replaced with 0.5mL of BCIP/NBT (3.5 μ L BCIP / 4.5 μ L NBT per mL of staining buffer) staining solution and placed in a °C incubator, in the dark. When the desired stain intensity was reached, embryos were returned to their original Eppendorf tubes and washed three times in PBSTw for 5 mins each to stop the reaction.

Double ISH protocol

For a double ISH the following modifications were made to the above ISH protocol;

Day 1: Both RNA probes, incorporating differently labelled UTPs, were added at 1:450 dilution after pre-hybridisation.

Day 3: After the staining and three washes in PBSTw, embryos were incubated in 100mM glycine pH 2.2 for 30 minutes to inactivate the first conjugated antibody. Embryos were then washed three times in PBSTw for 5 minutes before being transferred into blocking buffer for 3 hours. This was replaced with 200 μ L of either anti-DIG or Fluorescein AP-conjugated antibody solution (diluted 1:2000 with blocking buffer), depending on the first antibody used, and incubated overnight

Day 4: The antibody solution was discarded and embryos washed briefly in PBSTw. Embryos were then washed three times in PBSTw for 30 mins each before being placed in PBSTw over-night at 4°C.

Day 5: The PBSTw washes were continued, with two more 30 minute washes. Embryos were then washed three times for 5 minutes each in Fast Red (Roche) staining buffer and after the last wash embryos were transfer to a 24 well plate before having 500 μ L of Fast Red (1 tablet dissolved in 4mL of staining buffer) staining solution applied and being incubated at room temperature in the dark. When the desired stain intensity was reached, embryos were returned to their original eppendorf tubes and washed four times in PBSTw for 5 mins each. For both single and double ISH, if there was little background staining embryos were fixed in PFA after the final PBSTw washes. However if required, staining was cleared through MeOH washes. For this embryos were fixed in 4% PFA for 30 minutes before being washed for 5 mins in 33% MeOH, 5 mins in 66% then 100% MeOH for 10 minutes to remove excess staining. Embryos were then taken through the series in reverse before being washed twice in PBSTw for 10 minutes each. For imaging embryos were transferred into 37.5% glycerol/H₂O and washed for >10 minutes before finally being replaced with 75% glycerol.

ISH solutions

PBSTw	0.1% Tween in PBS
Hyb+	25mL Formamide, 2mL tRNA (10mg/ml), 12.5mL 20X SSC, 500 μ L 10% Tween-20, 50 μ L Heparin (50mg/mL), 460 μ L 1M Citric Acid and H ₂ O to 50mL
Hyb-	25mL Formamide, 12.5mL 20X SSC, 500 μ L 10% Tween-20, 460 μ L 1M Citric Acid and H ₂ O to 50mL.
20X SSC	140.2g 3M NaCl, 65.8g 0.3M Sodium Citrate dihydrate (pH to 7) then H ₂ O to 800mL. All dilutions (2x and 0.2x) are with MQH ₂ O.
(MAB) Blocking solution	5mL 1.5M maleic acid, 1mL 5M NaCl and H ₂ O to 35mL (pH to 7.5). Then add 1g blocking reagent (Roche), 500 μ L 10% Tween-20, 1ml FBS or sheep serum and make up to 50mL with H ₂ O. Heat to 60°C to dissolve the blocking reagent and either use immediately or store at -20°C.
BCIP/NBT staining buffer	5mL Tris pH 9.5 , 2.5mL 1M MgCl ₂ , 1mL 5M NaCl, 500 μ L 10% Tween-20 and H ₂ O to 50mL.
Fast Red staining buffer	5mL Tris pH 8.2 , 2.5mL 1M MgCl ₂ , 1mL 5M NaCl, 500 μ L 10% Tween-20 and H ₂ O to 50mL.

Table 2.14: Table of ISH solutions

2.2.14 Phalloidin staining of actin-rich stereocilia

3dpf embryos were fixed in 4% PFA over-night and washed three times in PBS for 10 minutes before then being permeabilised in 2% triton-X100 (Sigma) for 3-4 days at 4°C. Embryos were the washed three times in PBS for 5 minutes each and this was then replaced with FITC-phalloidin (1:20 dilution of working stock, Sigma) or Alexa Fluor 647-phalloidin (1:100 dilution, ThermoFisher) in PBS and left over-night at 4°C. The following day embryos were washed three times in PBS for 1 hour each before being dissected (eyes, forebrain, fins and trunk removed) in PBS and mounted in Vectashield (Vectorlabs) prior to confocal imaging.

2.2.15 Joint acetylated-tubulin antibody and phalloidin staining

Initially the kinocilia were labelled using anti acetylated-tubulin. This was then directly followed by phalloidin staining, carried out as previously described. Polarity maps from these were created by overlaying the stereociliary bundles with arrows pointing in the direction of the kinocilium in FIJI. When polarity could not be determined a dot was used to indicate a hair cell.

2.2.16 Heat-shock inducible misexpression

For standard misexpression, ≤ 60 embryos from either a hemizygous transgenic carrier (see Table 2.1) outcross or incross were transferred at the time points described from their incubation at 28°C to 25ml of preheated E3 in a 39°C water bath. Embryos were then left at this temperature for 30 minutes, as has been describe previously (Padanad et al., 2012). Heat-shocks ranging from 15 minutes to 2 hours at this high temperature have also been reported (Kidwell et al., 2017; Hammond and Whitfield, 2011; Padanad et al., 2012).

After the 39°C heat-shock, embryos were returned to their previous plates of E3, which had been incubated to 33°C during the heat-shock, before being incubated for a further 30 minutes at 33°C. This 33°C incubation, likely inducing a very low-level heat-shock response, has been suggested to extend transgene activation and also reduce cell death following heat-shock (personal communication with Professor B Riley) (Padanad et al., 2012; Zou et al., 1998).

Following their incubation at 33°C, embryos were returned to 28°C and incubated until they reached the desired stage for fixation, as described.

2.2.17 Embryo chemical treatment

Embryos applied with small molecule antagonists/agonists (table 14) were treated in 12-well plates with 3ml of the respective treatment and ≤ 30 embryos per well. Embryos treated with compounds dissolved in ethanol, such as cyclopamine, had their chorions punctured with a sterile hypodermic needle prior to treatment to allow penetration of the compound. For compounds dissolved in DMSO, chorion permeability is not an issue and therefore chorions were not punctured (Kais et al., 2013). All treatments were carried out at 28.5°C and following treatment, embryos were washed twice in E3 medium before either being fixed or grown on. Vehicle controls consisted of the solvent alone at the highest treatment concentration used.

Chemical	Supplier	Solvent/Vehicle control
InSolution Cyclopamine, V. californicum	Calbiochem (Merck Millipore)	Ethanol
DEAB 4-(diethylamino) benzaldehyde 99%	Sigma	DMSO
RA Retinoic Acid	Sigma	DMSO
InSolution SU5402	Calbiochem (Merck Millipore)	DMSO

Table 2.15: Treatment chemicals and their solvents

2.2.18 Vestibular analysis

To test motor coordination and balance, reflecting the vestibular function of the ear, tests previously established by Riley and Moorman, were used on 5dpf larvae (Riley and Moorman, 2000). For motor coordination, individual larvae were observed after a startle response induced by tapping the edge of the plate with the handle of a wooden seeker. Normally following such a startle response, larvae move rapidly in a straight line, whereas larvae with vestibular dysfunction swim in irregular patterns. The ability of larvae to balance was defined by whether they rested dorsal side up one minute after the startle stimulus. Each larvae was tested for both motor coordination and balance three times, with failure in two or more tests constituting a failure.

2.2.19 Statistics

Statistical analyses were performed in Graphpad Prism. Data normality was assessed using a D'Agostino-Pearson normality test on residuals (difference between individual measurements and the group mean for that condition), which were assessed as a whole experiment rather than for individual conditions. For normally distributed data, parametric tests such as an unpaired T-test or ANOVA with a post-hoc multiple comparison test such as Dunnett's, Sidak or Holms-Sidak were used. If non-normally distributed, non-parametric tests such as the Mann-Whitney test were used. Percentage data, if normally distributed, was tested using the same tests used for all other parametric data, whereas non-normally distributed, continuous percentage data was transformed with a log-10 transformation before being retested and a parametric test applied if appropriate. For testing association between categorical variables, a two-tailed Fisher's Exact Test was used.

Chapter 3

Identification of novel early markers of the posterior otic domain

3.1 Introduction

The role of the Fgf and Hh signalling pathways in determining the anterior and posterior character of the developing zebrafish ear have been well reported (see section 1.4.2). However, the transcriptional response by the otic placode to these signals before 24hpf has focused on transcription factors that have been shown to establish either the anterior sensory and morphological character or the anteroventral neurogenic domain in zebrafish (see section 1.4.3).

The response of a handful of posterior otic markers such as *fsta*, *pou3f3b* and *tbx1* to the same patterning signals have also been characterised in zebrafish. However, the requirement of Fsta and Pou3f3b in establishing or maintaining the posterior otic domain are not known and Tbx1, whilst having a well reported role in regulating the extent of the posteroventral non-neurogenic domain in vertebrates does not appear to respond as would be expected if it were regulating posterior otic character. This is despite the loss of pillars and fused maculae reported in the zebrafish *tbx1* mutants (Whitfield et al., 1996b; Bok et al., 2011; Maier and Whitfield, 2014; Radosevic et al., 2011).

Another characteristic of the establishment of the otic anterior-posterior (AP) axis in zebrafish previously reported by Hammond et al is the progressive loss of the posterior otic region's ability to adopt a duplicated anterior character by 17hpf (16ss) in response to either misexpression of *fgf3* or inhibition of Hh using cyclopamine (Hammond et al., 2010; Hammond and Whitfield, 2011). This progressive loss of competence could indicate the induction of an early determinant of posterior character with the initially equipotent posterior otic tissue, resisting changes in its posterior identity. This is unlikely to be either of the posterior markers that could have a role in establishing posterior otic character, *fsta* or *pou3f3b*, as they are first expressed within the zebrafish ear from 24hpf (Hammond et al., 2003; Kwak et al., 2002a).

Therefore to identify new, early markers of the posterior otic domain in zebrafish a comprehensive search of expression profiles on the ZFIN database, which includes data from a number of in situ hybridisation screens and published data, was carried out (Ruzicka et al., 2015). Possible novel posterior markers would be looked for and tested based on the features predicted for markers of posterior character.

Initially this would be expression within the posterior otic domain, likely more medially towards the posterior otic sensory epithelium as observed with *fsta* and *pou3f3b*, towards the end of the period during which the posterior otic domain appears competent to adopt anterior identity i.e around 17hpf (16ss) (Hammond et al., 2010; Hammond and Whitfield, 2011; Millimaki et al., 2007). Any posterior markers could also be tested against the prediction that if they reflect posterior character, in zebrafish, they should have lost or reduced expression domain after treatments that are known to lead to the duplication of anterior otic character such as misexpression of *fgf3* and the converse, an increase in their expression domain after treatments that are known to lead to the duplication of posterior otic character (Hammond et al., 2003; Hammond and Whitfield, 2011).

This approach was used as previous mutagenesis screens focussed on the ear have not identified any genes with a clear role in establishing posterior otic character (reviewed in Whitfield et al. 2002). A previous adult screen of mutants based on auditory response, a role thought to be primarily carried out by the posterior saccular macula, only reported mutants with defects in the Weberian ossicles and swim bladder, which are involved in conduction of auditory stimuli, rather than any changes in the posterior character of the ear itself (Popper and Fay, 1973; Bang et al., 2002).

The results of these searches and the characterisation of one of the candidates identified, including in response to changes in Fgf and Hh signalling are presented in this chapter.

3.2 Results

3.2.1 Search of expression data for genes with early restriction to the anterior and posterior otic domains

It was noted that early expression of *pax2a*, a marker of early otic induction and later the sensory hair cells, appeared to show lobed otic expression at the anterior-posterior poles of the otic placode just prior to the onset of otic AP patterning in zebrafish (10ss, 14hpf) (Hans et al., 2004; Hammond and Whitfield, 2011). It was hypothesised that this expression pattern may reflect an early patterning event across the otic AP axis. Such an early otic patterning event could be supported by the preliminary observation of an early (14-15hpf) concentration of cilia at both poles of the otic placode (Supplementary Figure 1), as the presence of cilia within the otic vesicle have been reported as being required for regulating Hh signalling in the otic vesicle (Stooke-Vaughan, 2013). Therefore a search of ZFIN gene expression data to identify other genes showing a similar lobed or restricted expression pattern to *pax2A* at early stages (14hpf) was carried out using the search string "otic placode between 1-4 to 10-13 somites".

Gene	Possible Role	Reference	Gene	Possible Role	Reference
ak7b	Cilia function	Panayiotou et al., 2011	irf6	Epithelial differentiation	Garza de la et al., 2013
ak8	Cilia function and epithelial cell migration	Panayiotou et al., 2011	irx4b	Unknown	
ccdc24	Unknown		katnal1	(katanin catalytic subunit A1 like 1) Unknown	
ccdc40	Cilia function	Becker-Heck et al., 2010	llgl2	Cilia and lumen formation	Tay et al., 2013
ccdc103	Cilia function	Panizzi et al., 2012	myod1	Myogenic differentiation	Pownall ME et al., 2002
Cdr2l	Unknown		prdm1a	Neural crest development	Powell et al., 2013
cyb5d1	Cilia function	McClintock et al., 2007	robo4	Epithelial migration	Paul et al., 2013
cyp2p10	Unknown		sb:eu592	Unknown	
dnah9	Cilia function	Bartoloni et al., 2001	sfrp2	(Secreted frizzled related protein-2) Wnt antagonist	Sugiyama et al., 2013
entpd1	Nucleotide catabolism possibly in the synaptic cleft	Broock Rosemberg et al., 2010	six2a	Unknown	
etv5b	Mediating Fgf regulation of the cell cycle	Bosco et al., 2013	slc34a2	(solute carrier family 34) Unknown	
has3	(Hyaluronan synthase) cell-ECM interactions	Rilla et al., 2012	sp7	Bone formation	Renn et al., 2014
hk1	(Hexokinase-1) Metabolism	Seilliez et al., 2013	tbx2b	Cardiac and pineal	Chi et al., 2008 and Snelson et al., 2008
ier2	Proliferation/migration	Neeb et al., 2012	zgc:172136	Unknown	
ift122	Cilia signalling transduction	Qin et al., 2011			

Table 3.1: ZFIN search using search terms: "otic placode" between 1-4 to 10-13 somites
Results from a search of the ZFIN gene expression database and genes with previously published otic phenotypes removed (for full table, see Supplementary Table S2). Transcription factors are highlighted in blue.

Fifty genes were identified and those with a known otic function were removed, leaving twenty-eight candidates (Table 3.1). Whilst a large subset were implicated in cilia function, a diverse range of possible functions were represented along with a number of transcription factors (highlighted blue). Of the twenty eight candidates, three, *adenylate kinase 8 (ak8)*, *cerebellar degeneration-related protein 2-like (cdr2l)* and *lethal giant larval 2 (llgl2)*, were taken forward for further characterisation. This was based on the fact they represented a broad range of functions and appeared to have strong otic expression with potential AP localisation at an early stage of otic patterning (Panayiotou et al., 2011; Simpson et al., 2008; O'Donovan et al., 2010; Tay et al., 2013).

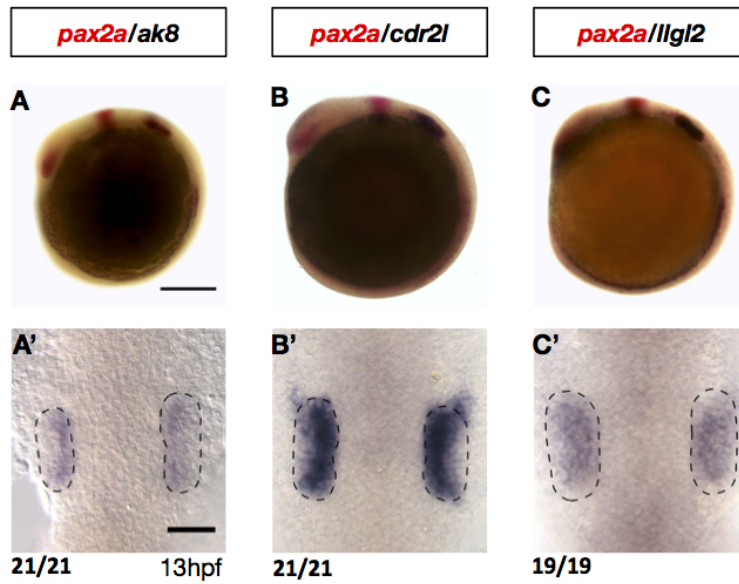


Figure 3.1: Expression of early otic markers *ak8*, *cdr2l* and *llgl2* at 13hpf

Genes of interest identified from a ZFIN search for early markers of the otic placode with possible AP restriction at 8ss (13hpf). Expression of adenylate kinase 8 (*ak8*) (A, A''); cerebellar degeneration-related 2 like (*cdr2l*) (B, B'') and lethal giant larvae 2 (*llgl2*) (C, C''). Images A-C are double in situ hybridisations for the genes mentioned and *pax2a* in red. A-C were taken using bright field with a 10x objective and A'-C' using DIC with a 40xW objective. A-C are lateral views and A'-C' are dorsal views. Scale bars: A; 200 μ M and A'; 50 μ M

Therefore, to confirm this early otic expression pattern, in situ hybridisations were carried out on wild-type embryos at 8ss (approximately 13hpf) (Figure 3.1). All three showed a broad expression across the early otic placode as marked by *pax2a* expression. At the AP poles, expression appeared to extend slightly medially for all three, possibly explaining why in lateral images this appears as a strengthening at either end (Figure 3.1A-C''). Out of these three, *ak8* expression appeared the weakest at this early stage and so *llgl2* and *cdr2l* were focused on.

Initially *llgl2* and *cdr2l* were further characterised by in situ hybridisations carried out at a number of later developmental time points (Figure 3.2). The broad otic domain of *cdr2l* expression at 13hpf appeared to be progressively lost in the anterior, being expressed in a single posterior domain by 18hpf (Figure 3.2A-B'). This posterior domain of otic *cdr2l* was all but lost by 20hpf (Figure 3.2C''), although a domain of expression abutting the anterior of the otic vesicle (Figure 3.2C', white arrow) was observed.

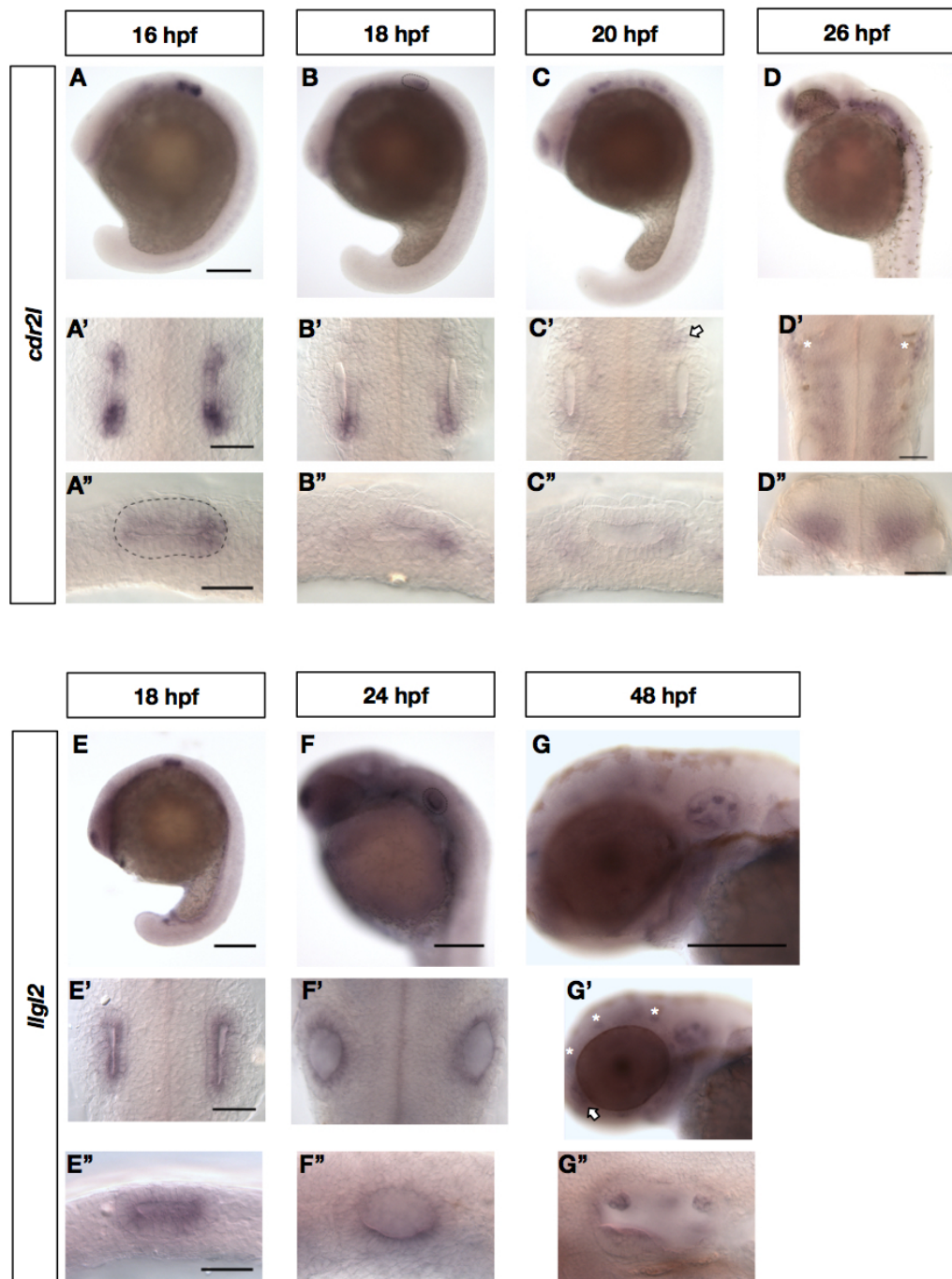


Figure 3.2: Expression of *cdr2l* between 16-20 hpf and *llgl2* between 18-48 hpf

(A–C'') Expression of *cdr2l* at 16 to 20hpf shows progressive loss from the anterior and then the posterior otic domain. At 20hpf weak expression anterior to the otic vesicle (white arrow, C') and in puncta along the anterior dorsal trunk (Supplementary Figure 10). At 26hpf, otic expression is not visible with expression in the adjacent ventrolateral hindbrain, forebrain and two patches lateral to the MHB (White asterisks, D). (E–G'') Expression of *llgl2* between 18 to 48hpf shows the broad otic expression at 18hpf appearing more ventrally localised by 24hpf. By 48hpf, expression within the ear is localised to the tips of the pillar projections and apical region of the maculae. Expression is also seen in the nasal placode (white arrow, G') and anterior neuromasts (white asterisks, G''). A - G G' were taken using bright field with a 10x objective. All other images were taken using DIC with a 40x objective. Scale bars: 50 μ M.

At 20hpf, expression of *cdr2l* within the anterior forebrain also appeared stronger with a domain of expression also now seen in a domain lateral to the mid-hindbrain boundary (MHB), possibly marking the trigeminal placode (Figure 3.2C). *Cdr2l* expression was also seen in small dorsal puncta in the anterior trunk, which could be Rohon-Beard mechanosensory neurons (Supplementary Figure 10). At 26hpf *cdr2l* expression persisted within this domain anterior to the otic vesicle along with the expression observed in the forebrain. The domain of expression adjacent to the posterolateral mid-hindbrain boundary appeared stronger by this time (Figure 3.2D, white asterisks), with a stripe of *cdr2l* expression also now clearly present in the ventrolateral hindbrain (Figure 3.2D and D”).

llgl2 expression did not show a similar early localisation to either of AP domains as seen with *cdr2l*. Instead at 18hpf *llgl2* remained broadly expressed across the otic vesicle although the staining appeared apically located within the cells (Figure 3.2E-E”). This is interesting as this apparent apical localisation of the transcript is in contrast to the previously reported basal membrane localisation of the Lgl2 peptide (Tay et al., 2013). This apically-localised, broad otic transcription persisted at 24hpf primarily within the ventral otic domain and at 48hpf expression appeared localised to the apical edge of the sensory patches along with the tips of the protruding pillars destined to form the semi-circular canals (Figure 3.2F-G”). At 48hpf *llgl2* was also expressed within the ciliated and epithelial structures of the neuromasts and nasal placodes (Figure 3.2G’ white asterisks and arrow, respectively).

The early AP lobed otic expression seen for *ak8*, *cdr2l* and *llgl2* did not appear to correlate with any later AP restriction in expression, as shown by the later otic expression of *cdr2l* and *llgl2* (Figure 3.2). Therefore this early AP restricted, lobed expression may instead reflect the morphology of the early otic placode rather than a restriction of expression. As this project aimed to study the dynamics of the patterning of the otic AP axis, a second search of the ZFIN gene expression database was carried out to identify other genes with posterior otic expression between 14-19 somites. Markers with posterior otic restriction were focused on due to the lack of clear early markers associated with the posterior otic domain in contrast to the anterior (Whitfield and Hammond, 2007). This search returned four results, two of which were transcription factors, with one of these, *tbx1* having a previously characterised role in posteroventral otic patterning (Supplementary Figure 3).

For the remaining three, *neuron navigator 3 (nav3)*, *nuclear factor, erythroid 2 (nfe2)* and *zgc:101731*, anti-sense RNA probes were synthesised to characterise their expression during early otic development. However, probes designed for *nfe2* (NM 175043.2) and *zgc:101731* (NM 1025558.2) failed to give any obvious staining at 24hpf or earlier, in contrast to their recorded expression on ZFIN (data not shown). *Nav3*, whilst not showing any otic expression at 14hpf (Figure 3.3A), by 16hpf showed a weak domain of medial expression within the posterior otic vesicle (Figure 3.3B-B”). At 18hpf the *nav3* staining in the posterior domain appeared stronger and now was also expressed along the dorsomedial otic domain (Figure 3.3C-C”). *nav3* has been found to be expressed as two post-splice isoforms, a longer *nav3a* transcript with a putative calponin-like domain, which likely mediates an interaction with actin filaments and a shorter *nav3b* transcript lacking this domain (Figure 3.3E) (Klein et al., 2011; Schmidt et al., 2009). The previously used *nav3* probe hybridised to a sequence shared by both transcripts (referred to as *nav3a/b* Figure 3.3E). Therefore to identify which isoform was expressed within the developing zebrafish ear, an in situ probe designed against the 5’ transcript sequence only present in the longer *nav3a* transcript was designed (Figure 3.3E).

This showed that the transcript expressed within the dorsomedial and posterior domains of the otic vesicle at 18hpf is that of *nav3a*. In contrast, the clear loss of expression in the somites when compared with the *nav3a/b* probe suggests this somite expression is that of the *nav3b* transcript and also supports the specificity of the *nav3a* probe (Figure 3.3D-D’’).

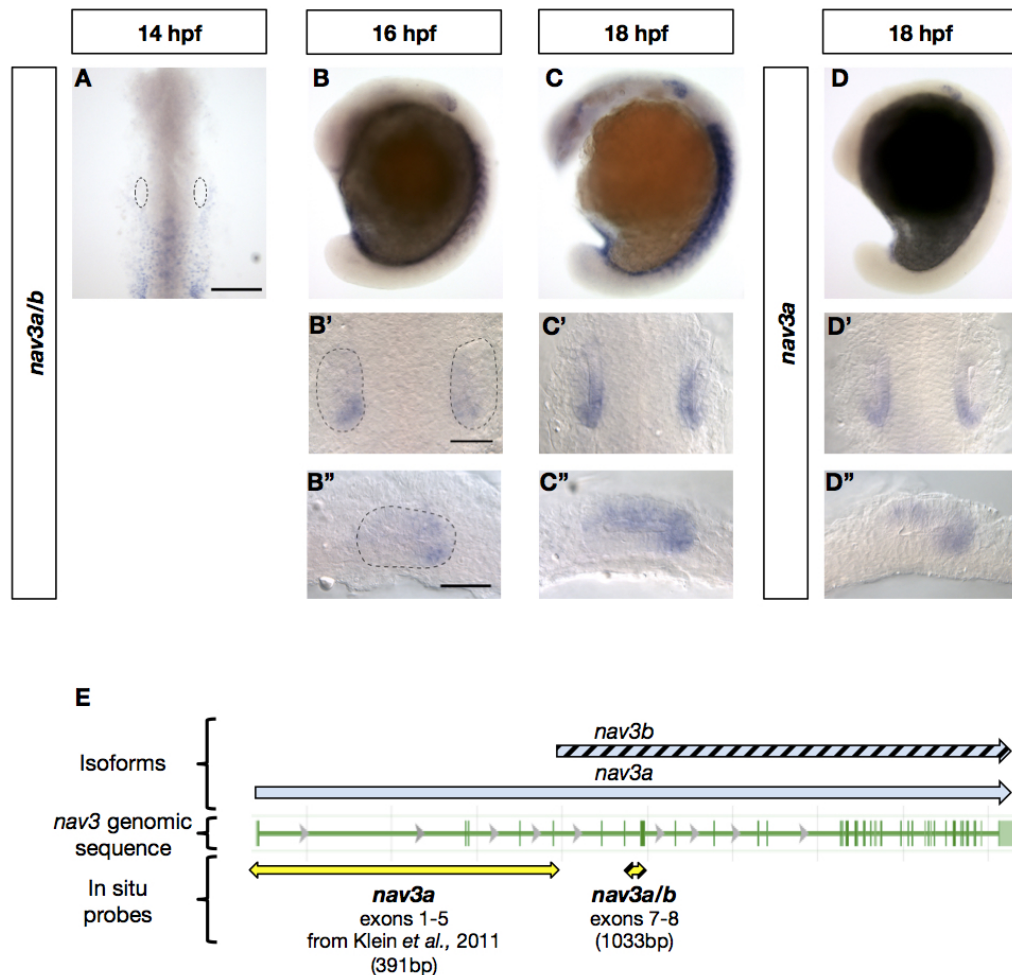


Figure 3.3: Expression of the posterior otic marker *nav3* and the differential expression of the isoform, *nav3a*

(A-C’’) Expression of *nav3* using a probe that hybridizes to both *nav3a* and *b* isoforms between 14 and 18hpf. At 14hpf (A), there is no obvious staining within the otic placode. However, by 16hpf (B-B’’), *nav3a/b* is expressed in the posteromedial domain of the otic placode, which appears both stronger and expanded across the dorsomedial domain by 18hpf (C-C’’). (D-E) Using a probe designed against the first five exons of *nav3*, which are divergent between the *a* and *b* isoforms, Klein *et al.*, 2011 (E). (D-D’’) Expression of *nav3a* at 18hpf is present within a similar domain to that seen in C-C’’ using the *nav3a/b* probe but expression within the somites is clearly lost. A-D were taken using bright field with a 10x objective. B’-D’’ were taken using DIC microscopy with a 40x objective. Scale bars: A; 200 μ M with B and B’’; 50 μ M.

3.2.2 *Cdr2l* expression persists in the anterior otic domain after loss of Fgf signalling but only transiently

As both *cdr2l* and *nav3a* represented novel posterior otic markers, I hypothesised that they should be up-regulated within the anterior otic domain when Fgf signalling is inhibited. This is because such loss of Fgf signalling during early otic development is known to duplicate posterior otic identity, including expression of posterior markers with a converse loss of anterior identity (Hammond and Whitfield, 2011). However, as expression of *nav3a* within the liver bud has been reported to be unaffected when Fgf signalling is reduced in *hs:dnfgfr1* embryos, *cdr2l* was initially focused on (Klein et al., 2011).

Cdr2l expression was initially observed by in situ hybridisation in the *fgf3* (*lia^{t21142}*) mutants, which have reduced anterior otic identity but not duplicated posterior identity (Hammond and Whitfield, 2011) (Figure 3.4A-J). Early during otic development at 10ss (14hpf), expression of *cdr2l* appears weaker in the *fgf3* mutants when compared to the wild-type siblings, although still appearing to have normal patterning (Figure 3.4A compared to B). In contrast, at 20-21ss (19hpf) *cdr2l* expression persists in the anterior otic domain as well as being present within the posterior domain rather than being lost in the anterior domain as seen in the siblings (Figure 3.4C compared to D). Despite this apparent persistence in the mutants, by 26hpf all otic expression of *cdr2l* appears lost in both the mutants and sibling (Figure 3.4E and F). In *fgf8a* (*ace^{ti282a}*) mutants, which have a milder reduction in anterior otic identity than *fgf3* mutants, expression of *cdr2l* at 10ss appears weaker and abnormally patterned (Figure 3.4H compared to G) (Léger and Brand, 2002). Yet at the 20-21ss, whilst the otic expression appears weaker, it is localised to the posterior otic domain rather than persisting at the anterior as seen in the *fgf3* mutants (Figure 3.4I). This suggests that the weaker and abnormally patterned expression seen at 10ss in the *fgf8a* mutants might reflect the role of *fgf8a* in the induction of the otic placode rather than being a direct effect on *cdr2l* (Phillips et al., 2001).

The persistence of anterior otic *cdr2l* expression after loss of Fgf function was also confirmed by transiently inhibiting all Fgf signalling. This was achieved by treating wild-type embryos between 14 (10ss) and 19hpf (20ss) with the pan-Fgf inhibitor SU5402, which can also be reported to duplicate anterior otic identity in zebrafish (Figure 3.4O) (Hammond and Whitfield, 2011). In embryos treated with 10 μ M of SU5402, 68% (17/25) showed a broader medial domain of *cdr2l* expression across the AP axis, although still appearing stronger in the posterior, compared to the vehicle controls (Figure 3.4M compared to L). *cdr2l* expression in the other 32% (8/25) of treated embryos appeared stronger in two domains at the AP poles, similar to the phenotype seen in the *fgf3* mutants (Figure 3.4M'). Treatment with a higher concentration of SU5402, 15 μ M, resulted in comparable phenotypes to treatment with 10 μ M of SU5402 but with a higher proportion 46% (12/26) of embryos displaying stronger expression in two AP-localised domains (Figure 3.4N and N'). Taken together, these results suggest that whilst Fgf signalling appears to have an inhibitory effect of *cdr2l* expression, the loss of *cdr2l* expression from the otic vesicle must also be in response to other non-Fgf3 dependent changes.

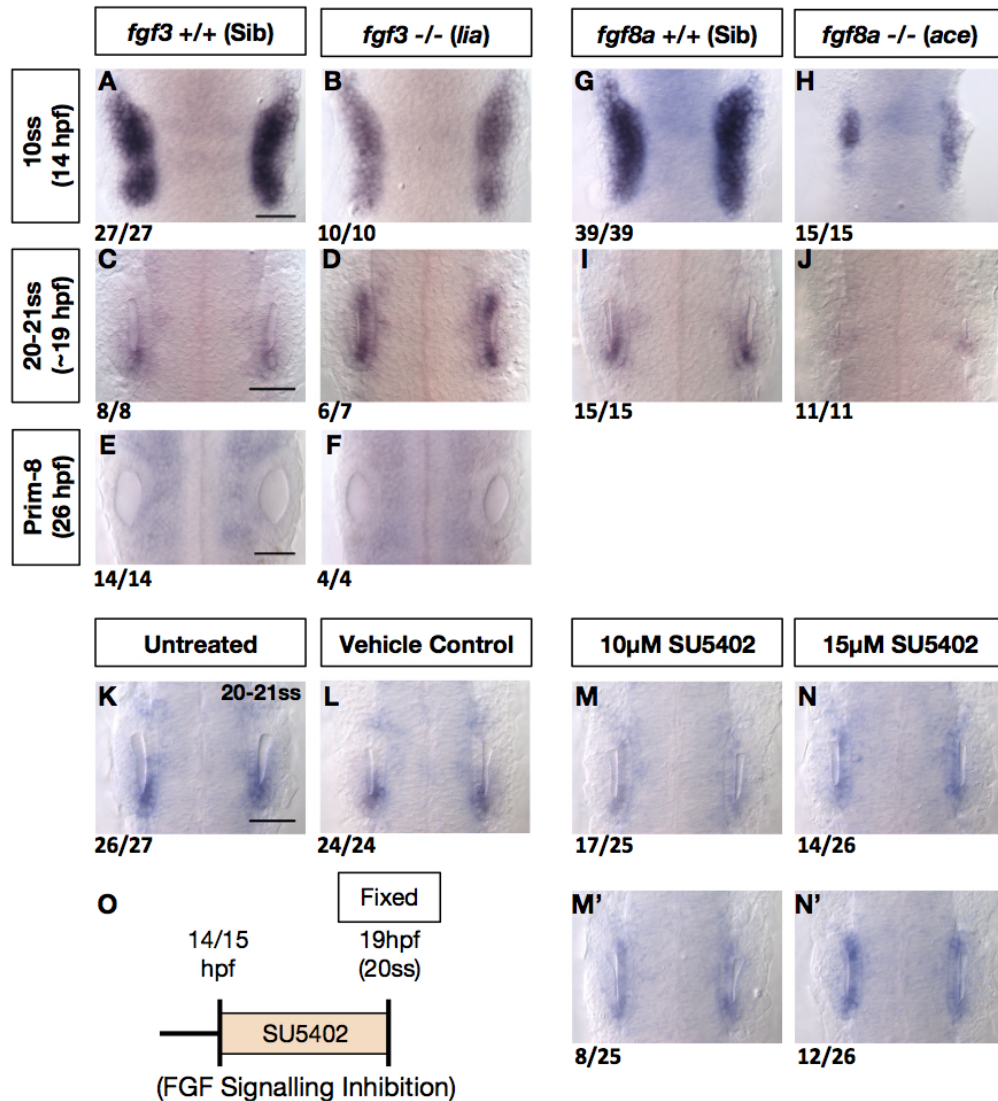


Figure 3.4: Expression of *cdr2l* between 16-20 hpf and *llg12* between 18-48 hpf

(A-F) In *fgf3* (*lia*) $-/-$ mutants at 10ss (14hpf), *cdr2l* expression appears weaker in the mutants (B) compared to their siblings (A). At 20-21ss (19hpf) *cdr2l* expression persists in the anterior otic domain in the *fgf3* mutants (D) rather than being restricted to the posterior otic domain as seen in the siblings (C). By 26hpf, *cdr2l* is lost in the otic vesicle of the *fgf3* $-/-$ mutants (F), similar to the siblings (E). (G-J) In *fgf8a* (*ace*) $-/-$ mutants at 10ss (14hpf), *cdr2l* expression appears weaker and abnormally patterned in the mutants (H) compared to their siblings (G). *Cdr2l* expression at 20-21ss is weaker within the posterior otic domain of the *fgf8a* mutants (J) relative to the siblings (I). Visible *cdr2l* expression within the *ace* mutants appears to be predominantly localised within the posterior domain as in the siblings, rather than persisting at the anterior (75% vs 92% with posterior expression only, respectively). (K-N') Treatment of embryos with the pan-FGF inhibitor, SU5402. Treatment with 10µM results in either broad expression of *cdr2l* across the medial edge (M) or strong expression primarily within two patches at the AP poles (M'). Treatment with 15µM leads to an increase in embryos showing stronger expression within two pole patches (N'). Both untreated (K) and the DMSO vehicle controls (L) show clear posterior otic expression of *cdr2l*. (O) Schematic of SU5402 treatment protocol. All images are dorsal views taken using DIC microscopy with a 40x objective. All scale bars: 50µM.

3.2.3 Otic *cdr2l* expression appears down regulated in response to over-expression of *fgf3*

As *cdr2l* appeared to persist, albeit transiently, in the anterior otic domain after a loss of Fgf signalling, over-expression should have the reverse phenotype of down-regulating *cdr2l*. Therefore to test this, *fgf3* and *fgf8a* were over-expressed using heat-shock inducible transgenic lines (Lecaudey et al., 2008; Millimaki et al., 2010). Embryos from a heterozygous incrosses of these transgenic lines were exposed to a 39°C, 30 minute heat shock at 14hpf, a stage at which over-expression of *fgf3* has been shown to induce a duplication of anterior otic identity (Hammond and Whitfield, 2011). These embryos were then fixed at 18hpf and assayed for *cdr2l* expression by in situ (Figure 3.5A-F). After over-expression of *fgf3*, all transgenic embryos showed a reduction in otic *cdr2l* expression (Figure 3.5B and C). 47% (7/15) of these transgenic *hs:fgf3* embryos showed a milder reduction in *cdr2l* expression within the anterior otic domain when compared to their siblings (Figure 3.5C). A possible slight increase in expression within the anterior hindbrain of the embryos was also noted. In the other 53% (8/15), a more dramatic loss in the anterior was seen (Figure 3.5B). After over-expression of *fgf8a*, otic *cdr2l* expression appeared reduced in all transgenic embryos but again this phenotype appeared variable (Figure 3.5E and F). 43% (9/21) of these *hs:fgf8a* transgenic embryos showed reduced anterior otic expression (Figure 3.5F) when compared to the siblings. However, the majority (57%, 12/21) showed a more evident reduction in otic expression of *cdr2l* than observed in the *hs:fgf3* embryos, although with a domain of posterior otic expression still being visible (Figure 3.5E). A stronger up-regulation of expression in the anterior forebrain compared to *hs:fgf3* was also observed in these embryos (Figure 3.5F, white arrow).

In both *hs:fgf3* and *hs:fgf8a* transgenic embryos heat-shocked at 14hpf, expression of *cdr2l* whilst reduced, was not completely lost in the posterior otic domain. This was surprising given the strong duplication of anterior otic identity previously reported after over-expression of *fgf3* using a similar heat-shock at 14hpf (Hammond and Whitfield, 2011). Therefore to identify whether this was due to insufficient levels of either *fgf3* or *fgf8a* over this four-hour time period, *hs:fgf3* and *hs:fgf8a* embryos were given a series of 15 minute, 39°C heat shocks at 14,16 and 18hpf before being fixed at 19hpf (Figure 3.5G-N). In the *hs:fgf3* transgenic embryos otic expression of *cdr2l* again appeared reduced, although this reduction appeared greater than previously observed after over-expression at 14hpf (Figure 3.5I and J). In 25% (3/12) of embryos, weak posterior otic *cdr2l* was observed but in the majority (75%, 9/12) of the transgenic embryos *cdr2l* no longer appeared expressed in the otic domain (Figure 3.5J). *hs:fgf8a* transgenic embryos also appeared to show a greater reduction in otic *cdr2l* expression when compared to embryos heat shocked a single time at 14hpf (Figure 3.5K-N). Interestingly, these serially heat shocked *hs:fgf8a* embryos showed a less pronounced reduction in expression than seen in the *hs:fgf3* embryos, the opposite to the phenotypes observed after over-expression at 14hpf.

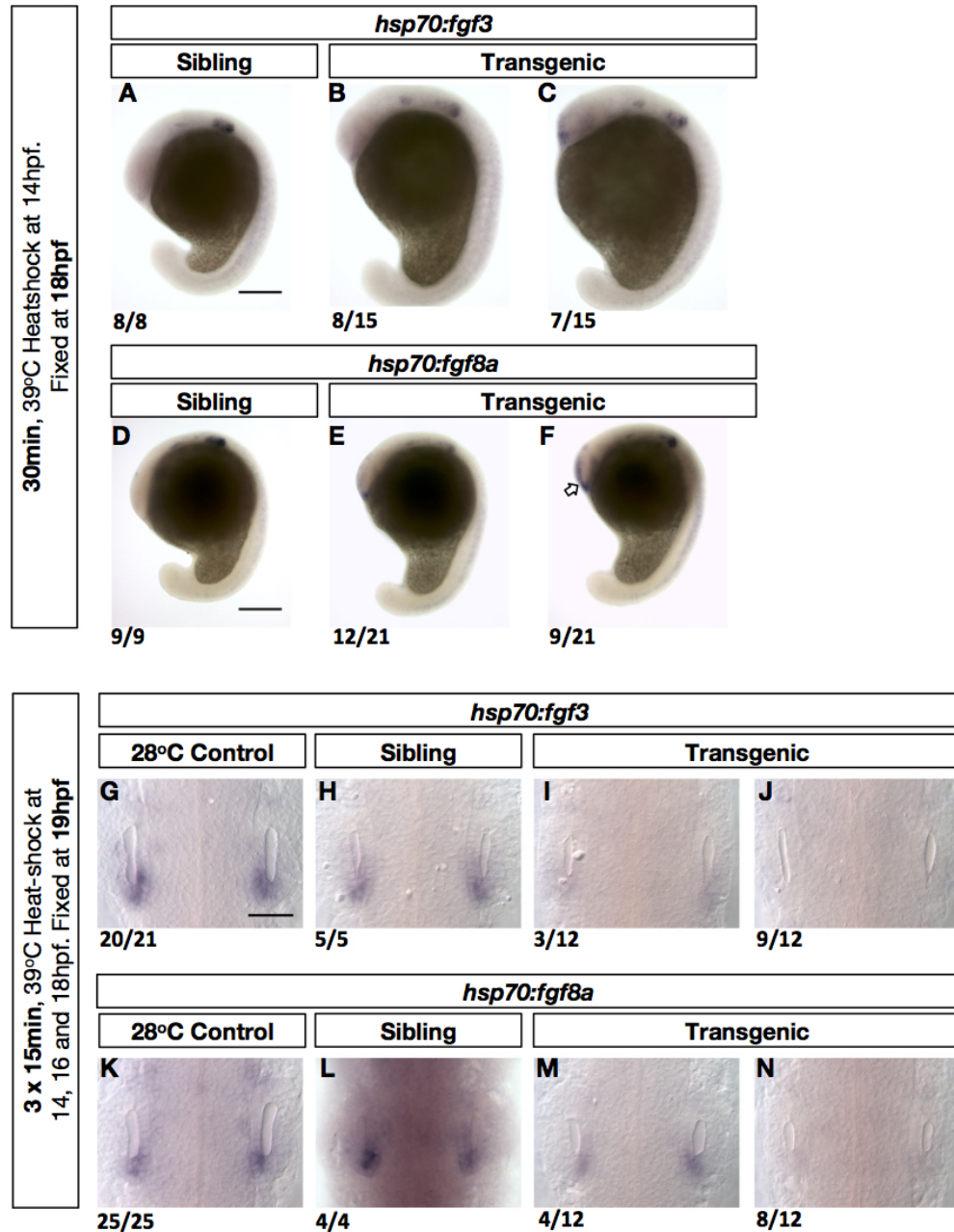


Figure 3.5: Cdr2l expression is reduced in response to over-expression of either *fgf3* or *fgf8a*
 (A-F) Expression of *cdr2l* at 19 hpf after 30-minute, heat-shock induced expression of either *fgf3* or *fgf8a* at 14hpf. (A-C) In embryos from a *hs:fgf3 +/-* incross, 8/15 transgenic embryos have weaker *cdr2l* expression throughout the vesicle (B). The remaining 7/15 have weaker throughout but still observable expression in the anterior domain. (D-F) In embryos from a *hs:fgf8a +/-* incross, the majority of transgenic embryos (12/21, E) have a stronger reduction in otic expression although retaining posterior expression than in the siblings. In the remaining 9/21 embryos posterior otic staining appears similar to that in the siblings although is weaker within the anterior domain (F). These embryos also show slightly stronger *cdr2l* staining within the forebrain (white arrow). (G-N) Expression of *cdr2l* at 19 hpf after 3x15 minute serial heat-shocks. (G-J) In *hs:fgf3 +/-* incross embryos, *cdr2l* expression is either only weakly present (I, 3/12) or lost (J, 9/12). (K-N). In *hs:fgf8a +/-* incross embryos, posterior otic *cdr2l* expression is weakly present in all. This is stronger in 4/12 (M) compared to the remaining 8/12 (N). A-F are lateral views taken using bright field with a 4x(2xmag) objective. G-N were taken using DIC microscopy with a 40x objective. Scale bars: A and G;150µM, D; 50µM.

As over-expression of *fgf3* or *fgf8a* resulted in reduced expression of *cdr2l* by 18-19hpf, I wanted to observe whether a similar reduction was seen in the strong otic *cdr2l* expression at 14ss (16hpf) after over-expression (Figure 3.2). Progeny from a heterozygous *hs:fgf3* and *hs:fgf8a* incross were therefore heat shocked at 39°C for 30 minutes, but earlier than previously, at 13hpf before being fixed at 16hpf (Figure 3.6). *hs:fgf3* embryos did not show any clear loss of expression across the AP axis (Figure 3.6A-A’), although expression appeared possibly weaker and less defined to varying degrees in approximately three-quarters of these (77%, 30/39) (Figure 3.6A and A’). In 16hpf *hs:fgf8a* embryos heat shocked at 13hpf, again no clear loss of *cdr2l* expression was seen (Figure 3.6B-B’). However, there was an apparent variability in otic expression, similar to that observed in *hs:fgf3* (64%, 23/36) (Figure 3.6B-B’). This difference in the severity of reduction in *cdr2l* expression between embryos at 16hpf and at 18-19hpf after over-expression of either *fgf3* or *8a* could reflect the normal difference in *cdr2l* expression seen between these time points.

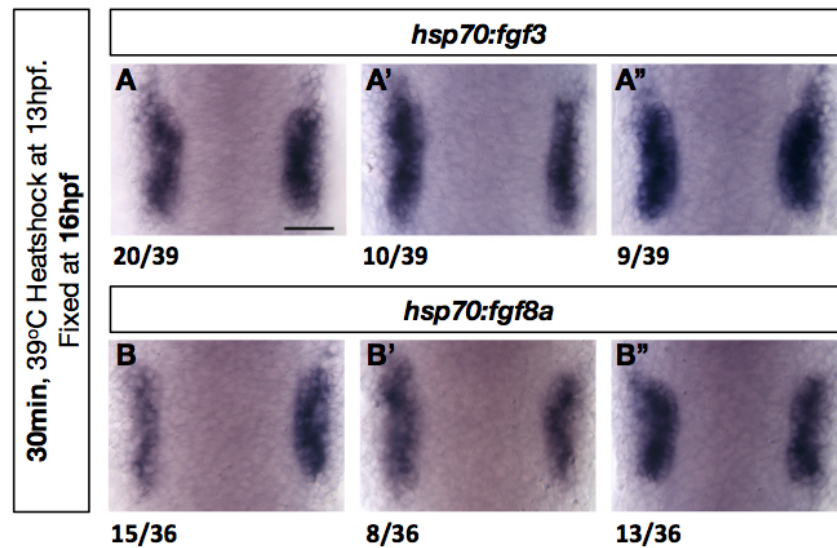


Figure 3.6: Cdr2l expression appears slightly reduced by 16hpf in response to over-expression of either *fgf3* or *fgf8a* at 13hpf

(A–A’’) Expression of *cdr2l* in progeny from a *hs:fgf3* +/- incross. In 77% of these (A & A’) *cdr2l* expression appears slightly weaker and the domain misshapen compared to A’’, which show stronger expression and likely represent non-transgenic siblings (23%). (B–B’’) Expression of *cdr2l* in progeny from a *hs:fgf8a* +/- incross. 64% of these (B & B’) show weaker and irregular domains of *cdr2l* expression compared to B’’ (36%). The embryos represented by B’’ therefore are likely the non-transgenic siblings. All images are dorsal views taken using DIC microscopy with a 40x objective. Scale bar in A: 50µM.

3.2.4 Otic *cdr2l* expression does not appear duplicated or strongly up-regulated when Hh signalling as constitutively active

If *cdr2l* is a marker of posterior otic identity, then in *ptch1^{-/-}; 2^{-/-}* Hh gain-of-function mutants, which have a duplication of posterior otic character, its expression should persist in the anterior domain (Hammond et al., 2010). In these mutants at 20ss (19hpf), otic *cdr2l* expression remained primarily localised to the posterior domain with no up-regulation observed within the anterior (Figure 3.7B).

However, posterior *cdr2l* expression when viewed laterally did appear to show a slight retention of expression along the both the dorsal and ventral edges of the otic domain when compared to the siblings (Figure 3.7D compared to C).

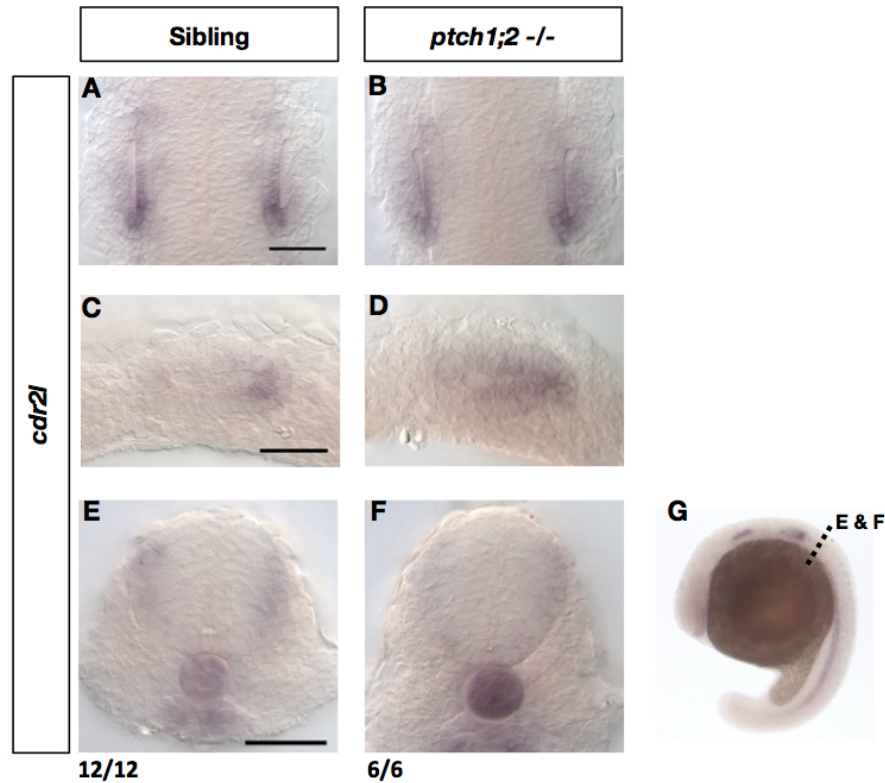


Figure 3.7: Aberrant activation of Hedgehog signalling results in a modest anterior retention of Cdr2l expression in both the medial and lateral otic domains
 (A–E) Expression of *cdr2l* in sibling embryos. (B–F) Expression of *cdr2l* in *ptch1;2* mutant embryos. (G) The black-dotted line represents the point at which the transverse trunk sections, B and F were taken from. A–B are dorsal views, C–D are lateral views and E–F are transverse trunk sections. All images were taken using DIC with a 40x objective. All scale bars: 50 μ M.

As Hh signalling is known to be a strong regulator of neuronal patterning, expression of *cdr2l* within the neural tube just posterior to the otic vesicle at 19hpf was also observed in transverse sections (Takamiya and Campos-Ortega, 2006; Cohen et al., 2013) (Figure 3.7E-F). This showed no clear change in *cdr2l* expression within the lateral neural tube, either in terms of dorsoventral positioning or strength in the *ptch1*^{-/-}; *2*^{-/-} mutants (Figure 3.7F).

3.3 Discussion

In this chapter I have presented data on identification of novel markers of both the early otic placode and the posterior otic domain through a search of previously published in situ expression data. This has led to a focus on the previously uncharacterised gene, *cdr2l*, due to its dynamic expression across the otic AP axis both during early otic development and in response to Fgf manipulation.

Using a search of the ZFIN expression database has inherent issues such low quality data and annotation and, as with all potential reverse genetic approaches, no guarantee of gene function (Junker et al., 2014). However, it also represents an easily-accessible, large dataset of potentially uncharacterised genes (>30,000) which may have undiscovered roles in development. Given the well-studied regionalisation of the otic placode by clearly defined domains of gene expression and the previous difficulty with identifying posterior otic markers using phenotypic means, this presents a good system for utilising such a search (Ruzicka et al., 2015; Whitfield and Hammond, 2007; Bang et al., 2002). This is supported by the number of known otic markers identified in the two searches performed. However, alongside this, an unbiased transcriptomics approach focused on characterising early otic genes differentially expressed either after perturbation or across the AP axis was also pursued, as discussed in Chapter Five.

Whilst the initial search for early otic markers with a lobed AP expression pattern gave a number of candidates, including *cdr2l*, this lobed pattern did not appear to reflect later AP localisation of expression or identity. *Llgl2*, one of the markers characterised from this search, rather than having expression restricted to the AP otic domains, did show an interesting apical localisation of its transcript within the ear. This is the opposite to the basal localisation of the peptide, which in zebrafish has been implicated in the formation of ciliated luminal organs, including the otic vesicle (Tay et al., 2013). As *Llgl2* is required for formation of hemidesmosomes at the basal membrane, it may play a role in establishing the early apical-basal polarity of cells of the otic placode (Sonawane et al., 2009). Such early establishment of otic apical-basal polarity has been shown to be important in determining the size of the otic lumen (Hoijsman et al., 2015). It would therefore also be interesting to study the function of *Llgl2* in pillar formation and fusion, given its later expression in the tips of the protruding luminal pillars.

In the second search for later posterior otic markers, which yielded a smaller number of candidates, *nav3a* was identified as being expressed in the posterior otic domain from 16hpf and later expanding anteriorly along the dorsal edge. Interestingly the anteroventral domain from which *nav3a* was excluded is marked by a number of anterior otic markers, such as *hmx3a*, and is strongly influenced by anterior Fgf signalling (Whitfield and Hammond, 2007; Maier and Whitfield, 2014). This localisation of *nav3a* expression, may indicate a role in regulating posterior identity. However, in the developing zebrafish liver bud expression of *nav3a* has been shown to be positively regulated by Wnt signalling but unaffected by loss of Fgf (Klein et al., 2011). Whilst Wnt signalling is not thought to be involved in patterning the AP otic axis (see section 1.4.1), Wnt emanating from the dorsal hindbrain in vertebrates has been implicated in otic dorsoventral (DV) patterning in mice with a similar role postulated in zebrafish (Riccomagno et al., 2005; Lecaudey et al., 2007). Therefore the dorsal expansion of *nav3a* seen after 16hpf, may be driven by dorsal sources of *wnt1* or *wnt3a* adjacent to the developing otic placode at 16hpf (Lecaudey et al., 2007). Intriguingly, *nav3a* is not thought to be a transcriptional activator, instead being implicated in axonal guidance and cellular movement (Klein et al., 2011). For that reason, identifying whether *nav3a* appears associated with posterior otic character would be a key initial question to address.

Following on from these two ZFIN searches, *cdr2l* was focused on as it showed dynamic expression across the AP otic axis during the period in which AP otic identity is thought to be assigned in zebrafish (Hammond and Whitfield, 2011). Whilst otic expression of *cdr2l* persisted in the anterior after a loss of *fgf3* or inhibition of Fgf signalling with SU5402, loss of *fgf8a* did not appear to have the same effect. As expression of *fgf3* within rhombomere 4 is still present in *fgf8a* mutants, this suggests *fgf3* might be the key regulator in the progressive loss of *cdr2l* expression from 16hpf onwards (Léger and Brand, 2002). Despite this difference, over-expression of either *fgf3* or *fgf8a* resulted in an obvious reduction in otic *cdr2l* expression by 18-19hpf. However, the loss of otic *cdr2l* expression, even when persisting in the anterior after loss of *fgf3*, at 26hpf puts into doubt *cdr2l* being involved in defining posterior identity. If this were the case, expression of *cdr2l* would be expected to persist as posterior identity is established. The lack of a clear anterior duplication of *cdr2l* after aberrant activation of Hh signalling, which has previously been shown to result in a strong duplication of posterior otic character, also supports this.

I have also shown that during development *cdr2l* is also expressed in neuronal structures such as the anterior forebrain, the assumed trigeminal placode, ventral hindbrain, lateral neural tube and anterior-dorsal neurons within the trunk, from 20hpf onwards. This may indicate another role for Cdr2l in the regulation of neuronal populations, possibly providing a link with its previously-describe characterisation within cerebellar Purkinje cells (Schubert et al., 2014). However the broad range of structures in which *cdr2l* is expressed during development also makes it difficult to infer how Cdr2l may be regulating neuronal development.

Given the interesting expression profile of *cdr2l*, along with the indication it may play role in determining posterior otic identity, this clearly asks the question - what is Cdr2l's function during otic development? Chapter Four begins to address this by presenting data from embryos where *cdr2l* has been either knocked-down or knocked-out.

3.4 Conclusions

- During early development of the otic placode a broad range of markers with potentially different functions are expressed, with a high proportion being linked to cilia function.
- *Cdr2l* and *nav3a* both represent novel markers of the posterior otic domain.
- *Cdr2l* persists until 26hpf in the anterior otic domain in loss of *fgf3* mutants or after treatment with the pan-Fgf signalling inhibitor, SU5402.
- Over-expression of either *fgf3* or *fgf8a* leads to a down-regulation of otic *cdr2l* expression but this is only clearly apparent at 18-19hpf.
- *Cdr2l* expression does not persist in the anterior otic domain and expression in the lateral neural tube appears unaffected when Hh signalling is aberrantly activated.

Chapter 4

The role of *cdr2l* in otic placode development

4.1 Introduction

CDR2L is a highly coiled, cell-membrane localised member of the cerebellar degeneration-related (CDR) family that has primarily been studied in relation to its role in Paraneoplastic Cerebellar Degeneration (PCD) (Eichler et al., 2013). In this human pathology it is thought that an autoimmune response against a highly-conserved antigenic epitope in CDR2L and CDR2, which share 45% identity in humans and 41% identity in zebrafish, occurs in reaction to ectopic expression of CDR2 within certain tumour types (Corradi et al., 1997; Sakai et al., 1990). The subsequent inhibition of endogenous CDR2L and CDR2 within cerebellar Purkinje cells results in their loss, possibly due to deregulation of calcium homeostasis or the cell cycle within these cells (Schubert et al., 2014; Eichler et al., 2013). However, the expression and function of both *Cdr2l* or *Cdr2* during development have not been reported.

In zebrafish, the dynamic expression of *cdr2l* across the anterior-posterior otic axis during early development, which appears responsive to changes in Fgf signalling, suggested a possible role for *Cdr2l* in otic patterning (Chapter Three). To identify any such function of *Cdr2l*, two approaches to reduce the expression of the wild-type *cdr2l* transcript were used. Firstly a synthetic morpholino oligo was injected into one cell embryos to block translation of *Cdr2l*. Translation-blocking morpholinos function by binding a complementary sequence of the transcript 5' to the translation start, thus sterically blocking binding of the ribosome to the transcript (Summerton, 1999). In zebrafish this has been used to produce gene-specific knock-down up to 50hpf (Nasevicius and Ekker, 2000). However, despite morpholinos representing a quick method for knocking-down genes of interest, their ability to recapitulate phenotypes observed in the corresponding mutant has recently been questioned (Kok et al., 2015). The use of morpholinos is also associated with off-target effects such as general craniofacial defects, trunk abnormalities and heart oedema (Robu et al., 2007; Bedell et al., 2011). These are estimated to occur in around 15-20% of morphants and despite the specificity of the morpholino function being controlled for, such artefacts can be misleading (Bedell et al., 2011).

Advances in generating targeted mutations, in particular CRISPRs, have presented reverse genetics as an alternative to transient knock-down approaches such as morpholinos. Such approaches now have high mutagenesis efficiencies and germline transmission rates along with low associated costs compared to previous reverse genetic techniques such as TILLING (Targeting Induced Local Lesions in Genomes) (Schulte-Merker and Stainier, 2014). Whilst the potential for mutation at off-target sites is still a consideration in CRISPR-generated mutants, this is only thought to occur

in around 1.1-2.5% of injected embryos (Hruscha et al., 2013). Therefore the second approach was to knock-out the wild-type zebrafish *cdr2l* gene by generating stable lines carrying targeted non-sense mutations in *cdr2l* utilising CRISPRs.

Recently, it has been suggested that in deleterious mutants a compensatory network of gene regulation may buffer against the effects of the deletion, which is not seen in morpholino-based knock-down approaches (Rossi et al., 2015). In light of this, comparing the phenotypes observed when *cdr2l* was either knocked-down or knocked-out allowed validation of the phenotypes seen. Given the drawbacks of each approach mentioned above, this therefore represents a comprehensive approach beginning to identify the function of Cdr2l during development.

4.2 Results

4.2.1 *cdr2l* morphant morphology

To knock-down expression of *cdr2l* during otic development, a morpholino (MO) was designed against the sequence upstream of the translation initiation site (+1, Figure 4.1A). Initially 1, 2 and 3nL of this MO at a concentration of 0.9mM (7.6ng/nl) were injected with a Ringer's solution control alongside into wild-type embryos. These were then characterised over five days for their survival and any otic phenotypes. At 2dpf a number of MO-injected embryos across all three injected volumes were observed to have either a single or no otolith phenotype, whereas the majority of the Ringer's injected controls (99%) had two normally-positioned otoliths. Interestingly though, the percentage of embryos having a single otolith at 2dpf appeared consistent across all three injection volumes at 1nl; 34%, 2nl; 40% and 3nl; 32% (Figure 4.1F) which could suggest a general developmental delay rather than a specific response to knock-down of *cdr2l*. However, at 3dpf the single otolith phenotype persisted, with the 1nl-injected batch having a slightly higher percentage, 37% (37/101) with one otolith and the 2nL-injected batch still having 40% (32/80) with one otolith compared to the Ringer's-injected controls, where all embryos (100%) had two otoliths (Figure 4.1A-E').

Despite the persistence of this phenotype at 3dpf, the otic morphology in the morphants with a single otolith generally appeared perturbed showing a lack of pillar formation and/or fusion (Figure 4.2D'), which was also observed to a lesser extent in the 2nL-injected embryos with two otoliths. Given this, along with other non-specific effects such as a smaller head and eyes as well as oedema seen, this perturbation of the pillars could reflect off-target effects commonly reported in morphants (see introduction 4.1). It was also observed that the otic vesicles generally appeared smaller in the morphants, although this may be due these embryos having an overall smaller head when compared to the controls. In embryos injected with a lower volume (0.5nl) of the same concentration (0.9mM) MO, only 9% of embryos had a single otolith phenotype in both ears; however, these embryos also displayed the most severe overall morphological defects (Supplementary Figure 4).

The survival of embryos over the first five days was also recorded (Figure 4.1G) and showed that all three MO injection volumes show a drop in survival at 4dpf, which was not observed in the Ringer's injected controls but the 1nL injection volume have the lowest drop in survival. Interestingly the batch of embryos injected with 2nL of MO showed a greater drop in survival at 4dpf than those injected with 3nL (28% vs 56% at 4dpf, respectively). As the 1nL injection volume gave the highest survival along with a possible otic phenotype this injection volume of the 0.9mM ATG MO was used in all subsequent experiments.

4.2.2 *Cdr2l* morphants show largely unaffected patterning of the anterior-posterior otic axis but a possible reduction in overall length

As otic expression of *cdr2l* appears negatively regulated by Fgf (Chapter 3), a key determinant of anterior otic identity in zebrafish (Hammond and Whitfield, 2011), and *cdr2l* the morphants show a partially penetrant loss of an otolith which could reflect altered otic patterning, markers of the otic anterior-posterior (AP) axis in *cdr2l* morphants were studied. Embryos were injected with either 1nL of a non-specific control MO at 0.9mM or 1nL of the *cdr2l* ATG MO at 0.9mM alongside an uninjected control and raised to either the 18-20ss (approximately 18-19hpf) or Prim-7 (26hpf) stage before being fixed.

18-20ss embryos were assayed for expression of the anteromedial marker, *hmx2* by in situ hybridisation. The *cdr2l* morphants showed no obvious differences in otic *hmx2*, either in strength or localisation, in staining when compared to the uninjected and control MO (Figure 4.2A-C). To confirm this the overall anterior-posterior length of the *hmx2* expression domain for all three conditions was measured from the lateral-most point of expression along the outer otic edge to the most posterior point. This showed no significant difference in the length of the *hmx2* expression domain, as would be expected if the domain was expanded or reduced either laterally or posteriorly, when either the non-specific control or *cdr2l* morphants were compared to the uninjected controls (Supplementary Figure 5).

Similar to *hmx2* the expression domain of the otic non-neural ventrolateral marker, *otx1b*, in Prim-7 staged *cdr2l* morphants did not appear drastically reduced in size or staining intensity relative to the uninjected and non-specific MO controls (Figure 4.2D-F). However, as the *otx1b* staining appeared irregular in shape in a number of embryos, for all injection conditions the percentage length of the expression domain relative to the overall anterior-posterior length was measured. To do this an ROI was bounded to the laterally imaged otic vesicles and the distance from the anterior edge to the posterior edge measured. Then the domain of *otx1b* staining was measured from the anterior-most to the posterior-most point and this value was then normalised against the total anterior to posterior length. This confirmed that the normalised anterior to posterior length of otic *otx1b* staining in the *cdr2l* morphants was not significantly different from the uninjected controls, with the non-specific controls also not differing significantly when compared to the uninjected (Supplementary Figure 6).

Few markers of posterior otic character have been identified but of these *fsta* has been previously shown to be associated with posterior otic character (Hammond and Whitfield, 2011). In the Prim-7 staged *cdr2l* morphants staining for *fsta* in 55% (6/11) appeared strikingly stronger within the medial hindbrain compared to the uninjected and non-specific controls (Figure 4.2G compared to I). Whilst staining in the posterior otic vesicle was present in all *cdr2l* morphants, the strength of staining appeared reduced, although possibly stronger within the mesenchyme just posterior to this (Figure 4.2I compared to G and H). Staining in the remaining 45% (5/11) of morphants showed staining within the hindbrain similar to that seen in the uninjected and non-specific controls and again, whilst staining was present within the posterior otic vesicle, it appear reduced in strength (Figure 4.2J).

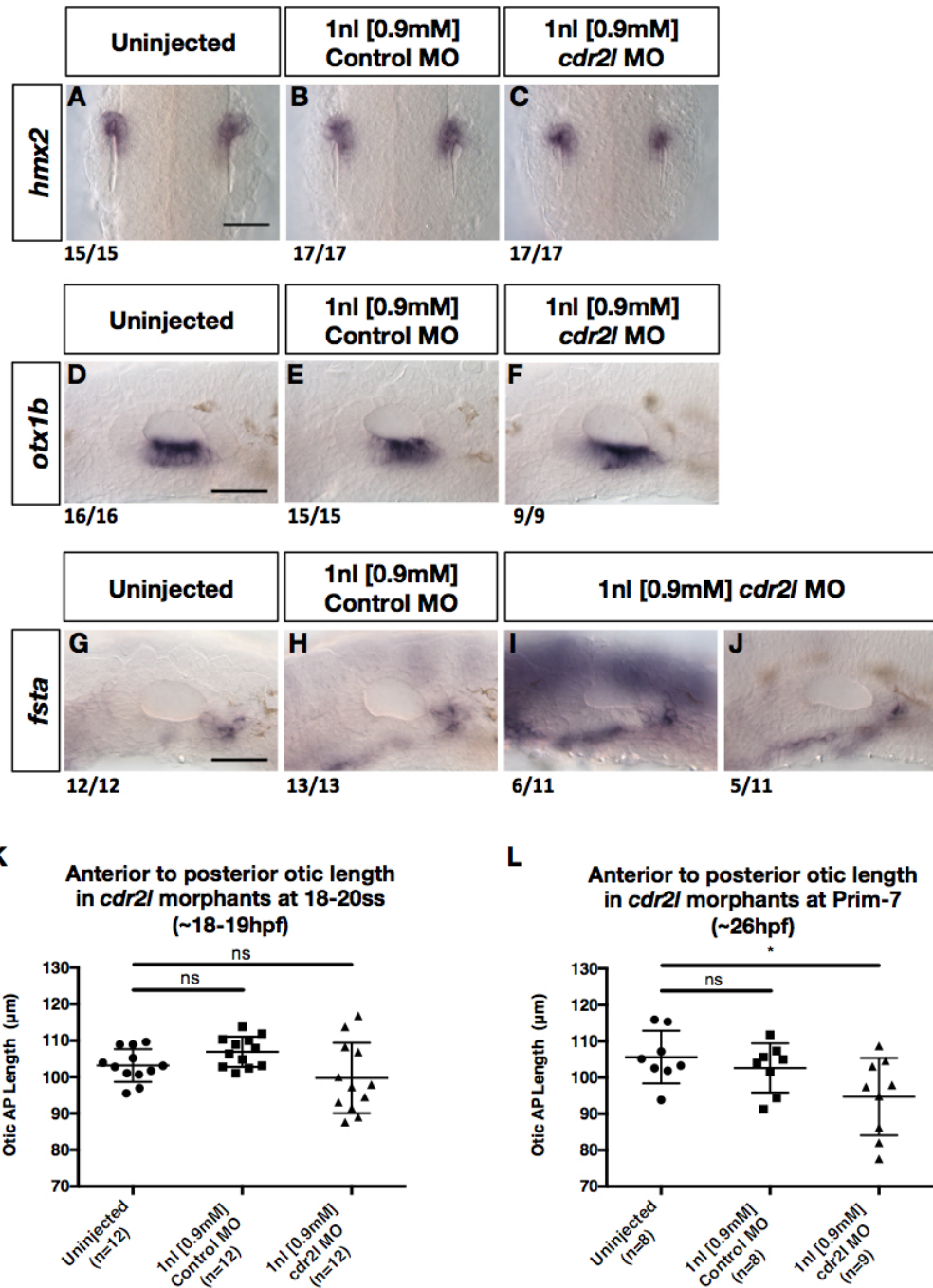


Figure 4.2: *cdr2l* morphants show no abnormal patterning of the anterior otic marker, *hmx2* or the ventrolateral otic marker, *otx1b* but the posterior otic marker, *fsta*, appears abnormal

(A–C) *hmx2* expression in *cdr2l* morphants at 18–20ss does not appear obviously expanded in the *cdr2l* morphants. (D–F) The domain of *otx1b* expression also does not appear strikingly different or expanded in the prim-7 staged morphants. (G–J) *fsta* staining in 6/11 morphants (I) appeared up-regulated within the medial hindbrain compared to both controls with expression within the posterior otic vesicle appearing reduced. Staining in the remaining 5/11 morphants (J) showed staining within the hindbrain similar to that seen in both controls with staining in the posterior otic vesicle again appearing slightly reduced. (K) Measurement of the anterior to posterior otic length for both ears from dorsal imaged 18–20ss embryos. This shows a significant difference in the mean AP length although post-hoc testing for multiple comparison to the uninjected control shows no significance (one-way ANOVA $p=0.0388$, Holm-Sidak adjusted $p=0.3182$ and 0.3182). (L) Measurement of the anterior to posterior otic length for Prim-7 (26hpf) embryos. This shows a significant difference between the mean AP length of the uninjected and *cdr2l* MO injected embryos (one-way ANOVA adjusted $p=0.0280$ with Dunnett's multiple comparison). N= number of individual embryos measured. In K, both ears were measured from 6 dorsal images for each condition (a total of 12 data points), whereas in L only the left ears could be measured due to the lateral perspective. A–C are dorsal views with all other images being lateral views. All images were taken using DIC with a 40x objective. Scale bars in A, D and G: 50μM.

The anterior to posterior length of the otic vesicle was also measured for all three injection conditions by bounding imaged otic vesicles with a Region Of Interest (ROI) within ImageJ and measuring from the anterior to posterior edges of this. For 18-20ss staged embryos, a significant difference in length between the conditions was found with the morphants having a smaller mean than either the uninjected and non-specific controls. However a multiple comparison test showed no significant difference between either the *cdr2l* morphants or non-specific controls when compared to the uninjected (Figure 4.2K). There was a significant difference in the variation between the groups (Brown-Forsythe $p=0.0222$ ** and Bartlett's $p=0.0072$ *); the standard deviation (SD) for the *cdr2l* morphants ($9.648\mu\text{m}$) was more than double that of the non-specific ($4.142\mu\text{m}$) and uninjected ($4.503\mu\text{m}$) controls (Figure 4.2L). The Prim-7 (26hpf) staged embryos also showed a significant difference in length between conditions, with the morphants again having a smaller mean AP length than both the control conditions. A multiple comparison test also identified a significant difference between the uninjected and *cdr2l* morphants but not the non-specific MO control. Interestingly, unlike the 18-20ss embryos, the difference in variance was not significant (Brown-Forsythe $p=0.4175$ and Bartlett's $p=0.4118$) although the *cdr2l* morphants did show a greater SD ($10.66\mu\text{m}$) when compared to the non-specific ($6.774\mu\text{m}$) and uninjected controls ($7.281\mu\text{m}$).

4.2.3 Markers of the delaminating otic neuroblasts and their subsequent differentiation display a modest reduction in expression in the *cdr2l* morphants

Alongside its role in determining and maintaining anterior identity, Fgf signalling, which appears to negatively regulate *cdr2l*, is also thought to positively regulate the number of neuroblasts that delaminate from an anteroventral otic domain (Maier and Whitfield, 2014). Given this, the expression of *neurog1*, a marker of delaminating otic cells destined to form the statoacoustic ganglion and *neurod1*, a marker of cells subsequently completing neuronal differentiation within the *neurog1*-expressing population (Andermann et al., 2002; Korzh et al., 1998) were assayed by in situ hybridisation in *cdr2l* morphants. In *cdr2l* morphants staged at 20-21ss (approximately 19-20hpf), *neurog1* staining is still observed within a similar anterior otic domain to the uninjected and non-specific controls (Figure 4.3A-C') and expression in the head and trunk also appears relatively consistent between all conditions (not shown). However, in the majority (70%, 33/47) of *cdr2l* morphants otic *neurog1* staining appeared slightly weaker and patchy when compared to the uninjected and non-specific controls (Figure 4.3C compared to A and B). *Neurod1* staining in high-pec staged (approximately 42hpf) *cdr2l* morphants in the domain anterior to the otic vesicle, appeared grossly similar in position as did staining posterior to the otic vesicle when compared to the uninjected and non-specific controls (Figure 4.3D-F). Interestingly, the domain of *neurod1* staining that extends anteriorly to the otic vesicle, likely comprised of the statoacoustic ganglion, the anterior lateral line ganglia and facial ganglion, does appear slightly reduced in overall size in the morphants compared to the controls, although this could reflect the morphants being smaller overall (Andermann et al., 2002).

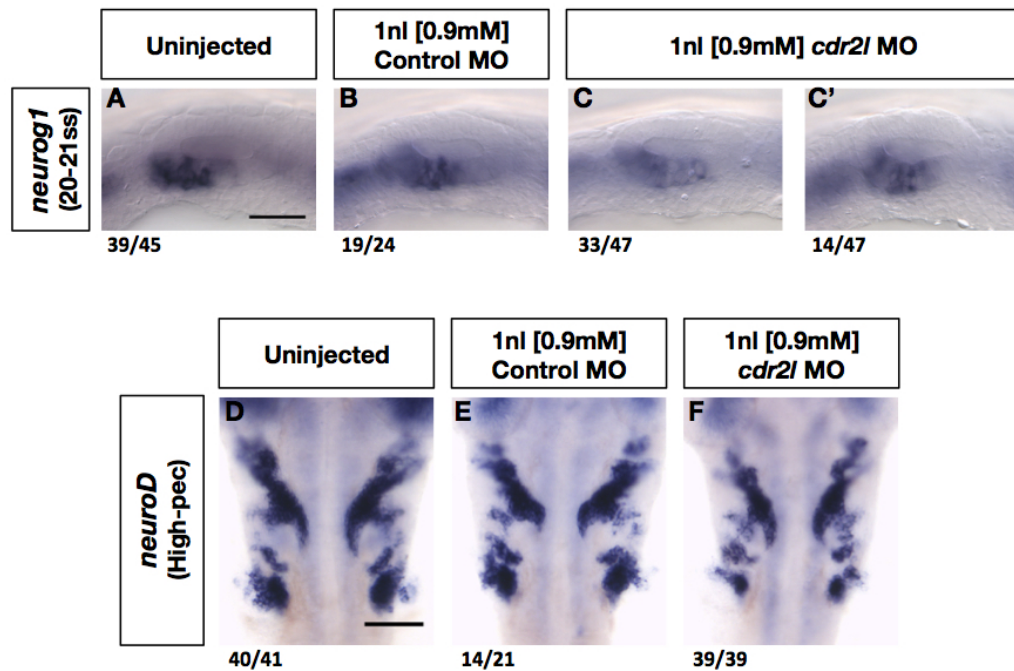


Figure 4.3: Cdr2l morphants show weakened neurog1 staining with a possible reduction in the anterior otic domain of neurod1 expression

(A–C') Expression of neurog1, a marker for delaminating otic neuroblasts, in uninjected (A), non-specific MO injected (B) and 0.9mM *cdr2l* MO injected (C & C') embryos at 20–21ss (approximately 19hpf).

(D–F) Expression of neurod1, a marker of neuronal differentiation, neuroblasts in uninjected (D), non-specific MO injected (E) and 0.9mM *cdr2l* MO injected (F & F) embryos at the high-pec stage (approximately 42hpf). A–C' were taken using DIC microscopy with a 40x objective and D–F using DIC microscopy with a 10x (1.6 mag) objective. Scale bars: A; 50 μ M and D; 100 μ M.

4.2.4 *Cdr2l* morphants have no apparent vestibular defects but a possible swim-bladder inflation phenotype by 5dpf

The zebrafish sensory maculae, in particular the utricle, are known to be required for detection of vestibular stimuli (Riley and Moorman, 2000). Defects either in the sensory epithelium itself or through their disrupted innervation result in a clear dysfunction in detecting vestibular stimuli (Kwak et al., 2006; Whitfield et al., 2002). Therefore if *cdr2l* plays a role in the development of either the sensory domains themselves or the neurogenic otic domain, the loss of *Cdr2l* in the morphants should dampen their response to vestibular stimuli.

Using a protocol previously published by Kwak et al, 2006 to test the vestibular response of larvae, *cdr2l* morphants injected with 1nL of 0.9mM MO were tested for their ability to respond to tap stimuli from a seeker handle (motor coordination test) and whether they were capable of balancing dorsal side up, one minute after this stimulus (balance test). All embryos were tested three times and were only scored as a fail if they did not respond or subsequently stay upright for two or more of the three tests (Figure 4.4A and B). In the motor coordination test, a subset of the *cdr2l* morphants tested failed to either respond or do so in a stereotypical manner (10%, 1/10) but this was not significantly different when compared to the number of non-specific control

MO-injected embryos that failed (7%, 1/15), with none of the uninjected controls failing (0/15) (Figure 4.4A). In the balance test, *cdr2l* morphants did show a higher number of embryos that were unable to balance after one minute, instead resting on their sides (40%, 4/10). Yet when compared to the control MO (13%, 2/15 failed) this higher percentage in the *cdr2l* morphants was not significantly different (Figure 4.4B).

Another suggested indicator of impaired motor function, although not necessarily impaired otic function, is a lack of swim bladder inflation due to the larvae being unable to reach the air-water interface (Riley and Moorman, 2000). In larvae injected with 1nL of 0.9mM *cdr2l* MO there was a significant association with a non-inflated swim bladder when compared to the uninjected controls (55% (6/11) vs 6% (1/17), $p=0.0069$, odds ratio=19.20) (Figure 4.4C). There was no such association seen when the non-specific control was compared to the uninjected controls (6% (1/16) vs 6% (1/17), $p=1.0000$), suggesting that the *cdr2l* morphants may have a reduced ability to inflate their swim bladders.

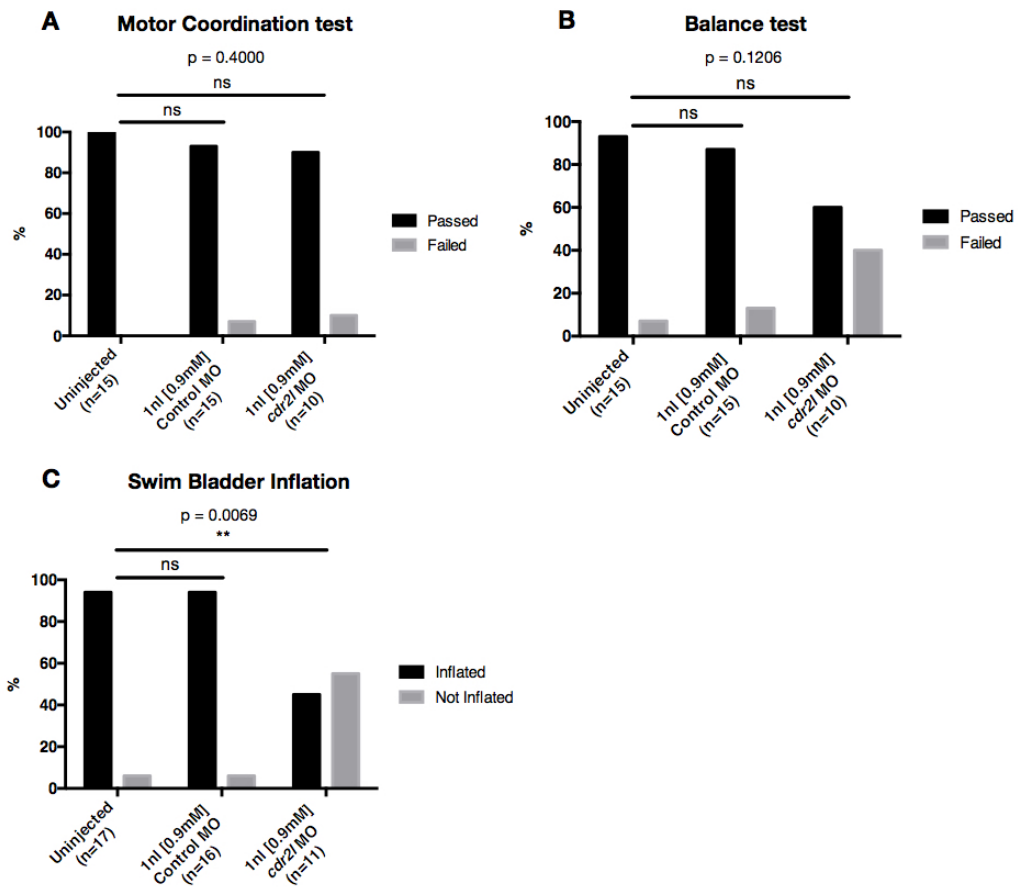


Figure 4.4: *cdr2l* morphants at 5dpf show no significant vestibular defects but reduced swim bladder inflation. Assessment of (A) motor coordination, (B) balance and (C) swim bladder inflation at 5dpf in uninjected embryos, non-specific control MO and 0.9mM *cdr2l* morphants. A two-tailed Fisher's exact test was used to separately compare the outcome count data from the uninjected controls to the control MO and 0.9mM *cdr2l* injected embryos for all tests.

N= number of individual larvae tested.

4.2.5 The *cdr2l* ATG morpholino inhibits translation of the *cdr2l* CDS *in vivo*

A CDR2L-eGFP fusion construct (pCS2+);

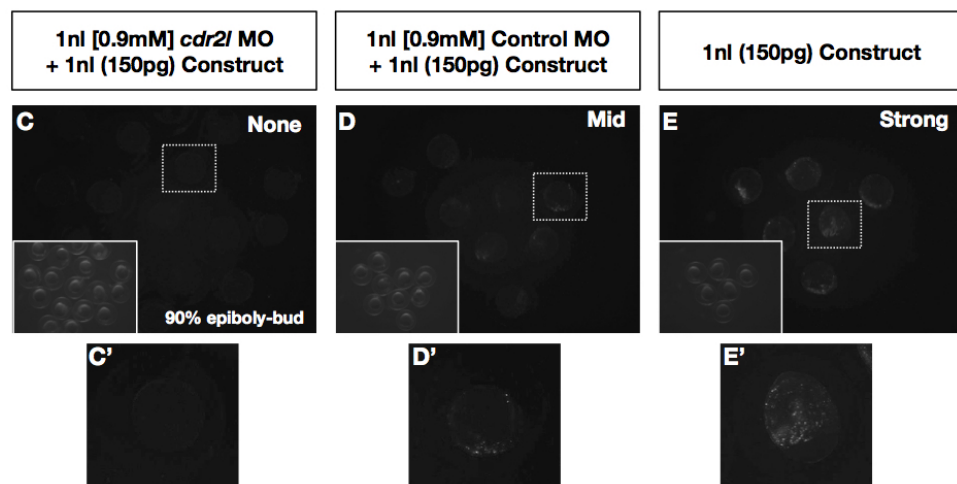
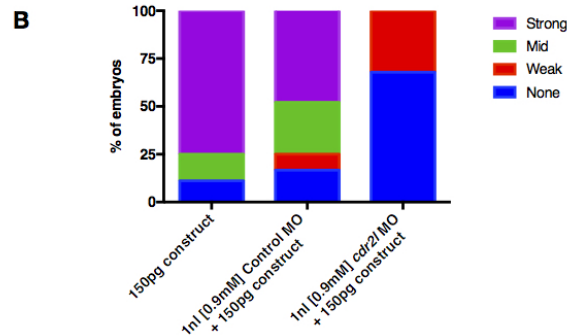


Figure 4.5: Co-injection of the *cdr2l* MO inhibits translation of a CDR2L-eGFP fusion construct

In vivo efficacy assay for *cdr2l* ATG morpholino binding and blocking. (A) Schematic of the CDR2L-eGFP fusion construct with the 5' morpholino binding sequence. (B) Graph of fluorescence phenotypes in construct-injected embryos after injection with either the non-specific control morpholino or the *cdr2l* morpholino. Embryos were grouped according to fluorescence, with (C, C') representing embryos grouped with no observable fluorescence, (D, D') having mid-strength fluorescence and (E, E') having strong fluorescence. Insets for C, D and E show bright-field images of the main panels with dotted-ROIs corresponding to magnified images C', D' and E', respectively. C-E were taken using 9x magnification. N= number of individual embryos.

As the *cdr2l* morpholino phenotype appeared subtle with no striking effect on otic development despite its strong expression during early otic development (Chapter three), I wanted to confirm that the morpholino, at the concentration being injected, did inhibit *cdr2l* translation *in vivo*. To test this, a construct was synthesised which contained the coding sequence (CDS) for *cdr2l*, including the 5' morpholino binding site, fused to the coding sequence for eGFP, and driven by a CMV promoter to allow constitutive expression of the fusion construct when injected at the one-cell stage (Figure 4.5A). 150pg of this construct were then injected either alone or alongside the non-specific control or the *cdr2l* morpholino and the embryos assessed for eGFP fluorescence at the 90% epiboly/bud stage (approximately 9-10 hours after injection) (Figure 4.5B).

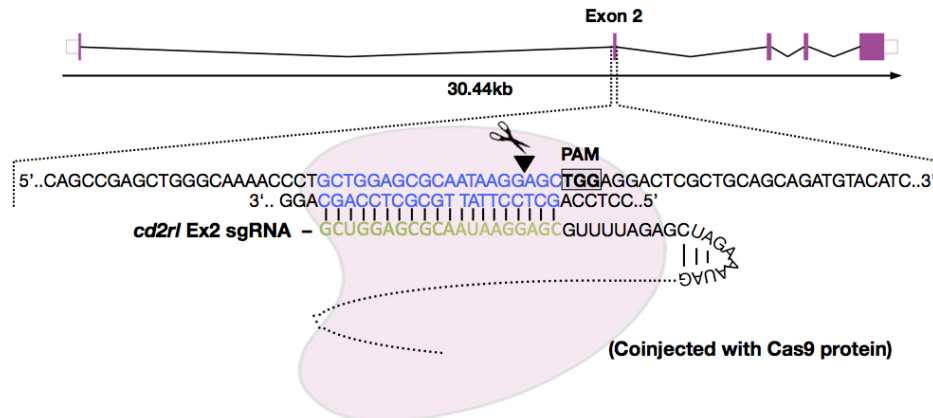
In embryos injected with 150pg of construct and 1nL of 0.9mM *cdr2l* morpholino, strong or mid-strength eGFP fluorescence was not seen (0%, 0/56) whereas a high percentage of embryos showed this degree of fluorescence in both the construct-injected (89%, 32/36) along with the construct and non-specific MO-injected (75%, 36/48) embryos (Figure 4.5C compared to D and E). This confirms that the *cdr2l* morpholino is capable of inhibiting translation of the *cdr2l* CDS-containing construct *in vivo* and therefore is also likely functioning to knock down endogenous *cdr2l* translation.

4.2.6 Generation of *cdr2l* CRISPR mutants

Due to this being the first reported knock-down of *cdr2l* in zebrafish and the issues associated with the use of morpholinos, in particular off-target effects and a lack of correlation with the corresponding mutant in the phenotypes reported, a *cdr2l* mutant was generated using CRISPR mutagenesis to confirm the subtle phenotypes in the variation of AP otic length and swim bladder inflation observed (Kok et al., 2015). The CRISPR system uses a guide RNA designed to a 20bp genomic target sequence adjacent to a protospacer adjacent motif (PAM) trinucleotide which when present with the protein Cas9 *in vivo* forms a complex around the genomic DNA, complementary to the target sequence and produces double stranded breaks. When these are repaired through non-homologous end joining there is a likelihood of insertions or deletions occurring (Hruscha et al., 2013).

For *cdr2l*, a guide RNA was designed to target exon 2 of the *cdr2l* genomic sequence (Figure 4.6A) and within the F1 generation generated using this guide RNA two mutations, a 4bp deletion and a five bp insertion along with a single bp deletion 5' to this (referred to as 5/1 InDel), were identified. Both of these mutations were predicted to produce frameshifts in the coding sequence resulting in a premature stop codon (Figure 4.6B). F1 fish carrying these mutations were used as founders to generate a stable heterozygous F2 line for each allele and when incrossed it was expected that 25% of the embryos would be homozygous for the mutations based on Mendelian inheritance.

A CRISPR design and *cdr2l* - exon 2 target sequence;



B Identified F1 *cdr2l* mutant alleles and their predicted peptide sequence;

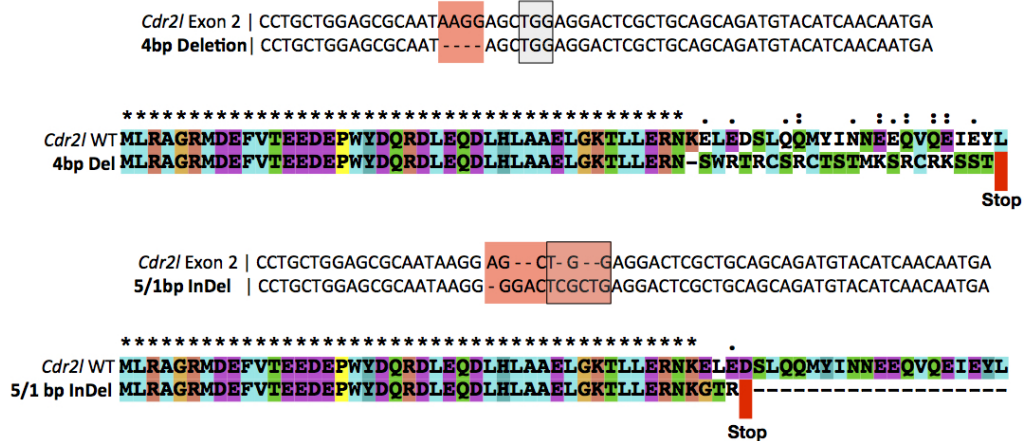


Figure 4.6: *cdr2l* exon 2 CRISPR design and identified alleles (A) Schematic of *cdr2l* exon structure and the 20bp guide sequence designed to recognise base pairs 34-54 of exon 2 (in blue) when transcribe as a single guide RNA (sgRNA, in green) with the scaffold sequence. In the presence of Cas9, this sgRNA should induce a double strand break approximately 3bp (black arrow) up-stream of the protospacer adjacent motif (PAM, grey box). (B) From the F1 population two mutant alleles were identified for carrying forward. A 4bp deletion (red box), 3bp upstream of the PAM (grey box), which is predicted to produce a frameshift within exon 2 and a premature stop codon at the start of exon 3, residue 66. Also a 5/1bp insertion/deletion (red box) within and upstream of the PAM (grey box), which is predicted to produce a frameshift within exon 2 and a premature stop codon at the end of exon 2, residue 47. Peptide sequence predicted with ExPASy (SIB) and aligned in MUSCLE (EBI).

4.2.7 *Cdr2l* mutants do not show any otolith, vestibular or swim bladder defects but do have a reduced anterior-posterior otic vesicle length

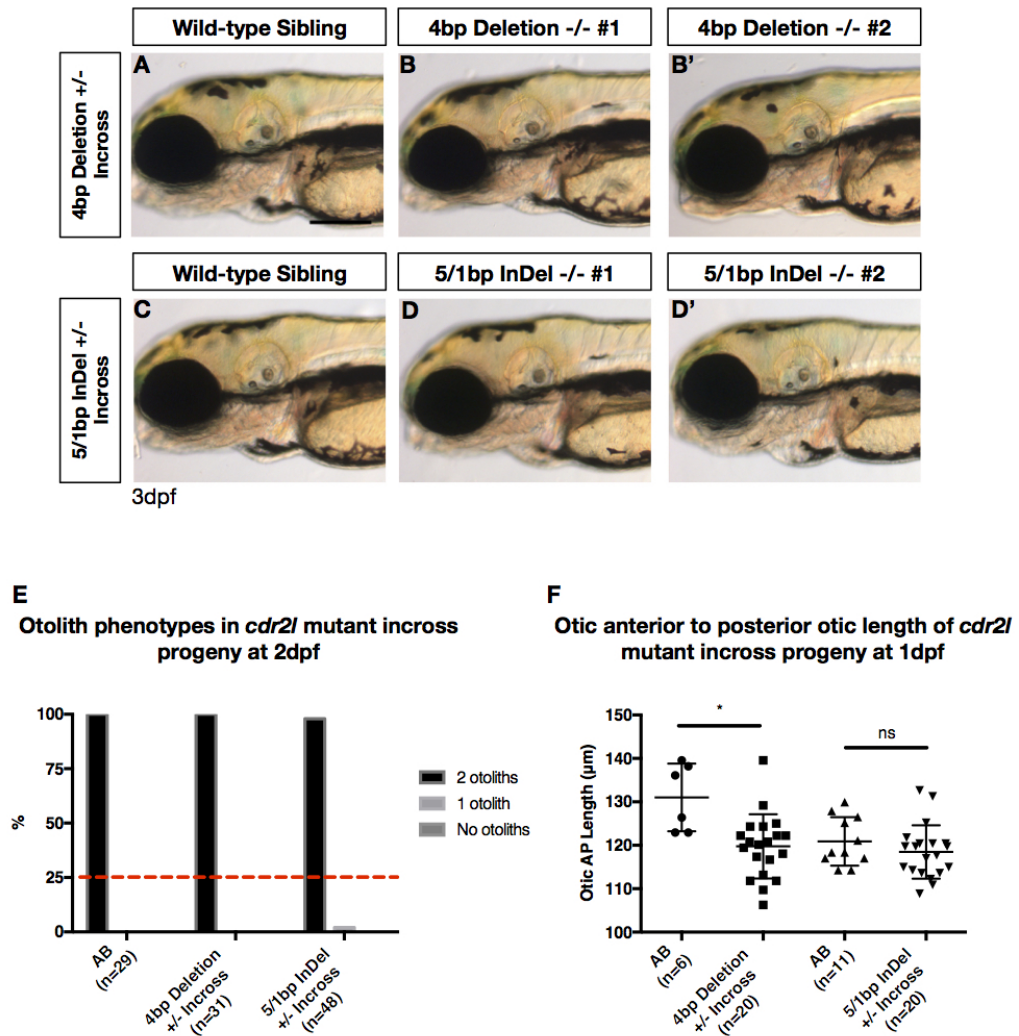


Figure 4.7: Neither the *cdr2l* 4bp deletion or the 5/1bp InDel mutant alleles show obvious otic morphological defects but may show a reduction in anterior to posterior length at 1dpf (A–D') Live images of 3dpf embryos. 4bp Deletion +/- incross sibling (A) and mutants (B–B') and 5/1bp InDel +/- incross sibling (C) and mutants (D–D'). (E) Otolith phenotypes at 2dpf in wild-type, 4bp Deletion incross and 5/1bp InDel incross progeny. There is no obvious change in otolith number in either allele, with neither the 1 otolith or no otolith phenotypes reaching 25% (red dotted line) as would be expected if a fully penetrant mutant phenotype. (F) Measurement of the anterior to posterior length of live, laterally-imaged; AB wild-types, 4bp deletion incross and 5/1bp InDel incross progeny at 1dpf. 4bp deletion progeny have a significantly shorter AP length than their wild-type counterparts (t test $p=0.0139$, $t=3.141$ $df=7.927$), whereas the 5/1bp InDel progeny have a shorter mean than their wild-type counterparts but this is not significant (t test $p=0.2742$, $t=1.121$ $df=22.55$). All images are lateral views taken with a 4x (2x mag) objective using DIC microscopy. Scale bars: A; $150\mu\text{M}$. N= number of individual embryos.

Progeny from heterozygous incrosses of both alleles showed no increase in mortality at 0dpf compared to wild-types or by 3dpf (Supplementary Figure 7). This suggests that homozygous *cdr2l* mutants for both alleles are likely viable. No obvious morphological abnormalities either within the ear or in general were observed in either allele by 3dpf (Figure 4.7A-D). When assessed for otolith number at 2dpf, following the observation that a number of *cdr2l* morphants had either single or no otoliths at a similar time point, both alleles showed the majority of embryos (4bp Del; 100%, 31/31 and 5/1bp InDel; 98%, 47/48) to have the expected number of otoliths with a similar distribution of phenotypes to the AB wild-type controls (100%, 29/29) and well below the 25% expected for any fully penetrant mutation (Figure 4.7E).

As *cdr2l* morphants also showed either a reduced anterior to posterior (AP) otic length or greater variation in this length (Chapter 3), twenty progeny from a heterozygous incross for both alleles were imaged at 1dpf and their otic AP length measured (Figure 4.7F). Wild-type embryos were imaged for comparison less than an hour before for 5/1bp InDel progeny and less than an hour after for 4bp deletion progeny. Interestingly, the embryos from the 4bp deletion incross showed a significantly smaller AP length when compared to the AB wild-type embryos ($119.8\mu\text{m} \pm 1.656$ vs $131.0\mu\text{m} \pm 3.179$), although there was no significant difference in variation (F test $p=0.7799$). For the 5/1bp InDel incross, embryos also had a smaller mean AP length than their AB counterparts ($118.5\mu\text{m} \pm 1.375$ vs $120.9\mu\text{m} \pm 1.681$). However, this reduction was not significant, with the difference in variation also being non-significant (F test $p=0.7742$).

To test whether *cdr2l* mutants displayed any abnormal vestibular response, given the slightly increased failure rate in the morphants, embryos at 5dpf from a 4bp deletion heterozygote incross were observed for their response and subsequent ability to balance after tap stimuli. For both the motor coordination and balance tests the majority of the incross embryos passed, with only 2% (1/48) failing the motor coordination test and none failing the balance test (Figure 4.8A and B). As 25% of the incross embryos are expected to be homozygous mutants, the low fail rate suggests that there are no strong vestibular defects in the homozygous mutants. A negative control, where 4bp deletion incross embryos were anaesthetised in a 1:25 dilution of tricaine was also run alongside. Within this group, 0% (0/12) passed the motor coordination test and only 25% (4/12) passed the balance test (data not shown).

cdr2l morphants were also observed to have a significantly higher percentage of non-inflated swim bladders at 5dpf when compared to the uninjected AB controls. However, in 5dpf larvae from both a 4bp deletion +/- incross and a 5/1bp InDel +/- incross, the number of larvae with non-inflated swim bladders (4%, 1/26 and 7%, 6/85 respectively) was not significantly different to the AB wild-type controls (11%, 3/28).

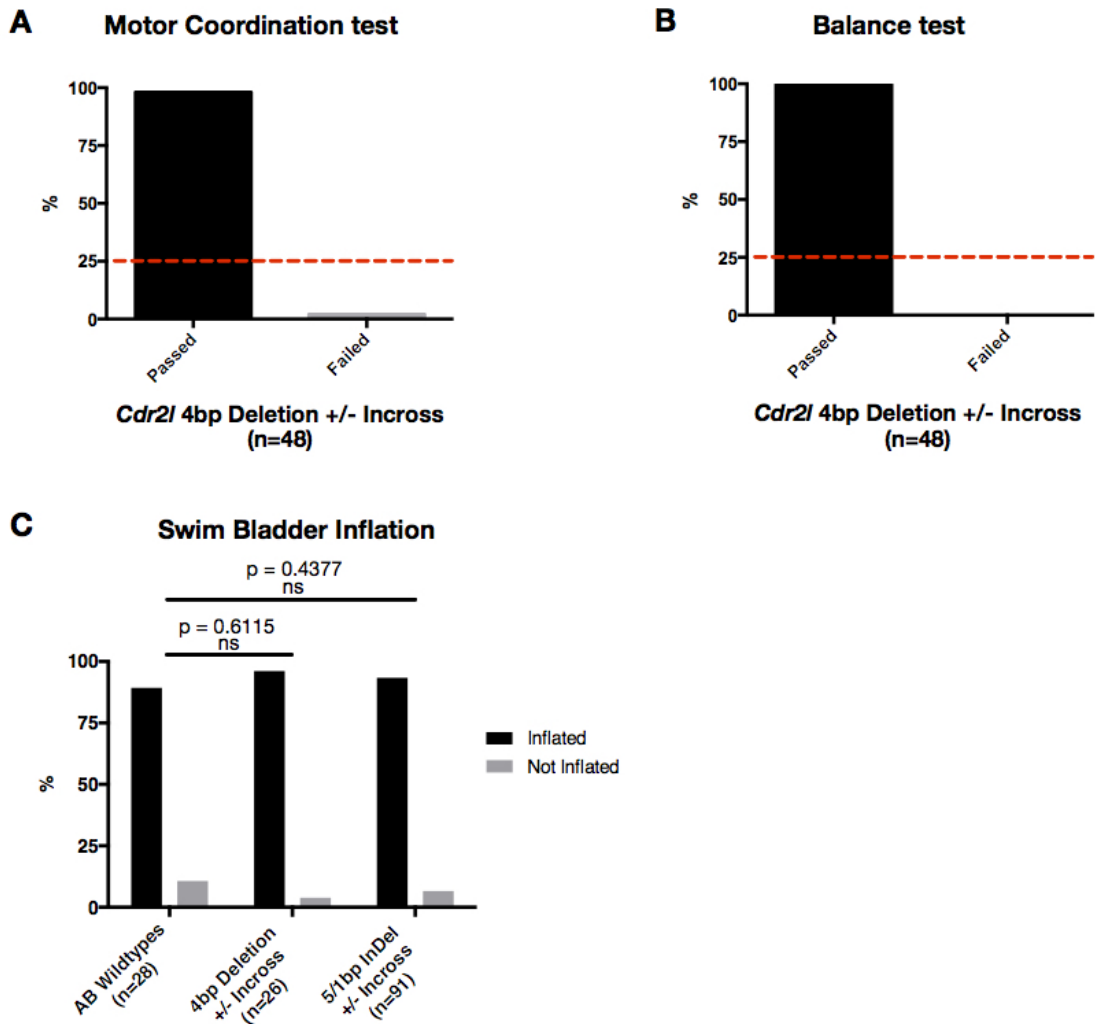


Figure 4.8: *cdr2l* 4bp deletion mutants at 5dpf show no obvious vestibular defects and neither the 4bp deletion or 5/1bp InDel alleles show a significant reduction in swim bladder inflation

Assessment of (A) motor coordination, (B) balance at 5dpf in progeny from a heterozygous *cdr2l* 4bp deletion incross suggest no obvious vestibular defects in the mutants, as less than 25% (expected number of mutants based on Mendelian inheritance, red dotted line) of embryos failed. Embryos were scored after observation of response to three, separate tap tests. (C) Swim bladder inflation in progeny from a heterozygous incross for both *cdr2l* mutant alleles compared against AB wild-type larvae shows no significant association between genotype and swim bladder inflation. A two-tailed Fisher's exact test was used to separately compare the outcome count data from the wild-types to the 4bp deletion and 5/1bp indel progeny. N = number of individual larvae tested.

4.2.8 *Cdr2l* 4bp deletion mutants show a loss of *cdr2l* full-length wild-type transcript by 14-16ss but no up-regulation of the potential paralogue *cdr2a*

The homozygous subset of embryos from the 4bp deletion heterozygous incross should have reduced or no transcription of the full-length wild-type *cdr2l* transcript due to the presence of the mutant sequence predicted to encode an early stop in exon 2, which should lead to the mutant transcript being degraded via non-sense mediated decay (Jopling, 2014). To determine whether this is the case, 14-16ss (approximately 16-17hpf) embryos from a 4bp deletion incross were assessed by in situ hybridisation for expression of the entire 1.39kb wild-type *cdr2l* transcript. In 38% (23/60) of embryos, staining for *cdr2l* was dramatically reduced in all regions in which it is normally expressed (Figure 4.9B compared to A) and this loss was consistently seen across two independent experiments. This suggests that in a subset of embryos, likely to be homozygous mutants, the full-length *cdr2l* transcript is not present. Based on this, the anterior to posterior (AP) otic length in nine embryos where *cdr2l* staining was lost was measured using an ROI bounded to the dorsally imaged otic vesicle. This was to observe whether in these embryos where expression of the *cdr2l* transcript is lost, if there is a reduction in otic AP length consistent with that previously observed in both the morphants and heterozygous mutant incrosses (Figure 4.9C). The *cdr2l* 4bp deletion (presumed homozygous) mutants showed a smaller mean length although this was not significantly different when compared to the siblings with strong wild-type *cdr2l* staining ($97.48\mu\text{m} \pm 2.522$ vs $98.95\mu\text{m} \pm 1.297$). However, there was a significant difference in the compared variances (F test $p=0.0090$, SD = $5.505\mu\text{m}$ vs $10.70\mu\text{m}$). Interestingly, this slight reduction in AP length with a significantly higher variation in length is similar to that observed in the *cdr2l* morphants (Figure 4.2).

A predicted paralogue of *Cdr2l* is *Cdr2a* (Ensembl), which shares 75% transcript identity over 26% of the *cdr2l* transcript with 75% identity over a region spanning exons 1 to 4 (out of 5) (Figure 4.9D). As it has been suggested that in deletion mutations, functional compensation is more likely than in knockdowns, such as morphants (Rossi et al., 2015), I wanted to confirm whether expression of *cdr2a*, as a potential paralogue of *Cdr2l*, was up-regulated in the 4bp deletion mutants. To confirm this an in situ hybridisation for *cdr2a* was carried out with 16hpf (14ss) progeny from a 4bp deletion heterozygous incross, which showed that *cdr2a* does not appear to be up-regulated in the mutant otic vesicle or expressed in the wild-type siblings, as none of the embryos showed any staining (Figure 4.9E). This is consistent with previous in situ hybridisation results using different *cdr2a* probes, which have shown that *cdr2a* does not obviously show any strong localised expression in the developing zebrafish.

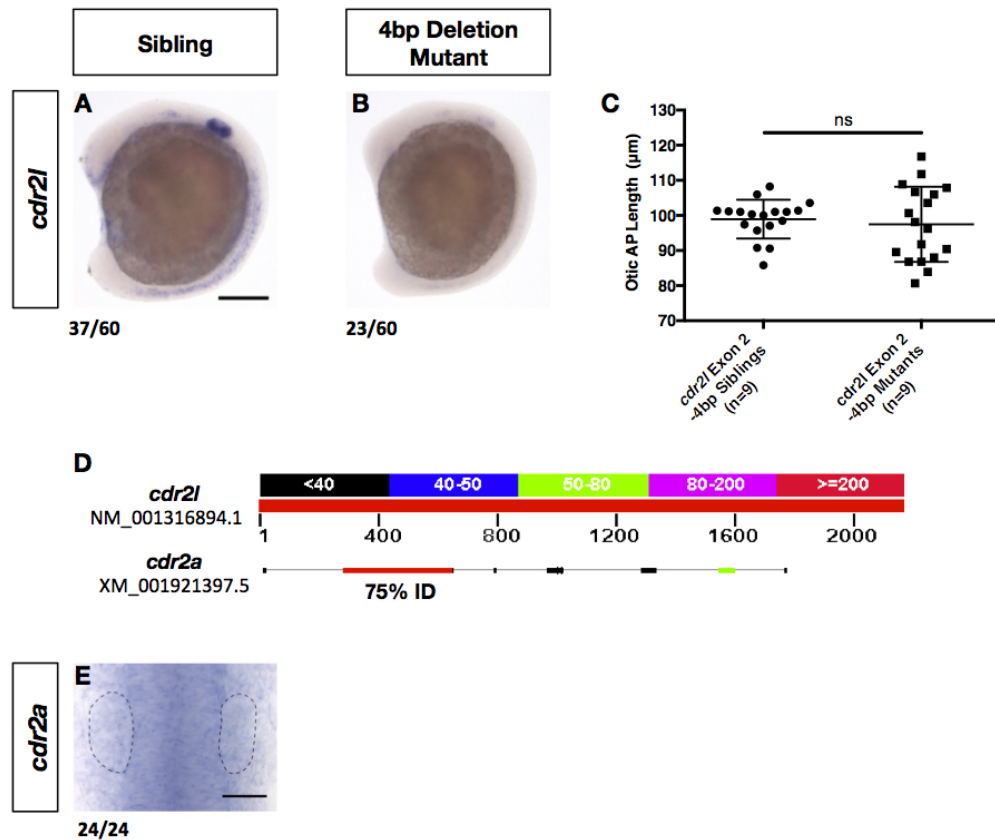


Figure 4.9: *cdr2l* 4bp deletion mutants show a reduction in *cdr2l* staining, which does not correlate with a significant difference in otic length or up-regulation of the possible paralogue, *cdr2a*

(A-B) Staining for *cdr2l* in 14-16ss (16–17hpf) embryos from a *cdr2l* 4bp deletion +/- incross, where 38% of embryos show a striking reduction in *cdr2l* staining (B). (C) The otic anterior to posterior length does not differ significantly between embryos showing staining (siblings) and those not (mutants) (t-test $p=0.6100$, $t=0.5165$ $df=25.41$), although there was a significant difference in variance (F test $p=0.0090$). (D) mRNA nucleotide BLAST alignment of the possible paralogue, *cdr2a* to *cdr2l*. (E) Staining for *cdr2a* in 14ss (16hpf) embryos from a *cdr2l* 4bp deletion +/- incross where all embryos showed no obvious otic staining or strengthening of staining. A and B were taken with a 4x (2x mag) objective and E with a 40x objective using DIC microscopy. Scale bars: A; $200\mu\text{M}$ and E; $50\mu\text{M}$. N= number of individual embryos. For C, both ears were measured from dorsal images (a total of 18 datapoints).

4.2.9 Otic expression of the positive cell cycle regulator *mycb* was not clearly altered in *cdr2l* mutants

The human protein, Cerebellar Degeneration Related protein 2 (CDR2), has previously been shown to directly interact with the cell cycle regulator C-MYC through a helix-leucine zipper motif, which leads to a reduction in C-MYC activity (Bretones et al., 2015; Okano et al., 1999; Fathallah-Shaykh et al., 1991). Alignment of the human CDR2 (NP 1793.1) peptide sequence to the zebrafish Cdr2 (XP 5169488.1) and Cdr2l (NP 1303823.1) sequences shows that all the leucine residues that form the helix-leucine zipper motif suggested to interact with c-Myc are conserved in the same position

(Figure 4.10E-G). Within these *mycb*-stained embryos, 69% (25/36) showed weak otic staining with the remaining 31% (11/36) showing strong staining within the posterior otic domain similar to that observed in the AB wild-types. However, when a subset of these embryos were genotyped, nine from each group, two homozygous mutants were identified in those embryos showing strong posterior otic staining (11/36) and one identified in the weak group (25/36) (Figure 4.10F and G). Wild-type siblings also found in both groups, although a higher number showed strong posterior otic staining (11/36)(Figure 4.10E). This suggests that loss of *cdr2l* in the 4bp deletion mutants does not have a clear effect on expression of *mycb* RNA at this time point.

4.2.10 Expression of *neurog1*, *neurod1* and *fsta* in the *cdr2l* mutants

It was also planned to observe expression of *neurog1*, *neurod1* and *fsta* in the mutants to confirm the phenotypes previously observed in the morphants. Unfortunately, due to time constraints this data could not be included within this thesis. However, preliminary data for *fsta* expression in embryos from a 4bp deletion +/- incross, suggests the strong up-regulation of *fsta* within the medial hindbrain seen in a subset of the morphants is not recapitulated in the mutants. Given the *cdr2l* mutants appear homozygous viable, adult homozygous mutants are being identified to generate greater numbers of homozygous embryos for future work, including conformation of the previous morphant phenotypes.

4.3 Discussion

This chapter has focused on data investigating the function of Cdr2l during otic development using two different approaches, morpholino-mediated knock-down and generation of *cdr2l* knock-out mutants using targeted CRISPR mutagenesis.

In *cdr2l* morphants the expression of markers associated with specifying the anterior and the ventral otic domains do not appear expanded or altered. However, otic expression of *fsta*, a BMP antagonist previously reported as a posterior otic marker, appeared reduced within the morphants vesicles (Figure 4.2J) (Erickson et al., 2010; Hammond and Whitfield, 2011). Whilst 55% of morphants also appeared to show an up-regulation of *fsta* within the hindbrain and mesenchyme abutting the posterior of the vesicle, a similar striking up-regulation was not observed in the 4bp deletion mutants (data not shown). Interestingly, such strong expression of *fsta* within the hindbrain was not reported in 19 or 30hpf embryos, making it unlikely this is reflecting a developmental delay in the morphants (Erickson et al., 2010; Hammond and Whitfield, 2011). The role of *fsta* within the posterior otic domain is unknown but is likely linked to the expression of *bmp7* within a similar domain at this time (Mowbray et al., 2001). In zebrafish, otic Bmp7a has been suggested to mediate the positive regulatory effect of Tfap2a on neuronal differentiation within the ventral domain (Kantarci et al., 2015). Interestingly, a gradient of Bmp7 has also been reported to be involved in defining the tonotopic axis in the chick basilar papilla in response to Hh signalling, although this does not appear to be conserved in mice (Mann et al., 2014; Son et al., 2015). Therefore the slight down-regulation of otic *fsta* seen in the morphants may reflect a requirement for Cdr2l in maturation or maintenance of the posterior otic domain rather than its specification. This is supported by the lack of posterior expansion seen in the expression of *hmx2* and *otx1b* in the morphants. Given the low numbers and differing phenotypes in the morphants, repeats of this experiment to gain higher numbers would be ideal both in the morphants and mutants. In the morphants, observing expression at later time points would also help confirm, in conjunction with the mutants, whether the up-regulation within the hindbrain is due to developmental delay.

In the *cdr2l* morphants I have also identified a possible reduction in the expression of *neurog1*, a marker of delaminating otic neuroblasts and *neurod1*, a marker of subsequent neuronal differentiation. These markers were examined at as Fgf signalling has been suggested to positively regulate the number of emerging otic neuroblasts but negatively regulate otic expression of *cdr2l*. Therefore it was hypothesised that loss of *cdr2l* transcription might lead to changes, possibly an up-regulation, of the number of delaminating neuroblasts, which should be reflected in the expression of both markers (Maier and Whitfield, 2014). While the weaker expression of otic *neurog1* could reflect a depletion of delaminating *neurog1*-positive cells, *neurod1* staining appeared reduced in area and remained grossly normally patterned around the otic vesicle. This reduction in *neurod1* staining is contrary to what would be expected if the number of delaminating neuroblasts had increased in response to a loss of *cdr2l*. This suggests that Cdr2l and Fgf are unlikely to be regulating otic neurogenesis in an opposing manner as hypothesised. Another possible explanation is that Cdr2l may influence this neural otic population by negatively regulating early maturation of otic cells destined to delaminate. This is supported by the loss of otic *cdr2l* expression in the anterior at 16hpf when neuroblast delamination begins and the lack of co-expression in the extra-otic domains of *neurod1* (Andermann et al., 2002). Whilst the morphants appeared to show altered expression of *fsta* and the neurogenic markers, no significant loss of motor coordination or ability to balance using a well established tap test was observed (Kwak et al., 2006). This was surprising, especially when considering a proportion of 1nL injected morphants were also observed to have a reduction in otolith number and indicates that loss of *cdr2l* likely has no significant impact on the the vestibular otic response.

Given the possible reduction in posterior otic *fsta* expression in the morphants, loss of *cdr2l* may be affecting the detection of auditory stimuli, thought to be primarily detected by the posterior, saccular macula (Bang et al., 2002). Therefore it would be interesting to carry out auditory testing on the morphants using a pre-pulse inhibition assay. However, the significant non-inflated swim bladder phenotype in the *cdr2l* morphants may confound any testing, as the swim bladder is thought to play a role in conducting auditory stimuli in otophys (Popper and Fay, 1973).

Whilst observation of the *cdr2l* CRISPR mutants confirmed that loss of *cdr2l* transcription does not affect motor coordination and balance in larval zebrafish, the reduction in otolith number and non-inflated swim bladder phenotypes observed was not reproduced. As this did not appear to be due to the *cdr2l* paralogue, *cdr2a*, acting redundantly in this knock-out, it suggests these are likely to be non-specific consequences of the morpholino injection. Therefore further work to confirm the *neurod1* and *fsta* morphant phenotypes in the mutants would also be beneficial. Interestingly, the *cdr2l* CRISPR mutants do appear to recapitulate the slight reduction in mean AP length and increased length variability noted in the morphants, which could point towards a role in regulating proliferation or apoptosis during early otic development as previously mentioned. Expression of *mycb*, which has been linked to proliferation in zebrafish, does not appear consistently up or down-regulated in response to knock-out of *cdr2l*, despite their possible interaction at the protein level (Lee et al., 2016). Therefore directly observing the levels of proliferation and apoptosis in developing otic placode of *cdr2l* mutants presents a better approach to confirm any changes which might influence otic AP length. A model with Cdr2l maintaining or reflecting otic proliferation would also fit with its down-regulation in response to Fgf manipulation, given that Fgf signalling can drive otic maturation (Hammond and Whitfield, 2011; Maier and Whitfield, 2014).

4.4 Conclusions

- *Cdr2l* expression is lost progressively across the otic AP axis during early otic development in zebrafish.
- Loss of *cdr2l* function does not appear to result in any consistent otic morphological defects or inability to detect vestibular stimuli.
- *Cdr2l* does not appear to regulate anterior otic patterning but may reduce otic expression of the posterior marker, *fstb*.
- Loss of *cdr2l* in morphants results in a reduction in the strength of *neurog1* and area of *neurod1* expression. This has yet to be confirmed in *cdr2l* mutants.
- *Mycb* is initially broadly expressed across otic AP axis during early otic development but this is progressively lost from the anterior otic domain and is ultimately lost in the majority of the otic epithelium by 26hpf.
- The general reduction and variation in otic AP length in both *cdr2l* morphants and mutants may indicate a role regulating proliferation within the developing otic placode, despite not having a clear influence on the expression of the positive cell-cycle regulator *myc*.

Chapter 5

Development of a transcriptomics approach to identifying differential gene expression associated with posterior otic identity

5.1 Introduction

The functional and morphological asymmetry of the inner ear is the result of the spatially and temporally dynamic transcription of a myriad of genes during its development (reviewed in (Whitfield and Hammond, 2007; Bok et al., 2007a)). Identification of these regulators in otic development has primarily been through reverse-genetic screens or analysis of genes with previously known functions in development or that are regulated by pathways acting during otic development (Whitfield et al., 1996a). However over the past decade, a rapid improvement in genome annotation and sequencing technologies have made it easier and cheaper to identify the majority of the transcriptome. Such transcriptomic approaches have continued to progress with improvement in next-generation sequencing techniques such as RNA-Seq seeing their increased use over hybridisation-dependent microarrays. Whilst currently requiring more intensive analysis, such next-generation techniques are being increasingly used as they have greater versatility, are not limited by prior annotation and provide better quantitation of transcript levels (reviewed in (Martin and Wang, 2011)). However, microarray-based systems are still a well-established tool for comparing differential expression and have been used to study transcriptional difference in otic tissue to changes in Fgf signalling in chick and mouse (Oshlack et al., 2010; Yang et al., 2013; Urness et al., 2010).

Whilst in zebrafish the anterior otic expression of a number of genes has been linked with establishing anterior otic character, an early transcriptional network defining the posterior has not been identified. Evidence for posterior-specific expression within the early otic placode has been presented previously in chapters Three and Four, where I described the expression of two novel markers expressed in the posterior domain during the time period over which AP patterning is thought to be occurring. The progressive reduction in the propensity of the posterior domain to adopt an anterior duplicated fate in response to over-expression of *fgf3* (discussed in Chapter Six) also supports a change in the posterior otic tissue. Therefore, using the well-characterised equipotent nature of the poles of the zebrafish otic placode to adopt either anterior or posterior character, a transcriptomics approach to study differential gene expression in otic tissue after posterior duplication was investigated, as described in this chapter.

5.2 Results

For utilising a transcriptomics approach, the first step is to isolate the tissue of interest, in this case the otic placode. This is of particular importance for the proposed isolation of duplicated otic tissue after signalling pathway manipulation, given that most tissues surrounding the otic placode will likely respond to manipulations of Fgf or Hh signalling.

Initially a transgenic *cldnb:lynGFP* line, which expresses GFP within the ear along with other sensory placodes, was identified as a potential marker of the otic tissue (Haas and Gilmour, 2006). It was planned that by GFP labelling the otic tissue in this way, after treatment to induce an AP duplication the otic cells could be isolated from a dissected tissue sample using fluorescence-activated cell sorting (FACS) before subsequently being processed for a transcriptomic approach. Proof-of-principle has already been demonstrated using this transgenic line, for isolating and profiling neuromasts of the posterior lateral line (Gallardo and Behra, 2013).

To test the feasibility of this approach for isolating otic cells, Tg(*cldnb:lynGFP*) embryos between 14hpf and 16hpf were dissected in Ringer's solution using transverse cuts to isolate either, the otic tissue, along with the adjacent hindbrain, the trunk as a negative control, or the head as a positive control (Figure 5.1A-C, white-dotted outlines). These tissue sections were then dissociated in a sterile solution of 0.25% porcine trypsin, 1mM EDTA and 10mg/mL proteinase K in PBS with gentle agitation for 20 minutes before being stopped and washed. After being spun-down following the final wash, cells were resuspended in PBS and the number of GFP-positive cells counted using flow cytometry. This confirmed that it was possible to identify a GFP-positive population of cells (6%, 759/12552), likely reflecting the otic placodal cells, from the section isolated containing hindbrain and otic vesicle tissue (Figure 5.1C'). This was done using negative and positive controls to set the gate threshold at which cells are considered GFP-positive (Figure 5.1A' and B').

However, expression of otic GFP within the *cldnb:lynGFP* line is only weakly observable at 14-16hpf, making it less ideal for isolating otic early during its development. Also, as mentioned previously, the *cldnb:lynGFP* line also marks other sensory placodes including the anterior and lateral line which arise adjacently to the otic placode within the posterior placodal area (PPA) (Ladher et al., 2010). Therefore it is likely that the GFP cells from the hindbrain sections isolated would represent a heterogeneous population of placodal fates.

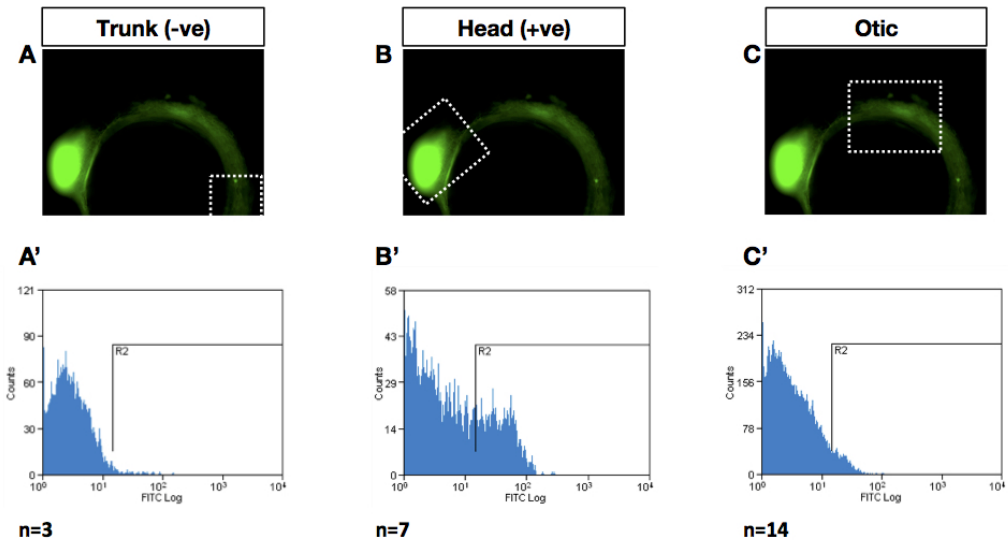


Figure 5.1: Isolation and counting of GFP positive otic cells from *Tg(cldnb:lynGFP)* embryos

(A–A') Sections of mostly GFP negative trunk tissue were used as a negative control. Flow cytometry confirmed a low count of GFP+ cells (R2 1.8%, 63/3507). (B–B') Head sections containing a large GFP positive population within the optic placode were used as a positive control. This was reflected in a high count of GFP+ cells (R2 26%, 822/3174). (C–C') The otic tissue was isolated as a section of hindbrain and a small population of GFP+ cells were identified based on thresholds set by the negative and positive controls (R2 6%, 759/12552). For the count plots; x axis = FITC intensity and y axis = cell count. White-dotted outline represent sections used. A–C were taken at a 30x zoom using epifluorescent imaging. N= number of pooled embryos used for each count.

To address the issue of otic specificity, other promoters with strong, early otic expression were examined. DeLaurier et al, 2010 utilised a BAC (CH73-243G6) containing the genomic *sp7* sequence to drive eGFP expression within the otic placode from 6ss (12hpf) onwards with no other obvious expression in other tissues, even by 24hpf (Figure 5.2B) (DeLaurier et al., 2010). Whilst duplicating the AP axis by perturbing Fgf and Hh signalling may identify responses to these treatments, some transcriptional differences present along the AP axis during normal development may be lost. Therefore, by using the otic specific *sp7* promoter to drive the photo-convertible protein, Kaede, it was hoped that the posteromedial otic cells from untreated embryos could be labelled in this way and isolated using FACS, an approach previously used (Figure 5.2A) (Brown et al., 2008). These isolated cells could then be used to characterise the early transcriptional state that under wild-type conditions results in posterior otic identity.

A construct with Kaede being driven by the *sp7* promoter, flanked by Tol2 insertion sites was generated through recombineering, with the kaede coding sequence inserted into the *sp7*-containing BAC at the same location used by DeLaurier et al, 2010 to ensure a similar expression profile. This construct was then injected into AB wild-type embryos with transposase, which facilitates genomic insertion (Suster et al., 2009). A stable F1 *Tg(sp7:kaede)* line was raised, which displayed the expected otic specific expression of Kaede and this was confirmed to be responsive to photo-conversion (Figure 5.2C).

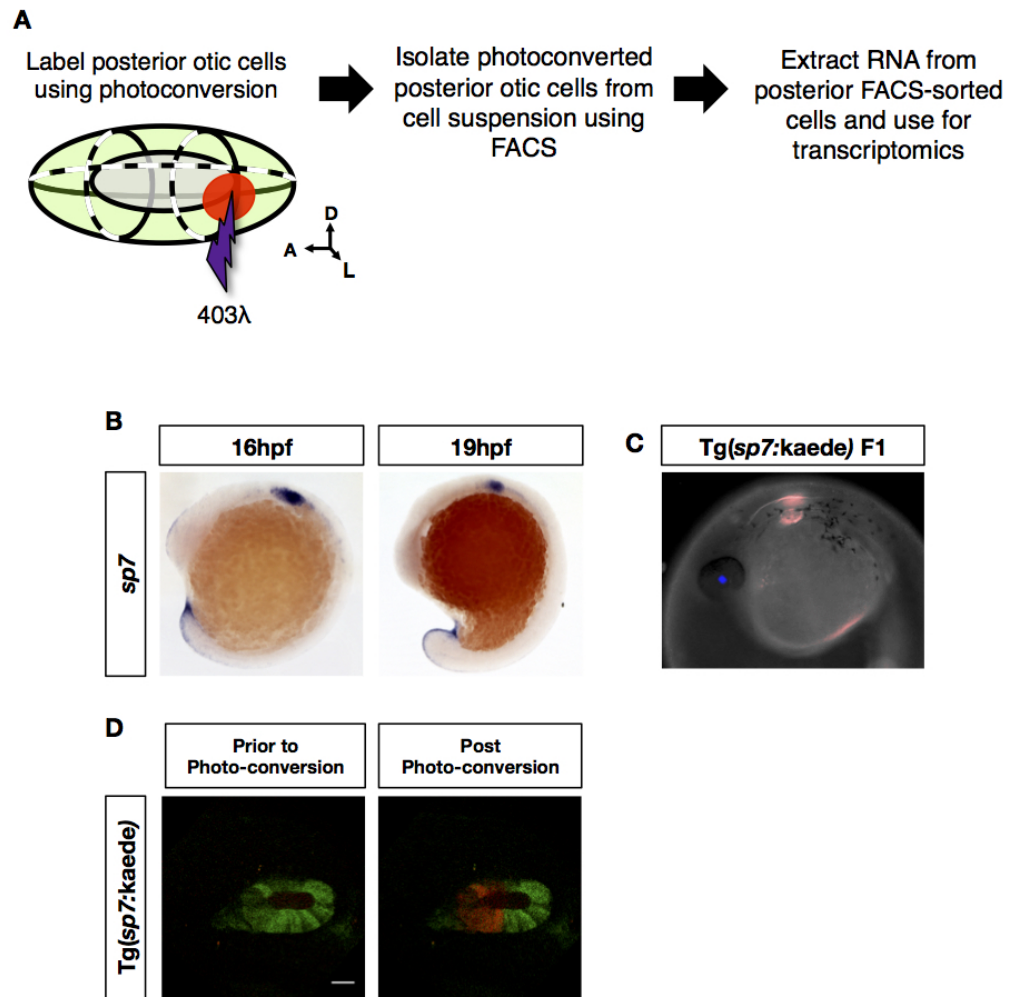


Figure 5.2: Targeted isolation of cells from the posterior otic domain using photo-conversion

(A) Schematic outline of the proposed approach for labelling and isolating cells from the posterior otic domain. (B) In situ staining for *sp7* shows otic specific expression at 16 and 19hpf. (C) The F1 generation of *Tg(sp7:kaede)* showed strong expression of kaede within the otic vesicle at 24hpf, which also appeared photoconvertible (red). Expression of the *crya:venus* selection marker can also be seen in the lens (blue). (D) Trial photo-conversion of the anterior otic domain at >18hpf using 39 seconds of exposure with a 403nm λ laser at 50.69%. Images in B were taken using 7x magnification and brightfield.

To test whether specific regions of the otic vesicle could be photo-converted, *Tg(sp7:kaede)* embryos were mounted, dorsal side down, in 1% low-melting point agarose before being photo-converted. Given the small size of the domain to be photo-converted, photoconversion was performed on a confocal microscope with a 40x objective. Photo-conversion of the anterior otic domain in 18hpf embryos was successfully achieved using three pulses of 403nm laser for 13 seconds (Figure 5.2D). Therefore using the same method, the anterior halves of both otic placodes were photo-converted in 15hpf *Tg(sp7:kaede)* embryos.

After photo-conversion, these *Tg(sp7:kaede)* embryos were dissociated as previously described and analysed by flow cytometry, with a non-transgenic negative control and unconverted sample run alongside (Figure 5.3).

In both the unconverted and anterior photo-converted samples, no clear green (y-axis) or red (x-axis) population of cells were present but a population of cells between the two was apparent (Figure 5.3B and C). In the photo-converted sample the proportion of this population of cells was greater at 0.08% compared to 0.03% in the unconverted. As Kaede is still being produced within the otic placode of these embryos, even after photo-conversion this might represent a mixture of both unconverted and converted Kaede.

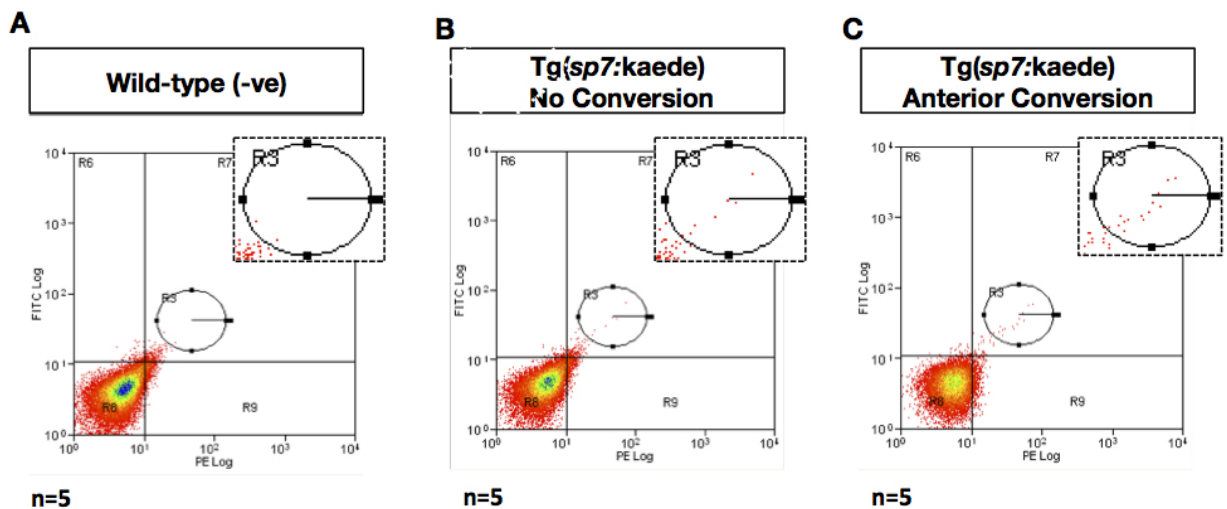


Figure 5.3: Isolation and counting of photo-converted Kaede positive otic cells from *Tg(sp7:kaede)* embryos

(A) Cells from dissociated wild-type embryos were used as a negative control. Flow cytometry confirmed a low count of kaede+ cells (R3 1×10^{-4}). (B) Plot of cells from dissociated, unconverted *Tg(sp7:kaede)* embryos show a population of positive cells both green and red (R3 3×10^{-4}). (C) Plot of cells from dissociated *Tg(sp7:kaede)* embryos where the anterior otic domain has been photo-converted. These show an increase in the population of positive cells both green and red (R3 8×10^{-4}). Black dotted box outline a zoom of the corresponding R3 region. For the plots; x axis = red (PE) (converted) intensity and y axis = green (FITC) (unconverted) intensity. N= number of pooled embryos used for each count.

The next stage was to test whether this transgenic line could be used to isolate otic cells using FACS with the view of confirming that the Kaede-positive cells isolated expressed otic markers. This test would also give an indication of the potential yield of positive cells after sorting. For this, 18hpf unconverted *Tg(sp7:kaede)* embryos were used with Kaede RNA-injected embryos and uninjected embryos run as positive and negative controls respectively (Figure 5.4).

A different protocol from before was used to dissociate the embryos in an attempt to reduce the time taken to dissociate the cells and improve the purity of the collected cells, based on previously published protocols and personal discussion with Dr S Baxendale. Briefly, after removing the majority of the yolk in sterile ca^{2+} -free Ringer's solution, embryos were dissociated in a 1.75mg/ml solution of collagenase/dispase (Roche), which has been suggested to be quicker and less damaging than trypsin, with gentle agitation (Lawson Lab (<http://lawsonlab.umassmed.edu>) and personal discussion with Dr S Baxendale). This dissociation generally took around 40 minutes with the cells then being washed in room temperature, sterile PBS. After being spun-down following the final wash, cells were resuspended in Hank's Buffered Saline Solution (HBSS - a pH and osmotically balanced solution) to increase their chances of survival.

The negative and positive control suspensions were used to set the gate intensity thresholds for unconverted Kaede-positive cells prior to sorting. Using this threshold a much smaller population of unconverted Tg(*sp7:kaede*) cells (4.2x10⁻⁴%, 90/211,723) (Figure 5.4C and C') were identified compared to the Kaede RNA injected positive control population (34%, 8,854/25,602) (Figure 5.4B and B').

This smaller population might be due to the fluorescent signal in the Tg(*sp7:kaede*) sample being weaker, as the population of cells just below the threshold (bracket population) appears larger than in the wild-type negative control (Figure 5.4A' compared to C'). However, given that there is overlap, lowering the selection gate to collect these cells would also potentially collect non-labelled cells.

The Tg(*sp7:kaede*) photo-conversion approach was initially followed due to the greater specificity of the promoter and the ability to target regions of the otic placode. However, given the small population of positive cells collected, possibly resulting from weak fluorescence, it was decided that this approach was not viable to produce the yield of cells needed for the required amount of RNA. Due to time constraints and other lines of experimental work, the planned transcriptomics assay was not pursued further.

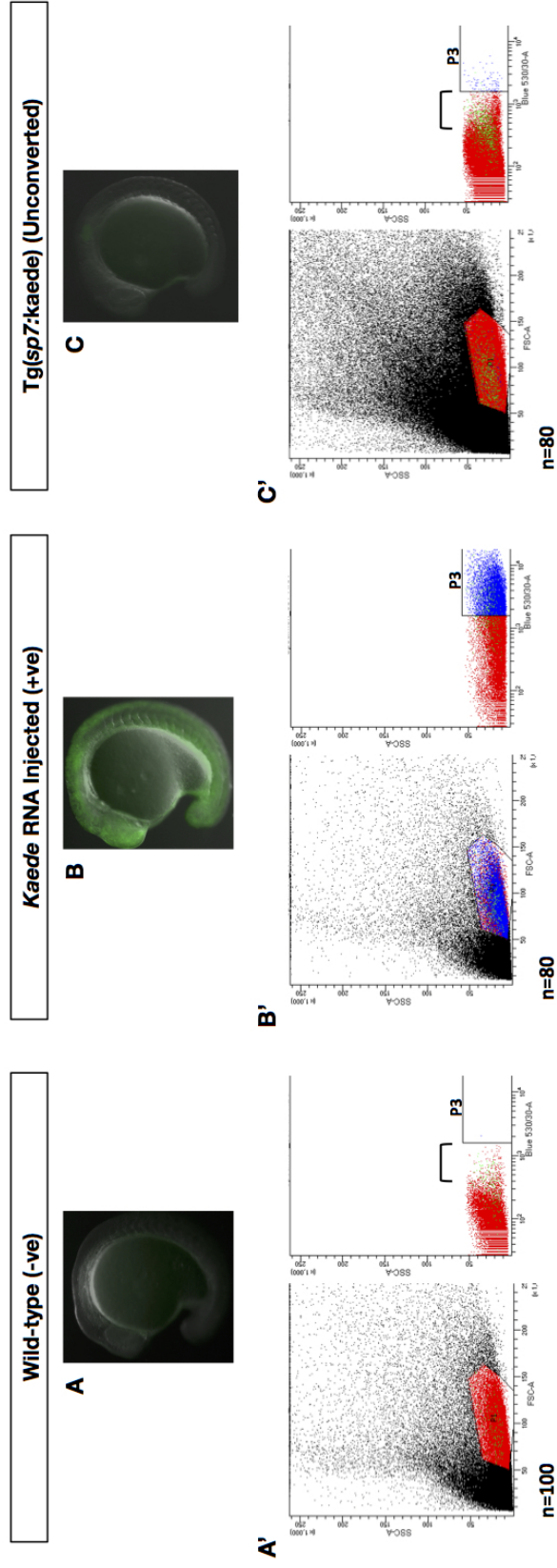


Figure 5.4: Isolation and FACS of unconverted Kaede positive cells from Tg(sp7:kaede) embryos

(A-A') FACS scatter (left) and count plots (right) from Kaede negative wild-type embryos used as a negative control. (B-B') Unconverted, wild-type embryos injected with Kaede RNA used as a positive control (P3 34%, 8,854/25,602) (B). (C-C') Tg(sp7:kaede) embryos, 90 events were recorded as positive, based on thresholds set by the negative and positive controls, representing 4.2x10⁻⁴% (P3 90/211,723). For all count plots, blue cells within the gate set by the positive and negative controls are counted as positive with red cells counted as negative. Green points represent an initial short run and were not counted. Images A-C were taken at a 30x zoom using epifluorescent imaging.

5.3 Discussion

In this chapter, I have explored approaches for isolating early otic tissue by FACS. This aim of this was to ultimately identify differential gene expression that may reflect regulation of anterior or posterior otic identity using transcriptomics. One of the key issues encountered was that of specificity, both in isolating just the otic tissue and going one step further, potentially isolating only the posterior otic tissue. In regards to the first of these, the *sp7* promoter certainly appeared to give better and earlier otic-specific expression than seen with the Tg(*cldnb:lynGFP*) line. Therefore the *sp7* promoter could be used to drive expression of a brighter fluorescent protein such as eGFP or mCitrine (Shaner et al., 2005). Whilst this would help isolate the early otic tissue, it would rely on perturbing the tissue with modulators of Hh or Fgf signalling to duplicate the otic tissue. This might be informative as ultimately this can give rise to ears with duplication across the AP axis in zebrafish. However, it may also be a less accurate representation of the patterning events that occur during normal otic development, discussed further in Chapter 7. Another issue with this approach is it still relies on FACS and the necessary dissociation step prior to this. Although the trialled approach did not appear to result in any high levels of cell death (Supplementary Figure 8.), it is conceivable that in the time between the initial dissociation and collecting the cells that transcriptional changes may have occurred.

The second issue was that of isolating tissue with regional specificity across the otic AP axis. As the otic placode is highly segregated into domains of varying gene expression, morphology and function an approach where the region of otic tissue could be decided seemed ideal. This would also allow isolation of the anterior and posterior medial otic domains under normal developmental conditions, which could then be compared. Unfortunately using the *sp7* promoter to drive otic expression of the photo-convertible protein Kaede did not work. This was due to the endogenous Kaede signal being too weak to identify the otic population clearly, let alone a smaller posterior subset. The use of Kaede RNA injection may be an alternative to this, as despite not being localised to the otic epithelium it is stronger in intensity and gives a clear population as shown in Figure 5.4 and previously reported (Brown et al., 2008). It would also ensure that labelled cells do not continue to produce new, unconverted Kaede, which may dilute the converted signal.

Another approach to gain information about spatial resolution of transcripts across the AP axis from whole otic isolates would be to screen any differentially expressed genes by in situ hybridisation. This would constitute a validation following any transcriptomics assay and could be done in a relatively high-throughput method. Another, more elegant approach to this would also be to use RNA tomography. This uses RNA isolated from serial sections of tissue, which is then uniquely labelled and subsequently analysed by RNA-seq. This allows a map of the transcriptome across the sections and ultimately the tissue to be built up (Junker et al., 2014).

An issue not addressed in this chapter is that of the time point at which the otic tissue would be isolated. The spatial localisation of expression across the AP otic axis is crucial in assigning anterior and most likely posterior identity to the otic placode. However, this dynamic localisation of otic expression occurs over a time period, reflecting differing interactions and regulatory relationships. Therefore the characterisation of these as presented in the next chapter (Chapter Six) might help address this point in consideration for future attempts at a transcriptomics analysis of otic patterning.

Chapter 6

Integration of Fgf and Hh signalling across the early otic placode

6.1 Introduction

The patterning and development of the vertebrate inner ear is known to be dependent on a number of signalling pathways, including those of BMP, Wnt, Retinoic Acid (RA), Hedgehog (Hh) and Fibroblast growth factor (Fgf) signalling (reviewed by (Bok et al., 2007a; Whitfield, 2015)). The integration of these signals, both directly and indirectly, regulates expression of otic genes with differing temporal and spatial dynamics producing a structure with asymmetry around all three axes. Whilst differences in the otic morphology are seen between vertebrate models, particularly in the auditory sensory organs, the overall structure of the inner ear is remarkably conserved. Similarly, despite the regulatory activity and function of a number of signalling ligands and otic genes differing between vertebrates during early otic morphogenesis, a number show conservation in their function and localisation. The Shh and Fgf signalling pathways exemplify this, as during otic development in zebrafish they are crucial for defining anterior-posterior otic identity, with Hh also being required for dorsoventral patterning. However, in chick and mouse otic development, Shh and Fgf signalling are primarily thought to pattern the early dorsoventral axis with RA being responsible for regulating the anterior-posterior axis (Bok et al., 2005; Brown and Epstein, 2011; Hatch et al., 2007; Hammond et al., 2010; Hammond and Whitfield, 2011; Freter et al., 2008; Ohta et al., 2016; Bok et al., 2011; Cadot et al., 2012). However, despite this difference, regulation by Hh and Fgf signalling of a number of genes required for patterning the otic tissue, albeit with differences in their function, do show some comparability between these vertebrate models (see Sections 1.4 and 1.5) .

The importance of the interaction between such extra-otic signals and the otic tissue during development is highlighted by the ability of the otic tissue in zebrafish, amphibians and chick to duplicate either the anterior or posterior otic structures in response to alterations in the signalling environment (Bok et al., 2011; Hammond and Whitfield, 2011; Waldman et al., 2007). In zebrafish, duplications of the anterior or posterior otic domains are easily achieved through perturbation of Hh or Fgf signalling, respectively and as such makes this an ideal system for understanding the regulatory dynamics occurring with the zebrafish otic placode that ultimately lead to asymmetry along the anterior-posterior axis. Whilst a number of genes that show differential expression after changes in Hh or Fgf signalling have been identified and their requirement in patterning of the otic tissue studied, the way in which these are regulated both in time and by both Hh and Fgf signalling, acting independently of each other is not clearly understood (Hammond and Whitfield,

2011). Another important feature identified for defining the response of the otic tissue to the signalling environment acting on the developing otic tissue is the competence of the tissue to respond. In zebrafish and chick, a time-window over which the anterior-posterior axis in particular is sensitive to perturbations in signalling has been reported and the role of Fgf, Hh and RA signalling in the induction, specification and maturation of the otic tissue in all three of these model organisms emphasises the need for such regionalised changes in response (Bok et al., 2011; Hammond and Whitfield, 2011; Whitfield, 2015).

In this chapter, I firstly discuss the differing timings seen in the onset of expression in the posterior otic domain of genes associated with anterior identity in response to two approaches, loss of Hh signalling and over-expression of *fgf3*, known to duplicate anterior otic morphology as I look to identify the earliest otic determinant of anterior identity and how Fgf and Hh signalling integrate to regulate this. Secondly, I ask how certain otic regions display competence to initiate but not maintain expression of anterior otic genes in response to over-expression of *fgf3* and how this itself appears to be transient. Finally, given the role of RA in patterning the anterior-posterior axis of sensory otic tissue in amniotes, I present preliminary data suggesting that any effect on the anterior-posterior identity of sensory tissue in zebrafish is limited, both in conjunction with Hh signalling and alone.

6.2 Results

6.2.1 Posterior otic morphology is lost in embryos treated with 100 μ M cyclopamine (CyA) between 14-15 and 22.5hpf

Treatment of embryos with 50 and 90 μ M of the Hh signalling inhibitor, CyA, prior to 15ss have been shown by separate groups to phenocopy the duplication of anterior otic identity seen in the severe Hh loss-of-function mutations in *dispatched1* (previously *chameleon*, *disp1*^{tf18b}) and *smoothened* (*smo*^{b641}) (Hammond et al., 2003, 2010; Sapède and Pujades, 2010). Given Hh's requirement for a number of developmental processes, inhibition of Hh signalling with CyA within a treatment time-window provides the advantage of reducing non-otic developmental effects.

Embryos treated with 50 μ M of CyA as previously used by Hammond et al, 2010, maintained expression of the Hh signalling readout marker *ptch2* albeit at a lower level (data not shown). Therefore, to ensure a strong response, embryos were treated with a higher dose at 100 μ M from 14-15hpf to 22.5hpf with embryos being washed, twice, following treatment and allowed to develop onwards to 3dpf (75hpf) (Figure 6.1G). This treatment consistently resulted (42/47 of treated embryos, 89%) in a lateral positioning of the posterior macula, as seen in the live images from the positioning of the posterior otolith (Figures 6.1C and C'), relative to that in the untreated and vehicle controls (Figures 6.1A and B, respectively). However, this lateral positioning of the posterior macula occurred with varying distance between the anterior and posterior otoliths, as shown by Figures 6.1C and C'.

To visualise the actin-rich stereociliary bundles of the otic sensory patches, including the macula underlying the otoliths, embryos were stained within FITC-conjugated phalloidin (Figures 6.1D-F'). In the CyA-treated embryos this clearly shows a loss of the stereotypical shape of the posterior macula stereociliary bundles (Figures 6.1F) when compared to the untreated (Figures 6.1A, D) and vehicle controls (Figures 6.1B). In the CyA-treated, phalloidin-stained embryos a supernumerary crista was also observed adjacent to the lateral crista in 3/6 (50%) of the embryos imaged (Figure 6.1F'), which has previously been reported in severe Hh loss-of-function mutants

but not in CyA-treated embryos (Hammond et al., 2003). In the untreated and vehicle controls, such supernumerary cristae were not seen.

This phenotype seen in the 100 μ M CyA-treated embryos, alongside the altered position and shape of the posterior macula, suggests this treatment between 14-15hpf to 22.5hpf is sufficient to result in a loss of posterior otic identity with the posterior macula resembling a duplicated anterior macula. This treatment appears have little impact on the other structures of the ear, as shown by the largely correct positioning and formation of the semicircular canals. However, treatment with 90 μ M CyA over a longer time period has been reported in zebrafish to lead to a reduction of hair cells within the posterior macula but this was not looked at in this study (Sapède and Pujades, 2010).

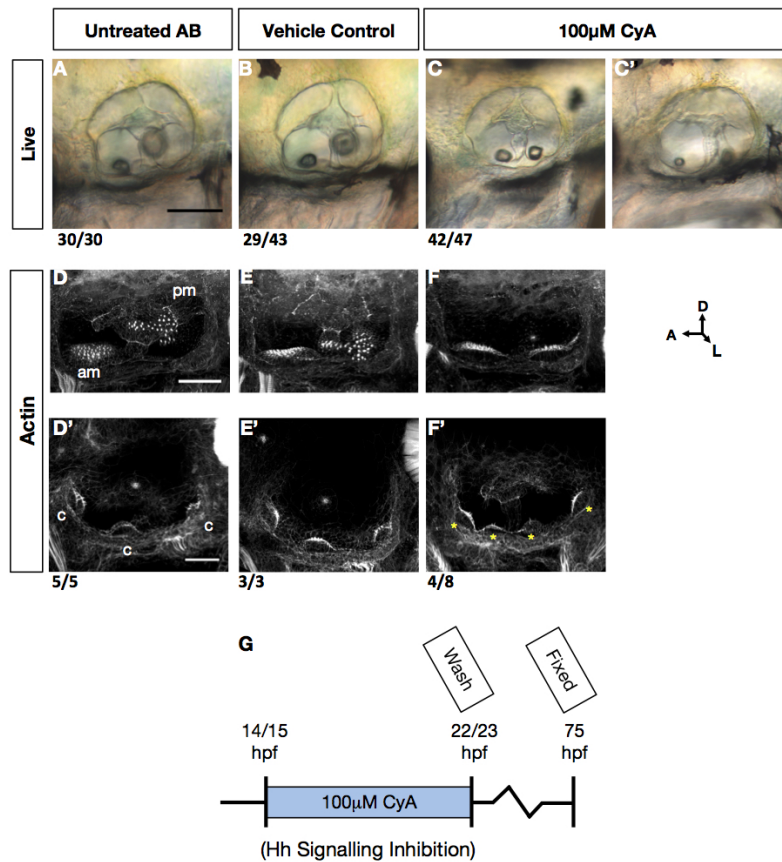


Figure 6.1: Inhibition of Hh signalling between 14/15 and 22/23 hpf results in a duplication of anterior otic morphology

(A–C') Images of live embryos at 3dpf. Treatment with cyclopamine (CyA) between 14/15 and 22/23hpf results in a laterally positioned, smaller posterior otolith resembling the anterior otolith (C–C') compared to the untreated (A) and vehicle controls (B). (D–F) Actin staining of the stereociliary bundles of the otic sensory patches highlights the lateral position of the posterior macula underlying the posterior otolith in CyA-treated embryos and the similarity in gross morphology to the anterior macula. (D'–F') Imaging of the cristae highlights that in 3/6 imaged embryos there is a supernumerary crista (yellow asterisks). (G) Schematic of CyA treatment. All images are lateral views. A–C' were taken using bright field with a 20x objective. D–F' were taken using confocal microscopy with a 40x oil objective. Scale bars: 50 μ M.

6.2.2 Inhibition of Hh signalling between 14-15 and 22.5hpf leads to delayed ectopic posterior otic expression of the anterior otic factors *fgf3*, *fgf8a* and *pax5*

As the treatment of embryos with 100 μ M from 14-15hpf to 22.5hpf appears sufficient to result in a loss of posterior otic identity and duplication of anterior macula morphology (Figure 6.1), I wanted to ask whether this resulted in a concomitant duplication of genes associated with anterior otic identity immediately after treatment, at 22.5hpf. While it has previously been shown that in the severe Hh loss-of-function mutants, *disp1*^{tf18b} and *smo*^{b641} at 24hpf, the anterior factors *fgf8a* and *pax5* do not show ectopic posterior otic expression (Hammond et al., 2003), the expression of anterior otic factors has not been studied after transient loss of Hh signalling.

Wild-type embryos were treated under the same conditions as used in section 6.1, to produce a loss of posterior and duplication of anterior otic identity with 100 μ M of CyA applied between 14-15hpf to 22.5hpf, before embryos were fixed and assayed by in-situ hybridisation (Figure 6.2K). After treatment with CyA the anterior markers *fgf3*, *fgf8a* and *pax5* (Figure 6.2B, D and H, respectively) show no ectopic posterior otic expression or expansion of their anterior otic expression domains at 22.5hpf. Interestingly, *fgf10a* staining was observed to be slightly strengthened in the anterior of the otic vesicle and also along the medial edge (Figure 6.2F). To confirm that the 100 μ M CyA treatment was reducing Hh signalling, in-situ hybridisation for *ptch2* was used. As a downstream negative regulator of Hh signalling, *ptch2* expression is dependent on levels Hh signalling (Lewis et al., 1999) and in treated embryos, *ptch2* staining is clearly reduced, although not lost completely (Figure 5.2J) when compared to the vehicle control (Figure 6.2I).

When *fgf3* is over-expressed under a heat-shock promoter, this results in a loss of posterior otic identity and duplication of anterior identity similar to that seen under loss of Hh conditions (Hammond et al., 2010; Hammond and Whitfield, 2011). Under these conditions, the anterior markers *pax5* and *hmx2* show expanded expression across the medial otic edge and into the posterior otic domain by 24hpf (Hammond and Whitfield, 2011). This suggests expanded or duplicated expression of anterior factors is likely required for the duplication of the anterior otic morphology seen and is further supported by the requirement of these factors for normal anterior otic identity both in zebrafish and other vertebrates (Feng and Xu, 2010; Kwak et al., 2006; Léger and Brand, 2002). Whilst no posterior duplicated expression of these anterior factors was observed either after transient inhibition of Hh signalling (Figure 6.2) or in the Hh loss-of-function mutants (Hammond et al., 2003), it had not been confirmed whether this represents a lack of a similar duplication of anterior factors in the posterior otic domain or a delayed onset of expression after 24hpf. Therefore treatment with 100 μ M of CyA, as used previously, was repeated but with the embryos being washed following treatment and then allowed to develop on until either 36 or 48hpf (Figure 6.3O). In treated embryos fixed at 36hpf, expression of the strong otic anteriorising signalling factors, *fgf3* (Figure 6.3C-D', white asterisk in C' and D') and *fgf8a* (Figure 6.3H and I), show expression within the posterior otic domain, not seen in the vehicle controls (Figure 6.3A-B' and E-F, respectively). These posterior domains of expression appear smaller in area than the domains of anterior otic expression, with *fgf3* staining appearing weaker than that of *fgf8a*. This could suggest *fgf8a* is more readily expressed within the posterior otic domain as *fgf8a* is also transiently expressed within the posterior otic domain at around 24hpf under normal development (Figure 6.2), also (Léger and Brand, 2002).

Expression of *pax5*, which is required for maintenance of anterior otic identity in zebrafish (Kwak et al., 2006), also appears to be duplicated within the posterior otic domain by 36hpf in 9/15 (60%) treated embryos (Figure 6.3M and N).

By 48hpf, under DIC microscopy it is also observable that the medial pseudo-stratified, thickened epithelium of the saccular (posterior) macula seen in the vehicle controls (Figure 6.3G, white arrow) is lost in 100 μ M CyA-treated embryos (Figure 6.3J, white arrow).

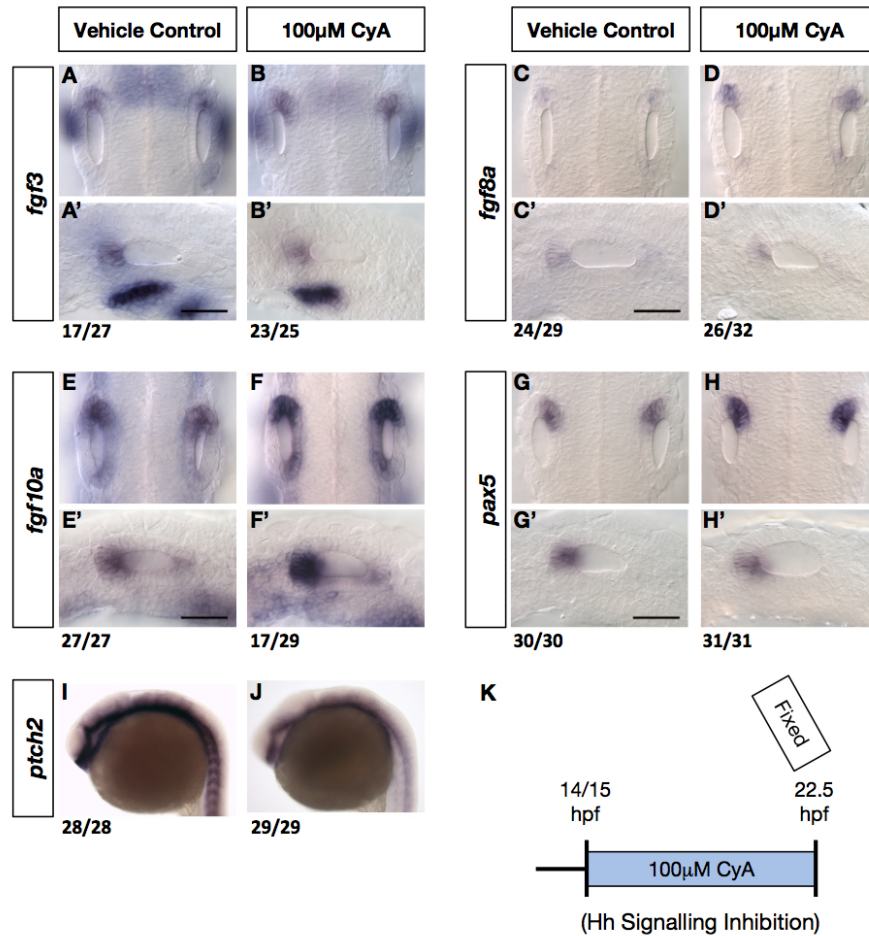


Figure 6.2: Inhibition of Hh signalling between 14/15 and 22/23 hpf does not lead to immediate expression of anterior factors within the posterior domain

(A–D'') Expression of the anteriorising factors, *fgf3* and *fgf8a* is neither duplicated or strengthened in the posterior domain at 22/23hpf after treatment with 100 μ M CyA. (E–F'') Expression of *fgf10a* appears slightly stronger along the medial edge and in the posterior otic domain in 17/29 embryos treated with CyA. (G–H'') Expression of *pax5* does not show any clear posterior expansion along the medial edge or expression within the posterior otic domain. (I–J) Treatment with 100 μ M CyA shows a clear reduction in *ptch2*, a downstream target and negative regulator of Hh, in all treated embryos (J, 29/29). (K) Schematic of CyA treatment. A–J are lateral views and A'–H' are dorsal views with the anterior to the left in all images. A–H' were taken using DIC microscopy with a 40x objective. Scale bars: 50 μ M.

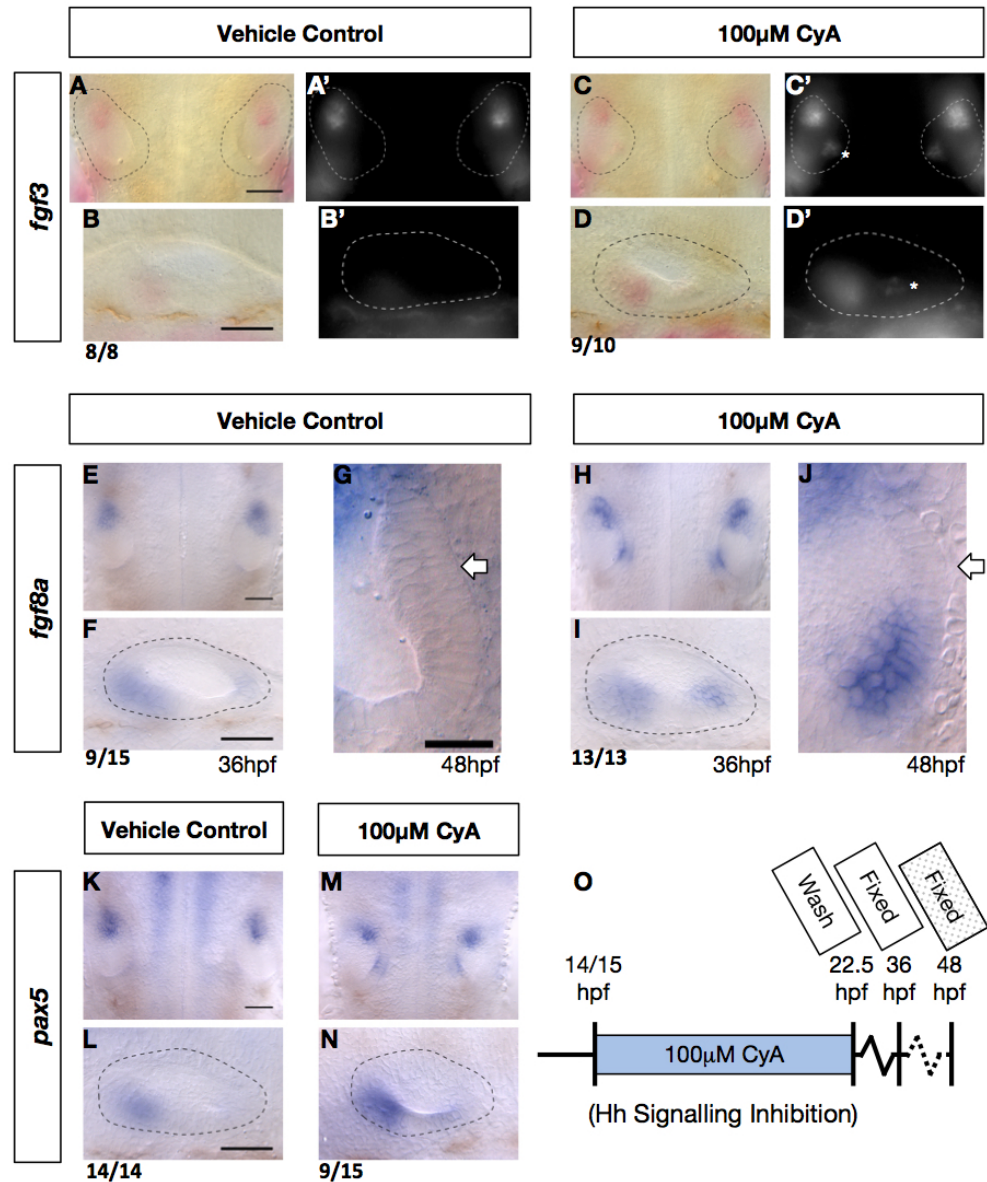


Figure 6.3: Inhibition of Hh signalling between 14/15 and 22/23 hpf does lead to expression of anterior factors within the posterior domain by 36hpf

(A–D') Expression of *fgf3* in vehicle control and treated embryos at 36hpf as shown by in-situ, imaged using both DIC (A–D) and fluorescent imaging (A'–D') to emphasise posterior staining in treated embryos (white asterisks). (E–J) *Fgf8a* expression is strongly duplicated by 36hpf in treated embryos (H–J) and at 48hpf treated embryos show a clear loss of the normal posterior macula morphology seen in the vehicle controls (white arrows). (K–N) Expression of *pax5* was also duplicated in the majority of treated embryos by 36hpf. (O) Schematic of CyA treatment. B/B', D/D', F, I, L N are lateral views with all others being dorsal. Anterior is to the left in all images. A'–D' were taken using epifluorescence microscopy with a 40x objective with the remain images being taken using DIC microscopy with a 40x objective. All scale bars except G: 50µM, G: 20µM.

These results suggest that the changes occurring prior to 22.5hpf in CyA-treated embryos, are sufficient to lead to the loss of posterior otic identity with a delayed duplication of *fgf3*, *fgf8a* and *pax5* and morphological changes observable by 48hpf.

6.2.3 Inhibition of Hh signalling between 14-15 and 22.5hpf directly results in a medial expansion of the early anterior otic factors *hmx2* and *hmx3a* by 22.5hpf

Despite loss of Hh signalling between 14 and 22.5hpf not resulting in the immediate induction of ectopic posterior expression of a number of anterior otic factors (section 6.2), in Hh loss-of-signalling mutants *hmx3a* (previously *nkx5.1*) has been previously shown to have a ventral expansion of expression into the posterior otic domain by 30hpf (Hammond et al., 2003). Given this and that *hmx3a* is the earliest known marker of the anterior otic domain in zebrafish, embryos were again treated with 100 μ M CyA from 14hpf to 22.5hpf, being immediately fixed after treatment to assess whether, unlike the other anterior otic markers, *hmx2* and *hmx3a* would show ectopic posterior otic expression by this time point (Feng and Xu, 2010). In the treated embryos, in-situ hybridisation for both *hmx2* (25/28) and *hmx3a* (25/25) showed expanded staining along the ventral edge of the otic vesicle (Figure 6.4B, B' and D, D') relative to the vehicle controls (Figure 6.4A, A' and C, C'). This expansion appeared stronger in 13/25 embryos for *hmx2* and 17/25 for *hmx3a*.

To confirm whether this expansion was significant over multiple treated embryos the length of staining along the medial otic edge was measured for both *hmx2* and *hmx3a* stained embryos. The medial edge was defined by placing a line at 66% of the overall width of a Region Of Interest (ROI) that bounded dorsally imaged otic vesicles. The length of staining was then measured from the anterior-most point of this line, along the medial edge, to the posterior-most point of staining. This measure was then continued to the posterior-most point along the medial line and the staining length was then reported as a percentage of this overall medial length (Figure 6.4G) to account for any differences in otic size and was repeated for both ears. Over the embryos imaged (n=8 vehicle controls; 10 treated for *hmx2* and n=8 vehicle controls; 9 treated for *hmx3a*), both *hmx2* and *hmx3a* show a highly significant increase in the percentage length of staining in the 100 μ M CyA-treated embryos compared to the vehicle controls (Figure 6.4C and F, respectively). Although *hmx3a* showed a greater difference in the mean percentage length between the treated and vehicle controls with a difference of 18.94% vs 9.87% for *hmx2*.

As expression of *hmx2* and *hmx3a* has been shown to be dependent on FGF signalling in zebrafish (Feng and Xu, 2010; Hammond and Whitfield, 2011) the expression of *etv4* (previously, *pea3*), a well established transcriptional readout of FGF-signalling (Raible and Brand, 2001) was assayed by in-situ hybridisation in embryos treated with 100 μ M CyA and vehicle controls. No obvious difference in *etv4* staining was observed in the treated embryos (Figure 6.4I and I'), either across the whole otic vesicle or the medial edge where *hmx2* and *3a* show expansion under these conditions when compared to the vehicle controls (Figure 5.4H and H'). This suggests that the expanded staining seen for *hmx2* and *hmx3a* in 100 μ M CyA-treated embryos is unlikely due to an up-regulation of FGF signalling in response to reduced Hh signalling. This is supported by data from (Hammond and Whitfield, 2011), where in-situ staining for *etv4* showed no change in either loss of Hh (*smo*^{b577-/-}) or aberrant Hh signalling (*ptc1*^{-/-}; *ptc2*^{-/-}) transgenic backgrounds.

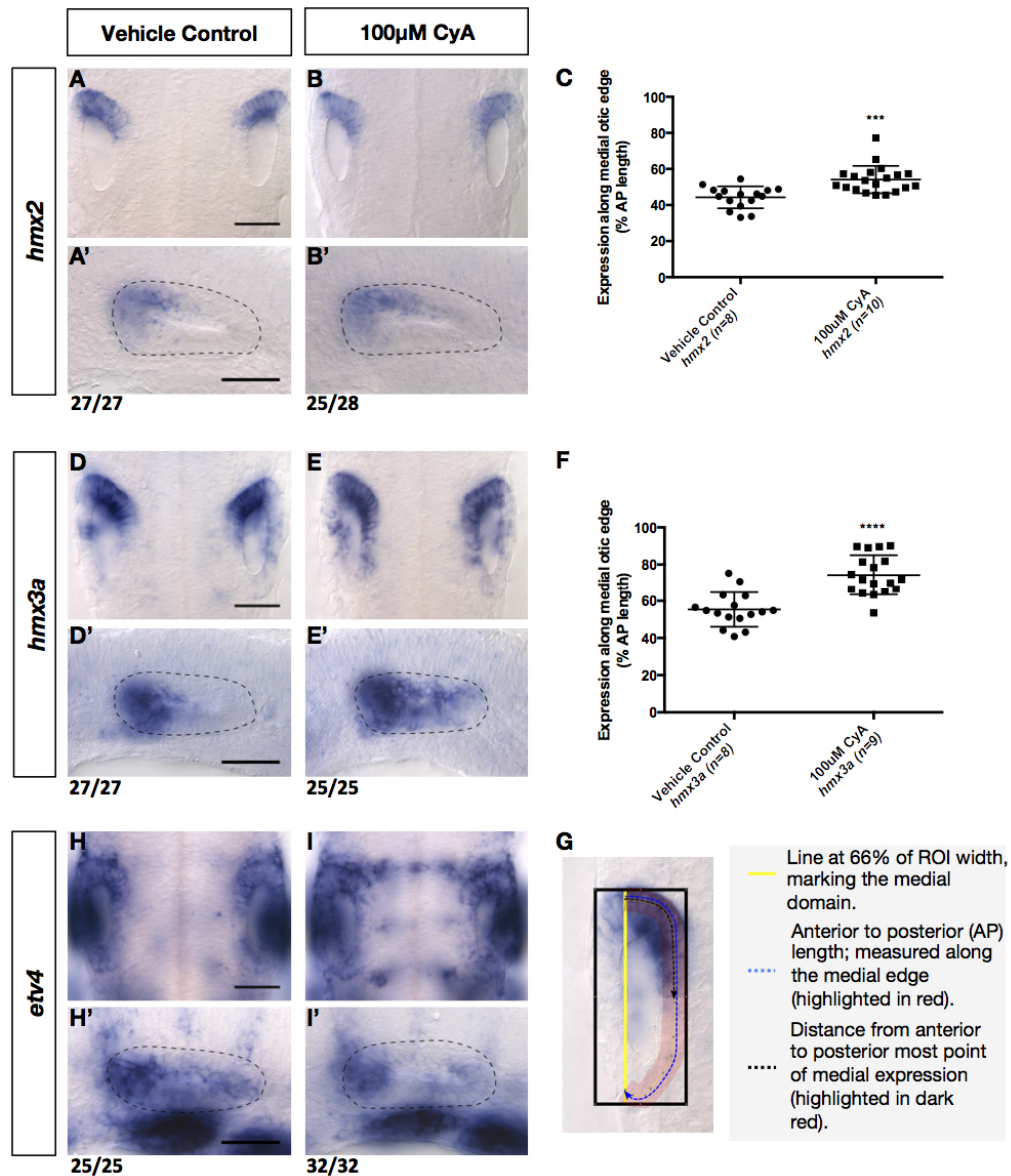


Figure 6.4: Inhibition of Hh signalling between 14/15 and 22/23 hpf leads to a posterior expansion of hmx2 and hmx3a expression

Expression in vehicle control and 100µM CyA-treated embryos at 22.5hpf as shown by in-situ hybridisation. (A–B') Expression of hmx2 is expanded medially in treated embryos (C) Quantification of hmx2 medial expression as a percentage of the overall medial anterior-posterior otic length shows a significant increase in the length of medial staining in treated embryos versus the vehicle controls (t-test on log-transformed data $p=0.0001$, $t=4.360$ $df=30.69$). (D–E') Expression of hmx3a in treated embryos shows a more dramatic expansion along the medial otic domain. (F) Quantification of hmx3a medial expression shows a significant increase in the length of medial staining in treated embryos versus the vehicle controls (t-test $p<0.0001$, $t=5.504$ $df=31.98$). (H–I') Expression of the Fgf transcriptional target, *etv4*, within the otic vesicle is unaltered in treated embryos. (G) Diagram of method used for quantification of staining. N= number of individual embryos. For C and F, both ears were measured from dorsal images. A–I are dorsal views with A'–I' being lateral views focused on the medial otic wall. Anterior is to the left in all images. All images were taken using DIC microscopy with a 40x objective. Scale bars: 50µM. N= number of individual embryos.

In the 100 μ M CyA-treated embryos it was observed that when the anterior to posterior length of the otic vesicle was measured using a bounding ROI the means of treated embryos for both *hmx2* and *hmx3a* in-situ hybridisations were smaller, although only significantly for those stained for *hmx2*, than the vehicle controls. Therefore to ensure the changes in otic expression of both *hmx2* and *hmx3a* were a consequence of altered Hh signalling rather than the otic tissue being smaller, the expression of *hmx2* and *hmx3a* was also studied in the strong Hh loss-of-signalling mutants, *smo*^{hi1640-/-}. Rather than being a point mutation such as the *smo*^{b641} and *smo*^{b577} alleles previously used in our lab (Hammond et al., 2003; Hammond and Whitfield, 2011), the *smo*^{hi1640} allele has a 6 kb proviral insertion within the first exon (Chen et al., 2001) and has been suggested to be a stronger loss-of-function *smoothened* mutation (personal communication with Drs S Elsworth and R Wilkinson). As the otic phenotype in *smo*^{hi1640-/-} mutants has not been described, homozygous mutants were morphologically identified and grown up alongside siblings to 3dpf at which point they were imaged (Figure 6.5A-B').

In the identified *smo*^{hi1640-/-} embryos, the predominant (61%, 17/28) otic phenotype was that of a smaller ear with two otoliths positioned next to one another on the ventral otic surface (Figure 6.5B') with the pillars either forming incorrectly or not at all, which resembles the phenotype seen in *smo*^{b641} mutants (Hammond et al., 2003). The other 39% of identified *smo*^{hi1640-/-} appeared to have a slightly milder phenotype with the otoliths still being positioned ventrally but spaced further apart and the ventral pillar also appearing more developed (Figure 6.5B), similar to the phenotypes reported for *disp1*^{tf18b} mutants and previously seen in 100 μ M CyA-treated embryos (Figure 6.1) (Hammond et al., 2003).

In the identified *smo*^{hi1640-/-} embryos fixed and stained with phalloidin (Figure 6.5C-D'), the sacular macula is clearly ventrally positioned abutting the anterior utricular macula (Figure 6.5D) unlike in the siblings (Figure 6.5C). In the phalloidin-stained *smo*^{hi1640-/-} embryos, we also observed a supernumerary lateral crista (Figure 6.5D', white asterisks) in 100% (8/8) of those imaged whereas this phenotype was not observed in any of the siblings imaged (6/6). Interestingly, despite showing phenotypic similarities to both *disp1*^{tf18b} and *smo*^{b641} mutants, the penetrance of this phenotype appears much higher in *smo*^{hi1640-/-} embryos than previously observed in the *disp1*^{tf18b} and *smo*^{b641} mutants (reported at 31% and 51%, respectively) (Hammond et al., 2003).

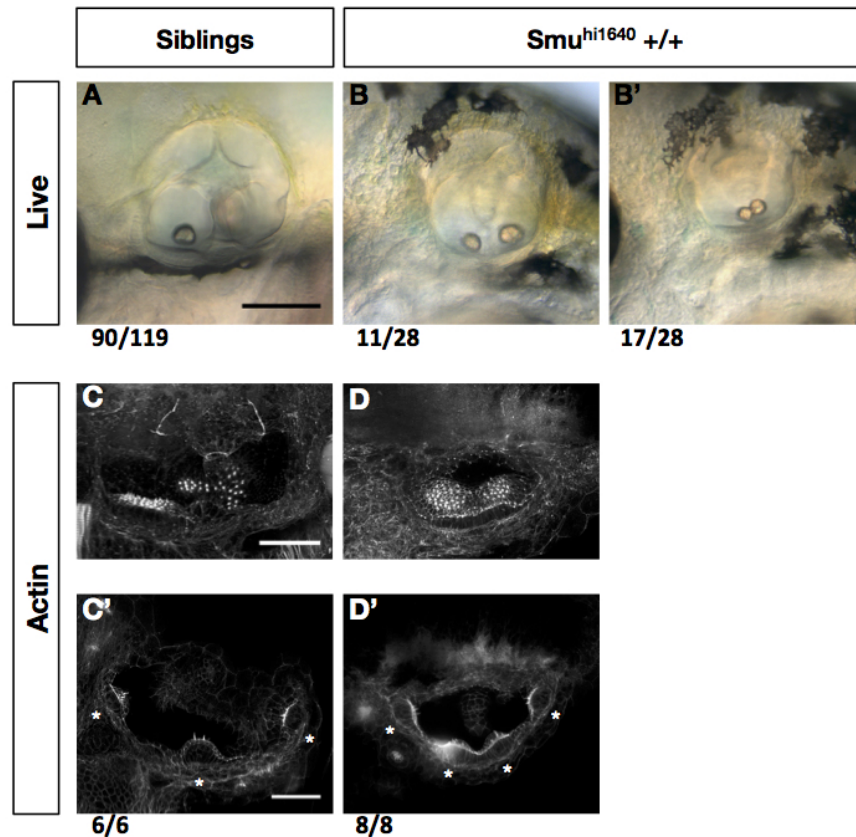


Figure 6.5: smu^{hi1640} homozygous embryos show a strong duplication of anterior morphology at 3dpf

(A–B') Live images of siblings and smu^{hi1640} mutants at 3dpf, showing a strong anterior duplication phenotype in the mutants (B–B'). (C–D') Phalloidin staining of the actin-rich stereociliary hair cells of the otic sensory patches. The posterior macula in the mutants (D) clearly shows a loss of the medially-located stereotypical fan morphology associated with posterior identity when compared to the siblings (C). Lateral views focusing on the cristae (C'–D') show a highly-penetrant supernumerary lateral crista phenotype. All images are lateral views with anterior to the left. A–B' were taken using brightfield microscopy with a 20x objective. C–D' were taken using confocal microscopy with a 40x oil objective. Scale bars: A; 50 μ M, C&C'; 25 μ M.

In smu^{hi1640} mutants and their siblings at 22.5hpf the expression of *hmx2* and *hmx3a* was then assayed using in-situ hybridisation. As seen in the 100 μ M CyA-treated embryos, staining for both *hmx2* and *hmx3a* appeared expanded along the ventromedial otic edge compared to the siblings (Figure 6.6B, B' and E, E', respectively). This was quantified using the same methodology as used in Figure 6.4 and confirmed the expansion in staining between the identified mutants and their respective siblings to be highly significant (Figure 6.6C and F), with a difference in mean percentage anterior-posterior length of 28% for *hmx2* and 22% for *hmx3a*.

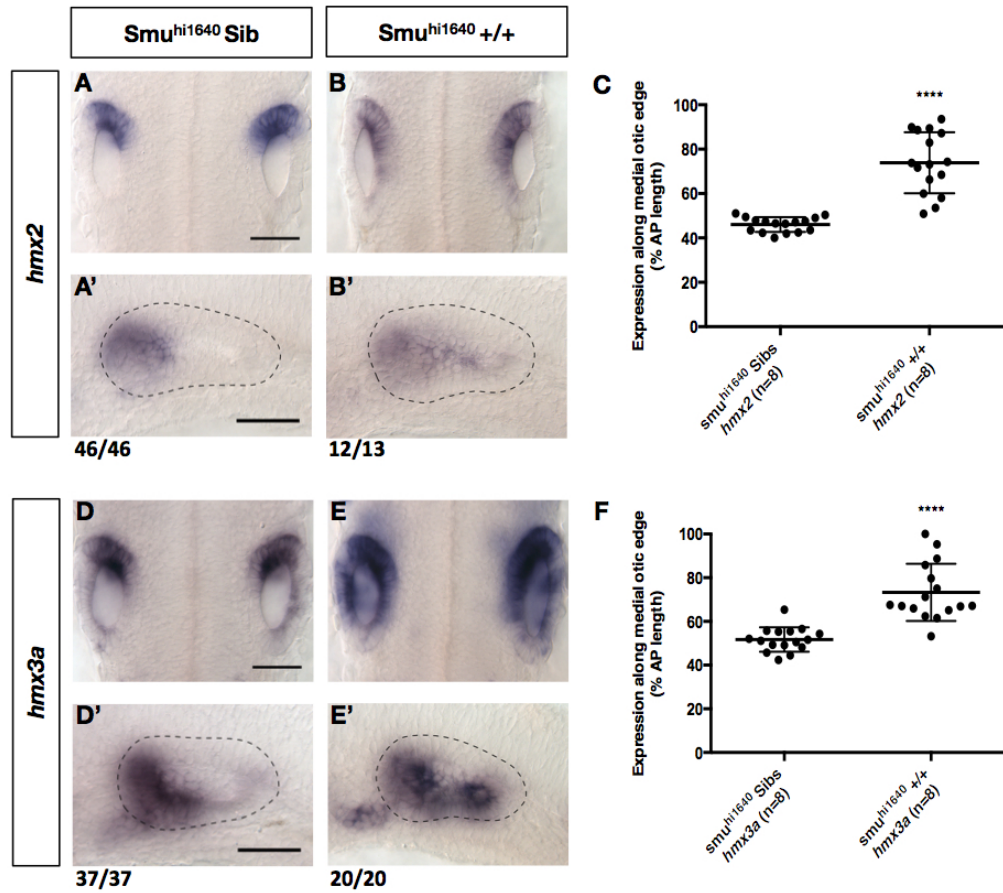


Figure 6.6: smu^{hi1640} homozygous embryos show a posterior expansion of $hmx2$ and $hmx3a$ at 22/23hpf

Expression in smu^{hi1640} mutants and their wild-type siblings at 22.5hpf as shown by in-situ. (A–B') Expression of $hmx2$ is expanded medially in smu^{hi1640} mutants when compared to the siblings. (C) The expansion of $hmx2$ staining in smu^{hi1640} mutants is a significant increase in the length of medial staining when compared to the siblings (t-test $p < 0.0001$, $t = 5.504$ $df = 31.98$). (D–E') Expression of $hmx3a$ is also expanded medially in mutant embryos relative to the siblings. (F) This expansion of $hmx3a$ staining in the mutants is significant when compared to the length of medial $hmx3a$ staining in the siblings (t-test $p < 0.0001$, $t = 6.069$ $df = 20.25$). N = number of individual embryos. For C and F, both ears were measured from dorsal images (a total of 16 datapoints). A–E are dorsal views with A'–E' being lateral views focused on the medial otic wall. Anterior is to the left in all images. All images were taken using DIC microscopy with a 40x objective. Scale bars: $50\mu M$. N = number of individual embryos.

6.2.4 The ventromedial expansion of *hmx2* and *hmx3a* expression after inhibition of Hh signalling between 14-15 and 22.5hpf persists at 36hpf

After treatment with CyA the other anterior markers, *fgf3*, *fgf8a* and *pax5* showed a clearly defined ectopic duplication of expression within the posterior domain by 36hpf (Figure 6.3). It was of therefore of interest to see whether the broad ventromedial domain of *hmx3a* expression observed by 22.5hpf (Figure 6.5) would later refine into two separate patches of expression at the anterior and posterior. Embryos were therefore treated with 100 μ M CyA between 14-15 and 22.5hpf, recapitulating the treatments used in Figures 6.3 but were grown on to 36hpf before being fixed.

To observe the otic expression of *hmx3a* in relation to the nascent utricular and saccular sensory domains, a double in-situ hybridisation was carried out with *hmx3a* (in red) and *atoh1a*, to mark developing otic sensory patches (in blue) (Figure 5.7) (Millimaki et al., 2007). In 100 μ M CyA-treated embryos, there is clear *hmx3a* staining across the entire otic ventral floor (Figure 6.7D-F') with expression persisting within the posterior otic domain (Figure 6.7E', white arrow) not seen in the vehicle controls (Figure 6.7A-C'). To observe whether this expansion was consistent across a sample (n=6) of the experimental population, the percentage of the posterior domain defined as the distance from the posterior of the anterior sensory domain marked by *atoh1a* to the most posterior point within the lumen with *hmx3a* staining was measured (Figure 5.7H) for both ears. This confirmed that the treated embryos showed a consistent significant expansion across almost the entire (treated mean; 96.55% \pm 1.114 vs vehicle control mean; 24.93% \pm 1.660) posterior domain when compared to the vehicle controls (Figure 6.7G). In the treated embryos, the anterior domain of *atoh1a* staining did not appear expanded compared to the vehicle controls and the posteromedial domain of *atoh1a* staining appears weakly in a more posterolateral position when compared to the vehicle controls (Figure 6.7D, F compared to A, C - white arrow).

In treated embryos, *hmx3a* staining also appears to be expanded medially (Figure 6.7F and F') relative to staining in the vehicle controls (Figure 6.7C and C'). Given the transient nature of the CyA inhibition of Hh signalling, this result suggests that loss of Hh signalling between 14-15 and 22.5hpf leads to changes within the otic vesicle that induce the persistence of *hmx3a* in a posteroventral region independently of the sensory domain.

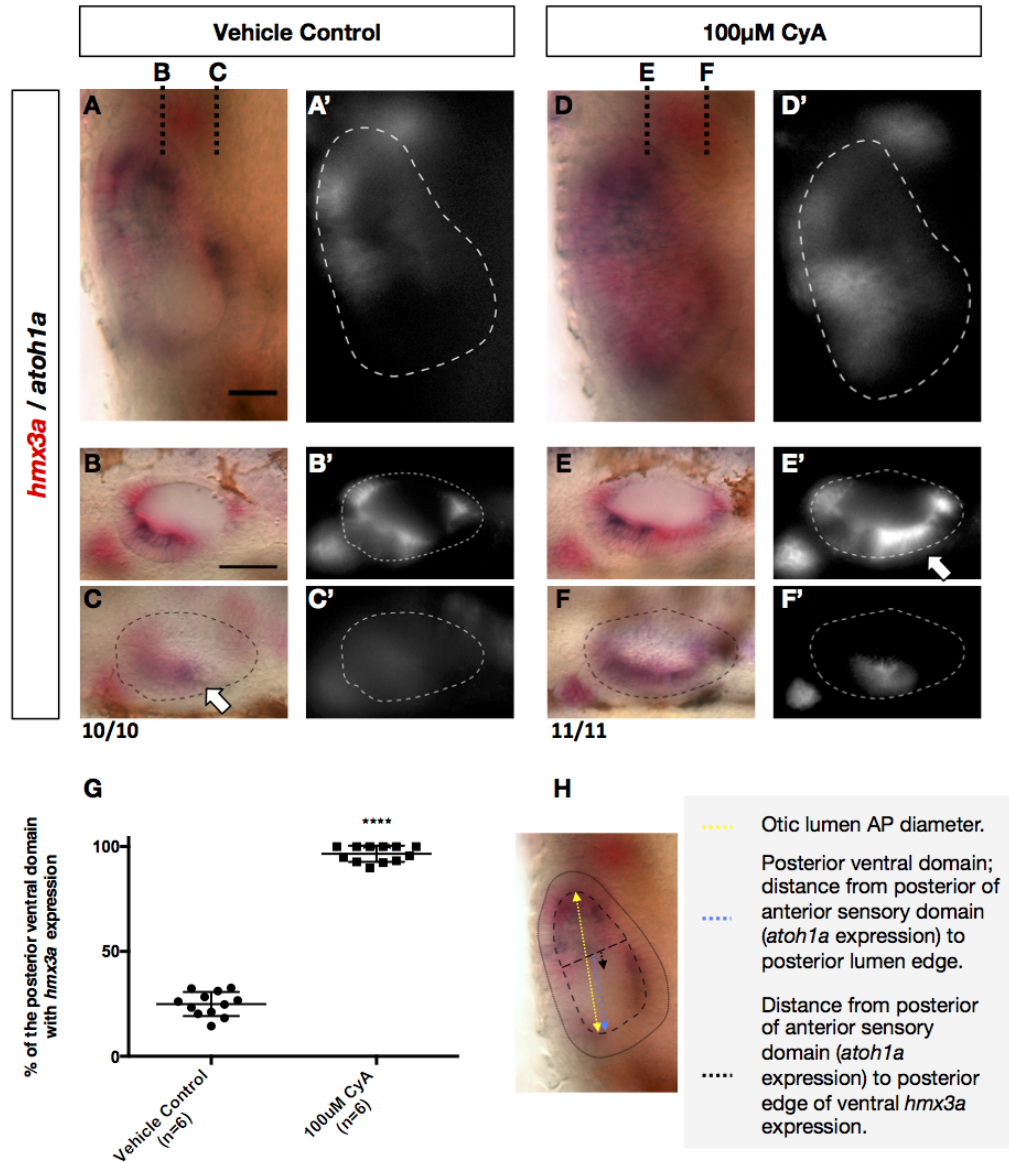


Figure 6.7: Inhibition of Hh signalling with 100uM CyA between 14/15 and 22/23 hpf result in a broad ventral domain of hmx3a by 36hpf

(A–F') Double in-situ for hmx3a (dark purple) and the sensory marker atoh1a (red) imaged using both DIC and fluorescent imaging (A'–F') to highlight hmx3a staining. (A–C') In vehicle control embryos, otic hmx3a is strongly localised to an anterior domain covering the anterior macula as marked by atoh1a but does not show co-localised staining with the posterior-medial sensory domain of atoh1a. (D–F')

In CyA-treated embryos, hmx3a but not atoh1a staining shows an expansion across the entire anterior-posterior length of the ventral floor (D–E', white arrow). Atoh1a expression also appears to be lost in the posterior-medial domain (F, D). (G) Quantification of hmx3a staining in the posterior otic domain shows a significant increase in treated embryos compared to the vehicle controls (t-test $p < 0.0001$, $t = 35.83$ $df = 19.24$) (H) Diagram of method used to quantify staining in the posterior otic domain. N = number of individual embryos. For G, both ears were measured from dorsal images. A, A', D, D' are dorsal views with all others being lateral views at different z-planes through the ear. Anterior is to the left in all images. Images were taken using DIC or epifluorescence microscopy with a 40x objective. Scale bars: 50µM.

6.2.5 Aberrant activation of Hh signalling does not lead to strong down-regulation of *hmx3a* by 14-16ss

As loss of Hh signalling, either through transient-treatment with CyA or in Hh loss-of-signalling mutants, leads to an expansion of *hmx2* and *hmx3a* expression that, for *hmx3a*, persists at 36hpf. I wanted to observe whether the converse, over-activation of Hh signalling, would lead to a loss of otic *hmx2* and *hmx3a* expression. It has previously been shown that when Hh signalling is elevated in either *shh* RNA injected embryos or *ptch1*^{-/-}; *2*^{-/-} mutants, *hmx3a* is reduced within the anterior otic domain (Hammond et al., 2003, 2010). However, this has been through observation of their expression at 30hpf and could reflect other transcriptional changes occurring prior to this within the anterior otic domain, as expression of both *fgf8a* and *pax5* have been shown to be down-regulated under these conditions by this time point (Hammond et al., 2003, 2010). Therefore *ptch1*^{-/-}; *2*^{-/-} mutants, in which Hh is aberrantly activated and their siblings were fixed at the 14-16ss (16-17hpf) before being assayed for *hmx2* and *hmx3a* expression via in-situ hybridisation (Figure 6.8).

At this stage *pax5* expression is only just detectable (Kwak et al., 2006) and neither of the strong anteriorising factors, *fgf3* (Millimaki et al., 2007) (own data) or *fgf8a* (Léger and Brand, 2002) are expressed within the otic vesicle so any changes in the expression of *hmx2* or *hmx3a* should be a consequence of an over-activation of Hh signalling. In the *ptch1*^{-/-}; *2*^{-/-} mutants at 14-16ss, *hmx3a* staining appears remarkably similar to that seen in the siblings (Figure 6.8A,A' compared to B,B'), although the medial staining in the *ptch1*^{-/-}; *2*^{-/-} mutants appeared slightly weaker. Measurement of the medial length of staining, as determined both by a calculated-threshold (Figure 6.8C and G) and by eye (data not shown), showed no significant difference between the siblings and identified double mutants. Interestingly, otic *hmx2* staining was visibly weaker in the *ptch1*^{-/-}; *2*^{-/-} mutants compared to the siblings (Figure 6.8D, D' compared to E, E'). However, measurement of *hmx2* staining using both threshold-calculated and by eye measurements again appeared to show no significant decrease in the length of medial staining, although the reduction in mean and standard deviation were greater than that of *hmx3a* in *ptch1*^{-/-}; *2*^{-/-} mutants (*hmx2* mean=45.69±3.942, S.D 15.77 vs *hmx3a* mean=51.34±2.787, S.D 10.43).

As *hmx3a* expression does not appear drastically reduced at 14-16ss (16-17hpf) when Hh signalling is aberrantly active in *ptch1*^{-/-}; *2*^{-/-} mutants but does later at 30hpf (Hammond et al., 2003), this gradual reduction implies that any inhibitory effect of Hh on *hmx3a* may be relatively weak compared to the response seen to changes in Fgf signalling (Hammond and Whitfield, 2011). It is also interesting that *hmx2* staining in *ptch1*^{-/-}; *2*^{-/-} mutants appears weaker than *hmx3a* under the same conditions. During normal development *hmx2* is expressed after *hmx3a* in the zebrafish otic placode (Hammond and Whitfield, 2011) (own data), and therefore this difference in expression might reflect a regulatory relationship between *hmx2* and *hmx3a*, that is affected by Hh signalling.

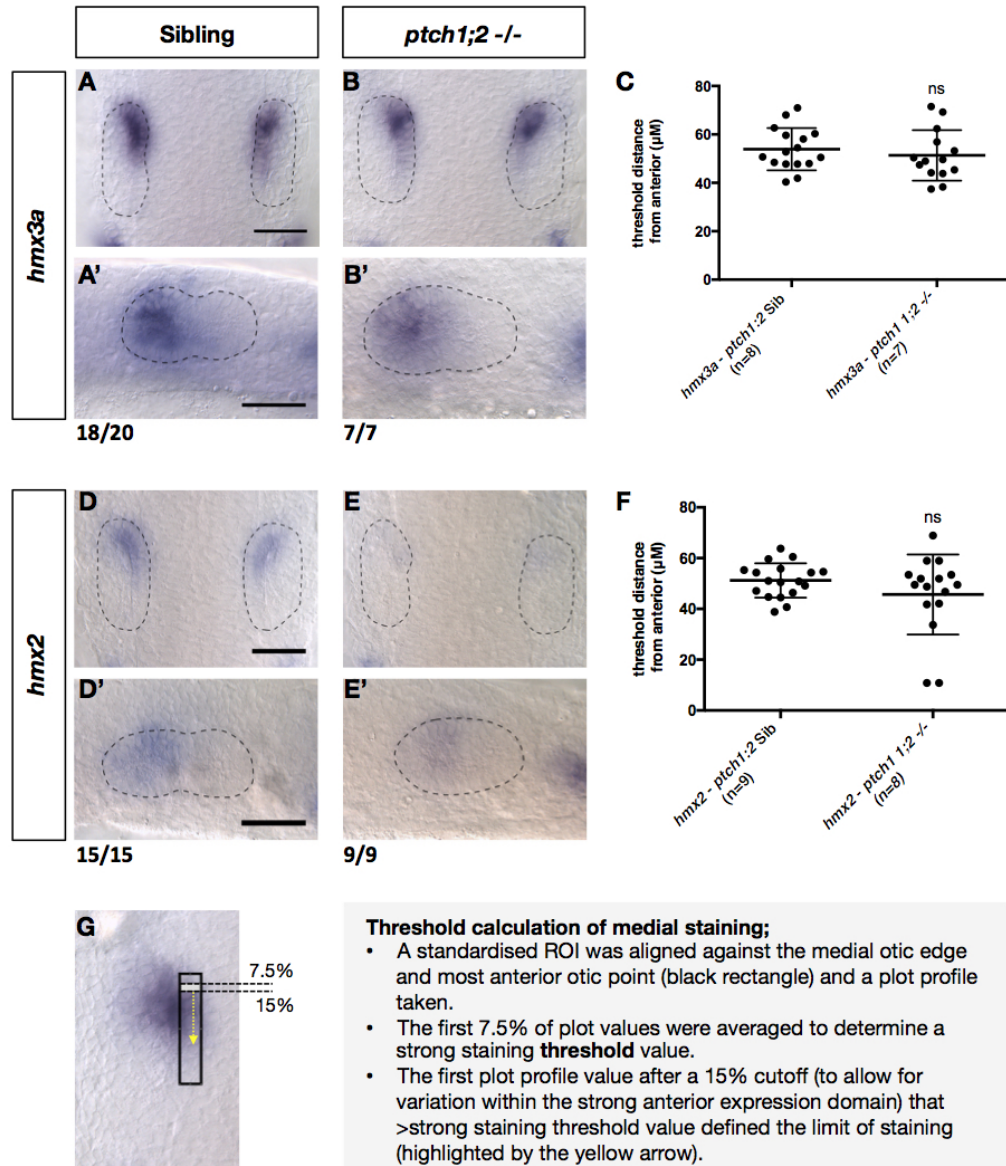


Figure 6.8: Aberrant activation of Hh signalling in *ptch1:2^{-/-}* double mutants does not significantly alter the domain of *hmx3a* but does result in an obvious weakening of *hmx2* expression at 14-16ss

(A–B') Expression of *hmx3a* in *ptch1:2^{-/-}* mutants does not appear obviously different from the siblings. (C) Despite a reduced mean, there was no significant difference in the threshold-length of medial staining between *ptch1:2^{-/-}* mutants and their siblings (*t*-test $p=0.4765$, $t=0.7225$ $df=25.56$) (D, E') Expression of *hmx2* in *ptch1:2^{-/-}* mutants appears clearly weaker relative to the siblings. (F) Despite *hmx2* staining appearing weaker and having a reduced mean, there was no significant difference in the threshold-length of medial staining between *ptch1:2^{-/-}* mutants and their siblings (Mann-Whitney $p=0.3605$, $U=117$) (G) Method for determining the threshold-calculated length of medial staining. N= number of individual embryos. For C and F, both ears were measured from dorsal images. Dotted lines outline the otic placodes with A–D being dorsal views and A'–D' being lateral views. Images were taken using DIC microscopy with a 40x objective. Scale bars: 50µM.

6.2.6 Over-expression of *fgf3* leads to an initially broad expansion in expression of anterior transcription factors which gradually resolves to the anterior and posterior otic poles

When Hh signalling was transiently inhibited, *pax5* along with *fgf3* and *fgf8a* did not show any posterior ectopic or expanded expression by 22.5hpf (Figure 6.2). Whereas *hmx2* and *hmx3a* showed a posterior expansion but were not strongly up-regulation within the posterior domain itself by 22.5hpf (Figures 6.4 and 6.6). Therefore to test whether the posterior otic domain is competent to express anterior factors at 22.5hpf and to also characterise expression of anterior factors at this time point after misexpression of *fgf3*, the heat-shock inducible, *hs:fgf3* transgenic line was used. Fgf misexpression was induced by a 39°C, 30 minute heat shock at 14-15hpf, a stage at which over-expression of *fgf3* has been shown to induce a duplication of anterior otic identity (Hammond and Whitfield, 2011), with embryos subsequently being fixed at 22.5hpf (Figure 6.9K).

The expression of the three *fgfs* that have been previously reported as influencing assignment of anterior otic character in zebrafish, *fgf3*, *fgf8a* and *fgf10a* were all observed after heat-shock induced over-expression of *Fgf3* (Hammond and Whitfield, 2011; Léger and Brand, 2002; McCarroll and Nechiporuk, 2013). *Fgf3* staining in the majority of transgenic embryos appeared weak across the dorsomedial otic domain with two stronger patches of staining at either pole (Figure 5.9B and B'), unlike the siblings which showed a single strong anterior domain of staining (Figure 6.9A and A').

In the transgenic embryos it was also observed that the expression of *fgf3*, normally observed within the pharyngeal pouches ventral to the ear is perturbed (Figure 6.9B' when compared to A'). *fgf8a* staining in the transgenic embryos was similar to *fgf3* with a clear anterior otic patch of staining along with patchy staining within the dorsoventral and posterior otic domain (Figure 6.9F and F'). Interestingly, the overall *fgf8a* staining in the transgenic embryos seemed weaker when compared to the siblings (Figure 6.9F, F' compared to E, E'), which may also account for why *fgf8a* staining in the posterior domain does not appear stronger. In contrast, *fgf10a* staining in transgenic embryos appears stronger across the dorsomedial edge and within the anterior-posterior otic pole domains (Figure 6.9J and J') when compared to the siblings (Figure 6.9I and I').

For *pax5* and *hmx3a*, staining within the transgenic embryos is consistently strong across the entire medial edge (Figure 6.9D, D' and H, H', respectively) rather than localised within the anterior domain as in the siblings (Figure 6.9C, C' and G, G'). Although at this stage, *pax5* staining does appear to be localised more dorsally than *hmx3a* (Figure 6.9D' vs H'). This result for *pax5* replicates that seen by Hammond et al, 2011 at 24hpf, after a similar over-expression of *fgf3*.

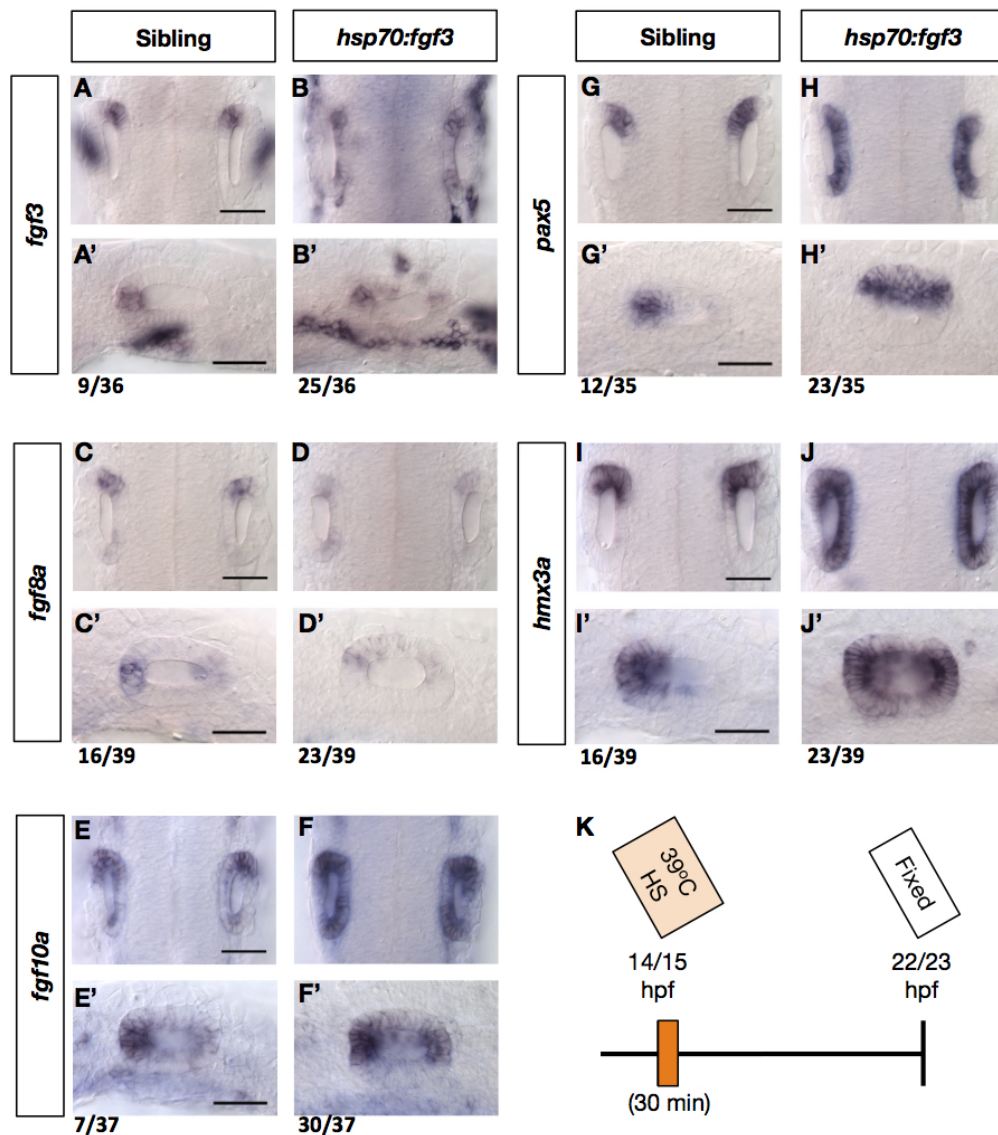


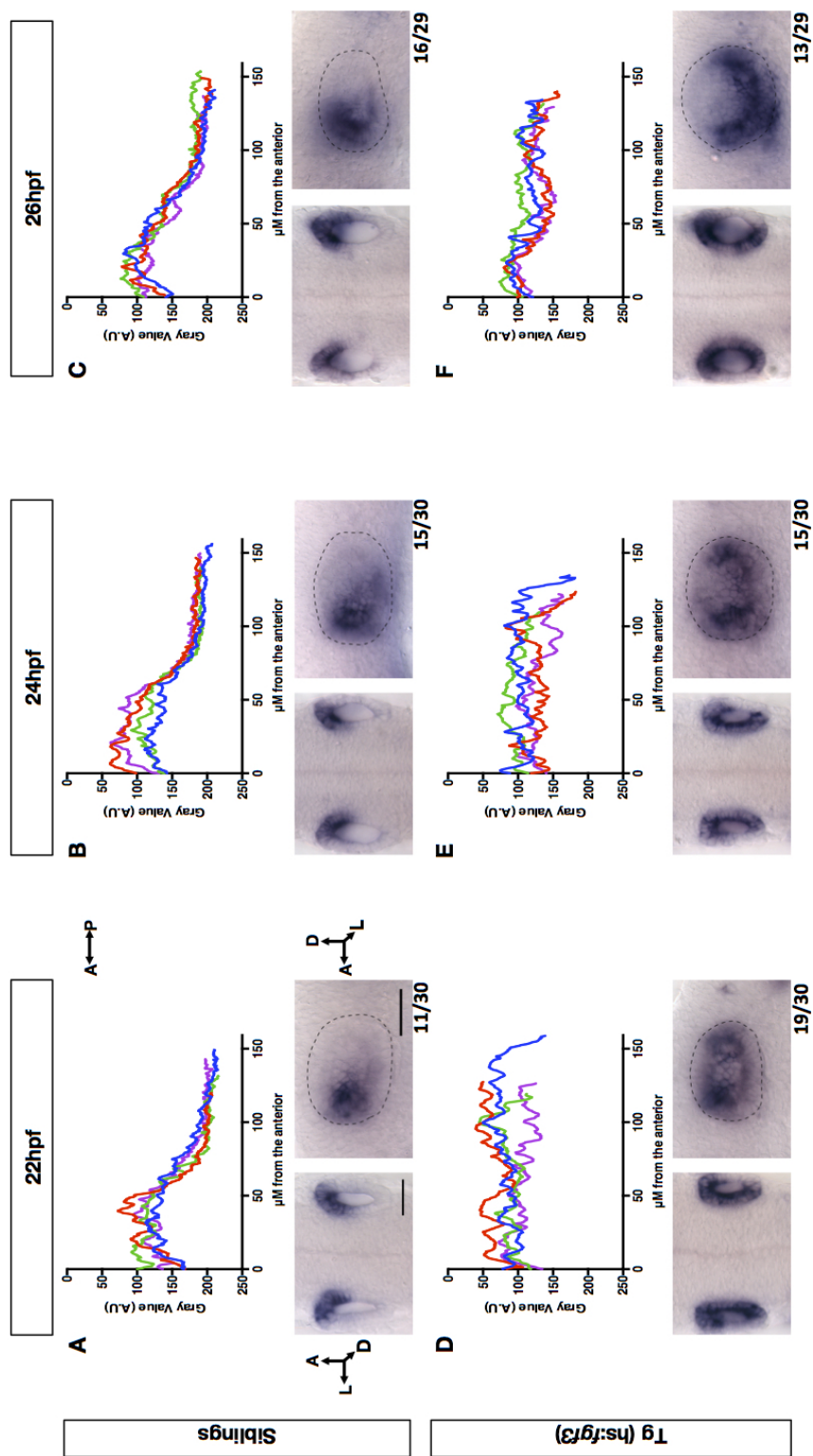
Figure 6.9: Over-expression of *fgf3* can result in up-regulation of *fgf10a*, *pax5* and *hmx3a* across the entire AP axis of the medial otic edge by 22.5hpf

(A–B') Expression of *fgf3* in heat-shocked transgenic (*hs:fgf3*) embryos at 22.5hpf shows staining in a patchy dorsomedial domain, strengthened at the anterior-posterior poles. (C–D') *Fgf8a* staining in transgenic embryos appears similar to *fgf3* spatially, although overall weaker. (E–F') *Fgf10a* staining, is stronger across the whole medial otic domain in transgenic embryos compared to their siblings. (G–H) *Pax5* expression appears as a broad dorsomedial domain in the transgenic embryos compared to a defined anterior domain in the siblings. (I–J) *Hmx3a* shows a similar broad medial expression to *pax5* in the transgenic embryos. (K) Schematic of heat-shock treatment. A–J are dorsal views with A'–J' being lateral. Images were taken using DIC microscopy with a 40x objective. Scale bars: 50 μ M.

Following the results observed at 22.5hpf after the over-expression of *fgf3* (Figure 6.9), where *fgf3* and *8a* showed primarily pole-localised expression compared to a broad, medial expression for *pax5* and *hmx3a*. I wanted to observe how over time this broad, medial expression of *hmx3a*, as the earliest anterior otic marker, resolves to form two separated domains of expression. Therefore progeny from a *hs:fgf3* +/- identified x AB-wildtype cross were heat-shocked using the same method and timings as used for Figure 5.9 (39°C, 30 minute heat shock at 14-15hpf) and fixed at 22, 24 and 26hpf (Figure 6.10).

In-situ hybridisations for *hmx3a* were carried out for these time points and plot profiles of staining within the medial edge for four embryos were plotted to clearly show any changes in expression and the consistency of these. In the transgenic embryos, at 22hpf, *hmx3a* shows strong expression across the entire medial otic domain with no clear difference in staining intensity between the anterior-posterior poles and centre when viewed dorsally (Figure 6.10D). At 24hpf, *hmx3a* staining still appears broadly across the medial edge, although appearing weaker than at 22hpf (Figure 6.10E) and also more ventrally-localised when viewed laterally. At 26hpf, the *hmx3a* staining still appears strong at the anterior and posterior poles but weaker within the central region of the medial edge (Figure 6.10D), a trend that is apparent in the majority of the staining profiles plotted. Compared to the transgenic heat-shocked embryos, siblings at all three time points show a consistent anterior domain of *hmx3a* staining (Figure 6.10A, B and C).

The data shown in Figure 6.10 suggests that after a broad otic induction of *hmx3a* expression, approximately 12 hours after over-expression of *fgf3*, expression of *hmx3a* is no longer maintained within the middle dorsomedial domain but is maintained at the AP poles and the ventral domain, similar to that seen after inhibition of Hh (Figure 6.7). As the expression of *fgf3* and *fgf8a* appear to be maintained at the poles at 22.5hpf after heat-shock induction of *fgf3* rather than the middle medial domain, this could explain why *hmx3a* expression persists in these domains given its dependence on Fgf signalling (Feng and Xu, 2010).



ph!

Figure 6.10: After over-expression of *fgf3*, *hmx3a* shows broad medial expression which progressively resolves to the AP poles (A–C) Sibling embryos from a *Tg(hs:fgf3)* +/- outcross, heat-shocked at 14hpf and fixed at 22 (A), 24 (B) and 26hpf (C), show strong anteromedial expression at all three time points. Plot profiles generated in FIJI of the medial edge highlight the consistency of this domain over multiple embryos. (D–F) *Tg(hs:fgf3)* +/- embryos heat-shocked under the same conditions show an initially broad medial expression domain at 22hpf (D). Between 22 and 26hpf, *hmx3a* expression weakens within the middle of the medial domain but remains strong at the anterior and posterior. The medial expression between 22 and 26hpf also appears to weaken dorsally and strengthen ventrally. Plot profiles are of ISH staining along the medial edge with each colour representing an individual embryo (n=4). The images below on the left are dorsal views and on the right, lateral. All images were taken with a 40x objective. Scale bar: 50 μM .

6.2.7 Localisation and maintenance of *fgf* expression within anterior and posterior otic domains

Given the localisation of *fgf3* and *fgf8a* expression to the anterior and posterior poles after misexpression of *fgf3* (Figure 6.9) and also for *fgf8a*, transiently during normal development (own data and (Léger and Brand, 2002)), the question arises of how the anterior and posterior pole domains differ from the middle medial otic domain. One mechanism could be that components of the Fgf signalling pathway are abundantly present or strongly maintained within the otic poles allowing indirect positive feedback on their expression, for example through *hmx2* and *hmx3a* (Feng and Xu, 2010). The expression of the known Fgf receptors has been studied in the vertebrate ear with *fgfR2* and *fgfR4* being suggested to show localised expression within the anterior and posterior otic domains in zebrafish (Ota et al., 2010; Maier and Whitfield, 2014). To confirm this, in-situ hybridisation using probes for both *fgfR2c* and *fgfR4* in wild-type embryos fixed at 26hpf were carried out. This showed *fgfR2c* is expressed within a posteromedial domain of the ear (Figure 6.11A-B') but not the anterior and that *fgfR4*, contrary to previous reports, has no obvious expression within the otic vesicle at this time (Figure 6.11C-D').

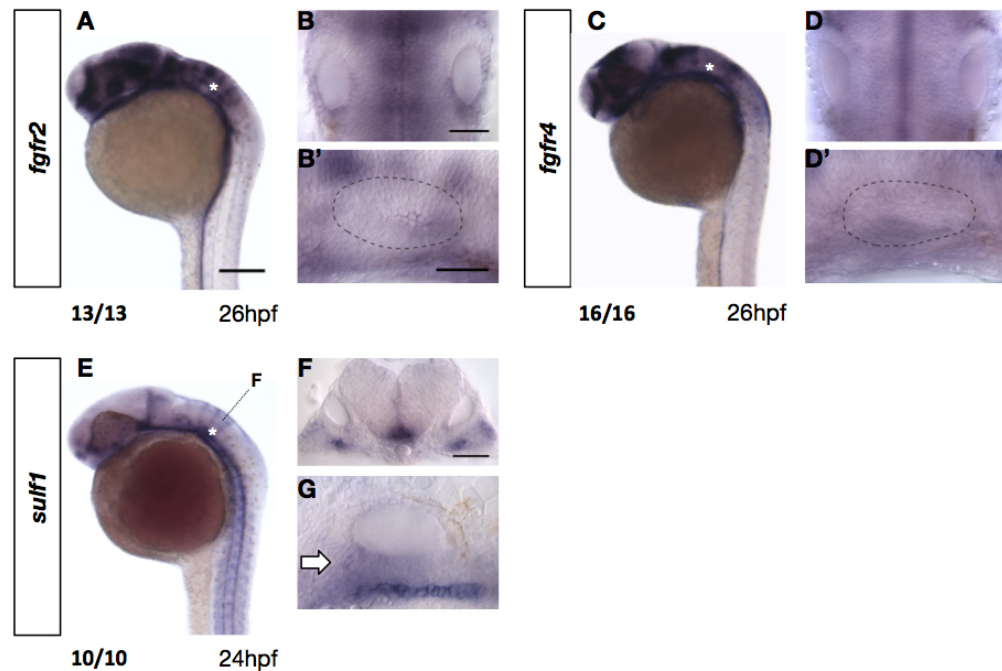


Figure 6.11: Fgfr2, fgfr4 and sulf1 do not show localised expression at both the anterior and posterior otic poles by 26hpf

(A–B') In situ hybridisation for *fgfr2* in 26hpf embryos shows expression within the hindbrain adjacent to the OV and weakly within the posteromedial otic domain (B–B'). (C–D') *Fgfr4* in 26hpf embryos shows weak expression anterior to the OV but none within the OV itself (D–D'). (E–G) *Sulf1* in 24hpf embryos shows weak expression in the anterior otic vesicle (white arrow) along with strong expression within the floor plate adjacent to the OV and weakly in a domain in the underlying mesoderm. White asterisks in A, C and E mark the position of the otic vesicle. Images A, C and E were taken using brightfield with a 4x objective (2x magnification). All other images were taken using DIC with a 40xW objective. Scale bar: A; 200 μ M for B, B' and F; 50 μ M.

As expression of the *fgf receptors* appear to have no obvious localisation to the anterior-posterior poles, expression of another Fgf signalling modulator, the heparan sulphate proteoglycans (HSPGs) were looked at. HSPGs are thought to form a ternary complex with Fgf receptors and ligands at the cell membrane during Fgf signalling and the glycosaminoglycan chains of HSPGs can be modified through sulfation resulting in structural and binding heterogeneity (reviewed in Brewer et al. 2016). In zebrafish this modulation of HSPG sulfation is achieved by the 6-O-endosulfatases, Sulf1 and Sulf2, with expression of *sulf1*, which has been implicated in modulating Fgf signalling in the lateral line, having also been observed in the otic vesicle (Meyers et al. 2013 and personal communication with Dr B Pownall). However, in-situ hybridisation against *sulf1* did not show any strong otic expression localised to both poles by 26hpf with only a weak anterior patch of anterior staining observed (Figure 6.11E-G, white arrow). *Sulf1* and *2* have been reported to be expressed in the otic tissue of chick and mice with double knock-outs in mice leading to an increase in hair cell number (Freeman et al., 2014). Therefore the anterior expression of *sulf1* seen in zebrafish at prim-5 (24hpf) may reflect a later role in regulating the sensory epithelium, possibly through Fgf signalling.

Another potential mechanism by which the expression of *fgfs*, and subsequently other anterior markers, could be localised to the poles is through localised regulation of transcription. As expression of *atoh1a/b* show early restriction to the anterior and posterior poles of the otic placode, specifying the sensory domains, a feedback loop between *Atoh1a* and anterior markers such as *fgf3* and *fgf8a* may account for why expression of these anterior markers are maintained within these discrete domains (Figure 1.6) (Millimaki et al., 2007; Sweet et al., 2011).

Mindbomb (*mib*^{ta52b}) mutants carry a missense mutation in the gene coding for a mis-sense RING E3 ubiquitin ligase required for Notch activation (Itoh et al., 2003) and in these mutants the early expression of *atoh1a* and *atoh1b* within the otic placode fails to restrict to the anterior and posterior poles and ectopic hair cells form (Millimaki et al., 2007). To observe if the broad expression of *atoh1a* is maintained at later stages in *mib* mutants and as a result, whether expression of *fgf3*, *fgf8a* and *hmx3a* are no longer localised, identified *mib* mutants were fixed alongside their siblings at 26hpf and assayed by in-situ hybridisation (Figure 6.12). Interestingly in the *mib* mutants, expression of *atoh1a* is maintained within the otic vesicle with two, slightly larger, pole patches of staining observed stereotypically positioned along the mediolateral axis (Figure 6.12B and B'). However, *atoh1a* staining within the dorsal hindbrain was strikingly absent in the mutants compared with their siblings (Figure 6.12B' compared to A'). *Fgf3* and *fgf8a* staining in the *mib* mutants, rather than showing ectopic or enlarge domains, appeared severely reduced within the anterior otic domain but not within the underlying branchial pouches (Figure 6.12E-F' and G-H', respectively) suggesting an otic-specific response.

For *hmx3a*, in the *mib* mutants, whilst the dorsoventral patterning of *hmx3a* appeared consistent with that seen in the siblings (Figure 6.12D' and C', respectively) the ventral domain of staining appeared both slightly less posteriorly expanded and appeared lost within a small anteroventral otic domain. A loss of staining within the cells anterior to the otic vesicle, presumed to be the anteroventral lateral line ganglion (gAV) (Figure 6.12D', white arrow) (Feng and Xu, 2010), was also observed in the mutants along with an drastic strengthening of staining in the dorsal trunk (not shown) compared to their siblings.

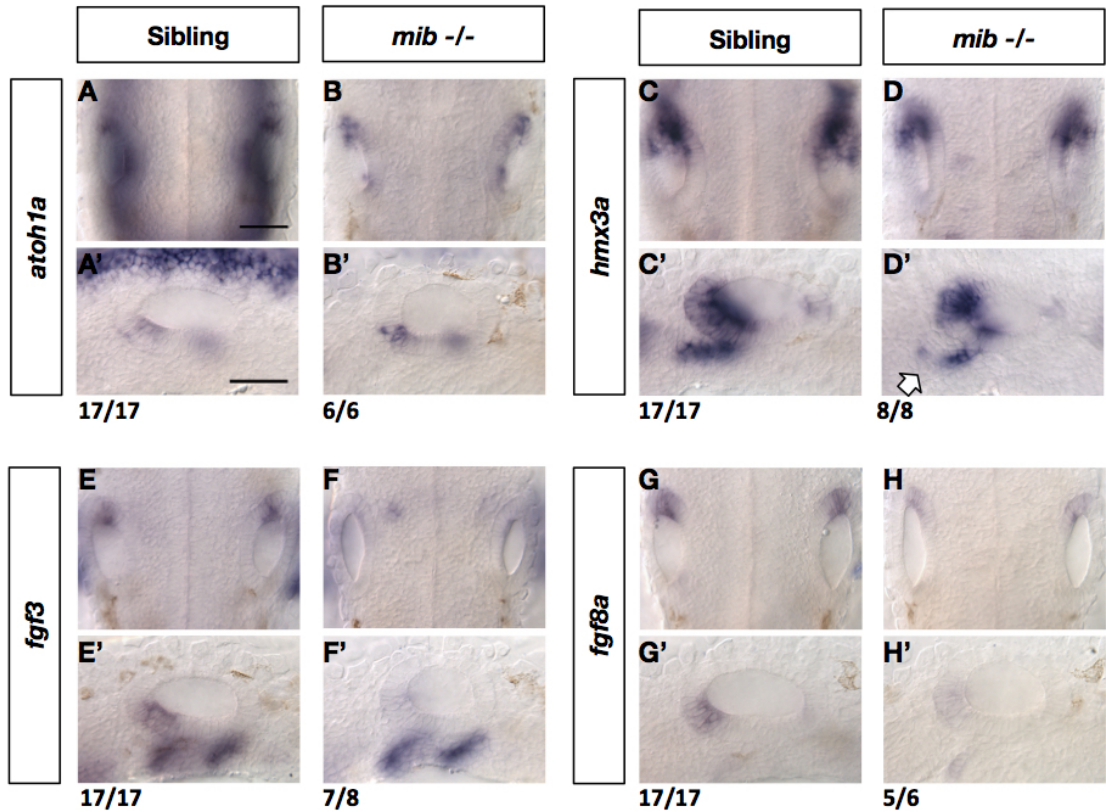


Figure 6.12: *fgf3*, *8a* and *hmx3a* expression in *mindbomb* E3 ubiquitin protein ligase (*mib*) mutants

Expression of *fgf3*, *8a* and *hmx3a* in 26hpf *mib* ^{+/+} mutants, where notch signalling is perturbed. (A–B') *atoh1a* expression in *mib* mutants is reduced in the dorsal hindbrain but expression domains with the OV appear slightly expanded and strengthened. (C'–D') *Hmx3a* expression in *mib* mutants appears to be lost in the anteroventral domain of the OV and SAG (D' white arrow). (E–F') *fgf3* expression in the anterior OV appears clearly reduced in *mib* mutants although expression in the pharyngeal pouches is similar to that in the siblings. (G–H) *fgf8a* expression in the anterior OV appears reduced in *mib* mutants and any changes in posterior OV expression were not obvious. All images were taken with DIC with a 40xW objective. Scale bars: 50 μ M.

6.2.8 Both *fgf3* or *fgf8a* have the ability, when over-expressed at 14hpf, to result in morphological duplications of anterior otic identity which is reduced by >18hpf

Whilst the ability of *Fgf3* when over-expressed to induce a transcriptional and morphological duplication of anterior otic identity has been well characterised in zebrafish (Hammond and Whitfield, 2011) the same cannot be said for *fgf8a*, despite having a clear, although possibly distinct, role in defining anterior otic identity (Phillips et al., 2001; Maier and Whitfield, 2014). Sweet et al. demonstrated that using a heat-shock promoter to drive over-expression of *fgf8a* can produce ectopic duplicated domains of *fgf3*, *pax5* and *hmx3* across the otic AP axis (Sweet et al., 2011). However to confirm whether over-expression of *fgf8a* also results in a morphological duplication of the anterior domain as seen with *fgf3*, embryos from a *hs:fgf8a* +/- incross and *hs:fgf3* +/- incross were heatshocked at 14-15hpf at 39°C for 30 minutes before being raised to 3dpf and fixed for phalloidin staining (Figure 6.13A-D'). This treatment resulted in a loss of posterior otic morphology for both transgenic lines, with the posterior sensory patch being positioned more ventrolaterally. The phenotypes seen after over-expression of *fgf8a* appear to be milder than those observed after over-expression of *fgf3*, with a reduced distance between what appears to be a remnant of the posterior macula and the now ventrolaterally-positioned majority of the posterior sensory patch (Figure 6.13D-D').

Given these differing phenotypes and also that *fgf3* and *fgf8a* may be working in slightly differing ways during otic patterning, I also wanted to confirm whether only *fgf8a* misexpression within a particular time window would result in a duplication of anterior morphology, as is the case for *fgf3* (Hammond and Whitfield, 2011; Léger and Brand, 2002; Maier and Whitfield, 2014). Therefore using the same *hs:fgf8a* +/- and *hs:fgf3* +/- crosses as previously, embryos were heat-shocked for the same period and temperature but at 18hpf rather than 14hpf. The result confirmed that over-expression of *fgf3* (Figure 6.13E-H) or *fgf8a* (Figure 6.13I-L) at time points >16hpf results in the majority of transgenic embryos having a grossly normal otic morphology similar to that of their siblings and clearly different from transgenics heat-shocked at 14hpf. From these results it appears that the competence of the otic placode to adopt an anterior sensory morphology in response to over-expression of *fgf* is lost at later stages (>18hpf) and is not specific to either *fgf3* or *fgf8a*.

To ask the question of whether this inability of the otic placode to produce an anterior duplication in response to a late over-expression of *fgf3* or *8a* is due to a loss of competence to respond at the transcriptional level, 18hpf heat-shocks were carried out as before on *hs:fgf3* incross embryos but were fixed at 22/23hpf (Figure 6.14H) before being assayed by in-situ hybridisation. *Pax5*, *hmx3a* and *fgf10a* (Figure 6.14) were previously shown to respond to over-expression of *fgf3* at 14hpf (Figure 5.9) and surprisingly, in the 18hpf heat-shocked transgenic embryos, *pax5* (Figure 6.14B and B') and *hmx3a* (Figure 6.14D and D') showed a similar staining across the entire medial edge. *Fgf10a* also showed broad staining along the medial edge of the otic vesicle but only in 5/28 embryos (23%) (Figure 6.14G) with the remaining transgenic embryos only having stronger staining within the posterior domain compared to the siblings (Figure 6.14F, F' compared to E, E').

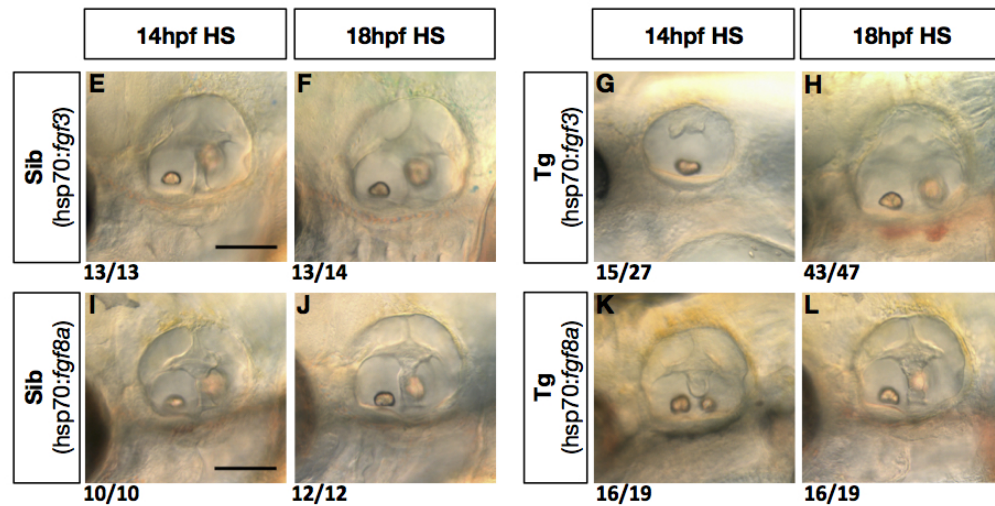
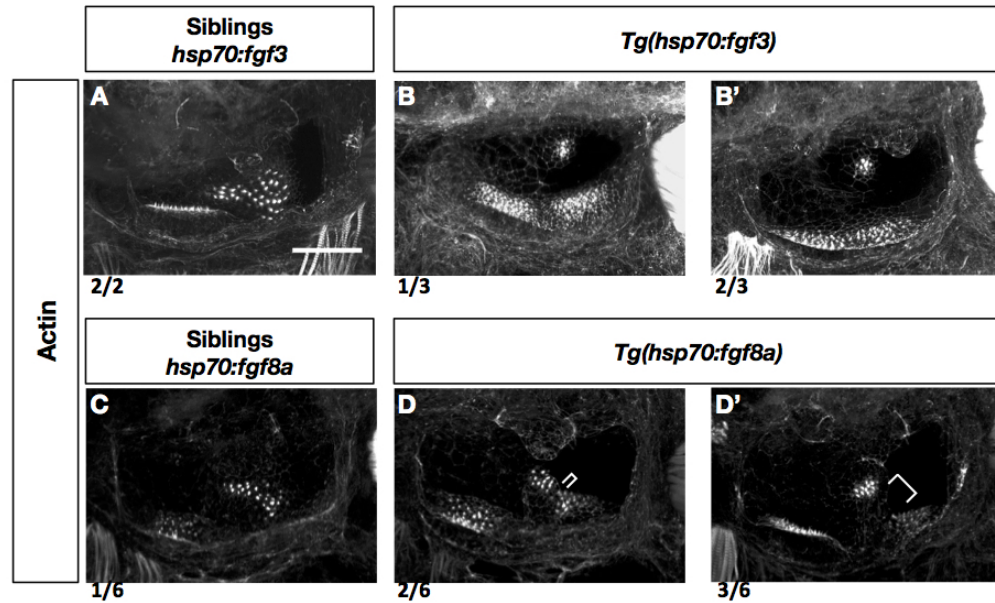


Figure 6.13: *fgf3* and *fgf8a*, when over-expressed, result in differing otic phenotypes but both show a reduction in ability to duplicate anterior otic morphology when heat-shocked at ≥ 18 hpf

(A–B') Transgenic *hs:fgf3* transgenic embryos heat-shocked at 14hpf show a clear loss of the stereotypical posterior macula morphology seen in the siblings (A) and two closely-positioned ventrolateral maculae (B–B'). (C–D') *Hs:fgf8a* embryos heat-shocked at 14hpf show abnormal patterning of the posterior macula, with the posterior most region of the sensory patch appearing to be laterally positioned to varying degrees (D&D', white lines). (E–H) *Hs:fgf3* embryos heat-shocked at 18hpf (H) rather than 14hpf (G) show a largely normal positioned posterior otolith, resembling the siblings (E–F). (I–L) Similarly, *hs:fgf8a* embryos heat-shocked at 18hpf (L) show a grossly normal positioning of the posterior otolith unlike in transgenic embryos heat-shocked at 14hpf (K) All images are lateral views. A–D were taken using confocal microscopy with a 40x oil objective. E–L were taken using DIC with a 20x objective.

Scale bars: A; 25 μ M, E&I; 50 μ M.

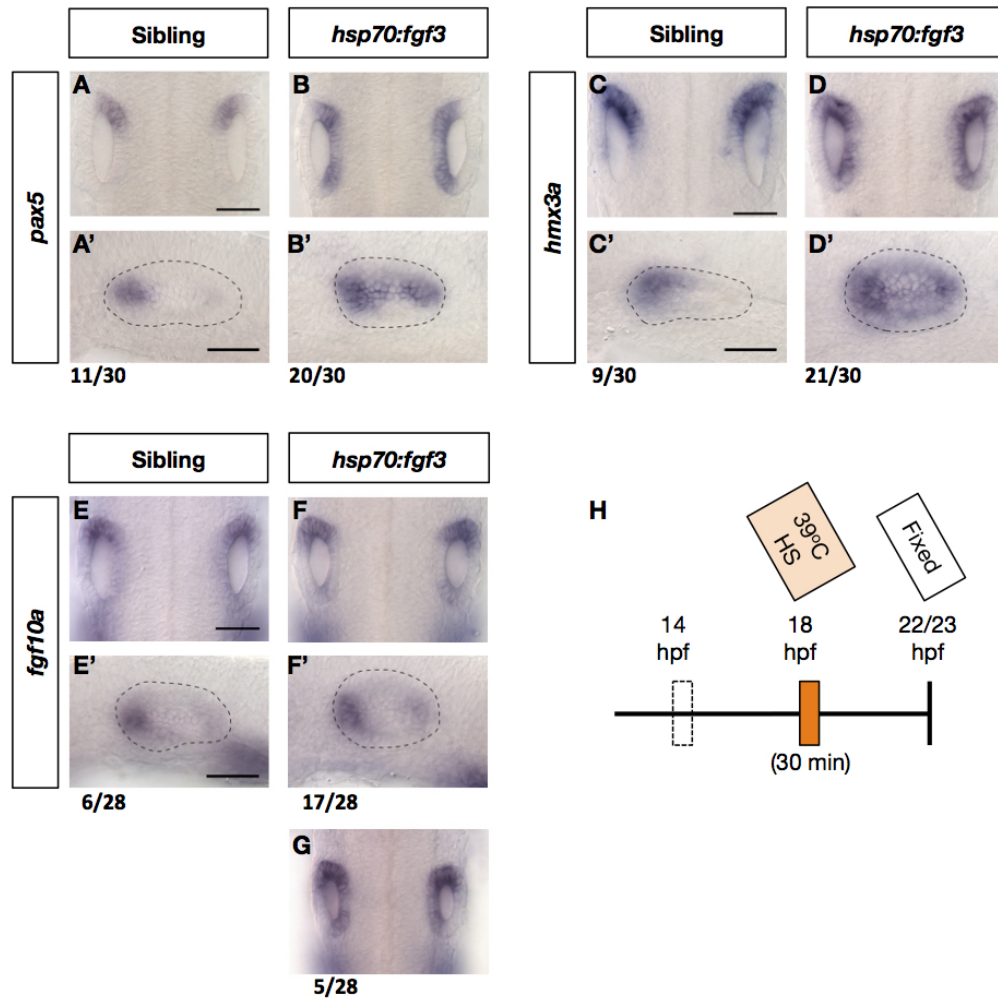


Figure 6.14: *pax5*, *hmx3a* and *fgf10a* at 22.5hpf are broadly expressed across the otic medial edge after over-expression of *fgf3* from 18hpf (A–B') Expression of *pax5* in transgenic (*hs:fgf3*) embryos heat-shocked at 18hpf show staining in a broad medial domain at 22.5hpf (B–B') unlike in the siblings (A–A'). (C–D') *hmx3a* staining in transgenic embryos appears similar to *pax5*, being present strongly present across the medial otic domain (D–D') rather than in a discrete anterior domain as seen in siblings (C–C'). (E–G) *Fgf10a* staining, is stronger across the whole medial otic domain in a subset of transgenic embryos (G) but the majority show an up-regulation in the posterior otic pole but not the middle medial domain (F–F'). (H) Schematic of 18hpf heat-shock treatment. A–G are dorsal views and A'–F' are lateral. Images were taken using DIC microscopy with a 40x objective. Scale bars: 50 μ M.

Based on the previously studied roles of *pax5* and *hmx3a* in anterior otic identity and that the medial expansion seen in the 18hpf heat-shocked embryos is similar to that in 14hpf heat-shocked embryos, this expansion appears at odds with the lack of a morphological duplication observed (Figure 6.13). Anterior and posterior otic identity can also be distinguished based on the hair cell polarity patterns of the respective macula, using phalloidin to mark the stereocilia and anti-acetylated tubulin to mark the kinocilia (see Section 1.4.3) (Haddon et al., 2000).

Therefore to observe whether the lack of a strong morphological duplication after an 18hpf heat-shock was accompanied by a stereotypical posterior hair cell polarity pattern *hs:fgf3* in cross embryos were heat-shocked at 18hpf as before (Figure 6.13 and 14) but were grown on to 3dpf (approximately 75hpf) before being imaged and subsequently fixed for staining (Figure 6.15K). In live, 3dpf embryos dorsally imaged, the majority (25/34, 74%) of transgenic, heat-shocked embryos showed a posterior otolith at a similar medial position to the non-transgenic, heat-shocked siblings but this was more ventrally located (Figure 6.15B compared to A). The remaining transgenic embryos (9/34, 26%) showed a stronger ventralisation in the position of the posterior otolith, although still remaining medial to the anterior otolith (Figure 6.15C).

Interestingly, the hair cell polarity of the posterior macula in heat-shocked, transgenic embryos showed the posterior 'pan' domain of the macula positioned, at varying degrees, in a separate and ventral location, which was not observed in the non-transgenic siblings (Figure 6.15E-I compared to D and D'). This ventral posterior domain of the macula in transgenic embryos also showed a loss of the stereotypical dorsoventral opposing hair cell polarity (Figure 6.15H-I). In contrast to this, the remaining anterior handle domain in most of the transgenic embryos imaged maintained a similar AP opposing hair cell patterning to that observed in the corresponding domain of the non-transgenic siblings.

Comparison of the number of hair cells within the handle domain displaying such anterior/posterior polarity showed no significant difference between the transgenics and their non-transgenic siblings (Figure 6.15J) and similarly no significant difference in the overall number of hair cells (defined in the non-transgenics as any hair cell anterior of and including, those marked in red - Figure 6.15D') was observed. This data suggests that despite appearing grossly morphologically normal after an 18hpf heat-shock, reported both in this project and previously, Tg(*hs:fgf3*) embryos actually do have a perturbed posterior macula morphology and hair cell patterning that might reflect the broad, medial ectopic otic expression of anterior factors such as *hmx3a* seen at 22.5hpf in such embryos.

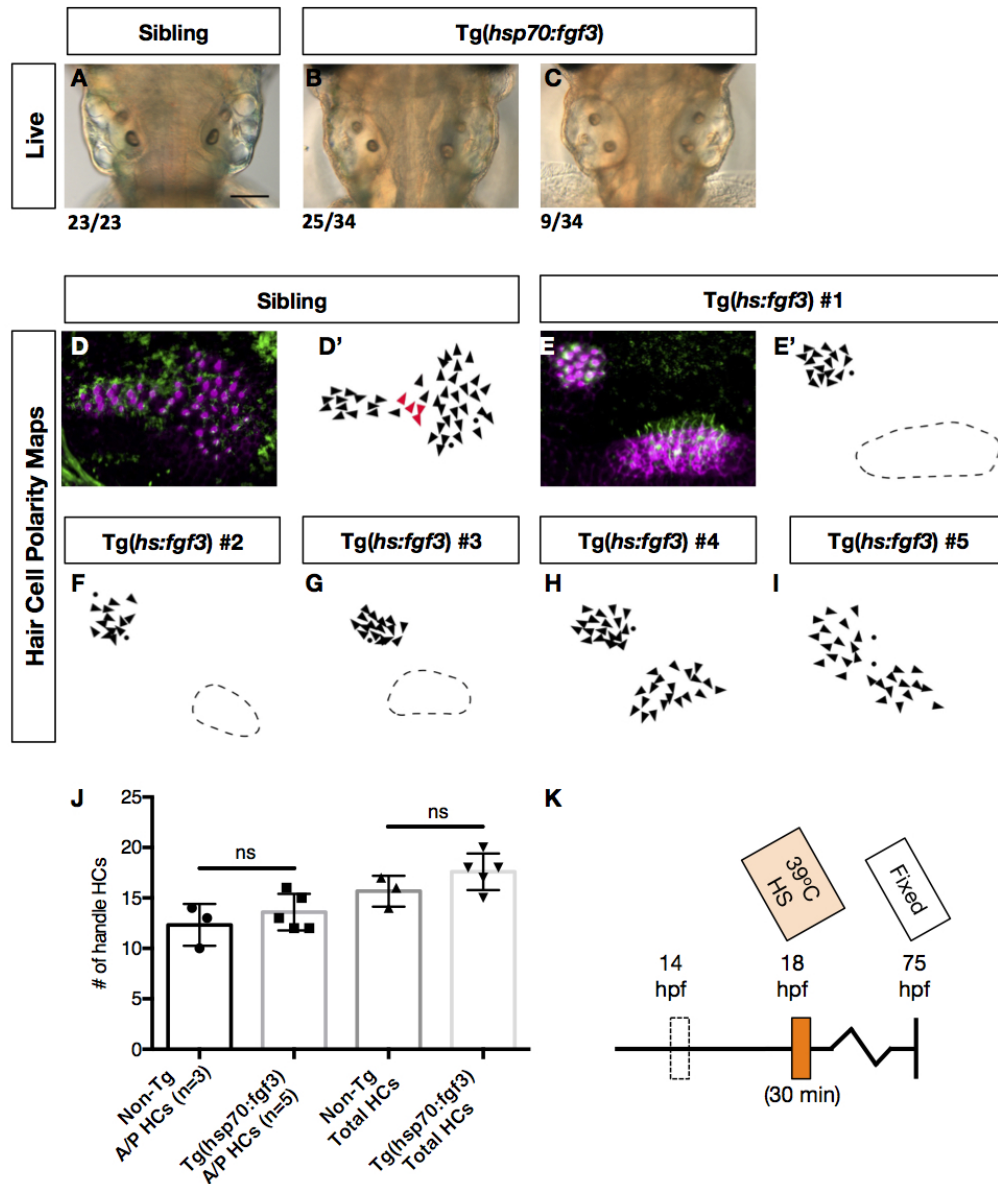


Figure 6.15: Over-expression of *fgf3* from 18hpf leads to a disrupted posterior macula with some anterior characteristics at 3dpf

Imaging of live and actin/acetylated-tubulin stained 3dpf (75hpf) embryos, heat-shocked at 18hpf. (A–C) Live, dorsally imaged embryos. (A) non-transgenic (Tg) embryos. (B) The majority of Tg(*hs:fgf3*) embryos had a posterior otolith positioned medially but at a more ventral location than the non-transgenic siblings. (C) A subset of Tg(*hs:fgf3*) embryos showed a more strikingly ventral posterior otolith. (D–I) Staining with phalloidin (purple) to mark the sensory stereocilia and anti-acetylated tubulin (green) to mark the kinocilia, allowing the polarity of the posterior macula to be mapped. In non-Tg siblings this shows a stereotypical pan morphology (D&D'), whereas Tg embryos display a range of perturbed patterning, with the posterior region of the macula generally more ventrally positioned (E–I). (J) The number of hair cells with a stereotypical anterior and posterior orientation within the handle region (hair cells left and including those highlighted in red D') is higher in the Tg embryos but not significantly (t -test $p=0.4337$, $t=0.8732$ $df=3.844$) with the total number of hair cells in this region also being higher but again not significantly ($p=0.1675$, $t=1.612$ $df=5.025$). (K) A schematic of experimental timings. N= number of individual embryos. Images A–C were taken using brightfield microscopy with a 10x (2xMag) objective and all others using confocal microscopy with a 60x oil lens. A–C are dorsal views with anterior to the top whereas D and E are lateral views with the anterior to the left. Scale bar: A; 100 μ M

6.2.9 Inhibition of retinoic acid signalling weakly potentiates the early loss of Hedgehog signalling transcriptional phenotype in the ear

Another signalling pathway that has been implicated in the anterior-posterior axial patterning of the vertebrate ear is Retinoic Acid (RA) (Bok et al., 2011). In zebrafish, during early otic development (>26hpf), RA has been shown to act within a negative feedback loop with Fgf to determine boundaries between sensory and neurogenic otic populations (Maier and Whitfield, 2014). At 20hpf in-situ hybridisation for the RA synthesising enzyme, *Aldh1a2* shows expression is within a region posterior ventral to the otic vesicle (Figure 6.16 A, A') which persists at 24hpf, although as a smaller domain (Figure 6.16 B, B').

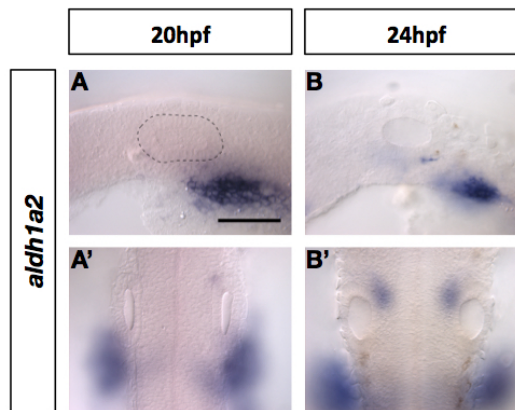


Figure 6.16: Aldehyde dehydrogenase 1 family, member A2 (*aldh1a2*) is expressed strongly in a domain adjacent to the posterior otic vesicle

In-situ hybridisation for *aldh1a2* in 20 and 24hpf AB wild-type embryos. (A-B') The RA synthesising enzyme, *Aldh1a2*, is expressed in a domain posterior-ventral to the otic vesicle at 20hpf (A & A') which although smaller, persists at 24hpf, with staining also starting to be observed anterior to the otic vesicle (B & B'). A-B are lateral views and A'-B' are dorsal views with the anterior to the left or top of the image, respectively. All images were taken using DIC microscopy with a 40x objective. Scale bar: 50 μ M.

RA and Fgf have been previously been reported to have negative regulatory relationship in the anterior otic domain around prim-5 (24hpf) but localised expression of *aldh1a2* adjacent to the posterior of the otic vesicle also makes it likely that high levels of free RA are also acting within the posterior otic domain (Figure 6.16) (Maier and Whitfield, 2014). This led to the hypothesised that sources of RA within the posterior otic domain could be inhibiting the up-regulation of any posterior *fgf* expression, possible contributing to the delayed ectopic expression of anterior markers observed after loss of hedgehog signalling (Figures 6.2-6.6). To test this, embryos from a loss of Hh signalling, *smo*^{hi1640/-} mutant incross were treated either with a competitive inhibitor of RA synthesis, N,N-diethylaminobenzaldehyde (DEAB) (Russo et al., 1988) at 50 μ M or a vehicle control between 14-15 and 22.5hpf before being fixed (Figure 6.17H). These embryos were then assayed by in-situ hybridisation for *fgf3*, *fgf8a* and *pax5* expression.

In the treated embryos assayed for *fgf3* expression, 3/27 (11%) showed staining within the posterior otic domain alongside the expected staining within the anterior (Figure 6.17B and B'), whereas none of the vehicle control treated embryos showed posterior staining (Figure 6.17A).

For *fgf8a* the majority of DEAB treated embryos had weak or no staining within the posterior otic domain and a strong anterior domain of staining (Figure 6.17D) with 9/26 (35%) having strong posterior staining alongside the expected anterior otic staining (Figure 6.17D'). However, within the *fgf8a* vehicle controls 9/28 (32%) embryos were also classified as having strong staining in the posterior otic domain (Figure 6.17C). In the DEAB-treated embryos assayed for *pax5* expression, the majority showed strong staining in the anterior otic domain with no obvious staining in the posterior (Figure 6.17F) with a similar phenotype observed for all the vehicle controls (Figure 6.17E). In contrast, 4/29 (14%) DEAB-treated embryos showed strong *pax5* staining in the posterior domain alongside that in the anterior (Figure 6.17E').

Despite there appearing to be a trend towards more embryos having strong anterior and posterior expression of *fgf3* and *pax5* after DEAB-treatment compared with the vehicle controls, this difference does not appear to be significant when tested with a Fisher's exact test (*fgf3*; $p=0.1055$, odds ratio= 0.1186 and *pax5*; $p=0.0522$, odds ratio= 0.09290) (Figure 6.17G). For *fgf8a*, the lack of difference in the groups observed between the DEAB-treated and vehicle controls was also confirmed to be highly non-significant ($p=0.7734$, odds ratio= 0.7953) (Figure 6.17G).

To identify if the weak trend for posterior expression of the anterior markers *fgf3* and *pax5* after treatment with DEAB was associated with a loss of Hh signalling background, embryos defined as showing strong ectopic posterior expression were genotyped. For both *fgf3* and *pax5*, those embryos showing strong posterior expression were also confirmed as being homozygous for *smo*^{hi1640-/-} (Figure 6.17G). However, the number of embryos showing this phenotype was clearly below the 25% (red line) expected for Mendelian inheritance suggesting the phenotype is not fully penetrant in these mutants. For *fgf8a*, despite the number of embryos classified as having strong posterior expression for both treated and vehicle controls being closer to the expected 25% (35% and 32%, respectively), these embryos for both conditions appear to be comprised of both mutants and siblings (Figure 6.17G). This suggests that for *fgf8a* RA and Hh likely have a negligible direct influence on expression of *fgf8a* within the posterior domain before 22.5hpf.

As inhibition of RA synthesis in combination with loss of Hh signalling appeared to result in a partial up-regulation of factors known to drive anterior otic within the posterior otic domain, I wanted to test whether treatment with a high concentration of RA would conversely reduce expression of these factors within the anterior otic domain. This would then support the hypothesis that posterior sources of RA might be inhibiting establishment of anterior otic character in the posterior otic domain of wild-type embryos, resulting in the transient expression of anterior markers seen around prim-5 (24hpf) (Léger and Brand, 2002; Kwak et al., 2006).

Treatment of zebrafish with lower doses (10nM) of RA, starting at a slightly early time point of 20ss (19hpf) have been reported to result in a reduction in *fgf3* and *fgf8a* expression within the anterior otic domain (Maier and Whitfield, 2014). Therefore, I predicted that treatment with a higher concentration (50nM) of RA at a time point that is slightly later starting but within the previously reported treatment timeframe, might result in reduced expression of *fgf3* and *8a* along with a concomitant reduction of other anterior factors that are known to be dependent on anterior Fgf signalling within the anterior otic domain. To test this, wild-type embryos were treated with a high concentration (50nM) of exogenous RA over an 6 hour period between 22.5 and 28-29hpf before being washed and grown on to 36hpf (Figure 6.18I).

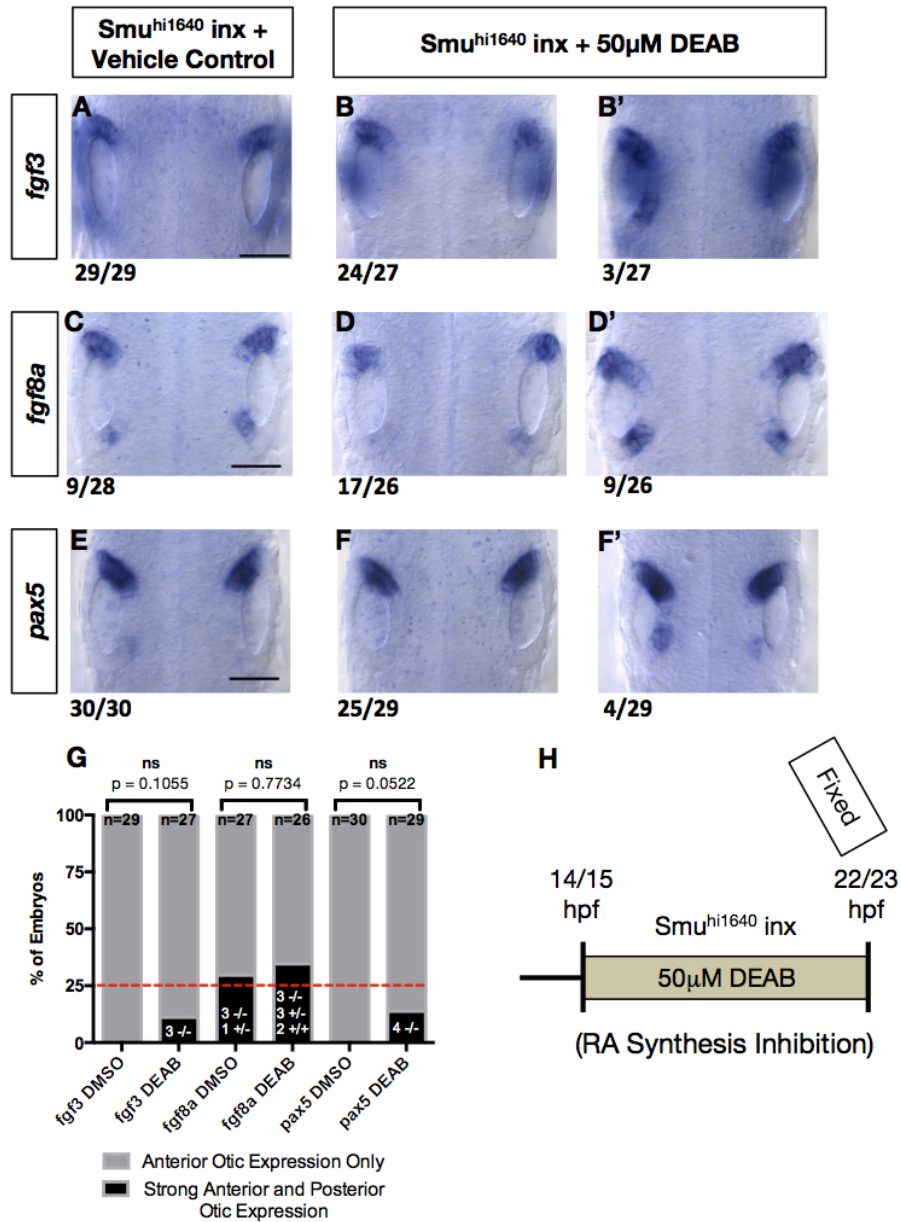


Figure 6.17: Inhibition of RA synthesis with 50µM DEAB partially potentiates expression of anterior markers in the posterior domain but only in a loss of Hh background (A–B') Expression of *fgf3* in the posterior otic domain is not seen in embryos from a *smu^{hi1640} +/-* incross treated with a vehicle control (A) but is strongly expressed in the posterior otic domain of a subset (B') of those treated with 50µM of DEAB. (C–D') Expression of *fgf8a* in vehicle control treated embryos shows strong anterior otic staining also clearly present in the posterior domain (C). In DEAB-treated embryos, the posterior otic *fgf8a* staining appears stronger in some embryos (D') but is also seen weakly in the majority (D). (E–F') *pax5* expression in the posterior otic domain is not seen in the vehicle controls (E) but is strongly expressed in the posterior otic domain of a subset (F') of those treated with 50µM DEAB. (G) Quantification of phenotypes and genotyping of those with strong posterior otic expression. A two-tailed Fishers exact test was used to separately compare the count data for DMSO and DEAB treatments for each probe. The red dotted line represents 25%, the expected number of homozygous mutants from a *smu^{hi1640} +/-* incross. (H) Schematic of DEAB treatment. N= number of individual embryos. All are dorsal views with anterior to the left. Images were taken using DIC microscopy with a 40x objective. Scale bars: 50µM.

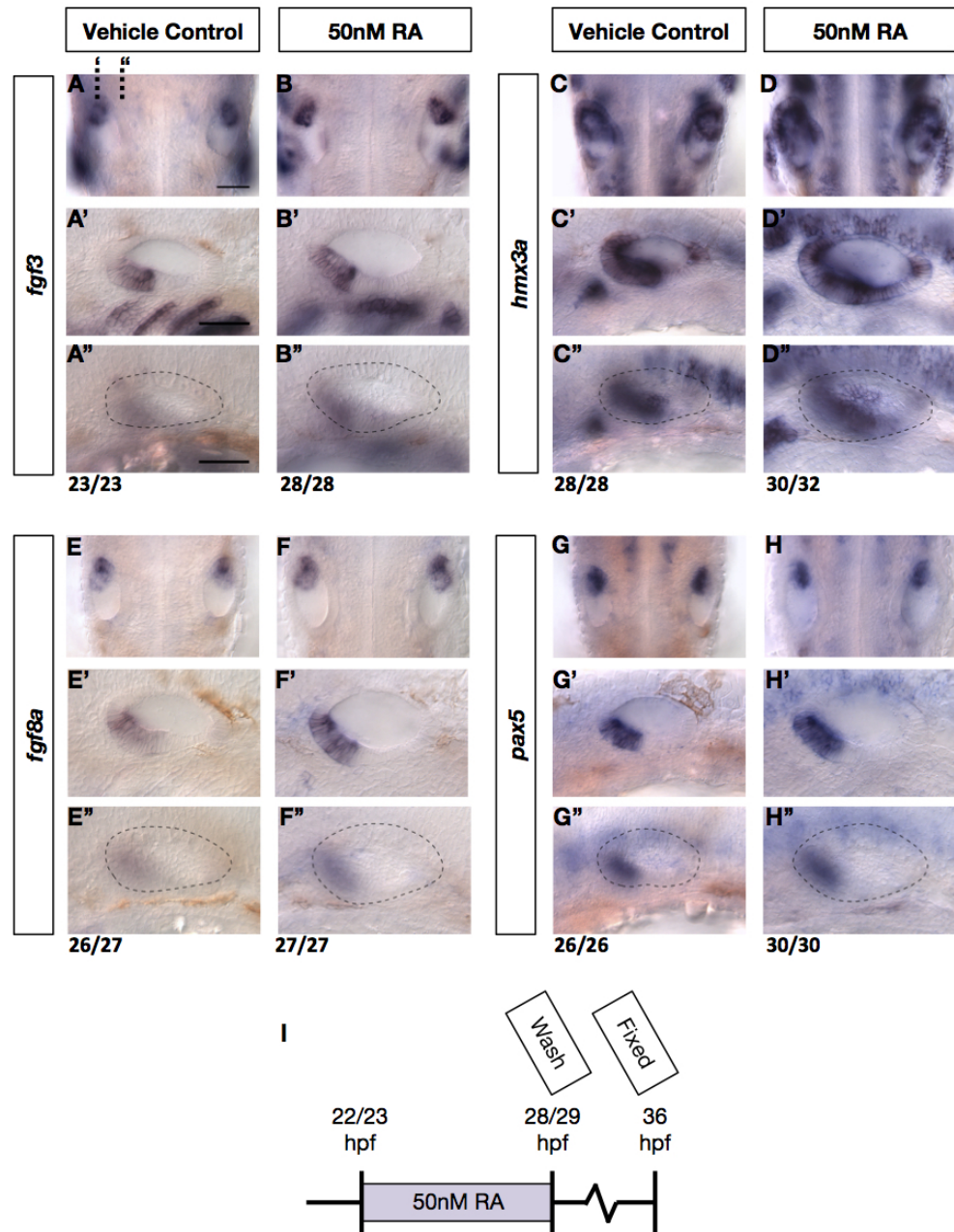


Figure 6.18: Application of exogenous RA alone after 22.5hpf does not appear to weaken anterior identity or induce expression of anterior markers within the posterior domain. Anterior otic expression of (A–B'') *fgf3*, (E–F'') *fgf8a* and (G–H'') *pax5* at 36hpf appears unaltered after treatment with 50nM of exogenous RA between 22.5 and 28–29hpf. (B–D'') *Hmx3a* staining in the anterior otic domain does not appear expanded along the medial edge after RA treatment but does show expanded staining along the lateral otic edge (D–D'). A–H are dorsal views with all others being lateral views at different z-planes through the ear. Images were taken using DIC microscopy with a 40x objective. Scale bars: 50 μ M

Expression of *fgf3* and *fgf8a* in 50nM RA-treated embryos (Figure 6.18B-B'' and F-F'', respectively) appeared similar in anterior localisation and strength of staining relative to the vehicle controls (Figure 6.18A-A'' and E-E''). However, RA-treated embryos assayed for *fgf3* expression did show a consistent change in expression within the ventral branchial pouches with this expression domain appearing as a single broad domain abutting the ventral edge of the otic vesicle rather than discrete domains (Figure 6.18B'). Expression of *pax5* also showed no obvious changes in either positioning along the anterior-posterior axis or staining strength (6.18H-H'') compared to the vehicle controls. *Hmx3a* staining in RA-treated embryos did appear to be expanded slightly along the ventrolateral domain in 30/32 embryos (94%) when compared to the vehicle controls (Figure 6.18D, D' compared to C, C') and staining in the dorsal hindbrain and within the domain just anterior to the otic vesicle was also stronger in treated embryos (Figure 6.18D-D''). Therefore, my predictions were not fulfilled as none of the anterior markers, including *fgf3* and *8a*, showed a persistent reduction in their anterior otic expression.

A batch of embryos treated with 50nM of RA alongside those fixed at 36hpf were grown on to 3dpf. These RA-treated embryos showed a strong pectoral fin overgrowth phenotype (27/27, 100%), which was not observed in untreated embryos (30/30) and supports the activity of the exogenous RA treatment (Grandel et al., 2002).

6.3 Discussion

The morphological and transcriptional duplication of anterior otic identity in response to a loss of Hedgehog (Hh) signalling or increase in Fgf signalling has been previously reported later than 24hpf. Strikingly, the duplication of anterior otic morphology observed in response to manipulation of these two pathways appears remarkably similar. However, despite determination of AP otic identity occurring early during otic development, the transcriptional response of anterior factors, such as *fgf3*, *fgf8a*, *hmx2*, *hmx3a* and *pax5* prior to 24hpf and how this differs between manipulations of the two pathways has not been studied.

I have shown that under loss of Hh conditions, which are sufficient to produce a duplication of the anterior otic morphology, the anterior factors *pax5*, *fgf3* and *fgf8a* show a slow transcriptional response. In contrast, *hmx2*, *hmx3a* and *fgf10a* show a robust expansion of expression into the posterior otic domain by 22.5hpf. As *fgf10a* and its paralogue, *fgf10b*, do not have a strong impact on anterior identity (Maulding et al., 2014), *hmx2* and *hmx3a* were focused on.

The posterior expansion of *hmx2* and *3a* in response to a loss of Hh signalling appeared to be direct rather than reflecting any reduction in the size of the otic tissue or elevated Fgf signalling. A similar up-regulation of *hmx3* along the otic DV axis in chick has been reported in response to Gli3R, which is associated with low Hh signalling (Ohta et al., 2016). Therefore it was unexpected that early otic expression of *hmx3a* appeared only weakly reduced in *ptch1* $-/-$; $2-/-$ mutants, where Hh signalling is constitutively active, yet expression of *hmx2* was almost lost. This could suggest *hmx3a* expression is more sensitive to anterior extra-otic Fgf signalling than *hmx2*, which may initially offset the inhibitory effect of increased Hh signalling. Such a difference in regulation is supported by reduced *hmx3a* expression in *ptch1* $-/-$; $2-/-$ mutants by 30hpf and its earlier induction in the anterior otic domain compared to *hmx2* during wild-type otic development (Hammond et al., 2010; Feng and Xu, 2010).

Early over-expression of *fgf3* has previously been shown to produce a similar anterior duplication to that seen in a loss of Hh signalling background. This duplication was also reflected in the duplicated expression of a number of known anterior otic factors such as *hmx2* and *pax5* (Hammond and Whitfield, 2011). I showed that in 22.5hpf embryos, after over-expression of *fgf3*, *hmx3a* and *fgf10a* show a stronger posterior expansion of expression than observed at 22.5hpf after loss of Hh signalling. In contrast, while *pax5* shows no posterior otic expression after loss of Hh at 22.5hpf, over-expression of *fgf3* leads to an expansion of *pax5* expression across the AP axis. Similarly, *fgf3* expression also appears up-regulated in a discrete posterior otic domain at 22.5hpf after its earlier over-expression. This is in contrast to the slow up-regulation occurring by 36hpf observed after loss of Hh. These differing responses represent a clear difference in the transcriptional response to manipulation of Hh compared to Fgf signalling, even though the morphological outcome is similar.

I have also expanded upon previous data from Hammond et al, 2011 by showing that the stereotypical morphology of the posterior macula is altered after over-expression of *fgf* at time points greater than 16hpf. However, this is milder than the phenotypes observed after over-expression of *fgf* at 14hpf, making this change in posterior morphology less clear in live embryos. This loss of stereotypical morphology was also confirmed to be concomitant with a posterior expansion of anterior factor expression. These data support the posterior otic placode becoming progressively less able to adopt anterior identity during development, highlighting the requirement for early (<18hpf) transcriptional changes in determining the anterior otic domain. It would be interesting to identify whether the transcriptional response of anterior factors in response to *fgf* over-expression reflects the weaker phenotype seen at these later developmental time points.

Based on these observations, I propose a model where otic *hmx3a* expression is dependent on integrating both Fgf and Hh signalling to define the extent of the anterior otic domain during early otic development. This model would support the early expansion of *hmx3a* expression in loss of Hh embryos inducing anterior identity within the posterior domain. However, the current data do not identify whether *hmx3a* and/or *hmx2* are sufficient to induce anterior identity independently of Fgf signalling. Therefore further work to identify whether, when Fgf signalling is inhibited, over-expression of *hmx3a* is sufficient to rescue the posterior duplication phenotype seen. It is also possible that other signalling pathways may be later impact upon otic AP identity, as discussed later.

A previous model for patterning along the otic AP axis in zebrafish suggested the presence of a pre-pattern upon which either anterior or posterior identity is assigned (Hammond and Whitfield, 2011). I have shown that when *fgf3* is over-expressed, the otic expression of both *fgf3* and *fgf8a* appears strengthened in two domains located at the anterior and posterior poles. A similar maintenance within these two AP pole domains is seen with *hmx3a* following its initially broad expression across the medial otic edge in response to *fgf3* over-expression. This restriction of *hmx3a* to these domains and its loss within the middle dorsal domain may reflect the localised expression of *fgf3* expression at either pole under these duplicating conditions.

In wild-type embryos, I have shown that three regulators of the Fgf signalling pathway, Fgf Receptors 2, 4 and Sulf1, do not show any spatial restricted expression to both poles, suggesting that Fgf signalling is unlikely to be tightly restrained to these pole domains either by localization of receptors or correctly sulfated HSPGs. This is despite wild-type embryos having expression of both *fgf8a* and *fgf10a* in the posterior otic domain around prim-5 (24hpf). However, it would be interesting to confirm whether *fgfR4* or *sulf1* show any posterior expression in embryos after over-expression of *fgf3*. It is also possible that other FgfRs, such as FgfR1 may be localised to the

poles, although this is not seen in their wild-type expression (Maier and Whitfield, 2014). Given the importance of FgfRs in otic patterning it could also be that their transcripts, if localised to the AP poles, may be present at sub-detection levels (Hammond and Whitfield, 2011).

Another mechanism by which *fgf* expression could be localised is through its interaction with *Atoh1a*. *Atoh1a* is expressed in two discrete pole domains during early otic development and has been shown to act in a positive feedback loop with Fgf signalling (Sweet et al., 2011). *Atoh1a* has previously been shown in 14hpf mind bomb mutants, where Notch signalling is lost, to be broadly expressed across the otic placode rather than refining into two domains (Millimaki et al., 2007). Therefore to explore whether otic *fgf* expression is broadened in response to ectopic otic *atoh1a* expression, 26hpf *mib* mutants were observed. However, in these mutants at 26hpf, *atoh1a* did not show broad expression and instead appeared resolved into two discrete domains. Interestingly, otic expression of *fgf3* and *fgf8a* was lost in these mutants yet an anterior domain of *hmx3a* expression was still present. This highlights that by 26hpf, otic expression of *fgf3* and *fgf8a* is dependent on the presence of a differentiated otic population, likely the supporting cells of the sensory domain, which are lost in *mib* mutants (Haddon et al., 2000). It also presents the possibility that there is still sufficient extra-otic Fgf signalling at this time to maintain anterior otic expression of *hmx3a*.

RA has been shown to play a role in otic patterning in chick (Bok et al., 2011), mouse (Niederreither et al., 2000; Romand et al., 2013) and zebrafish (Hans et al., 2007; Maier and Whitfield, 2014; Radosevic et al., 2011), where it is thought to be initially present as a posterior (high) to anterior (low) gradient across the otic tissue. In zebrafish, RA has been suggested to regulate the balance of sensory, neurogenic and non-neural otic tissue through negative feedback regulation of anterior Fgf signalling between 18- 26hpf (Maier and Whitfield, 2014). A similar negative regulation by RA on *fgf* expression within the otic tissue has also been observed in mice (Cadot et al., 2012; Frenz et al., 2010). I therefore hypothesised that posterior RA could be contributing to the delayed duplication of anterior factors seen when Hh signalling is lost. However, reduction of RA synthesis using DEAB only partially potentiated the up-regulation of duplicated anterior factors at 22.5hpf and only when hedgehog signalling was also lost. This suggests that any repression by RA on the posterior otic domain before 22.5hpf is weak. As treatment with DEAB has variable efficiencies in producing the same otic phenotype (Maier and Whitfield, 2014; Radosevic et al., 2011), I also tried to confirm this result using a dominant-negative Retinoic acid receptor transgenic line (Kikuchi et al., 2011). This line has been used previously to study RA signalling during otic development (Maier and Whitfield, 2014; Rubbini et al., 2015); however, attempts at using this transgenic resulted in embryo lethality and no clear effect on RA patterning. An unexpected embryo-wide up-regulation of *pax5* was observed, although this may be an off-target effect (Supplementary Figure 9).

Application of a high concentration of exogenous RA after 22.5hpf did not appear to strongly influence the expression of anterior factors supporting a weak effect of RA on determining otic AP identity. Interestingly, this is contrary to the loss of anterior otic *fgf3* and *fgf8a* expression reported when 10nM of RA was applied from a slightly earlier time point (Maier and Whitfield, 2014). However, embryos treated with 50nM of RA embryos were not fixed after treatment but rather were washed and grown on to 36hpf. Therefore, an earlier reduction in the expression of anterior factors may have occurred but subsequently recovered. Alternatively, the anterior otic tissue may have lost its competence to respond to elevated RA by 22.5hpf, result in no change in the anterior expression. Despite these possible explanations, the result seen suggests that transient treatment with 50nM of RA from 22.5hpf does not alter anterior otic character. Further work to examine expression after the earlier application of RA and directly after treatment would help validate this hypothesis.

6.4 Conclusions

- Transient inhibition or loss of Hedgehog signalling leads to a progressive duplication of the otic anterior factors *fgf3*, *fgf8a* and *pax5* between 22.5hpf and 36hpf but an early expansion of *hmx2* and *hmx3a* across the medial otic domain.
- After transient inhibition or loss of Hedgehog signalling, *hmx3a* expression persists across the entire ventral otic floor at 36hpf.
- Despite leading to an expansion of otic *hmx3a* expression, aberrant Hedgehog signalling does appear to directly lead to a reduction of anterior otic *hmx3a* expression by 16-17hpf (14-16ss) but does reduce *hmx2* expression.
- Misexpression of *fgf3* at 14hpf results in a broad medial expression of *hmx3a*, *pax5* and *fgf10a* by 22.5hpf with *fgf3* and *fgf8a* expression being localised to the anterior and posterior otic poles. Subsequently, the broad medial expression of *hmx3a* progressively resolves into two domains at the anterior and posterior otic poles, and is not maintained within the central region of the medial otic domain.
- Components known to regulate the Fgf signalling pathway do not show any expression localised to both the anterior and posterior otic domains in wildtype embryos.
- Inhibition of Notch signalling in *mind bomb* mutants results in an *atoh1a*-independent loss of otic *fgf3* and *fgf8a* expression, which does not affect the otic anterior-posterior profile of *hmx3a* expression by 26hpf.
- Misexpression of *fgf8a* at 14hpf results in a weaker loss of posterior identity at 3dpf compared with embryos where *fgf3* has been over-expressed at the same time point.
- The response of the otic tissue to over-expression of either *fgf3* or *fgf8a* at 18hpf is far weaker than that seen at 14hpf; however, over-expression of *fgf3* at 18hpf does still result in a similar broadened expression of *hmx3a* and *pax5* across the medial otic domain and also a disruption of the posterior-most region of the posterior macula.
- Inhibition of RA synthesis weakly potentiates the transcriptional anterior duplication phenotype seen after loss of Hedgehog signalling at 22.5hpf, but a high concentration of exogenous RA applied transiently at 22.5hpf does not reduce anterior transcriptional identity.

Chapter 7

Overall Discussion

7.1 Overview of Results

This thesis presents data characterising the early patterning dynamics that occur across the AP axis of the developing zebrafish otic placode. In an attempt to better model how the polarity in otic anterior and posterior character is established. In Chapter Three, I reported the expression of two new early markers of the posterior otic domain, *nav3a*, which is expressed from 16hpf in a posteromedial domain, later spreading dorsally and *cdr2l*, which is initially expressed broadly across the otic placode but is then successively lost from the anterior and then the posterior domains. Given the stronger expression and dynamic nature of otic *cdr2l* expression, this marker was explored further, with otic *cdr2l* expression identified as being negatively regulated by Fgf signalling early during otic development.

In Chapter Four, I built upon this previous characterisation of otic *cdr2l* expression by testing the function of *cdr2l* in the otic epithelium through morpholino knock-down and CRISPR-generated mutants. This showed that loss of *cdr2l* does not appear to affect otic AP patterning, although the posterior marker *fstb* may show a slight reduction in its otic expression in the *cdr2l* morphants. In the *cdr2l* morphants, a possible reduction in the population of differentiated neurons within the anterior hindbrain, as marked by *neurod1*, was observed. It was also noted that both the ears of *cdr2l* morphants and mutants showed a slight reduction in otic AP length, accompanied by an increase in variation, compared to the controls. This led to the hypothesis that Cdr2l may play a role in regulating proliferation/maturation of the zebrafish otic placode.

In Chapter Five, I have also discussed developing approaches to isolate the otic tissue for identification of the transcriptional differences that define anterior and posterior otic character through subsequent transcriptomics. However, due to technical issues and time constraints, ultimately this was not pursued.

Finally in Chapter Six, I present data showing the differing early transcriptional responses of known anterior markers, within the otic tissue, in response to a loss of Hh signalling. This was to identify the early transcriptional changes that likely drive the duplication around the otic AP axis under such conditions. This highlighted *hmx3a* and *hmx2* as showing an early (prior to 22.5hpf) posterior expansion, with the other known markers showing a delayed duplication of expression. This was in contrast to the expression of the anterior markers after over-expression of *fgf3*, which showed an up-regulation of the majority of anterior markers within the posterior otic domain by 22.5hpf.

I also confirmed that the whole medial edge of the otic placode is competent to express these anterior markers after their broad up-regulation by *fgf3* over-expression. However, this broad expression, as demonstrated with *hmx3a*, is only maintained in two domains at the AP poles, which I propose reflects a positive feedback between Fgf and Atoh1a along with differentiation within these regions.

Within Chapter Six, I also present preliminary data integrating the role of Retinoic Acid (RA) and Hh signalling in the regulation of posterior otic character. This suggests that RA may be acting to weakly inhibit *fgf* expression within this domain, as has been shown in the anterior otic domain, possibly in combination with a Hh mediated inhibition of other anterior factors. I also present data showing that the application of a high concentration of RA after 22.5hpf does not have the ability to alter anterior otic identity, despite its previously published role in regulating anterior *fgf* expression (Maier and Whitfield, 2014).

In the discussion below, I have attempted to place these data in the context of what is already known in relation to early otic development in zebrafish and also otic development across other vertebrates. Finally, I also propose a model, which looks to expand upon those previously proposed for patterning across the otic AP axis, in light of my data.

7.2 Early markers of the posterior otic domain; a role for *Cdr2l* in otic development?

While a number of early (>24hpf) transcriptional responses have been linked with anterior otic identity in zebrafish, none have been found for the posterior. This led to a search for markers which showed an early and localised expression profile within the posterior domain (Chapter Three). I identified two candidate posterior markers but focussed on *cdr2l* due to its initially strong expression across the otic placode at 14hpf (10ss) and the novel dynamics observed in its progressive loss of expression across the AP axis of the otic domain.

7.2.1 Dynamic expression of *cdr2l* across the early otic AP axis, reflective of maturation?

As shown in Chapter Four, loss of *cdr2l* does not appear to alter AP patterning within the ear. This supports data from Chapter Three, where expression of *cdr2l* failed to persist in either the anterior or posterior domains of wild-type or loss of Fgf signalling embryos, as would be expected if it were associated with AP identity (Hammond and Whitfield, 2011). Therefore the progressive loss of *cdr2l* expression across the AP axis (Chapter Three) could be reflecting transcriptional changes associated with assignment of anterior and posterior identity at either end along the otic AP axis, which is supported by the asynchronous development of the anterior and posterior maculae reported in zebrafish (Sapède and Pujades, 2010). The onset of anterior otic *hmx3a* expression at 14hpf (10ss) represents the earliest known differential expression within the anterior otic domain (Feng and Xu, 2010) with expression of *pax5*, a down-stream target of *hmx3a* and *hmx2*, observable within the anterior domain at around 16hpf (Feng and Xu, 2010; Kwak et al., 2006). This progressive induction of anterior markers between 14-16hpf, coincides with the loss of anterior *cdr2l* expression. In the posterior otic domain, expression of *nav3a*, the other early posterior marker characterised in this thesis, was observed from 16hpf (Chapter Three). This is prior to the loss of *cdr2l* expression within the posterior otic domain at 18-19hpf and therefore

could support the hypothesis that the progressive loss of otic *cdr2l* expression is in response to maturation/specification of the anterior and posterior domains. However, as onset of all other posterior markers, such as *fsta* and *pou3f3b* occur around 24hpf, it cannot be confirmed that posterior character has been established prior to this at 18-19hpf (Kwak et al., 2002b; Hammond and Whitfield, 2009). However, even if *nav3a* is not regulating posterior otic character, it must mark an event that induces its localised expression within a posterior domain. This therefore supports a model where the progressive loss of *cdr2l* expression across the otic AP axis is mirroring maturation or commitment of the otic placode across the AP axis, as supported by the expression of the known AP markers. A similar idea of the otic tissue undergoing progressive commitment has also been suggested to occur in chick explants, although not across an axis (Freter et al., 2008).

To identify whether Cdr2l does play a role in maturation of the otic tissue, further work looking at whether expression of *pax5* and *neurog1* show delayed induction after injection of *cdr2l* RNA would be interesting. Especially as *cdr2l* expression within the anterior domain is lost around the time of their onset. Conversely, observing whether otic *cdr2l* expression is lost after over-expressing *hmx3a* or *pax5* early on during otic development could support *cdr2l* expression reflecting otic maturation. Identifying if *nav3a* does reflect posterior identity, through knock-down and characterisation of its expression in duplicated ears would also be of interest to confirm whether assignment of posterior identity does occur as early as 16hpf.

7.2.2 A role for otic Cdr2l in proliferation?

Recent work in mature rat cerebellar tissue has linked CDR2L and another CDR family member, CDR2 with calcium homeostasis within the synapses of Purkinje cells. Here it is proposed that the disruption of this homeostatic role of CDR2L and CDR2, due to the autoimmune response against an epitope shared by CDR2 and CDR2L, contributes to the PCD pathology (Schubert et al., 2014). However, regulation of cellular calcium levels have not been implicated in otic development, despite elevated levels of Ca^{2+} reported within the otic placode at 14hpf (Créton et al., 1998).

Another possible role for otic Cdr2l could be in regulating proliferation within the early otic placode. Whilst the function of Cdr2l during embryonic development has not been studied, its function in tumours, which as they develop share some similarities with embryonic development (reviewed in Ma et al. 2010), has been linked to cell-cycle regulation (O'Donovan et al., 2010). As CDR2 has been shown to co-precipitate with the positive cell-cycle regulator, C-MYC, it was suggested CDR2 may negatively regulate proliferation through this (Okano et al., 1999). However, the most recent study by O'Donovan et al. suggested loss of CDR2 in cancer cell lines results in reduced proliferation and increased apoptosis (O'Donovan et al., 2010). Although it is not clear if CDR2L is present in cancerous tissues associated with PCD, it shares a high peptide sequence homology with CDR2 (Corradi et al., 1997; Eichler et al., 2013). The highest homology is within a region previously proposed to interact with C-MYC (Fathallah-Shaykh et al., 1991), of which a paralogue, *mycb*, is expressed during early development of the zebrafish otic placode (Chapter Four). However, loss of *cdr2l* did not appear to robustly alter otic expression of *mycb*, which has been linked to hair cell proliferation and regeneration in neuromasts (Lee et al., 2016). As CDR2 has not been shown to regulate *C-MYC* expression directly, altered expression of *mycb* in the *cdr2l* mutants may not be expected. The apparent lack of regulation of *mycb* by Cdr2l, could also reflect differences in localisation with CDR2. As CDR2L in cell culture has been shown to localise to the cell membrane, whereas CDR2 appeared localised to the cytoplasm (Eichler et al., 2013).

Despite not showing any clear regulation of *mycb*, both the *cdr2l* morphants and mutants did show a non-significant but consistent decrease in otic AP length, generally with greater variability, when compared to the controls (Chapter Four). Although this needs further confirmation from further measurement of homozygous mutants, it could be indicative of a role in regulating proliferation within the ear. Directly studying proliferation and apoptosis in early *cdr2l* mutants using techniques such as using a phospho-histone H3 antibody and TUNEL staining would help directly confirm any changes that may not be reflected in *mycb* expression.

7.2.3 Does expression of *cdr2l* in other neural cell types provide an indication of a possible function?

In contrast to the proposed loss of *cdr2l* expression during maturation of the otic placode, the neural expression of *cdr2l* from 20hpf onwards appears to be in structures thought to be in the process of differentiating. Within the trigeminal placode, in which *cdr2l* appears to be expressed, differentiation is thought to peak with *neurog1* at 16hpf, with little *neurog1* expression observed in these cells at 26hpf (Andermann et al., 2002). Similarly, the ventrolateral expression of *cdr2l* within the hindbrain marks a domain thought to contain differentiating neurons moving from the dorsal ventricular zone (Nikolaou et al., 2009). The puncta of *cdr2l* expression within the dorsal trunk observed from 18-20hpf (Chapter Three), presumed to be Rohon-Beard neurons, also represents a differentiated neuronal cell type marked by *cdr2l* expression. Differentiation of Rohon-Beard neurons is thought to occur early in development, as they express *neurod1* and *elavl3*, both canonical markers of differentiating neurons, from 14hpf (10ss) onwards (Park et al., 2000; Korzh et al., 1998). Interestingly the otic placode, trigeminal placode and Rohon-Beard neurons do share early developmental similarities. All three have been shown to require Dlx3b and Dlx4b for their specification and Tfp2 has also been shown to be required to varying degrees during their development. This could suggest the loss of *cdr2l* expression is reflecting changes either in BMP signalling or neural crest contributions; although either would still support the loss of *cdr2l* expression in the otic placode reflecting maturation of this tissue as previously proposed (Hans et al., 2013; Kaji and Artinger, 2004; Barralho-Gimeno et al., 2004; Li and Cornell, 2007).

Other possible reasons for a weak otic phenotype after loss of *cdr2l*

Despite *cdr2l* showing strong and dynamic expression during early otic development, data from the morphants and mutants do not identify a clear otic phenotype associated with a loss of *cdr2l*. This lack of a strong phenotype could reflect a robustness in the process *cdr2l* regulates, possibly the cell-cycling, to being perturbed. In mice, despite being expressed in the ear, loss of a putative regulator of cell proliferation and the cell cycle, *c-Myc* does not disrupt otic morphology but loss of another Myc family member, *n-Myc*, does (Domínguez-Frutos et al., 2011). Another possibility is that despite *cdr2l* being expressed in the otic placode, the corresponding peptide may not be translated. Whilst murine CDR2 has been shown to be widely expressed in a number of tissues, the peptide is thought only to be present in the testis and neurons, which has been suggested to be due to these tissues being immune privileged. (Corradi et al., 1997). The early nature of otic *cdr2l* expression makes it unlikely that either an innate or adaptive immune response to the otic Cdr2l peptide is occurring (reviewed in Meijer and Spaink 2011). However, confirming the presence of the peptide within the placode during early development would rule out a lack of peptide as causing the weak otic phenotype seen after a loss of *cdr2l*.

7.3 Early integration of extra-otic signalling in defining the anterior and posterior otic domains during otic development

Previous work by Hammond et al. identified the otic placode in zebrafish as being equipotent in its ability to adopt either anterior or posterior morphology in response to Fgf or Hh, respectively (Hammond and Whitfield, 2011). Whilst a posterior duplication in response to RA has been reported in chick and mouse, neither the otic placode in chick or mice show a similar response to Fgf or Hh manipulation or the same propensity for duplication of either anterior or posterior sensory character reported in zebrafish (Bok et al., 2011). However, the anterior-posterior axis of all vertebrate models has been reported to show a restricted period over which changes to anterior and posterior character can be made (Hammond et al., 2010; Hammond and Whitfield, 2011; Bok et al., 2005, 2011). Therefore, early transcriptional changes across the AP axis under duplicating conditions are likely necessary for producing a strong morphological duplication for all vertebrates, even if this only prevents differentiation.

In this thesis I have shown that out of the previously characterised regulators of anterior otic character, only *hmx3a*, and *hmx2* show an early posterior expansion under loss of Hh conditions that result in anterior duplication. In contrast to this early posterior expansion, the other known otic anterior factors, *pax5*, *fgf8a* and *fgf3* show a slower up-regulation of expression in the posterior domain of these duplicated ears (Chapter Six). From this I proposed a model whereby the early posterior expansion of *hmx3a* and *hmx2* is the key determinant in driving the anterior duplication phenotype. This sequential up-regulation of anterior otic factors within the posterior domain after a loss of Hh, with *hmx3a* and *hmx2* showing the earliest response, is strikingly similar to the progressive establishment of the anterior otic domain observed in wild-type embryos (Figure 7.1). Therefore I propose this early posterior expansion of *hmx3a* and *hmx2* is the key determinant in effecting the extent of the anterior domain established and therefore also duplication of the anterior under perturbed conditions.

The early otic expression of *hmx2* and *hmx3* in chick and mouse have a number of similarities with zebrafish, being expressed early during otic development and initially localised to the anterior otic domain (Herbrand et al., 1998; Wang et al., 1998). Yet their later expression in the chick and mice otocyst are primarily thought to direct patterning of the DV axis (Riccomagno et al., 2005; Hatch et al., 2007). However, as mentioned previously in the general introduction, *hmx2* and *hmx3* in chick and mouse may play a role in sensory AP patterning, albeit possibly not to the same extent as seen in zebrafish (Wang et al., 2004). The early expression of *hmx2* and *hmx3* with the anterior otic domain could therefore represent a conserved early state of otic patterning between vertebrates which subsequently diverges. This may reflect the proposed ancestral function of the Hmx gene family in patterning, highlighted by the ability of the *Drosophila hmx* CDS to replace *hmx2* and *hmx3* in mice (Wang et al., 2004).

1. Feng et al., 2010 (*hmx3a*; 11.5hpf and *hmx2*; 14hpf).
2. McCarrol et al., 2013 and own data (14hpf and 16hpf, respectively).
3. kwak et al., 2006. (17hpf).
4. Leger and Brand., 2002 (18hpf).
5. Millimaki et al., 2007 and own data (22hpf and 19/20hpf, respectively).
6. Maier et al., 2014 (22-24ss).

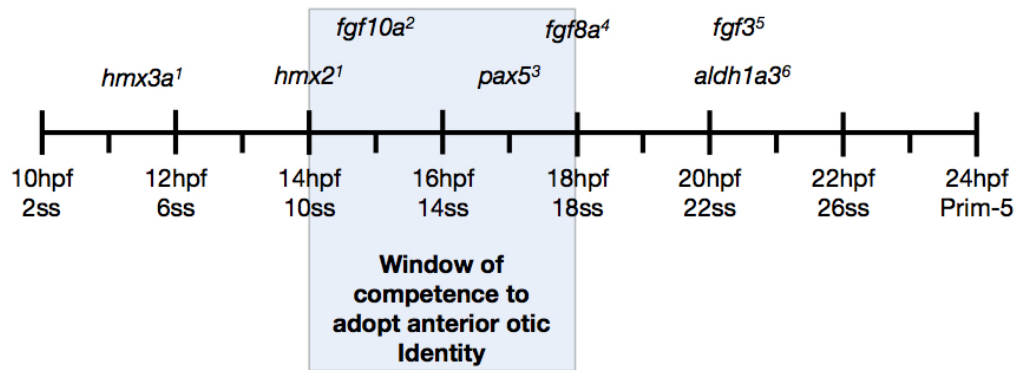


Figure 7.1: Timeline showing sequential onset of expression within the anterior otic placode

7.3.1 Are *hmx3a* and *hmx2* sufficient to assign posterior identity?

When *fgf3* is over-expressed, a different early transcriptional response is seen compared to when Hh signalling is lost, with all the anterior otic factors appearing up-regulated either across the whole medial otic edge or at the AP poles (Chapter Six). This is consistent with Fgf3 being up-stream of *hmx3a*, *hmx2* and *pax5* and capable of producing duplications of anterior otic character when over-expressed (Hammond and Whitfield, 2011). It has been proposed that an anterior to posterior gradient of Fgf3 and 8a emanating from rhombomere 4 is likely present across the otic placode from the initial establishment of the otic placode onwards, which is likely augmented by a ventral source of Fgf signalling in the endoderm of the epibranchial pouches (Hammond and Whitfield, 2011; McCarroll and Nechiporuk, 2013). Such a gradient of Fgf signalling across the otic placode is supported by the expression of canonical Fgf signalling readout genes such as *dusp6*, *etv4* and *spry4*, which show graded expression from the anterior of the placode. However, at around 24hpf, weak *etv4* expression within the posterior is apparent (data not shown). This expression may reflect a the transient expression of *fgf8a* reported within this domain around 24hpf, possibly in combination with the more persistent posterior *fgf10a* expression (Léger and Brand, 2002) (own data).

Data from Chapter Six confirmed that a loss of Hh signalling does not appear to effect Fgf signalling in or around the otic placode, with a weak domain of *etv4* still observed at 22.5hpf in CyA-treated embryos. Therefore based on the known positive-regulation of Fgf signalling on the anterior otic domain, the delayed duplication of anterior factors following a loss of Hh signalling may reflect the initially weak Fgf signalling within the posterior rather than the progressive expansion of *hmx3a*.

The positive feedback loop between *fgf3* and *fgf8a* with *hmx2* and *hmx3a* makes it difficult to identify which of these is the key early regulator in driving duplication of anterior otic character (Feng and Xu, 2010; Hammond and Whitfield, 2011). Therefore future work identifying whether *hmx3a* misexpression alone is sufficient to induce anterior character would help clarify this. If *hmx3a* over-expression alone is sufficient, it would support the previously proposed model where early expansion of *hmx3a* is primarily responsible for establishing the extent of the anterior duplication, which is subsequently reinforced by its feedback loop with Fgf.

7.3.2 Is posterior otic identity duplicated after knock-down of *hmx3a* and *hmx2*?

If *hmx2* and *hmx3a* are the key early regulators of defining the extent of the anterior otic domain then it would also be expected that knocking these down would lead to a duplication of posterior otic identity. Knock-down of *hmx2* and *hmx3a* in zebrafish, previously reported by Feng et al. showed in these morphants the ear has a merged medial sensory patch retaining primarily saccular identity but not a duplication (Feng and Xu, 2010). However, in these double morphants and also the mouse *hmx2;hmx3* mutants, there is a reported loss of anterior hair cells, which could mask any posterior morphology present in the remaining anterior sensory patch (Feng and Xu, 2010; Wang et al., 2004). Interestingly, the merger of the utricle and saccule seen in the *hmx2;hmx3* morphants is similar to that seen in the *hmx3* mouse mutants, whereas loss of both *hmx2* and *hmx3* in mice resulted in a progressive loss of both the utricle and saccule (Wang et al., 1998, 2004). Despite the *hmx2;hmx3* morphants not showing an obvious morphological loss of anterior otic identity, at the transcriptional level a clear loss of the otic anterior factors, *fgf3*, *8a*, *10a* and *pax5* was reported (Feng and Xu, 2010).

A possible explanation for these differing phenotypes is that in zebrafish, *hmx3* appears to be duplicated with two paralogues, *hmx3a* (NM 131634.2) and a predicted *hmx3b* (XM 017358610.1). Feng et al. reported that *hmx3a* and *hmx2* have functional redundancy within the zebrafish ear and the previously mentioned ability of the *Drosophila hmx* CDS to replace *hmx2* and *hmx3a* in mice supports a strong conservation of function in this transcription factor family (Feng and Xu, 2010; Wang et al., 2004). Zebrafish *hmx2*, *hmx3a* and *hmx3b* all contain a highly conserved region (Figure 7.2) and therefore based on this *hmx3b* is likely to be acting redundantly with *hmx3a* if expressed within the ear.

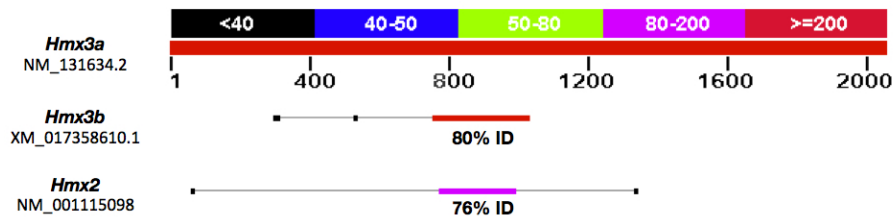


Figure 7.2: Blastn alignment of zebrafish *hmx3b* and *hmx2* against *hmx3a* mRNA sequence shows homology within an overlapping region 47% of the predicted *hmx3b* coding sequence shares 80% of its sequence identity with that of *hmx3a*. *Hmx2*, which has been shown to act redundantly with *hmx3a* during otic development, has 28% of its coding sequence sharing 76% sequence identity with that of *hmx3a*. This sequence homology appears to be within the same region for both *hmx2* and *hmx3a*.

7.3.3 Insight into assignment of posterior otic identity in zebrafish

Data in this thesis, along with that already published, seem to suggest that despite Hh being required for posterior otic identity in zebrafish, its effect appears weak when compared to that of Fgf (Hammond et al., 2010) (Hammond and Whitfield, 2011). In chick and mouse, as Hh is still expressed primarily within the ventral midline structures, it has been suggested to manifest as a ventral to dorsal gradient across the hindbrain adjacent to the otocyst. This has also been suggested to be reflected in a similar gradient of the Hh transcriptional effector, Gli3A across the DV axis (Bok et al., 2005, 2007b; Ohta et al., 2016). Aberrant Hh signalling in zebrafish also results in ventralised otic tissue, possibly suggesting a conservation of Hh's function during otic development between vertebrates. However, a converse loss of Hh does not expand the dorsal domain (Hammond et al., 2010, 2003).

As previously mentioned, RA has been shown to play a greater role in AP otic patterning in chick and mouse than appears to be the case in zebrafish (Bok et al., 2011). However, despite only chick showing a strong posterior duplication in response to RA, all three vertebrate models show a similar transcriptional response in the anterior expansion of *tbx* and reduction in *neurod1* (Bok et al., 2011; Radosevic et al., 2011; Maier and Whitfield, 2014). In zebrafish and mice, RA has also been shown to negatively regulate *fgf* expression within the otic tissue (Maier and Whitfield, 2014; Cadot et al., 2012; Frenz et al., 2010). Another interesting characteristic of RA signalling during otic development is how its regulatory effect appears to differ dependent upon its levels and the time at which these are increased or decreased (Chapter Six) (Maier and Whitfield, 2014; Frenz et al., 2010). Therefore, whilst RA may appear to have strikingly different effects on otic development between vertebrates, it may highlight temporal and spatial differences in transcription between these rather than the way in which RA is acting.

In zebrafish, Shh and RA appear to positively regulate posterior identity, although this appears weak relative to the anteriorising effect of Fgf signalling on the placode (Chapter Six). Therefore their combined action may be required to counter the strong anteriorising effect that Fgf exerts. Shh and RA are likely regulation of different targets, given RA is a known inhibitor of *fgf* expression during early otic development and Hh does not appear to directly influence Fgf signalling (Maier and Whitfield, 2014; Hammond and Whitfield, 2011). Interestingly, this potential combinatorial regulation of posterior otic identity by Hh and RA is in contrast to their opposing effect in patterning the ventral otic floor (Radosevic et al., 2011).

7.3.4 A new model for patterning of the otic AP axis in zebrafish

Building upon the model previously put forward by Hammond et al. for otic AP patterning with the data presented in this thesis, I propose a new model for patterning the otic AP axis in zebrafish. This supports an anterior to posterior gradient of Fgf but which drives early expression of *hmx3a* and *hmx2* in a similar gradient across the otic placode. When Hh signalling is present as a dorsoventral gradient originating from ventral midline structures this inhibits *hmx3a* and *hmx2* expression weakly but enough to limit its expression to an anterior domain. However, when Hh signalling is lost this inhibition is lifted, allowing a posterior expansion of *hmx3a* and *hmx2* expression. The positive feedback loop between otic *hmx3a* and *hmx2* with *fgf3* and *fgf8a* subsequently leads to reinforcement of anterior identity within the posterior domain leading to a duplication. The reinforcement of this network is likely also driven by the positive feedback relationship between *fgf3* and *fgf8a* and the localised *atoh1a* at either AP pole (Figure 7.3).

Within the posterior otic domain, RA appears to contribute to preventing adoption of anterior character, likely by inhibiting expression of *fgf* alongside the action of Hh in inhibiting *hmx3a* and *hmx2*. The combined effect of RA and Hh allows posterior expression of markers, such as *nav3a*, from 16hpf onwards; progressively defining posterior character. This progressive maturation of the anterior and posterior domains as outlined in the model above is also reflected in the loss of *cdr2l* expression, initially from the anterior but also from the posterior otic domain from 18hpf.

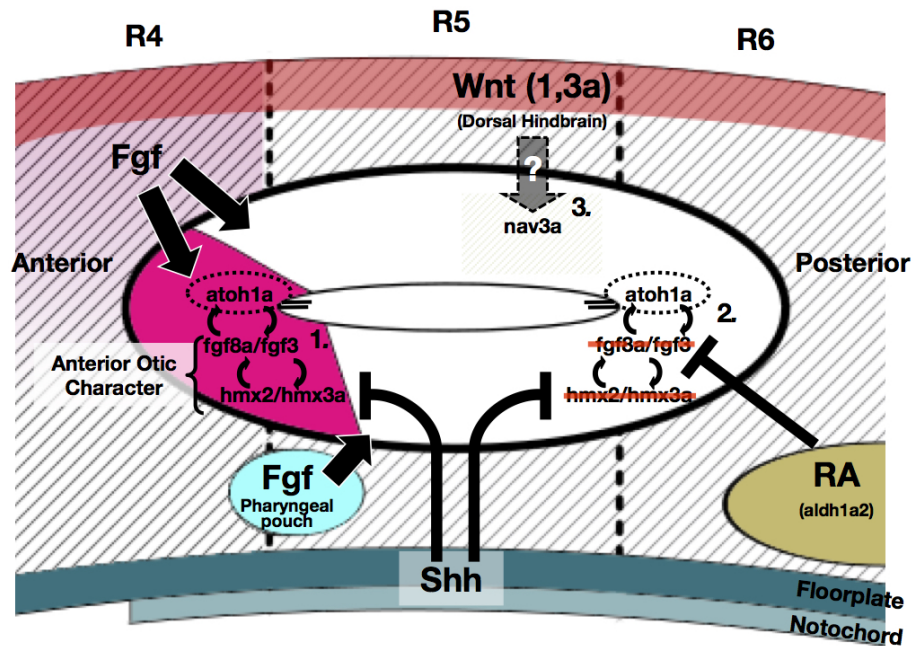


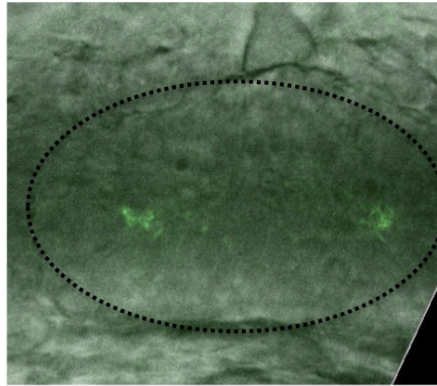
Figure 7.3: A new model for patterning of the otic AP axis in zebrafish

1. High levels of extrinsic Fgf signalling induces expression of *hmx2* and *hmx3a*, overcoming any inhibitory effect of Shh, which in turn establish anterior identity early on and subsequently driving expression of *fgf3* and *fgf8a* within the anterior. Maintenance of *fgf* expression within the anterior is also dependent on establishment of the sensory domains due to its positive feedback with Atoh1a in this region and expression from within the supporting cells. 2. In the posterior under normal conditions, due to the weaker presence of Fgf signalling early in development, expression of *hmx2* and *hmx3a* is inhibited by Hh. Within this region, early posterior RA may also inhibit *fgf* expression, which also dampens any positive reinforcement through either Hmx2, Hmx3a or Atoh1a. 3. At 16hpf, *nav3a* is induced within the posterior domain that later extends dorsally, which could reflect a response to dorsal hindbrain sources of Wnt signalling. Whether this impacts posterior otic identity is unclear. The establishment of the anterior and posterior domains, may also be marked by the progressive loss of *cdr2l* expression in an anterior to posterior-graded manner.

7.4 Future work

While the model defined in Figure, based upon the data presented in this thesis begins to give a better overview of the transcriptional relationships and dynamics likely to be patterning the zebrafish ear during early development, a number of questions still remain. Three in particular would be the initial focus of any future work; the first is identifying if *hmx3a* over-expression is sufficient to assign anterior identity without Fgf signalling. The second would be understanding how the persistence of anterior *hmx3a* expression after constitutive activation of Hh can be accounted for by the proposed model. One possible explanation could be that Hh signalling indirectly prevents the activity of Hmx3a, which could account for why expression of *hmx2*, a target of Hmx3a, appeared more strongly reduced in the gain-of-function Hh mutants compared to *hmx3a* (Chapter Six). The third focus would be confirming whether *nav3a* regulates posterior otic character or is only a marker. If *nav3a* is associated with posterior identity, it would clearly indicate that differentiation of the posterior otic domain is occurring earlier than signified by the other known posterior markers. This would support the proposed model, including *cdr2l* reflecting maturation of the otic tissue.

Supplementary data



S1: Localisation of cilia at the otic AP poles in 14-15hpf embryos

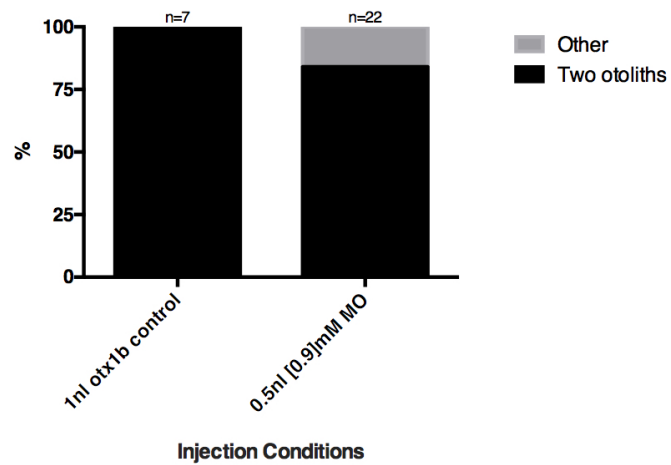
Cilia labelled using the *tg(arl13b:GFP)* line at 14-15hpf, prior to the formation of the otic lumen.

Search terms: "otic placode" between 1-4 to 10-13 somites (30/08/13)		
Gene	Expression Data (current status)	Stage Range
ak7b	Fig. 2 from Thisse <i>et al.</i> , 2004	1-4 somites to 10-13 somites
ak8	Fig. 2 from Thisse <i>et al.</i> , 2004	1-4 somites to 10-13 somites
atoh1b	3 figures from Millimaki <i>et al.</i> , 2007	1-4 somites to 10-13 somites
ccdc24	Fig. 2 from Thisse <i>et al.</i> , 2004	1-4 somites to 10-13 somites
ccdc40	Fig. 2 from Becker-Heck <i>et al.</i> , 2011	75%-epiboly to 5-9 somites
ccdc103	Fig. S11 from Panizzi <i>et al.</i> , 2012	75%-epiboly to Long-pec
cdr2l	Fig. 2 from Thisse <i>et al.</i> , 2004	1-4 somites to 10-13 somites
cxcl14	Fig. 2 from Thisse <i>et al.</i> , 2005	1-4 somites to 10-13 somites
cyb5d1	Fig. 2 from Thisse <i>et al.</i> , 2004	1-4 somites to 10-13 somites
cyp2p10	Fig. 2 from Thisse <i>et al.</i> , 2004	1-4 somites to 10-13 somites
dlx3b	6 figures from 5 publications	90%-epiboly to 20-25 somites
dlx4b	2 figures from 2 publications	1-4 somites to 10-13 somites
dnah9	2 figures from 2 publications	1-4 somites to 10-13 somites
entpd1	Fig. 2 from Thisse <i>et al.</i> , 2004	1-4 somites to 10-13 somites
etv5b	Fig. 7 from Esterberg <i>et al.</i> , 2009	5-9 somites
fgf24	2 figures from Padanad <i>et al.</i> , 2011	1-4 somites to 14-19 somites
fgfr1a	Fig. 7 from Esterberg <i>et al.</i> , 2009	5-9 somites
fgfr2	Fig. 7 from Esterberg <i>et al.</i> , 2009	5-9 somites
fgfr3	Fig. 7 from Esterberg <i>et al.</i> , 2009	5-9 somites
foxi1	3 figures from 3 publications	1-4 somites to Prim-5
foxj1b	3 figures from 3 publications	Dome to Protruding-mouth
gas8	Fig. S1 from Colantonio <i>et al.</i> , 2009	5-9 somites to 14-19 somites
ghrl2b	Fig. 3 from Han <i>et al.</i> , 2011	5-9 somites to Long-pec
has3	Fig. 2 from Thisse <i>et al.</i> , 2005	1-4 somites to 10-13 somites
hk1	Fig. 2 from Thisse <i>et al.</i> , 2004	1-4 somites to 10-13 somites
hmx3	Fig. S2 from Feng <i>et al.</i> , 2010	5-9 somites to Prim-25
ier2	Fig. S3 from Hong <i>et al.</i> , 2009	High to Prim-25
ift122	Fig. 2 from Thisse <i>et al.</i> , 2004	1-4 somites to 10-13 somites
irf6	Fig. 1 from Sabel <i>et al.</i> , 2009	64-cell to Protruding-mouth
irx4b	2 figures from Lecaudey <i>et al.</i> , 2005	1-4 somites to 20-25 somites
katnal1	Fig. 2 from Thisse <i>et al.</i> , 2004	1-4 somites to 10-13 somites
llgl2	Fig. 2 from Thisse <i>et al.</i> , 2004	1-4 somites to 10-13 somites
msxc	Fig. 2 from Phillips <i>et al.</i> , 2006	Bud to 5-9 somites
myod1	Fig. 11 from Hamade <i>et al.</i> , 2006	1-4 somites to 10-13 somites
pax2a	21 figures from 16 publications	Bud to Prim-25
pax8	11 figures from 5 publications	Bud to 5-9 somites
prdm1a	Fig. 1 from Birkholz <i>et al.</i> , 2009	5-9 somites to Long-pec
prox1a	Fig. 1 from Pistocchi <i>et al.</i> , 2008	1-4 somites to Days 7-13
robo4	Fig. 2 from Thisse <i>et al.</i> , 2008	1-4 somites to 10-13 somites
sb:eu592	Fig. 2 from Thisse <i>et al.</i> , 2005	1-4 somites to 10-13 somites
sfrp2	Fig. 3 from Tendeng <i>et al.</i> , 2006	5-9 somites to Long-pec
six2a	text only from Weber <i>et al.</i> , 2008	5-9 somites to Long-pec
slc34a2b	Fig. 2 from Thisse <i>et al.</i> , 2004	1-4 somites to 10-13 somites
sox3	Fig. 3 from Padanad <i>et al.</i> , 2011	5-9 somites
sox9a	3 figures from 3 publications	1-4 somites
sox9b	4 figures from 4 publications	1-4 somites to 5-9 somites
sox10	3 figures from 3 publications	1-4 somites to Prim-25
sp7	2 figures from 2 publications	1-4 somites to Day 4
sp8a	Fig. 2 from Thisse <i>et al.</i> , 2004	1-4 somites to 10-13 somites
tbx2b	2 figures from 2 publications	Bud to 26+ somites
zgc:172136	Fig. 2 from Thisse <i>et al.</i> , 2004	1-4 somites to 10-13 somites

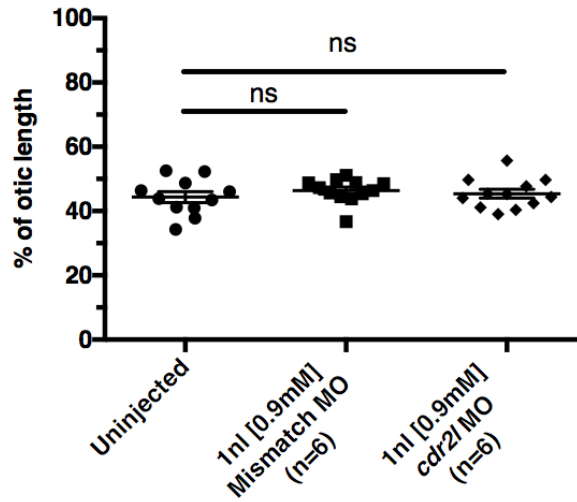
S2: Full ZFIN search using search terms: "otic placode" between 1-4 to 10-13 somites
 Full results from a search of the ZFIN gene expression database. Genes previously characterised as having an otic function are highlighted in orange.

Search terms: "posterior otic placode" between 14 to 20 somites		
Gene	Expression	Stage Range
nav3	-	16 -18.5 hpf (14 - 19 som)
nfe2	blood, ventral mesenchyme, ventral mesoderm	16 -18.5 hpf
zgc:101731	Not mentioned (see comments)	16 -18.5 hpf
tbx1	Non-neurogenic otic tissue	15 hpf +

S3: Full ZFIN search using search terms: "posterior otic placode" between 10 to 20 somites
Full results from a search of the ZFIN gene expression database.

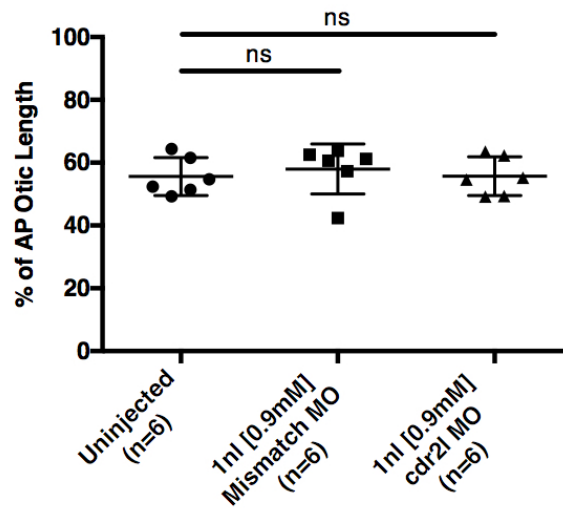


S4: Otolith phenotypes in 0.5nl 0.9mM *cdr2l* MO-injected embryos and control *otx1b* morphants



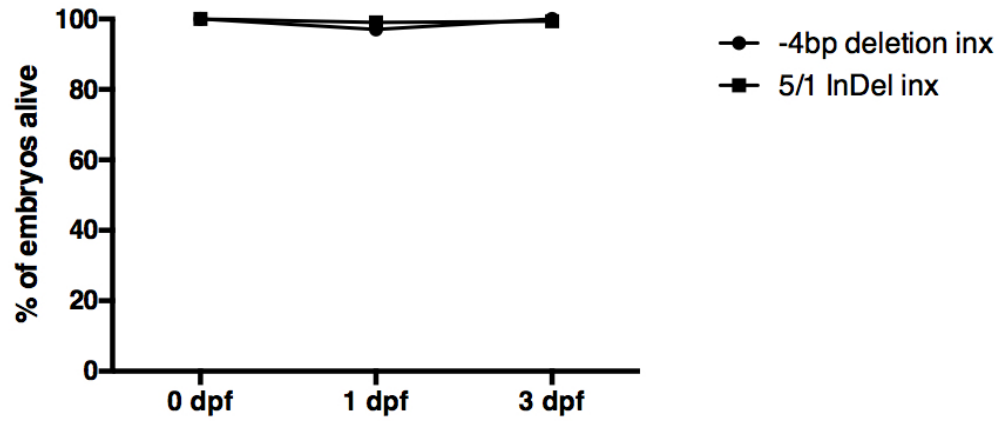
S5: % AP length of the *hmx2* domain in *cdr2l* morphants

n = 6 x dorsally imaged embryos per condition. One-way Anova (Non significant, $p=0.5882$) with Dunn's multiple comparison to the uninjected (both non significant. Adjusted p; Non-specific MO = 0.4850 and *cdr2l* MO = 0.8137)

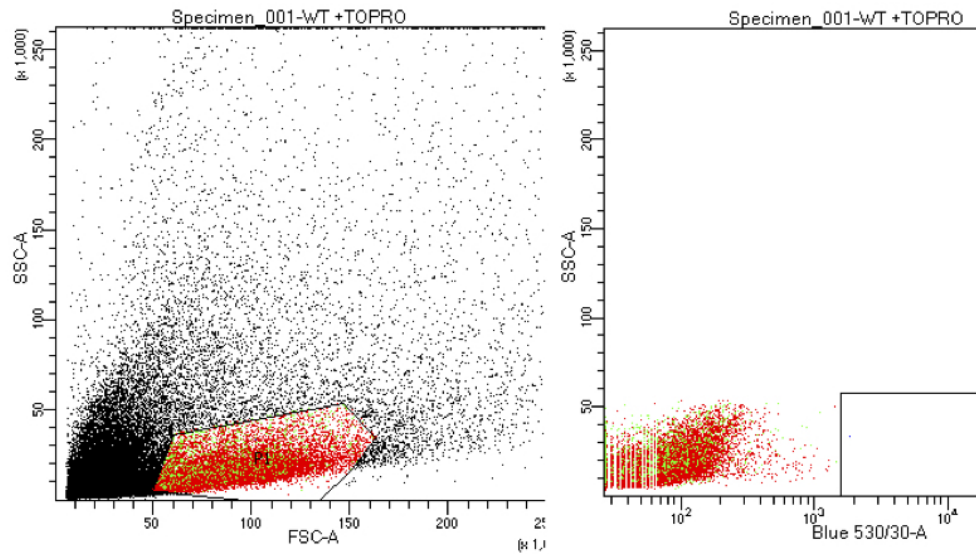


S6: % AP length of the *otx1b* domain in *cdr2l* morphants

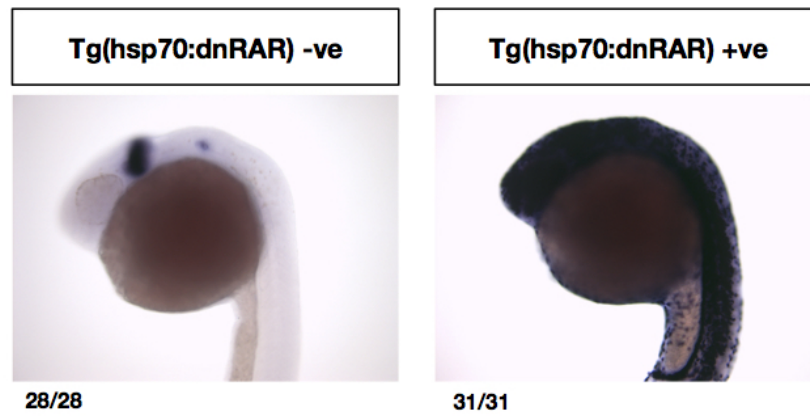
n = 6 x laterally imaged embryos per condition. One-way Anova (non-significant, $p=0.7917$) with Dunnett's multiple comparison to the uninjected (both are non-significant. Adjusted p; MM MO = 0.7698 and *cdr2l* MO = 0.9994)



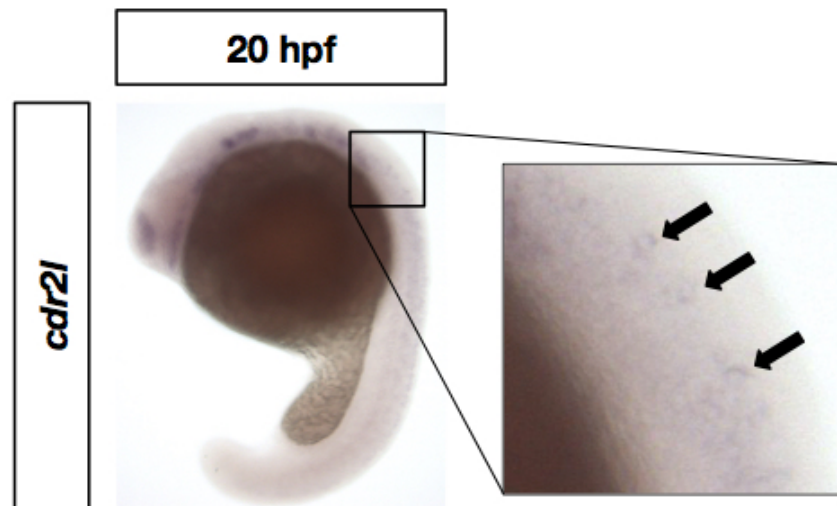
S7: Mortality curves for -4bp del incross and 5/1bp InDel incross over the first three days of development
 -4bp del incross n = 75, 5/1bp InDel incross n= 175



S8: Flow cytometry scatter plot on dissociated cell stained with TOPRO
 TOPRO stains compromised cells, which is associated with cell death. In the P3 gate only 4.2% of the population appeared non-viable.



S9: Expression of *pax5* in Tg(hs:dnRAR) embryos and their siblings after heatshock



S10: Expression of *cdr2l* at 20hpf with a zoomed image to show the dorsal puncta

Bibliography

- L. Abbas and T. T. Whitfield. Nkcc1 (Slc12a2) is required for the regulation of endolymph volume in the otic vesicle and swim bladder volume in the zebrafish larva. *Development (Cambridge, England)*, 136(16):2837–48, aug 2009. doi: 10.1242/dev.034215.
- S. Ali, D. L. Champagne, H. P. Spaink, and M. K. Richardson. Zebrafish embryos and larvae: A new generation of disease models and drug screens. *Birth Defects Research Part C: Embryo Today: Reviews*, 93(2):115–133, jun 2011. doi: 10.1002/bdrc.20206.
- B. Alsina, G. Abelló, E. Ulloa, D. Henrique, C. Pujades, and F. Giraldez. FGF signaling is required for determination of otic neuroblasts in the chick embryo. *Developmental Biology*, 267(1):119–134, 2004. doi: 10.1016/j.ydbio.2003.11.012.
- B. Alsina, F. Giraldez, and C. Pujades. Patterning and cell fate in ear development. *The International journal of developmental biology*, 53(8-10):1503–13, jan 2009. doi: 10.1387/ijdb.072422ba.
- Y. Alvarez, M. T. Alonso, V. Vendrell, L. C. Zelarayan, P. Chamero, T. Theil, M. R. Bösl, S. Kato, M. Maconochie, D. Riethmacher, and T. Schimmang. Requirements for FGF3 and FGF10 during inner ear formation. *Development (Cambridge, England)*, 130(25):6329–38, 2003. doi: 10.1242/dev.00881.
- P. Andermann, J. Ungos, and D. W. Raible. Neurogenin1 defines zebrafish cranial sensory ganglia precursors. *Developmental biology*, 251(1):45–58, 2002. doi: 10.1006/dbio.2002.0820.
- R. Ando, H. Hama, M. Yamamoto-Hino, H. Mizuno, and A. Miyawaki. An optical marker based on the UV-induced green-to-red photoconversion of a fluorescent protein. *Proceedings of the National Academy of Sciences of the United States of America*, 99(20):12651–6, oct 2002. doi: 10.1073/pnas.202320599.
- W. Y. Aw and D. Devenport. Planar cell polarity: global inputs establishing cellular asymmetry. *Current Opinion in Cell Biology*, 2016. doi: 10.1016/j.ceb.2016.08.002.
- P. I. Bang, W. F. Sewell, and J. J. Malicki. Morphology and cell type heterogeneities of the inner ear epithelia in adult and juvenile zebrafish (*Danio rerio*). *Journal of Comparative Neurology*, 438(2):173–190, 2001. doi: 10.1002/cne.1308.
- P. I. Bang, P. C. Yelick, J. J. Malicki, and W. F. Sewell. High-throughput behavioral screening method for detecting auditory response defects in zebrafish. *Journal of Neuroscience Methods*, 118(2):177–187, 2002. doi: 10.1016/S0165-0270(02)00118-8.
- A. Barrallo-Gimeno, J. Holzschuh, W. Driever, and E. W. Knapik. Neural crest survival and differentiation in zebrafish depends on mont blanc/tfap2a gene function. *Development (Cambridge, England)*, 131(7):1463–77, 2004. doi: 10.1242/dev.01033.

- S. Baxendale, C.-K. Chen, H. Tang, C. Davison, L. V. Hateren, M. D. R. Croning, S. J. Humphray, S. J. Hubbard, and P. W. Ingham. Expression screening and annotation of a zebrafish myoblast cDNA library. *Gene expression patterns : GEP*, 9(2):73–82, feb 2009. doi: 10.1016/j.gep.2008.10.003.
- V. M. Bedell, S. E. Westcot, and S. C. Ekker. Lessons from morpholino-based screening in zebrafish. *Briefings in Functional Genomics*, 10(4):181–188, 2011. doi: 10.1093/bfgp/elr021.
- C. A. Beretta, I. Brinkmann, and M. Carl. All four zebrafish Wnt7 genes are expressed during early brain development. *Gene Expression Patterns*, 11(3-4):277–284, 2011. doi: 10.1016/j.gep.2011.01.004.
- N. Bhat, H.-J. Kwon, and B. B. Riley. A gene network that coordinates preplacodal competence and neural crest specification in zebrafish. *Developmental Biology*, 373(1):107–117, jan 2013. doi: 10.1016/j.ydbio.2012.10.012.
- O. Birol, T. Ohyama, R. K. Edlund, K. Drakou, P. Georgiades, and A. K. Groves. The mouse Foxi3 transcription factor is necessary for the development of posterior placodes. *Developmental Biology*, 409(1):139–151, jan 2016. doi: 10.1016/j.ydbio.2015.09.022.
- J. Bok, M. Bronner-Fraser, and D. K. Wu. Role of the hindbrain in dorsoventral but not anteroposterior axial specification of the inner ear. *Development (Cambridge, England)*, 132(9):2115–24, may 2005. doi: 10.1242/dev.01796.
- J. Bok, W. Chang, and D. K. Wu. Patterning and morphogenesis of the vertebrate inner ear. *The International journal of developmental biology*, 51(6-7):521–33, jan 2007a. doi: 10.1387/ijdb.072381jb.
- J. Bok, D. K. Dolson, P. Hill, U. Rütther, D. J. Epstein, and D. K. Wu. Opposing gradients of Gli repressor and activators mediate Shh signaling along the dorsoventral axis of the inner ear. *Development (Cambridge, England)*, 134(9):1713–1722, 2007b. doi: 10.1242/dev.000760.
- J. Bok, S. Raft, K.-A. Kong, S. K. Koo, U. C. Dräger, and D. K. Wu. Transient retinoic acid signaling confers anterior-posterior polarity to the inner ear. *Proceedings of the National Academy of Sciences of the United States of America*, 108(1):161–6, jan 2011. doi: 10.1073/pnas.1010547108.
- M. Bouchard, D. de Caprona, M. Busslinger, P. Xu, and B. Fritzschn. Pax2 and Pax8 cooperate in mouse inner ear morphogenesis and innervation. *BMC developmental biology*, 10:89, 2010. doi: 10.1186/1471-213X-10-89.
- G. Bretones, M. D. Delgado, and J. León. Myc and cell cycle control. *Biochimica et biophysica acta*, 1849(5):506–516, 2015. doi: 10.1016/j.bbagr.2014.03.013.
- J. R. Brewer, P. Mazot, and P. Soriano. Genetic insights into the mechanisms of Fgf signaling. pages 751–771, 2016. doi: 10.1101/gad.277137.115.GENES.
- A. S. Brown and D. J. Epstein. Otic ablation of smoothened reveals direct and indirect requirements for Hedgehog signaling in inner ear development. *Development (Cambridge, England)*, 138(18):3967–76, sep 2011. doi: 10.1242/dev.066126.
- J. L. Brown, M. Snir, H. Noushmehr, M. Kirby, S.-K. Hong, A. G. Elkahloun, and B. Feldman. Transcriptional profiling of endogenous germ layer precursor cells identifies *dusp4* as an essential gene in zebrafish endoderm specification. *Proceedings of the National Academy of Sciences of the United States of America*, 105(34):12337–12342, 2008. doi: 10.1073/pnas.0805589105.

- G. R. Buckles, C. J. Thorpe, M.-c. Ramel, and A. C. Lekven. Combinatorial Wnt control of zebrafish midbrain hindbrain boundary formation. *Mechanisms of Development*, 121:437–447, 2004. doi: 10.1016/j.mod.2004.03.026.
- S. Cadot, D. Frenz, and M. Maconochie. A novel method for retinoic acid administration reveals differential and dose-dependent downregulation of Fgf3 in the developing inner ear and anterior CNS. *Developmental Dynamics*, 241(4):741–758, 2012. doi: 10.1002/dvdy.23748.
- W. Chang, J. V. Brigande, D. M. Fekete, and D. K. Wu. The development of semicircular canals in the inner ear: role of FGFs in sensory cristae. *Development (Cambridge, England)*, 131(17):4201–11, 2004. doi: 10.1242/dev.01292.
- W. Chen, S. Burgess, and N. Hopkins. Analysis of the zebrafish smoothed mutant reveals conserved and divergent functions of hedgehog activity. *Development (Cambridge, England)*, 128(12):2385–96, jun 2001.
- M. Cohen, J. Briscoe, and R. Blassberg. Morphogen Interpretation: The Transcriptional Logic Of Neural Tube Patterning. *Current Opinion in Genetics and Development*, 23(4):423–428, 2013. doi: 10.1016/j.gde.2013.04.003.
- J. P. Corradi, C. Yang, J. C. Darnell, J. Dalmau, and R. B. Darnell. A post-transcriptional regulatory mechanism restricts expression of the paraneoplastic cerebellar degeneration antigen cdr2 to immune privileged tissues. *The Journal of neuroscience : the official journal of the Society for Neuroscience*, 17(4):1406–15, 1997.
- R. Créton, J. E. Speksnijder, and L. F. Jaffe. Patterns of free calcium in zebrafish embryos. *Journal of cell science*, 111 (Pt 1:1613–1622, 1998.
- A. Davies, C. Formstone, I. Mason, and J. Lewis. Planar polarity of hair cells in the chick inner ear is correlated with polarized distribution of c-flamingo-1 protein. *Developmental Dynamics*, 233(3):998–1005, 2005. doi: 10.1002/dvdy.20376.
- A. DeLaurier, B. F. Eames, B. Blanco-Sánchez, G. Peng, X. He, M. E. Swartz, B. Ullmann, M. Westerfield, and C. B. Kimmel. Zebrafish sp7:EGFP: a transgenic for studying otic vesicle formation, skeletogenesis, and bone regeneration. *Genesis (New York, N.Y. : 2000)*, 48(8):505–11, aug 2010. doi: 10.1002/dvg.20639.
- a. Dick, M. Hild, H. Bauer, Y. Imai, H. Maifeld, a. F. Schier, W. S. Talbot, T. Bouwmeester, and M. Hammerschmidt. Essential role of Bmp7 (snailhouse) and its prodomain in dorsoventral patterning of the zebrafish embryo. *Development (Cambridge, England)*, 127(2):343–354, 2000.
- E. Domínguez-Frutos, I. López-Hernández, V. Vendrell, J. Neves, M. Gallozzi, K. Gutsche, L. Quintana, J. Sharpe, P. S. Knoepfler, R. N. Eisenman, A. Trumpp, F. Giráldez, and T. Schimmang. N-myc controls proliferation, morphogenesis, and patterning of the inner ear. *The Journal of neuroscience : the official journal of the Society for Neuroscience*, 31(19):7178–89, 2011. doi: 10.1523/JNEUROSCI.0785-11.2011.
- B. W. Draper, D. W. Stock, and C. B. Kimmel. Zebrafish fgf24 functions with fgf8 to promote posterior mesodermal development. *Development*, 130(19):4639–4654, 2003. doi: 10.1242/dev.00671130/19/4639 [pii].
- K. Dutton, L. Abbas, J. Spencer, C. Brannon, C. Mowbray, M. Nikaido, R. N. Kelsh, and T. T. Whitfield. A zebrafish model for Waardenburg syndrome type IV reveals diverse roles for Sox10 in the otic vesicle. *Disease models & mechanisms*, 2(1-2):68–83, 2009. doi: 10.1242/dmm.001164.

- K. a. Dutton, A. Pauliny, S. S. Lopes, S. Elworthy, T. J. Carney, J. Rauch, R. Geisler, P. Haffter, and R. N. Kelsh. Zebrafish *coloAess* encodes *sox10* and specifies non-ectomesenchymal neural crest fates. *Development (Cambridge, England)*, 128(21):4113–25, nov 2001.
- T. W. Eichler, C. Totland, M. Haugen, T. H. Qvale, K. Mazengia, A. Storstein, B. I. Haukanes, and C. a. Vedeler. CDR2L Antibodies: A New Player in Paraneoplastic Cerebellar Degeneration. *PLoS one*, 8(6):e66002, jan 2013. doi: 10.1371/journal.pone.0066002.
- M. Ekker, M. A. Akimenko, R. Bremiller, and M. Westerfield. Regional expression of three homeobox transcripts in the inner ear of zebrafish embryos. *Neuron*, 9(1):27–35, 1992.
- T. Erickson, C. R. French, and A. J. Waskiewicz. *Meis1* specifies positional information in the retina and tectum to organize the zebrafish visual system. *Neural development*, 5(June):22, 2010. doi: 10.1186/1749-8104-5-22.
- R. Esterberg and A. Fritz. *dlx3b/4b* are required for the formation of the preplacodal region and otic placode through local modulation of BMP activity. *Developmental biology*, 325(325(1)): 189–199, 2009. doi: 10.1016/j.ydbio.2008.10.017.dlx3b/4b.
- H. Fathallah-Shaykh, S. Wolf, E. Wong, J. B. Posner, and H. M. Furneaux. Cloning of a leucine-zipper protein recognized by the sera of patients with antibody-associated paraneoplastic cerebellar degeneration. *Proceedings of the National Academy of Sciences of the United States of America*, 88(April):3451–3454, 1991. doi: 10.1073/pnas.88.8.3451.
- Y. Feng and Q. Xu. Pivotal role of *hmx2* and *hmx3* in zebrafish inner ear and lateral line development. *Developmental biology*, 339(2):507–18, mar 2010. doi: 10.1016/j.ydbio.2009.12.028.
- S. D. Freeman, K. Keino-Masu, M. Masu, and R. K. Ladher. Expression of the Heparan Sulfate 6-O-endosulfatases, *Sulf1* and *Sulf2*, in the Avian and Mammalian Inner Ear Suggests a Role for Sulfation during Inner Ear Development. *Developmental dynamics : an official publication of the American Association of Anatomists*, 244(2):168–80, 2014. doi: 10.1002/dvdy.24223.
- D. A. Frenz, W. Liu, A. Cvekl, Q. Xie, L. Wassef, L. Quadro, K. Niederreither, M. Maconochie, and A. Shanske. Retinoid signaling in inner ear development: A "Goldilocks" phenomenon. *American Journal of Medical Genetics, Part A*, 152 A(12):2947–2961, 2010. doi: 10.1002/ajmg.a.33670.
- S. Freter, Y. Muta, S.-S. Mak, S. Rinkwitz, and R. K. Ladher. Progressive restriction of otic fate: the role of FGF and Wnt in resolving inner ear potential. *Development (Cambridge, England)*, 135(20):3415–24, oct 2008. doi: 10.1242/dev.026674.
- H. Fujii, T. Sato, S. Kaneko, O. Gotoh, Y. Fujii-Kuriyama, K. Osawa, S. Kato, and H. Hamada. Metabolic inactivation of retinoic acid by a novel P450 differentially expressed in developing mouse embryos. *The EMBO journal*, 16(14):4163–73, 1997. doi: 10.1093/emboj/16.14.4163.
- J. a. Gagnon, E. Valen, S. B. Thyme, P. Huang, L. Ahkmetova, A. Pauli, T. G. Montague, S. Zimmerman, C. Richter, and A. F. Schier. Efficient mutagenesis by Cas9 protein-mediated oligonucleotide insertion and large-scale assessment of single-guide RNAs. *PLoS ONE*, 9(5):5–12, 2014. doi: 10.1371/journal.pone.0098186.
- V. E. Gallardo and M. Behra. Fluorescent activated cell sorting (FACS) combined with gene expression microarrays for transcription enrichment profiling of zebrafish lateral line cells. *Methods (San Diego, Calif.)*, 62(3):226–31, aug 2013. doi: 10.1016/j.ymeth.2013.06.005.

- L. V. Goodrich and D. Strutt. Principles of planar polarity in animal development. *Development (Cambridge, England)*, 138(10):1877–92, 2011. doi: 10.1242/dev.054080.
- H. Grandel, K. Lun, G.-J. Rauch, M. Rhinn, T. Piotrowski, C. Houart, P. Sordino, A. M. Kuchler, S. Schulte-Merker, R. Geisler, N. Holder, S. W. Wilson, and M. Brand. Retinoic acid signalling in the zebrafish embryo is necessary during pre-segmentation stages to pattern the anterior-posterior axis of the CNS and to induce a pectoral fin bud. *Development*, 129(12):2851–2865, 2002.
- A. Groves and D. Fekete. Shaping sound in space : the regulation of inner ear patterning. *Development*, 826:245–257, 2012. doi: 10.1242/dev.
- A. K. Groves and C. LaBonne. Setting appropriate boundaries: Fate, patterning and competence at the neural plate border. *Developmental Biology*, 389(1):2–12, 2014. doi: 10.1016/j.ydbio.2013.11.027.
- P. Haas and D. Gilmour. Chemokine Signaling Mediates Self-Organizing Tissue Migration in the Zebrafish Lateral Line. *Developmental Cell*, 10(5):673–680, 2006. doi: 10.1016/j.devcel.2006.02.019.
- C. Haddon, C. Mowbray, T. Whitfield, D. Jones, S. Gschmeber, and J. Lewis. Hair cells without supporting cells: further studies in the ear of the zebrafish mind bomb mutant. *Journal of neurocytology*, 28(10-11):837–850, 2000. doi: 10.1023/A:1007013904913.
- K. L. Hammond and T. T. Whitfield. The developing lamprey ear closely resembles the zebrafish otic vesicle: *otx1* expression can account for all major patterning differences. *Development*, 133(7):1347–1357, 2006. doi: 10.1242/dev.02306.
- K. L. Hammond and T. T. Whitfield. Expression of zebrafish *hip*: response to Hedgehog signalling, comparison with *ptc1* expression, and possible role in otic patterning. *Gene expression patterns : GEP*, 9(6):391–6, sep 2009. doi: 10.1016/j.gep.2009.06.006.
- K. L. Hammond and T. T. Whitfield. Fgf and Hh signalling act on a symmetrical pre-pattern to specify anterior and posterior identity in the zebrafish otic placode and vesicle. *Development (Cambridge, England)*, 138(18):3977–87, sep 2011. doi: 10.1242/dev.066639.
- K. L. Hammond, R. E. Hill, T. T. Whitfield, and P. D. Currie. Isolation of three zebrafish *dachshund* homologues and their expression in sensory organs, the central nervous system and pectoral fin buds. *Mechanisms of Development*, 112(1-2):183–189, 2002. doi: 10.1016/S0925-4773(01)00637-2.
- K. L. Hammond, H. E. Loynes, A. A. Forlarin, J. Smith, and T. T. Whitfield. Hedgehog signalling is required for correct anteroposterior patterning of the zebrafish otic vesicle. *Development*, 130(7):1403–1417, apr 2003. doi: 10.1242/dev.00360.
- K. L. Hammond, H. E. Loynes, C. Mowbray, G. Runke, M. Hammerschmidt, M. C. Mullins, V. Hildreth, B. Chaudhry, and T. T. Whitfield. A late role for *bmp2b* in the morphogenesis of semicircular canal ducts in the zebrafish inner ear. *PLoS One*, 4(2):e4368, 2009. doi: 10.1371/journal.pone.0004368.
- K. L. Hammond, F. J. M. van Eeden, and T. T. Whitfield. Repression of Hedgehog signalling is required for the acquisition of dorsolateral cell fates in the zebrafish otic vesicle. *Development (Cambridge, England)*, 137(8):1361–71, apr 2010. doi: 10.1242/dev.045666.

- S. Hans and M. Westerfield. Changes in retinoic acid signaling alter otic patterning. *Development (Cambridge, England)*, 134(13):2449–58, jul 2007. doi: 10.1242/dev.000448.
- S. Hans, D. Liu, and M. Westerfield. Pax8 and Pax2a function synergistically in otic specification, downstream of the Foxi1 and Dlx3b transcription factors. *Development (Cambridge, England)*, 131(20):5091–102, oct 2004. doi: 10.1242/dev.01346.
- S. Hans, J. Christison, D. Liu, and M. Westerfield. Fgf-dependent otic induction requires competence provided by Foxi1 and Dlx3b. *BMC developmental biology*, 7:5, jan 2007. doi: 10.1186/1471-213X-7-5.
- S. Hans, A. Irmscher, and M. Brand. Zebrafish Foxi1 provides a neuronal ground state during inner ear induction preceding the Dlx3b/4b-regulated sensory lineage. *Development (Cambridge, England)*, 140(9):1936–45, may 2013. doi: 10.1242/dev.087718.
- R. Harrison. RELATIONS OF SYMMETRY IN THE DEVELOPING EAR OF AMBLYSTOMA PUNCTATUM. *Proceedings of the National Academy of Sciences of . . .*, pages 238–247, 1936.
- E. Hatch, C. Noyes, and X. Wang. Fgf3 is required for dorsal patterning and morphogenesis of the inner ear epithelium. *Development*, 134(20):3615–3625, 2007.
- G. Hauptmann and T. Gerster. Combinatorial Expression of Zebrafish Brn-1- and Brn-2- Related POU Genes in the Embryonic Brain , Pronephric Primordium , and Pharyngeal Arches. *Developmental Dynamics*, 218:345–358, 2000.
- H. Herbrand, S. Guthrie, T. Hadrys, S. Hoffmann, H. H. Arnold, S. Rinkwitz-Brandt, and E. Bober. Two regulatory genes, cNkx5-1 and cPax2, show different responses to local signals during otic placode and vesicle formation in the chick embryo. *Development (Cambridge, England)*, 125(4): 645–654, 1998.
- E. Hoijsman, D. Rubbini, J. Colombelli, and B. Alsina. Mitotic cell rounding and epithelial thinning regulate lumen growth and shape. *Nature Communications*, 6:7355, 2015. doi: 10.1038/ncomms8355.
- A. Hruscha, P. Krawitz, A. Rechenberg, V. Heinrich, J. Hecht, C. Haass, and B. Schmid. Efficient CRISPR/Cas9 genome editing with low off-target effects in zebrafish. *Development (Cambridge, England)*, 140(May):4982–7, 2013. doi: 10.1242/dev.099085.
- P. Huang, Z. Zhu, S. Lin, and B. Zhang. Reverse Genetic Approaches in Zebrafish. *Journal of Genetics and Genomics*, 39(9):421–433, 2012. doi: 10.1016/j.jgg.2012.07.004.
- M. Itoh, C.-h. Kim, G. Palardy, T. Oda, Y.-j. Jiang, D. Maust, S.-y. Yeo, K. Lorick, G. J. Wright, L. Ariza-mcnaughton, A. M. Weissman, J. Lewis, S. C. Chandrasekharappa, and A. B. Chitnis. Mind Bomb Is a Ubiquitin Ligase that Is Essential for Efficient Activation of Notch Signaling by Delta. 4:67–82, 2003.
- T. Jiang, K. Kindt, and D. K. Wu. Transcription factor Emx2 controls stereociliary bundle orientation of sensory hair cells. *eLife*, 6(972), mar 2017. doi: 10.7554/eLife.23661.
- C. J. Jopling. MicroRNA-mediated repression of nonsense mRNAs. *eLife*, 3:e03032, 2014. doi: 10.7554/eLife.03032.
- J. P. Junker, E. S. Noel, V. Guryev, K. A. Peterson, G. Shah, J. Huisken, A. P. McMahon, E. Berezikov, J. Bakkers, and A. Van Oudenaarden. Genome-wide RNA Tomography in the Zebrafish Embryo. *Cell*, 159(3):662–675, 2014. doi: 10.1016/j.cell.2014.09.038.

- B. Kais, K. E. Schneider, S. Keiter, K. Henn, C. Ackermann, and T. Braunbeck. DMSO modifies the permeability of the zebrafish (*Danio rerio*) chorion-Implications for the fish embryo test (FET). *Aquatic Toxicology*, 140-141:229–238, 2013. doi: 10.1016/j.aquatox.2013.05.022.
- T. Kaji and B. Artinger. *dlx3b* and *dlx4b* function in the development of Rohon-Beard sensory neurons and trigeminal placode in the zebrafish neurula. 276(2):523–540, 2004. doi: 10.1016/j.ydbio.2004.09.020. *dlx3b*.
- H. Kantarci, R. K. Edlund, A. K. Groves, and B. B. Riley. *Tfap2a* Promotes Specification and Maturation of Neurons in the Inner Ear through Modulation of Bmp, Fgf and Notch Signaling. *PLOS Genetics*, 11:e1005037, 2015. doi: 10.1371/journal.pgen.1005037.
- Y. Kawano and R. Kypta. Secreted antagonists of the Wnt signalling pathway. *Journal of cell science*, 116(13):2627–2634, 2003. doi: 10.1242/jcs.00623.
- G. M. Kelly, P. Greenstein, D. F. Erezylmaz, and R. T. Moon. Zebrafish *Wnt8* and *Wnt8B* Share a Common Activity But Are Involved in Distinct Developmental Pathways. *Development*, 121(6):1787–1799, 1995.
- S. B. Khatri and A. K. Groves. Expression of the *Foxi2* and *Foxi3* transcription factors during development of chicken sensory placodes and pharyngeal arches. *Gene expression patterns : GEP*, 13(1-2):38–42, 2013. doi: 10.1016/j.gep.2012.10.001.
- S. B. Khatri, R. K. Edlund, and A. K. Groves. *Foxi3* is necessary for the induction of the chick otic placode in response to FGF signaling. *Developmental Biology*, 391(2):158–169, 2014. doi: 10.1016/j.ydbio.2014.04.014.
- C. U. Kidwell, C.-Y. Su, M. Hibi, and C. B. Moens. Multiple zebrafish *atoh1* genes specify a diversity of neuronal types in the zebrafish cerebellum. *bioRxiv*, 2017. doi: <https://doi.org/10.1101/098012>.
- A. E. Kiernan, A. L. Pelling, K. K. H. Leung, A. S. P. Tang, D. M. Bell, C. Tease, R. Lovell-Badge, K. P. Steel, and K. S. E. Cheah. *Sox2* is required for sensory organ development in the mammalian inner ear. *Nature*, 434(7036):1031–1035, apr 2005. doi: 10.1038/nature03487.
- K. Kikuchi, J. E. Holdway, R. J. Major, N. Blum, R. D. Dahn, G. Begemann, and K. D. Poss. Retinoic Acid Production by Endocardium and Epicardium Is an Injury Response Essential for Zebrafish Heart Regeneration. *Developmental Cell*, 20(3):397–404, 2011. doi: 10.1016/j.devcel.2011.01.010.
- C. B. Kimmel, W. W. Ballard, S. R. Kimmel, B. Ullmann, and T. F. Schilling. Stages of embryonic development of the zebrafish. *Developmental dynamics : an official publication of the American Association of Anatomists*, 203(3):253–310, jul 1995. doi: 10.1002/aja.1002030302.
- C. Klein, J. Mikutta, J. Krueger, K. Scholz, J. Brinkmann, D. Liu, J. Veerkamp, D. Siegel, S. Abdelilah-Seyfried, and F. le Noble. Neuron navigator 3a regulates liver organogenesis during zebrafish embryogenesis. *Development (Cambridge, England)*, 138(10):1935–45, may 2011. doi: 10.1242/dev.056861.
- A. K. Knecht and M. Bronner-Fraser. Induction of the neural crest: a multigene process. *Nature reviews. Genetics*, 3(6):453–461, 2002. doi: 10.1038/nrg819.

- F. O. Kok, M. Shin, C. W. Ni, A. Gupta, A. S. Grosse, A. VanImpel, B. C. Kirchmaier, J. Peterson-Maduro, G. Kourkoulis, I. Male, D. F. DeSantis, S. Sheppard-Tindell, L. Ebarasi, C. Betsholtz, S. Schulte-Merker, S. A. Wolfe, and N. D. Lawson. Reverse genetic screening reveals poor correlation between morpholino-induced and mutant phenotypes in zebrafish. *Developmental Cell*, 32(1):97–108, 2015. doi: 10.1016/j.devcel.2014.11.018.
- V. Korzh, I. Sleptsova, J. Liao, J. He, and Z. Gong. Expression of zebrafish bHLH genes *ngn1* and *nrd* defines distinct stages of neural differentiation. *Developmental Dynamics*, 213(1):92–104, 1998. doi: 10.1002/(SICI)1097-0177(199809)213:1;92::AID-AJA9;3.0.CO;2-T.
- K. Kotkamp, E. Kur, B. Wendik, B. K. Polok, S. Ben-Dor, D. Onichtchouk, and W. Driever. Pou5f1/Oct4 promotes cell survival via direct activation of myc expression during zebrafish gastrulation. *PLoS ONE*, 9(3), 2014. doi: 10.1371/journal.pone.0092356.
- S.-J. Kwak, B. T. Phillips, R. Heck, and B. B. Riley. An expanded domain of *fgf3* expression in the hindbrain of zebrafish *valentino* mutants results in mis-patterning of the otic vesicle. *Development (Cambridge, England)*, 129(22):5279–87, 2002a.
- S.-J. Kwak, B. T. Phillips, R. Heck, and B. B. Riley. An expanded domain of *fgf3* expression in the hindbrain of zebrafish *valentino* mutants results in mis-patterning of the otic vesicle. *Development (Cambridge, England)*, 129(22):5279–87, nov 2002b.
- S.-j. Kwak, S. Vemaraju, S. J. Moorman, D. Zeddies, A. N. Popper, and B. B. Riley. Zebrafish *pax5* Regulates Development of the Utricular Macula and Vestibular Function. *Developmental Dynamics*, (September):3026–3038, 2006. doi: 10.1002/dvdy.20961.
- H. J. Kwon, N. Bhat, E. M. Sweet, R. a. Cornell, and B. B. Riley. Identification of early requirements for preplacodal ectoderm and sensory organ development. *PLoS Genetics*, 6(9), 2010. doi: 10.1371/journal.pgen.1001133.
- R. K. Ladher. Changing shape and shaping change: Inducing the inner ear. *Seminars in Cell & Developmental Biology*, 2016. doi: 10.1016/j.semcdb.2016.10.006.
- R. K. Ladher, P. O’Neill, and J. Begbie. From shared lineage to distinct functions: the development of the inner ear and epibranchial placodes. *Development (Cambridge, England)*, 137(11):1777–85, jun 2010. doi: 10.1242/dev.040055.
- N. D. Lawson. Reverse Genetics in Zebrafish: Mutants, Morphants, and Moving Forward. *Trends in Cell Biology*, 26(2):77–79, 2016. doi: 10.1016/j.tcb.2015.11.005.
- V. Lecaudey, E. Ulloa, I. Anselme, A. Stedman, S. Schneider-Maunoury, and C. Pujades. Role of the hindbrain in patterning the otic vesicle: a study of the zebrafish *vhnf1* mutant. *Developmental biology*, 303(1):134–43, mar 2007. doi: 10.1016/j.ydbio.2006.10.041.
- V. Lecaudey, G. Cakan-Akdogan, W. H. J. Norton, and D. Gilmour. Dynamic Fgf signaling couples morphogenesis and migration in the zebrafish lateral line primordium. *Development (Cambridge, England)*, 135(16):2695–705, aug 2008. doi: 10.1242/dev.025981.
- E. C. Lee, D. Yu, J. Martinez de Velasco, L. Tessarollo, D. a. Swing, D. L. Court, N. a. Jenkins, and N. G. Copeland. A highly efficient *Escherichia coli*-based chromosome engineering system adapted for recombinogenic targeting and subcloning of BAC DNA. *Genomics*, 73(1):56–65, apr 2001. doi: 10.1006/geno.2000.6451.

- S. G. Lee, M. Huang, N. D. Obholzer, S. Sun, W. Li, M. Petrillo, P. Dai, Y. Zhou, D. A. Cotanche, S. G. Megason, H. Li, and Z.-Y. Chen. Myc and Fgf Are Required for Zebrafish Neuromast Hair Cell Regeneration. *Plos One*, 11(6):e0157768, 2016. doi: 10.1371/journal.pone.0157768.
- S. Léger and M. Brand. Fgf8 and Fgf3 are required for zebrafish ear placode induction, maintenance and inner ear patterning. *Mechanisms of Development*, 119(1):91–108, 2002. doi: 10.1016/S0925-4773(02)00343-X.
- A. C. Lekven, C. J. Thorpe, J. S. Waxman, and R. T. Moon. Zebrafish wnt8 Encodes Two Wnt8 Proteins on a Bicistronic Transcript and Is Required for Mesoderm and Neurectoderm Patterning. *Developmental Cell*, 1(1):103–114, 2001. doi: 10.1016/S1534-5807(01)00007-7.
- A. C. Lekven, G. R. Buckles, N. Kostakis, and R. T. Moon. wnt1 and wnt10b function redundantly at the zebrafish midbrain hindbrain boundary. *Developmental biology*, 254:172–187, 2003. doi: 10.1016/S0012-1606(02)00044-1.
- K. E. Lewis, J. P. Concordet, and P. W. Ingham. Characterisation of a second patched gene in the zebrafish *Danio rerio* and the differential response of patched genes to Hedgehog signalling. *Developmental biology*, 208:14–29, 1999. doi: 10.1006/dbio.1998.9169.
- W. Li and R. Cornell. Redundant activities of Tfp2a and Tfp2c are required for neural crest induction and development of other non-neural ectoderm derivatives in zebrafish embryos. 304 (1):338–354, 2007. doi: 10.1016/j.pestbp.2011.02.012.Investigations.
- X. Li, J. D. Sanneman, D. G. Harbidge, F. Zhou, T. Ito, R. Nelson, N. Picard, R. Chambrey, D. Eladari, T. Miesner, A. J. Griffith, D. C. Marcus, and P. Wangemann. SLC26A4 Targeted to the Endolymphatic Sac Rescues Hearing and Balance in Slc26a4 Mutant Mice. *PLoS Genetics*, 9(7), 2013. doi: 10.1371/journal.pgen.1003641.
- J. K. Liang, J. Bok, and D. K. Wu. Distinct contributions from the hindbrain and mesenchyme to inner ear morphogenesis. *Developmental biology*, 337(2):324–34, jan 2010. doi: 10.1016/j.ydbio.2009.11.001.
- G. J. Lieschke and P. D. Currie. Animal models of human disease: zebrafish swim into view. *Nature reviews. Genetics*, 8(5):353–367, 2007. doi: 10.1038/nrg2091.
- D. Liu, L. Maves, Y. Yan, P. Morcos, J. Postlethwait, and M. Westerfield. Fgf3 and Fgf8 dependent and independent transcription factors are required for otic placode specification. *Development*, 130(10):2213–2224, may 2003. doi: 10.1242/dev.00445.
- Z. Lu and A. a. DeSmidt. Early development of hearing in zebrafish. *Journal of the Association for Research in Otolaryngology : JARO*, 14(4):509–21, aug 2013. doi: 10.1007/s10162-013-0386-z.
- W.-R. Ma and J. Zhang. Jag1b is essential for patterning inner ear sensory cristae by regulating anterior morphogenetic tissue separation and preventing posterior cell death. *Development*, 142(4):763–773, 2015. doi: 10.1242/dev.113662.
- Y. Ma, P. Zhang, F. Wang, J. Yang, Z. Yang, and H. Qin. The relationship between early embryo development and tumorigenesis. *Journal of Cellular and Molecular Medicine*, 14(12):2697–2701, 2010. doi: 10.1111/j.1582-4934.2010.01191.x.
- M. D. Mackereth, S.-j. Kwak, A. Fritz, and B. B. Riley. Zebrafish pax8 is required for otic placode induction and plays a redundant role with Pax2 genes in the maintenance of the otic placode. *Development (Cambridge, England)*, 132(2):371–382, 2005. doi: doi:10.1242/dev.01587.

- E. C. Maier and T. T. Whitfield. RA and FGF Signalling Are Required in the Zebrafish Otic Vesicle to Pattern and Maintain Ventral Otic Identities. *PLoS genetics*, 10(12):e1004858, dec 2014. doi: 10.1371/journal.pgen.1004858.
- A. Mandal, A. Rydeen, J. Anderson, M. R. Sorrell, T. Zygmunt, J. Torres-Vázquez, and J. S. Waxman. Regions of Available Embryonic Retinoic Acid. 242(8):989–1000, 2014. doi: 10.1002/dvdy.23987.Transgenic.
- Z. F. Mann, B. R. Thiede, W. Chang, J.-B. Shin, H. L. May-Simera, M. Lovett, J. T. Corwin, and M. W. Kelley. A gradient of Bmp7 specifies the tonotopic axis in the developing inner ear. *Nature Communications*, 5(4):395–401, may 2014. doi: 10.1038/ncomms4839.
- J. a. Martin and Z. Wang. Next-generation transcriptome assembly. *Nature Reviews Genetics*, 12(10):671–682, 2011. doi: 10.1038/nrg3068.
- K. Maulding, M. S. Padanad, J. Dong, and B. B. Riley. Mesodermal Fgf10b Cooperates With Other Fibroblast Growth Factors During Induction of Otic and Epibranchial Placodes in Zebrafish. *Developmental Dynamics*, pages 1–11, 2014. doi: 10.1002/DVDY.24119.
- L. Maves, W. Jackman, and C. B. Kimmel. FGF3 and FGF8 mediate a rhombomere 4 signaling activity in the zebrafish hindbrain. *Development (Cambridge, England)*, 129(16):3825–37, aug 2002.
- M. N. McCarroll and A. V. Nechiporuk. Fgf3 and fgf10a work in concert to promote maturation of the epibranchial placodes in zebrafish. *PloS one*, 8(12):e85087, jan 2013. doi: 10.1371/journal.pone.0085087.
- M. N. McCarroll, Z. R. Lewis, M. D. Culbertson, B. L. Martin, D. Kimelman, and A. V. Nechiporuk. Graded levels of Pax2a and Pax8 regulate cell differentiation during sensory placode formation. *Development (Cambridge, England)*, 139(15):2740–50, aug 2012. doi: 10.1242/dev.076075.
- N. D. Meeker, S. a. Hutchinson, L. Ho, and N. S. Trede. Method for isolation of PCR-ready genomic DNA from zebrafish tissues. *BioTechniques*, 43(5):610–614, 2007. doi: 10.2144/000112619.
- A. H. Meijer and H. P. Spaik. Host-pathogen interactions made transparent with the zebrafish model. *Current drug targets*, 12(7):1000–17, 2011. doi: 10.2174/138945011795677809.
- P. Mercier, A. Simeone, F. Cotelli, and E. Boncinelli. Expression pattern of two otx genes suggests a role in specifying anterior body structures in zebrafish. *International Journal of Developmental Biology*, 39(4):559–573, 1995.
- J. R. Meyers, J. Planamento, P. Ebrom, N. Krulewitz, E. Wade, and M. E. Pownall. Sulfl modulates BMP signaling and is required for somite morphogenesis and development of the horizontal myoseptum. *Developmental Biology*, 378(2):107–121, 2013. doi: 10.1016/j.ydbio.2013.04.002.
- B. Millimaki, E. Sweet, and B. Riley. Sox2 is required for maintenance and regeneration, but not initial development, of hair cells in the zebrafish inner ear. *Developmental biology*, 338(2), 2010. doi: 10.1016/j.ydbio.2009.12.011. Sox2.
- B. B. Millimaki, E. M. Sweet, M. S. Dhason, and B. B. Riley. Zebrafish atoh1 genes: classic proneural activity in the inner ear and regulation by Fgf and Notch. *Development (Cambridge, England)*, 134(2):295–305, jan 2007. doi: 10.1242/dev.02734.

- I. Mirkovic, S. Pylawka, and A. J. Hudspeth. Rearrangements between differentiating hair cells coordinate planar polarity and the establishment of mirror symmetry in lateral-line neuromasts. *Biology open*, 1(5):498–505, 2012. doi: 10.1242/bio.2012570.
- C. Mowbray, M. Hammerschmidt, and T. T. Whitfield. Expression of BMP signalling pathway members in the developing zebrafish inner ear and lateral line. *Mechanisms of Development*, 108(1-2):179–184, 2001. doi: 10.1016/S0925-4773(01)00479-8.
- R. Murphey and L. Zon. Small molecule screening in the zebrafish. *Methods*, 39(3):255–261, jul 2006. doi: 10.1016/j.ymeth.2005.09.019.
- A. Naidoo, K. Naidoo, N. Yende-zuma, and T. N. Gengiah. Compensatory regulation of the size of the inner ear in response to excess induction of otic progenitors by FGF signaling. *Developmental Dynamics*, 19(2):161–169, 2014. doi: 10.3851/IMP2701.Changes.
- A. Nasevicius and S. C. Ekker. Effective targeted gene ‘knockdown’ in zebrafish. *Nature genetics*, 26(2):216–220, 2000. doi: 10.1038/79951.
- A. Nechiporuk, T. Linbo, K. D. Poss, and D. W. Raible. Specification of epibranchial placodes in zebrafish. *Development (Cambridge, England)*, 134(3):611–623, 2007. doi: 10.1242/dev.02749.
- J. Neves, C. Parada, M. Chamizo, and F. Giráldez. Jagged 1 regulates the restriction of Sox2 expression in the developing chicken inner ear: a mechanism for sensory organ specification. *Development (Cambridge, England)*, 138(4):735–44, feb 2011. doi: 10.1242/dev.060657.
- K. Niederreither, P. McCaffery, U. C. Dräger, P. Chambon, and P. Dollé. Restricted expression and retinoic acid-induced downregulation of the retinaldehyde dehydrogenase type 2 (RALDH-2) gene during mouse development, 1997.
- K. Niederreither, J. Vermot, B. Schuhbaur, P. Chambon, and P. Dollé. Retinoic acid synthesis and hindbrain patterning in the mouse embryo. *Development (Cambridge, England)*, 127(1):75–85, 2000.
- N. Nikolaou, T. Watanabe-Asaka, S. Gerety, M. Distel, R. W. Köster, and D. G. Wilkinson. Lunatic fringe promotes the lateral inhibition of neurogenesis. *Development*, 136(15):2523–33, 2009. doi: 10.1242/dev.034736.
- F. Nin, T. Yoshida, S. Sawamura, G. Ogata, T. Ota, T. Higuchi, S. Murakami, K. Doi, Y. Kurachi, and H. HIBINO. The unique electrical properties in an extracellular fluid of the mammalian cochlea; their functional roles, homeostatic processes, and pathological significance. *Pflugers Archiv European Journal of Physiology*, pages 1–13, 2016. doi: 10.1007/s00424-016-1871-0.
- K. J. O’Donovan, J. Diedler, G. C. Couture, J. J. Fak, and R. B. Darnell. The onconeural antigen cdr2 is a novel APC/C target that acts in mitosis to regulate c-myc target genes in mammalian tumor cells. *PLoS one*, 5(4):e10045, jan 2010. doi: 10.1371/journal.pone.0010045.
- S. Ohta, B. Wang, S. L. Mansour, and G. C. Schoenwolf. BMP regulates regional gene expression in the dorsal otocyst through canonical and non-canonical intracellular pathways. *Development*, (May):dev.137133, 2016. doi: 10.1242/dev.137133.
- T. Ohyama and A. K. Groves. Expression of mouse Foxi class genes in early craniofacial development. *Developmental dynamics : an official publication of the American Association of Anatomists*, 231(3):640–6, nov 2004. doi: 10.1002/dvdy.20160.

- T. Ohyama, O. a. Mohamed, M. M. Taketo, D. Dufort, and A. K. Groves. Wnt signals mediate a fate decision between otic placode and epidermis. *Development (Cambridge, England)*, 133(5): 865–75, mar 2006. doi: 10.1242/dev.02271.
- H. J. Okano, W. Y. Park, J. P. Corradi, and R. B. Darnell. The cytoplasmic Purkinje onconeural antigen cdr2 down-regulates c-Myc function: Implications for neuronal and tumor cell survival. *Genes and Development*, 13(16):2087–2097, 1999.
- D. Olaya-Sánchez, L. Ó. Sánchez-Guardado, S. Ohta, S. C. Chapman, G. C. Schoenwolf, L. Puelles, and M. Hidalgo-Sánchez. Fgf3 and Fgf16 expression patterns define spatial and temporal domains in the developing chick inner ear, mar 2016.
- A. Oshlack, M. D. Robinson, and M. D. Young. From RNA-seq reads to differential expression results. *Genome Biology*, 11(12):220, 2010. doi: 10.1186/gb-2010-11-12-220.
- S. Ota, N. Tonou-Fujimori, N. Tonou-Fujimori, Y. Nakayama, Y. Ito, A. Kawamura, and K. Yasu. FGF receptor gene expression and its regulation by FGF signaling during early zebrafish development. *Genesis*, 48(12):707–716, 2010. doi: 10.1002/dvg.20682.
- M. S. Padanad and B. B. Riley. Pax2/8 proteins coordinate sequential induction of otic and epibranchial placodes through differential regulation of foxi1, sox3 and fgf24. *Developmental biology*, 351(1):90–98, 2011. doi: 10.1016/j.ydbio.2010.12.036.Pax2/8.
- M. S. Padanad, N. Bhat, B. Guo, and B. B. Riley. Conditions that influence the response to Fgf during otic placode induction. *Developmental biology*, 364(1):1–10, apr 2012. doi: 10.1016/j.ydbio.2012.01.022.
- C. Panayiotou, N. Solaroli, Y. Xu, M. Johansson, and A. Karlsson. The characterization of human adenylate kinases 7 and 8 demonstrates differences in kinetic parameters and structural organization among the family of adenylate kinase isoenzymes. *The Biochemical journal*, 433(3):527–34, feb 2011. doi: 10.1042/BJ20101443.
- H. C. Park, S. K. Hong, H. S. Kim, S. H. Kim, E. J. Yoon, C. H. Kim, N. Miki, and T. L. Huh. Structural comparison of zebrafish Elav/Hu and their differential expressions during neurogenesis. *Neuroscience Letters*, 279(2):81–84, 2000. doi: 10.1016/S0304-3940(99)00940-4.
- S. Pauley, T. J. Wright, U. Pirvola, D. Ornitz, K. Beisel, and B. Fritsch. Expression and function of FGF10 in mammalian inner ear development. *Developmental Dynamics*, 227(2):203–215, 2003. doi: 10.1002/dvdy.10297.
- B. T. Phillips, K. Bolding, and B. B. Riley. Zebrafish fgf3 and fgf8 encode redundant functions required for otic placode induction. *Developmental biology*, 235(2):351–65, jul 2001. doi: 10.1006/dbio.2001.0297.
- B. T. Phillips, E. M. Storch, A. C. Lekven, and B. B. Riley. A direct role for Fgf but not Wnt in otic placode induction. *Development (Cambridge, England)*, 131(4):923–31, feb 2004. doi: 10.1242/dev.00978.
- M. Piast, I. Kustrzeba-Wójcicka, M. Matusiewicz, and T. Banaś. Molecular evolution of enolase. *Acta Biochimica Polonica*, 52(2):507–513, 2005. doi: 10.1016/S.
- A. N. Popper and R. R. Fay. Sound detection and processing by teleost fishes: a critical review. *The Journal of the Acoustical Society of America*, 53(6):1515–29, 1973. doi: 10.1121/1.1913496.

- M. Radosevic, A. Robert-Moreno, M. Coolen, L. Bally-Cuif, and B. Alsina. Her9 represses neurogenic fate downstream of Tbx1 and retinoic acid signaling in the inner ear. *Development (Cambridge, England)*, 138(3):397–408, feb 2011. doi: 10.1242/dev.056093.
- S. Raft, S. Nowotschin, J. Liao, and B. E. Morrow. Suppression of neural fate and control of inner ear morphogenesis by Tbx1. *Development (Cambridge, England)*, 131(8):1801–12, 2004. doi: 10.1242/dev.01067.
- F. Raible and M. Brand. Tight transcriptional control of the ETS domain factors Erm and Pea3 by Fgf signaling during early zebrafish development. *Mechanisms of Development*, 107:105–117, 2001.
- F. Reifers, J. Adams, I. J. Mason, S. Schulte-Merker, and M. Brand. Overlapping and distinct functions provided by fgf17, a new zebrafish member of the Fgf8/17/18 subgroup of Fgfs. *Mechanisms of Development*, 99(1-2):39–49, 2000. doi: 10.1016/S0925-4773(00)00475-5.
- M. M. Riccomagno, L. Martinu, M. Mulheisen, D. K. Wu, and D. J. Epstein. Specification of the mammalian cochlea is dependent on Sonic hedgehog. *Genes and Development*, 16(18):2365–2378, 2002. doi: 10.1101/gad.1013302.
- M. M. Riccomagno, S. Takada, and D. J. Epstein. Wnt-dependent regulation of inner ear morphogenesis is balanced by the opposing and supporting roles of Shh. *Genes & Development*, pages 1612–1623, 2005. doi: 10.1101/gad.1303905.sal.
- B. B. Riley and S. J. Moorman. Development of utricular otoliths, but not saccular otoliths, is necessary for vestibular function and survival in zebrafish. *Journal of Neurobiology*, 43(4): 329–337, 2000. doi: 10.1002/1097-4695(20000615)43:4<329::AID-NEU2;3.0.CO;2-H.
- B. B. Riley, M.-y. Chiang, L. Farmer, and R. Heck. The deltaA gene of zebrafish mediates lateral inhibition of hair cells in the inner ear and is regulated by pax2 . 1. 5678:5669–5678, 1999.
- M. E. Robu, J. D. Larson, A. Nasevicius, S. Beiraghi, C. Brenner, S. A. Farber, and S. C. Ekker. P53 Activation By Knockdown Technologies. *PLoS Genetics*, 3(5):787–801, 2007. doi: 10.1371/journal.pgen.0030078.
- R. Romand, W. Krezel, M. Beraneck, L. Cammas, V. Fraulob, N. Messaddeq, P. Kessler, E. Hashino, and P. Dolle. Retinoic Acid Deficiency Impairs the Vestibular Function. *Journal of Neuroscience*, 33(13):5856–5866, 2013. doi: 10.1523/JNEUROSCI.4618-12.2013.
- A. Rossi, Z. Kontarakis, C. Gerri, H. Nolte, S. Hölper, M. Krüger, and D. Y. R. Stainier. Genetic compensation induced by deleterious mutations but not gene knockdowns. *Nature*, Aug 13(524): 230–3, 2015. doi: 10.1038/nature14580.
- D. Rubbini, A. Robert-Moreno, E. Hoijsman, and B. Alsina. Retinoic Acid Signaling Mediates Hair Cell Regeneration by Repressing p27kip and sox2 in Supporting Cells. *Journal of Neuroscience*, 35(47):15752–15766, 2015. doi: 10.1523/JNEUROSCI.1099-15.2015.
- J. E. Russo, D. Hauquitz, and J. Hilton. Inhibition of mouse cytosolic aldehyde dehydrogenase by 4-(diethylamino)benzaldehyde. *Biochemical Pharmacology*, 37:1639–1642, 1988.
- L. Ruzicka, Y. M. Bradford, K. Frazer, D. G. Howe, H. Paddock, S. Ramachandran, A. Singer, S. Toro, C. E. Van Slyke, A. E. Eagle, D. Fashena, P. Kalita, J. Knight, P. Mani, R. Martin, S. A. T. Moxon, C. Pich, K. Schaper, X. Shao, and M. Westerfield. ZFIN, The zebrafish model organism database: Updates and new directions. *Genesis*, 53(8):498–509, 2015. doi: 10.1002/dvg.22868.

- I. Sahly, P. Andermann, and C. Petit. The zebrafish *eya1* gene and its expression pattern during embryogenesis. *Development Genes and Evolution*, 209(7):399–410, 1999. doi: 10.1007/s004270050270.
- K. Sakai, D. J. Mitchell, T. Tsukamoto, and L. Steinman. Isolation of a complementary DNA clone encoding an autoantigen recognized by an anti-neuronal cell antibody from a patient with paraneoplastic cerebellar degeneration. *American Neurological Association*, 28(5):692–8, 1990. doi: 10.1002/ana.410280515.
- L. Ó. Sánchez-Guardado, L. Puelles, and M. Hidalgo-Sánchez. Fgf10 expression patterns in the developing chick inner ear. *Journal of Comparative Neurology*, 521(5):1136–1164, 2013. doi: 10.1002/cne.23224.
- D. Sapède and C. Pujades. Hedgehog signaling governs the development of otic sensory epithelium and its associated innervation in zebrafish. *The Journal of neuroscience : the official journal of the Society for Neuroscience*, 30(10):3612–23, mar 2010. doi: 10.1523/JNEUROSCI.5109-09.2010.
- T. Schimmang. Expression and functions of FGF ligands during early otic development. *The International journal of developmental biology*, 51(6-7):473–81, jan 2007. doi: 10.1387/ijdb.072334ts.
- J. Schindelin, I. Arganda-Carreras, E. Frise, V. Kaynig, M. Longair, T. Pietzsch, S. Preibisch, C. Rueden, S. Saalfeld, B. Schmid, J.-Y. Tinevez, D. J. White, V. Hartenstein, K. Eliceiri, P. Tomancak, and A. Cardona. Fiji: an open-source platform for biological-image analysis. *Nature Methods*, 9(7):676–682, 2012. doi: 10.1038/nmeth.2019.
- K. L. Schmidt, N. Marcus-Gueret, A. Adeleye, J. Webber, D. Baillie, and E. G. Stringham. The cell migration molecule UNC-53/NAV2 is linked to the ARP2/3 complex by ABI-1. *Development (Cambridge, England)*, 136(4):563–574, 2009. doi: 10.1242/dev.016816.
- M. Schubert, D. Panja, M. Haugen, C. R. Bramham, and C. a. Vedeler. Paraneoplastic CDR2 and CDR2L antibodies affect Purkinje cell calcium homeostasis. *Acta neuropathologica*, oct 2014. doi: 10.1007/s00401-014-1351-6.
- S. Schulte-Merker and D. Y. R. Stainier. Out with the old, in with the new: reassessing morpholino knockdowns in light of genome editing technology. *Development*, 141:3103–3104, 2014. doi: 10.1242/dev.112003.
- N. C. Shaner, P. A. Steinbach, and R. Y. Tsien. A guide to choosing fluorescent proteins. *Nature methods*, 2(12):905–909, 2005. doi: 10.1038/nmeth819.
- U. J. Sienknecht. Current concepts of hair cell differentiation and planar cell polarity in inner ear sensory organs. *Cell and Tissue Research*, 361(1):25–32, 2015. doi: 10.1007/s00441-015-2200-1.
- M. Simões-Costa and M. E. Bronner. Establishing neural crest identity: a gene regulatory recipe. *Development (Cambridge, England)*, 142(2):242–57, 2015. doi: 10.1242/dev.105445.
- K. J. Simpson, L. M. Selfors, J. Bui, A. Reynolds, D. Leake, A. Khvorova, and J. S. Brugge. Identification of genes that regulate epithelial cell migration using an siRNA screening approach. *Nature cell biology*, 10(9):1027–1038, 2008. doi: 10.1038/ncb1762.
- K. S. Solomon, T. Kudoh, I. B. Dawid, and A. Fritz. Zebrafish *foxi1* mediates otic placode formation and jaw development. *Development*, 130(5):929–940, mar 2003. doi: 10.1242/dev.00308.

- K. S. Solomon, S.-J. Kwak, and A. Fritz. Genetic interactions underlying otic placode induction and formation. *Developmental dynamics : an official publication of the American Association of Anatomists*, 230(3):419–33, jul 2004. doi: 10.1002/dvdy.20067.
- E. J. Son, J.-H. Ma, H. Ankamreddy, J.-O. Shin, J. Y. Choi, D. K. Wu, and J. Bok. Conserved role of Sonic Hedgehog in tonotopic organization of the avian basilar papilla and mammalian cochlea. *Proceedings of the National Academy of Sciences of the United States of America*, 112(12):3746–51, 2015. doi: 10.1073/pnas.1417856112.
- M. Sonawane, H. Martin-Maischein, H. Schwarz, and C. Nüsslein-Volhard. Lgl2 and E-cadherin act antagonistically to regulate hemidesmosome formation during epidermal development in zebrafish. *Development (Cambridge, England)*, 136(8):1231–40, apr 2009. doi: 10.1242/dev.032508.
- B. Steventon, C. Araya, C. Linker, S. Kuriyama, and R. Mayor. Differential requirements of BMP and Wnt signalling during gastrulation and neurulation define two steps in neural crest induction. *Development (Cambridge, England)*, 136(5):771–9, 2009. doi: 10.1242/dev.029017.
- G. A. Stooke-Vaughan. *The Role of Cilia in Inner Ear Development and Otolith Formation in the Zebrafish Otic Vesicle*. PhD thesis, University of Sheffield., 2013.
- G. a. Stooke-Vaughan, P. Huang, K. L. Hammond, A. F. Schier, and T. T. Whitfield. The role of hair cells, cilia and ciliary motility in otolith formation in the zebrafish otic vesicle. *Development (Cambridge, England)*, 139(10):1777–87, may 2012. doi: 10.1242/dev.079947.
- A. Streit. The preplacodal region: an ectodermal domain with multipotential progenitors that contribute to sense organs and cranial sensory ganglia. *The International journal of developmental biology*, 51(6-7):447–61, jan 2007. doi: 10.1387/ijdb.072327as.
- T. J. Stuhlmiller and M. I. García-Castro. Current perspectives of the signaling pathways directing neural crest induction. *Cellular and Molecular Life Sciences*, 69(22):3715–3737, 2012. doi: 10.1007/s00018-012-0991-8.
- J. Summerton. Morpholino antisense oligomers: The case for an RNase H-independent structural type. *Biochimica et Biophysica Acta - Gene Structure and Expression*, 1489(1):141–158, 1999. doi: 10.1016/S0167-4781(99)00150-5.
- S.-K. Sun, C. T. Dee, V. B. Tripathi, A. Rengifo, C. S. Hirst, and P. J. Scotting. Epibranchial and otic placodes are induced by a common Fgf signal, but their subsequent development is independent. *Developmental biology*, 303(2):675–86, mar 2007. doi: 10.1016/j.ydbio.2006.12.008.
- M. L. Suster, K. Sumiyama, and K. Kawakami. Transposon-mediated BAC transgenesis in zebrafish and mice. *BMC genomics*, 10:477, jan 2009. doi: 10.1186/1471-2164-10-477.
- E. M. Sweet, S. Vemaraju, and B. B. Riley. Sox2 and Fgf interact with Atoh1 to promote sensory competence throughout the zebrafish inner ear. *Developmental biology*, 358(1):113–21, oct 2011. doi: 10.1016/j.ydbio.2011.07.019.
- M. Takamiya and J. A. Campos-Ortega. Hedgehog signalling controls zebrafish neural keel morphogenesis via its level-dependent effects on neurogenesis. *Developmental Dynamics*, 235(4):978–997, 2006. doi: 10.1002/dvdy.20720.
- B. Tarchini, A. L. Tadenev, N. Devanney, and M. Cayouette. A link between planar polarity and staircase-like bundle architecture in hair cells. *Development*, (September):dev.139089, 2016. doi: 10.1242/dev.139089.

- H. G. Tay, S. K. Schulze, J. Compagnon, F. C. Foley, C.-P. Heisenberg, H. J. Yost, S. Abdelilah-Seyfried, and J. D. Amack. Lethal giant larvae 2 regulates development of the ciliated organ Kupffer's vesicle. *Development (Cambridge, England)*, 140(7):1550–1559, apr 2013. doi: 10.1242/dev.087130.
- B. Thisse and C. Thisse. Fast Release Clones: A High Throughput Expression Analysis., 2004.
- H. Thompson, A. Ohazama, P. T. Sharpe, and A. S. Tucker. The origin of the stapes and relationship to the otic capsule and oval window. *Developmental Dynamics*, 241(9):1396–1404, 2012. doi: 10.1002/dvdy.23831.
- J. A. Tucker, K. A. Mintzer, and M. C. Mullins. The BMP Signaling Gradient Patterns Dorsoventral Tissues in a Temporally Progressive Manner along the Anteroposterior Axis. *Developmental Cell*, 14(1):108–119, jan 2008. doi: 10.1016/j.devcel.2007.11.004.
- L. D. Urness, C. N. Paxton, X. Wang, G. C. Schoenwolf, and S. L. Mansour. FGF signaling regulates otic placode induction and refinement by controlling both ectodermal target genes and hindbrain Wnt8a. *Developmental biology*, 340(2):595–604, apr 2010. doi: 10.1016/j.ydbio.2010.02.016.
- E. H. Waldman, A. Castillo, and A. Collazo. Ablation studies on the developing inner ear reveal a propensity for mirror duplications. *Developmental dynamics : an official publication of the American Association of Anatomists*, 236(5):1237–48, may 2007. doi: 10.1002/dvdy.21144.
- J. Walshe and I. Mason. Fgf signalling is required for formation of cartilage in the head. *Developmental Biology*, 264(2):522–536, 2003. doi: 10.1016/j.ydbio.2003.08.010.
- W. Wang, T. Van De Water, and T. Lufkin. Inner ear and maternal reproductive defects in mice lacking the Hmx3 homeobox gene. *Development (Cambridge, England)*, 125(4):621–34, 1998.
- W. Wang, E. K. Chan, S. Baron, T. Van de Water, and T. Lufkin. Hmx2 homeobox gene control of murine vestibular morphogenesis. *Development (Cambridge, England)*, 128(24):5017–5029, 2001.
- W. Wang, J. F. Grimmer, T. R. Van De Water, and T. Lufkin. Hmx2 and Hmx3 homeobox genes direct development of the murine inner ear and hypothalamus and can be functionally replaced by Drosophila Hmx. *Developmental Cell*, 7(3):439–453, 2004. doi: 10.1016/j.devcel.2004.06.016.
- W. D. Wang, D. B. Melville, M. Montero-Balaguer, A. K. Hatzopoulos, and E. W. Knapik. Tfap2a and Foxd3 regulate early steps in the development of the neural crest progenitor population. *Developmental Biology*, 360(1):173–185, 2011. doi: 10.1016/j.ydbio.2011.09.019.
- J. S. Waxman and D. Yelon. Zebrafish retinoic acid receptors function as context-dependent transcriptional activators. *Developmental biology*, 352(1):128–40, 2011. doi: 10.1016/j.ydbio.2011.01.022.
- T. Weber and R. Köster. Genetic tools for multicolor imaging in zebrafish larvae. *Methods (San Diego, Calif.)*, 62(3):279–91, aug 2013. doi: 10.1016/j.ymeth.2013.07.028.
- M. Westerfield. *The Zebrafish Book. A guide for the laboratory use of zebrafish (Danio rerio)*. University of Oregon Press, Eugene, 4th edition, 2000.
- R. J. White, Q. Nie, A. D. Lander, and T. F. Schilling. Complex regulation of cyp26a1 creates a robust retinoic acid gradient in the zebrafish embryo. *PLoS biology*, 5(11):e304, nov 2007. doi: 10.1371/journal.pbio.0050304.

- T. T. Whitfield. Zebrafish as a model for hearing and deafness. *Journal of Neurobiology*, 53(2): 157–171, 2002. doi: 10.1002/neu.10123.
- T. T. Whitfield. Development of the inner ear. *Current Opinion in Genetics & Development*, 32: 112–118, 2015. doi: doi.org/10.1016/j.gde.2015.02.006.
- T. T. Whitfield and K. L. Hammond. Axial patterning in the developing vertebrate inner ear. *The International journal of developmental biology*, 51(6-7):507–20, jan 2007. doi: 10.1387/ijdb.072380tw.
- T. T. Whitfield, M. Granato, F. J. van Eeden, U. Schach, M. Brand, M. Furutani-Seiki, P. Haffter, M. Hammerschmidt, C. P. Heisenberg, Y. J. Jiang, D. a. Kane, R. N. Kelsh, M. C. Mullins, J. Odenthal, and C. Nüsslein-Volhard. Mutations affecting development of the zebrafish inner ear and lateral line. *Development (Cambridge, England)*, 123:241–54, dec 1996a.
- T. T. Whitfield, M. Granato, F. J. M. VanEeden, U. Schach, M. Brand, M. FurutaniSeiki, P. Haffter, M. Hammerschmidt, C. P. Heisenberg, Y. J. Jiang, D. A. Kane, R. N. Kelsh, M. C. Mullins, J. Odenthal, and C. NussleinVolhard. Mutations affecting development of the zebrafish inner ear and lateral line. *Development*, 123(SI):241–254, 1996b.
- T. T. Whitfield, B. B. Riley, M.-y. Chiang, and B. Phillips. REVIEWS Development of the Zebrafish Inner Ear. *Developmental Dynamics*, 458(February):427–458, 2002. doi: 10.1002/dvdy.10073.
- D. K. Wu, F. D. Nunes, and D. Choo. Axial specification for sensory organs versus non-sensory structures of the chicken inner ear. *Development (Cambridge, England)*, 125(1):11–20, jan 1998.
- L. Yang, P. O’Neill, K. Martin, J. C. Maass, V. Vassilev, R. Ladher, and A. K. Groves. Analysis of FGF-Dependent and FGF-Independent Pathways in Otic Placode Induction. *PloS one*, 8(1): e55011, jan 2013. doi: 10.1371/journal.pone.0055011.
- D. Yao, F. Zhao, Y. Wu, J. Wang, W. Dong, J. Zhao, Z. Zhu, and D. Liu. Dissecting the differentiation process of the preplacodal ectoderm in zebrafish. *Developmental Dynamics*, 243(10):1338–1351, 2014. doi: 10.1002/dvdy.24160.
- J. Zou, Y. Guo, T. Guettouche, D. F. Smith, and R. Voellmy. Repression of heat shock transcription factor HSF1 activation by HSP90 (HSP90 complex) that forms a stress-sensitive complex with HSF1. *Cell*, 94:471–480, 1998. doi: 10.1016/S0092-8674(00)81588-3.
- Y. Zou, S. S. Mak, H. Z. Liu, D. Y. Han, H. X. Zhuang, S. M. Yang, and R. K. Ladher. Induction of the chick columella and its integration with the inner ear. *Developmental Dynamics*, 241(6): 1104–1110, 2012. doi: 10.1002/dvdy.23788.

Acknowledgements

I would like to acknowledge and thank both Tanya Whitfield and Nick Monk for their continued discussion and support throughout, including the last minutes, of this PhD project. I would also like to thank all the other members of the Whitfield lab, past and present, who have advised and helped me along the way. This project would not have been possible without funding from the White Rose-BBSRC DTP.

To my friends and family, thank you for your welcomed distractions. Most importantly, I want to thank my fiancée Sarah. Words cannot do justice to how invaluable her support has been.

"We're just two lost souls swimming in a fish bowl, year after year" - Roger Waters.